THE UNIVERSITY OF ALBERTA

LAMINAR FORCED CONVECTION IN NONCIRCULAR DUCTS

by

MOHAMMAD JAMIL, B.Sc.

(West Pakistan University)

A THESIS

SUBMITTED TO THE FACULTY OF GRADUATE STUDIES

IN PARTIAL FULFILMENT OF THE REQUIREMENTS FOR THE DEGREE

OF MASTER OF SCIENCE

DEPARTMENT OF MECHANICAL ENGINEERING

EDMONTON, ALBERTA

APRIL 1967

THE UNIVERSITY OF ALBERTA

LAMINAR FORCED CONVECTION IN NONCIRCULAR DUCTS

by

MOHAMMED IMBIL, B.Sc.
(Moss Farkiadh University)

A THESIS

SUBMITTED TO THE FACULTY OF GRADUATE STUDIES

IN PARTIAL FULFILLMENT OF THE REQUIREMENTS FOR THE DEGREE

OF MASTER OF SCIENCE

DEPARTMENT OF MECHANICAL ENGINEERING

EDMONTON, ALBERTA

APRIL 1967

UNIVERSITY OF ALBERTA

FACULTY OF GRADUATE STUDIES

The undersigned certify that they have read, and recommend to the Faculty of Graduate Studies for acceptance, a thesis entitled "LAMINAR FORCED CONVECTION IN NONCIRCULAR DUCTS" submitted by MOHAMMAD JAMIL in partial fulfilment of the requirements for the degree of Master of Science.

ABSTRACT

Theoretical investigations for fully developed laminar heat transfer in noncircular ducts were carried out using both the point matching and variational methods. The thermal boundary conditions of axially uniform wall heat flux and equal wall temperature at a given axial position are considered for: (a) circular ducts with diametrically opposite flat sides: (b) ducts of multiply connected cross sections in the form of regular polygons with a central circular hole and circular ducts with a central regular polygonal hole. Heat transfer results for regular polygonal ducts with thermal boundary conditions of both peripherally and axially uniform heat flux were obtained using the point matching method.

Extensive numerical results are presented for local quantities such as the velocity distribution, temperature distribution, temperature gradient at the wall and for overall quantities such as the mass flow rate, friction factor, average wall temperature, bulk fluid temperature, and Nusselt number. Graphical results are presented for the shear stress distribution, temperature gradient at the wall, mass flow rate, friction factor - Reynolds number results and average Nusselt number. Velocity and temperature profiles are also presented for the representative cases.

Abstract

ACKNOWLEDGEMENTS

The author wishes to extend his appreciation to

- Dr. K.C. Cheng for his supervision of this thesis,
- The members of the Computing Science Department for their advice and cooperation in computer programing,
- Miss Lynne Fiveland for typing the thesis,
- The National Research Council of Canada for financial support under grant NRC A-1655 (Cheng).

TABLE OF CONTENTS

Table of Contents

Page

Page

LIST OF FIGURES

List of Figures

FIGURE PAGE

FIGURE PAGE

FIGURE PAGE

FIGURE PAGE

LIST OF TABLES

TABLE PAGE

TABLE PAGE

NOMENCLATURE

A	cross sectional area
A_j, B_j	series coefficients for velocity
A_j', B_j'	series coefficients for temperature
a	radius of circumscribed circle for regular polygon
b	radius of inner circular boundary
c	radius of outer circular boundary
c_1	axial pressure gradient, $c_1 = dp/dz$
c_2	axial temperature gradient, $c_2 = \partial t/\partial z$
c_p	specific heat at constant pressure
D_e	equivalent hydraulic diameter, 4x(cross section area)/S
f	Fanning friction factor
h	fully developed heat transfer coefficient
i,j	summation index
K	constant defined by $w = \rho K \left(-\frac{1}{\mu}\frac{dp}{dz}\right) a^4$
k	thermal conductivity or summation index
L	constant defined by $w = \rho L \left(-\frac{1}{\mu}\frac{dp}{dz}\right) c^4$
M	constant defined by $M = -u_m/(c_1 a^2/\mu)$
N	number of sides of regular polygon
n	normal to the regular polygon boundary
Nu	Nusselt number, hD_e/k
R	dimensionless radial coordinate, r'/c
Re	Reynold number, $D_e\ u_m\ \rho/\mu$

r	dimensionless radial coordinate, r'/a
r'	radial coordinate
S	circumference of cross section
t	local temperature
t_m	average temperature
t_w	local wall temperature
u	local axial velocity
u_m	average velocity
u_x	velocity derivative with respect to x
u_y	velocity derivative with respect to y
w	mass flow rate
x,y,z	rectangular coordinates
Z	constant defined by equation (24)
α	thermal diffusivity, $k/\rho c_p$
β	opening angle defined in Figure 1 or $\beta = \pi/N$
Γ	boundary curves of cross section
γ	ratio defined by $\gamma = c/(a \cos \pi/N)$
η	b/a
θ	temperature difference, $\theta = t - t_w$
θ_b	bulk fluid temperature
θ_h	homogeneous solution for temperature difference θ
θ_p	particular solution for temperature difference θ
θ_w	wall temperature, $\theta_w = t_w - t_m$
θ_{wm}	average wall temperature
θ'	temperature variable, $\theta' = t - t_m$

x	coordinate [axial component], x_1
$\bar{x}$	radial coordinate
θ	circumferential or skew angle
λ	local compression
λ_m	minimum compression
λ_s	local wall compression
μ	local wall viscosity
ν	Poisson ratio
ν_m	molecular diffusivity with respect to x
ν_t	molecular diffusivity with respect to y
π	3.14159...
ρ, ρ_1, ρ_2	fluid densities
σ	constant defined by equation (23)
τ	shearing stress, $\eta(\partial u/\partial y)$
ϕ	viscous dissipation function $2[(\partial u/\partial x)^2 + (\partial v/\partial y)^2 + \frac{1}{2}(\partial u/\partial y + \partial v/\partial x)^2]$
χ	boundary curve of cross section
ψ	ratio defined by $\lambda = \cos\psi$
ω	$\sqrt{\lambda}$
Δ	temperature difference, $\theta_w - \theta_\infty$
Δ_m	axial flux thickness
Δ_t	momentum thickness for temperature difference θ
Δ_u	displacement thickness for temperature difference θ
Δ_w	wall temperature, $\theta_w - \theta_\infty = \theta_0 - \theta_\infty$
Δ_{wm}	minimum wall temperature
Δ'	temperature gradient, $\theta_w' - \theta_\infty'$

λ	ratio defined by $\lambda = (a \cos \pi/N)/b$
μ	viscosity
ρ	density
τ	local wall shear stress
$\overline{\tau}$	average wall shear stress
Φ	angular coordinate
ψ	uniform temperature gradient at wall, $\partial t/\partial n$

CHAPTER I

INTRODUCTION

Laminar forced convection heat transfer in non-circular ducts, under developing or fully developed conditions, has been the subject of investigation for many years. The analytical solutions for such problems generally include three basic thermal boundary conditions:

(a) Uniform heat flux per unit length but uniform peripheral wall temperature (Dirichlet type thermal boundary condition),

(b) Uniform heat flux, axially and peripherally (Neumann type thermal boundary condition),

(c) Uniform wall temperature (Dirichlet type thermal boundary condition).

It has been shown recently that the point matching technique gives an approximate solution for many boundary-value or eigen-value problems involving the Laplace, Poisson or biharmonic equations, with either linear or homogeneous boundary conditions. Barta [1]* and Conway [2] applied this method to solve a number of torsion and plate problems involving triangular, square, hexagonal and rhombic shapes. Sparrow [3] has accurately determined the flow characteristics for laminar flow in isosceles

---

* Numbers in brackets denote references given on page 68 .

CHAPTER 1

INTRODUCTION

---

triangular ducts with various apex angles. Cheng [4] applied this method to fully developed laminar flow in noncircular passages consisting of regular polygons with Dirichlet type boundary conditions. In this thesis, the same approach is utilized for fully developed laminar flow in circular ducts with diametrically opposite flat sides, regular polygonal ducts with a central circular hole, and circular ducts with a central regular polygonal hole. All ducts are treated for Dirichlet-type boundary conditions with the exception of regular polygonal ducts where the Neumann boundary conditions are considered.

The variational method has been used by Sparrow and Siegel [5] to solve the problem of rectangular and circular-sector ducts with various thermal boundary conditions. Because of its success in the above problems, the method has been used here for evaluating the heat transfer and flow characteristics for circular ducts with diametrically opposite flat sides with Dirichlet-type boundary conditions. The Raleigh-Ritz variational method [6] has proved to be as successful as the point matching technique, but involves a great deal of work if accuracy is desired. The results obtained using this method are found to be quite comparable with those computed from the point matching technique.

The solutions for laminar heat transfer for both

parallel-plate channels and circular ducts with Dirichlet boundary conditions are available in the literature. Carter [7] and Ōkubo [8] give approximate solutions for the Saint-Venant torsion problem for circular cross sections with diametrically opposite flat sides. These approximate results, when interpreted in terms of flow problems, by analogy, substantially agree with those obtained from the point matching and variational methods.

A comprehensive study on heat transfer in annular passages for hydrodynamically fully-developed laminar flow with arbitrarily prescribed wall temperature or heat fluxes is presented by Lundberg, McCuen and Reynolds [9]. The problem of bilateral heat transfer in annuli for slug and laminar flows was studied by Dwyer [10] Gaydon and Nuttall [11] established the upper and lower bounds for volume flow rate through cylindrical tubes of square and hexagonal cross sections with a central circular hole, using the Schwartz inequality for various hole diameters. The present study for doubly connected boundaries with Dirichlet-type boundary conditions is based upon the method of point matching. Series solutions have been utilized by satisfying the boundary conditions at the inner circular boundary exactly: the case considered is that of regular polygonal ducts with a central regular polygonal hole [12]. The results for circular

potential-plate rheometer and stirrer media with multiple boundary conditions are available in the literature. Carter [3] and Happe [8] give approximate solutions for the Saito-Owens torsion pendulum for circular sections with elementarily geometric axes. These approximate results, when interpreted in terms of flow problems, by analogy, unfavorably agree with those obtained from the point-matching and variational methods.

A comparatively newly or lines attempted to develop passages for hydrodynamically fully-developed laminar flow with arbitrarily geometrically connected or near flukes is presented by Lundberg, Mcqueen and Reynolds [9]. The problem of flattened heat channels to annuli for wind can laminar flows was studied by Davis [10] wherein the finite [11] established the upper and lower bounds for volume flow rate through cylindrical tubes of square and rectangular cross sections with a central circular bore, using the geometric inequality for various body dimensions. The present study for annuli eccentric channels is based upon the method of point matching. Earlier solutions have been restored by restricting the boundary conditions of the three circular boundary ensembly: the case considered is that of annular polygonal ducts with a central circular eccentric hole [12]. The results for flattened

ducts with a central regular polygonal hole approximate very closely those for regular polygonal ducts with a central circular hole when the number of sides for the regular polygon approaches a very large number, e.g. twenty.

The case of rectangular ducts with uniform peripheral heat flux was solved by Cheng [13] in the form of an infinite series using separation of variables. Numerical results are given for aspect ratios of 1, 2, 4 and 10. Sparrow and Siegel [5] approached the same problem with aspect ratios of 1 and 10 using the variational method. Eckert, Irvine and Yen [14] presented the heat transfer results for circular sector ducts with apex angles ranging from 11° 25' 20" to 60° using a classical analytical method for both Dirichlet and Neumann type thermal boundary conditions. Recently, Sparrow and Haji-Sheikh [15] presented a computation-oriented method of analysis for ducts of arbitrary shape with arbitrary thermal boundary conditions by using orthonormal functions: numerical results are also given for ducts of circular-segment cross section. The method of point matching has also been used for evaluating the heat transfer results for regular polygonal ducts with Neumann type boundary conditions in this thesis.

CHAPTER II

THEORETICAL ANALYSIS

2.1 Governing Equations

The governing equations and the associated boundary conditions for a fully developed, constant property and non-dissipating laminar flow are [5]

$$\frac{\partial^2 u}{\partial r'^2} + \frac{1}{r'}\frac{\partial u}{\partial r'} + \frac{1}{r'^2}\frac{\partial^2 u}{\partial \phi^2} = \frac{1}{\mu}\frac{dp}{dz} = \frac{c_1}{\mu} \tag{1}$$

$$\frac{\partial^2 t}{\partial r'^2} + \frac{1}{r'}\frac{\partial t}{\partial r'} + \frac{1}{r'^2}\frac{\partial^2 t}{\partial \phi^2} = \frac{u}{\alpha}\frac{\partial t}{\partial z} = \frac{uc_2}{\alpha} \tag{2}$$

(a) Dirichlet type boundary conditions.

$$u = \theta = 0, \quad \text{on } \Gamma \tag{3}$$

(b) Neumann type boundary conditions.

$$u = 0, \quad \frac{dt}{dn} = \psi, \quad \text{on } \Gamma \tag{4}$$

2.2 Series Solution for Velocity

The general solution of equation (1) in polar coordinates (r,ϕ) for a symmetrical cross section (see Figures 1, 17, 32, 45) is [3]

CHAPTER II

GOVERNING EQUATIONS

2.1 Governing Equations

The governing equations and the corresponding boundary conditions for a fully developed, laminar pulsatory and non-axisymmetric laminar flow are [1]

$$\frac{\partial^2 u}{\partial r^2} + \frac{1}{r}\frac{\partial u}{\partial r} + \frac{1}{r^2}\frac{\partial^2 u}{\partial \theta^2} = \frac{1}{\mu}\frac{\partial p}{\partial z} = -\frac{\omega}{\nu} \qquad (1)$$

$$\frac{\partial^2 v}{\partial r^2} + \frac{1}{r}\frac{\partial v}{\partial r} + \frac{1}{r^2}\frac{\partial^2 v}{\partial \theta^2} = \frac{1}{\mu}\frac{\partial p}{\partial \theta} = -\frac{m\omega}{\nu} \qquad (2)$$

(a) Periodic type boundary conditions:

$$u = v = 0, \quad r = 1 \qquad (3)$$

(b) Pressure gradient boundary conditions:

$$\frac{\partial u}{\partial r} = E_1 \cos \omega t, \quad r = 1 \qquad (4)$$

2.2 Boundary Conditions for Velocity

The general solution of equation (1) in polar coordinates (r, θ) for a symmetrical tube section (see figure 1, r_1, r_2, and α is [1]

$$u = \frac{r'^2}{4}\left(\frac{1}{\mu}\frac{dp}{dz}\right) + A_o + B_o \ln r' + \sum_{k=1,2,\ldots}^{\infty}\left(A_k r'^{k} + B_k r'^{-k}\right)\cos k\phi \qquad (5)$$

The above solution for velocity may be used in evaluating the flow characteristics for different types of noncircular ducts, as discussed below, with no-slip boundary conditions.

(a) Circular Ducts with Diametrically Opposite Flat Sides

With the requirement that the velocity is finite everywhere and in particular at r' = 0 (see Figure 1) it follows that

$$B_o = 0, \qquad B_k = 0 \qquad (6)$$

From $\frac{\partial u}{\partial \phi} = 0$ at $\phi = \frac{\pi}{2}$

$k = 2j$ where $j = 1,2,3,\ldots$

Using the above results in equation (5), the velocity equation is,

$$u = \left(\frac{-a^2}{\mu}\frac{dp}{dz}\right)\left[-\frac{r^2}{4} + \sum_{j=0,1,2}^{\infty} A_j r^{2j}\cos 2j\phi\right] \qquad (7)$$

(b) Regular Polygonal Ducts with a Central Circular Hole

The velocity distribution for regular polygonal ducts with a central circular hole is [4],

$$u = \left(-\frac{a^2}{\mu}\frac{dp}{dz}\right)\left[-\frac{r^2}{4} + A_o + B_o \ln r + \sum_{j=1,2,3}^{\infty}\left(A_j r^{jN} + B_j r^{-jN}\right)\cos jN\phi\right] \quad (8)$$

The unknown coefficients can be selected so as to satisfy the boundary condition u = 0, on the inner circular boundary (see Figure 17). The results are

$$B_o = \frac{1}{\ln \eta}\left(\frac{1}{4}\eta^2 - A_o\right) \quad (9)$$

$$B_j = -A_j \eta^{2jN} \quad (10)$$

Substituting B_o and B_j into equation (8), we get

$$u = \left(-\frac{a^2}{\mu}\frac{dp}{dz}\right)\left[-\left(\frac{r^2}{4} - \frac{\eta^2}{4}\frac{\ln r}{\ln \eta}\right) + A_o\left(1 - \frac{\ln r}{\ln \eta}\right) + \sum_{j=1,2,3}^{\infty} A_j\left(r^{jN} - \frac{\eta^{2jN}}{r^{jN}}\right)\cos jN\phi\right] \quad (11)$$

(c) Circular Ducts with a Central Regular Polygonal Hole

The general solution of equation (1), for circular ducts with a central regular polygonal hole is [4]

$$u = \left(-\frac{c^2}{\mu}\frac{dp}{dz}\right)\left[-\frac{R^2}{4} + A_o + B_o \ln R + \sum_{j=1,2,3}^{\infty} \left(A_j R^{jN} + B_j R^{-jN}\right)\cos jN\Phi\right] \quad (12)$$

To satisfy the boundary condition u = 0 on the outer circular boundary the unknown coefficients must be selected as,

$$A_o = \frac{1}{4}$$
$$B_j = -A_j \quad (13)$$

Substituting the above constants into equation (12)

$$u = \left(-\frac{c^2}{\mu}\frac{dp}{dz}\right)\left[-\frac{R^2}{4} + \frac{1}{4} + B_o \ln R + \sum_{j=1,2,3}^{\infty} A_j \left(R^{jN} - R^{-jN}\right)\cos jN\Phi\right] \quad (14)$$

(d) Regular Polygonal Ducts

If the velocity is finite everywhere and particularly at r = 0 (see Figure 45) then from equation (8)

$$B_o = 0, \qquad B_j = 0 \quad (15)$$

and the remaining equation gives

$$u = \left(-\frac{a^2}{\mu}\frac{dp}{dz}\right)\left[-\frac{r^2}{4} + \sum_{j=0,1,2}^{\infty} A_j\, r^{jN} \cos jN\Phi\right] \tag{16}$$

2.3 Series Solution for Temperature

The general solution to the temperature equation (2) can be expressed as the sum of both the particular and homogeneous solutions

$$\theta = \theta_p + \theta_h \tag{17}$$

where the homogeneous solution of the temperature equation for a symmetrical duct (see Figure 1, 17, 32) from [4] is

$$\theta_h = \left(\frac{c_1 c_2}{\mu\alpha}\right)\left[A'_o + B'_o \ln r' + \sum_{j=1,2,3}^{\infty} A'_j\, r'^{jN} + B'_j\, r'^{jN}\right) \cos jN\Phi\Big] \tag{18}$$

The particular solution θ_p can be obtained by selecting or evaluating some function, for the individual case separately as discussed below.

(a) Circular Ducts with Diametrically Opposite Flat Sides

With the velocity field given by equation (7), the particular solution of equation (2) can always be obtained.

and the associated equation gives

$$\varepsilon = \left(\frac{\omega}{\omega_p}\right)^2 \left[1 + \frac{3}{k^2} \int_{-\infty}^{\infty} \frac{\partial f_0}{\partial v} \frac{1}{v - \frac{\omega}{k}} dv\right] \tag{10}$$

4.3 Plasma Dielectric Permittivity

The general solution to the homogeneous equation (9) can be expressed in the sum of both the particular and homogeneous solutions

$$E = E_p + E_h \tag{11}$$

where the homogeneous solution or the longitudinal oscillation for a symmetrical wave (see Figure 3) from (3) gives

$$E_h = \left(\frac{C_1 - C_2}{2}\right) \int_{-\infty}^{\infty} g(v) \, dv + \frac{C_1 + C_2}{2} \int_{-\infty}^{\infty} g(v) \, e^{-\frac{\omega}{k} t} \, dv \tag{12}$$

$$\left| \right| \tag{13}$$

The particular solution E_p can be derived by assuming an excitation wave function for the individual wave separately in Laplace form.

(a) Electron Wave with Time-Varying Charge Sine Wave

Since the velocity [illegible] of excitation [illegible] the [illegible] solution of equation (9) can always be obtained.

For instance, considering only the jth term in equation (7), the particular solution is

$$\theta_p = \left(-\frac{a^4 c_1 c_2}{\mu\alpha}\right)\left[A_j/(8j+4)\right] r^{2j+2} \cos 2j\phi \qquad (19)$$

The above particular solution of equation (7) and the homogeneous solution represented by equation (18), provide us with the temperature distribution

$$\theta = \left(\frac{a^4 c_1 c_2}{\mu\alpha}\right)\left[\frac{r^4}{16} - \sum_{j=0,1,2}^{\infty} \frac{A_j r^{2j+2}}{(8j+4)} \cos 2j\phi + A'_o + B'_o \ln r + \sum_{j=1,2,3}^{\infty}\left(A'_j r^{jN} + B'_j r^{-jN}\right)\cos jN\phi\right] \qquad (20)$$

For $\frac{\partial\theta}{\partial\phi} = 0$ at $\phi = \pi/2$, gives

$$N = 2$$

and θ being finite at $r = 0$, requires that

$$B'_j = 0$$

Therefore equation (20) reduces to the following form,

$$\theta = \left(\frac{a^4 c_1 c_2}{\mu\alpha}\right)\left[\frac{r^4}{16} - \sum_{j=0,1,2}^{\infty} \frac{A_j r^{2j+2}}{(8j+4)} \cos 2j\phi + \sum_{j=0,1,2}^{\infty} A'_j r^{2j} \cos 2j\phi\right] \qquad (21)$$

(b) Regular Polygonal Ducts with a Central Circular Hole

The particular solution of the energy equation (2) can be found with the velocity field given by equation (11). The general solution for equation (2) can be written as

$$\theta = \left(\frac{a^4 c_1 c_2}{\mu\alpha}\right)\left[\frac{r^4}{64} - \frac{\eta^2}{4\ln\eta}\left\{\frac{r^4}{4}(\ln r - 1)\right\} - A_o\left\{\frac{r^2}{4} - \frac{r^2}{4\ln\eta}(\ln r - 1)\right\} - \sum_{j=1,2,3}^{\infty} A_j \left(\frac{r^{jN+2}}{4jN+4} + \frac{\eta^{2jN} r^{-jN+2}}{4jN-4}\right)\cos jN\phi + A'_o + B'_o \ln r + \sum_{j=1,2,3}^{\infty}\left(A'_j r^{jN} + B'_j r^{-jN}\right)\cos jN\phi\right] \quad (22)$$

At the inner boundary, $\theta = 0 (r = b)$, we get,

$$B'_o = -\frac{1}{\ln\eta}(A'_o + Z) \quad (23)$$

with the condition that,

$$Z = \frac{\eta^4}{64} - \frac{\eta^2}{4\ln\eta}\left[\frac{1}{4}\eta^2(\ln\eta - 1)\right] - A_o\left[\frac{1}{4}\eta^2 - \frac{\eta^2}{4\ln\eta}(\ln\eta - 1)\right] \quad (24)$$

and

$$B'_j = \frac{A_j \eta^{2(jN+1)}(jN)}{2\left[(jN)^2 - 1\right]} - A'_j \eta^{2jN} \quad (25)$$

On substitution of B_o' and B_j' into equation (22), the temperature difference θ becomes,

$$\theta = \left(\frac{a^4 c_1 c_2}{\mu\alpha}\right)\left[\frac{r^4}{64} - \frac{\eta^2}{4\ln\eta}\left\{\frac{r^2}{4}(\ln r - 1)\right\} - A_o\right.$$

$$\left\{\frac{r^2}{4} - \frac{r^2}{4\ln\eta}(\ln r - 1)\right\} - \sum_{j=1,2,3}^{\infty} A_j \left\{\frac{r^{jN+2}}{4jN+4}\right.$$

$$\left. + \frac{\eta^{2jN} r^{-jN+2}}{4jN-4} - \frac{\eta^{2jN+2} r^{-jN}(jN)}{2\left[(jN)^2 - 1\right]}\right\} \cos jN\phi$$

$$+ A_o'\left(1 - \frac{\ln r}{\ln\eta}\right) - \frac{Z \ln r}{\ln\eta} + \sum_{j=1,2,3}^{\infty} A_j'$$

$$\left.\left(r^{jN} - \eta^{2jN} r^{-jN}\right) \cos jN\phi\right] \qquad (26)$$

(c) Circular Ducts with a Central Regular Polygonal Hole

The particular solution of the energy equation (2) can be found by using equation (14). Therefore the general solution to equation (2) can be written as,

$$\theta = \left(\frac{c^4 c_1 c_2}{\mu\alpha}\right)\left[\frac{R^4}{64} - \frac{R^2}{16} - \frac{B_o R^2}{4}(\ln R - 1)\right.$$

$$\left. - \sum_{j=1,2,3}^{\infty} A_j \left(\frac{R^{jN+2}}{4jN+4} + \frac{R^{-jN+2}}{4jN-4}\right) \cos jN\phi\right.$$

$$+ A'_o + B'_o \ln R + \sum_{j=1,2,3}^{\infty} \left(A'_j R^{jN} + B'_j R^{-jN} \right) \cos jN\Phi \Big] \quad (27)$$

On satisfying the boundary condition $\theta = 0$ at the outer circular boundary and setting $r' = c$, we obtain,

$$A'_o = \frac{3}{64} - \frac{B_o}{4}$$

$$B'_j = \frac{A_j\,(jN)}{2\left[(jN)^2 - 1\right]} - A'_j \quad (28)$$

On substituting A'_o and B'_j in equation (27), the temperature difference θ can be expressed as

$$\theta = \left(\frac{c^4\, c_1 c_2}{\mu\alpha}\right) \left[\frac{R^4}{64} + \frac{3}{64} - \frac{R^2}{16} - \frac{B_o}{4}\left(R^2 \ln R - R^2 + 1\right)\right.$$

$$- \sum_{j=1,2,3}^{\infty} A_j \left\{ \frac{R^{jN+2}}{4jN + 4} + \frac{R^{-jN+2}}{4jN - 4} - \frac{R^{-jN}\,(jN)}{2\left[(jN)^2 - 1\right]} \right\}$$

$$\cdot \cos jN\Phi + B'_o \ln R + \sum_{j=1,2,3}^{\infty} A'_j \left(R^{jN} - R^{-jN}\right)$$

$$\left. \cdot \cos jN\Phi \right] \quad (29)$$

(d) Regular Polygonal Ducts

The solution to equation (2), for the regular polygonal ducts can be expressed as follows [4],

$$\theta' = \left(\frac{a^4 c_1 c_2}{\mu\alpha}\right)\left[\frac{r^4}{64} - \sum_{j=0,1,2}^{\infty} \frac{A_j\, r^{jN+2}}{4jN+4} \cos jN\phi + \sum_{j=0,1,2}^{\infty} A'_j\, r^{jN} \cos jN\phi\right] \tag{30}$$

2.4 Analysis by the Point Matching Method

(a) Evaluation of Unknown Coefficients

The boundary conditions for various noncircular ducts are usually difficult to satisfy exactly. However, a completely circular boundary provides no difficulty. The other boundary e.g. with circular ducts with diametrically opposite flat sides and regular polygonal ducts, still requires the evaluation of the unknown coefficients A_j, B_j, A'_j and B'_j in their respective equations.

In solving these equations one might apply Fourier series [3]. Unfortunately the nature of these equations precludes the use of Fourier analysis and therefore some other approach must be found for obtaining these coefficients.

The method used here is the point matching method which invokes an approximate solution by taking the sum of the first j terms of an infinite series. The require-ment that the boundary condition be satisfied at discrete

points on the remaining unsatisfied boundary leads to a system of nonhomogeneous, algebraic equations for the unknown coefficients A_j, B_j, A'_j and B'_j, which can be easily solved using a digital computer. To check the accuracy of the result the entire procedure may be repeated by taking more points at the boundary. With an increasing number of points at the boundary one can observe the results approaching a definite value but in practice there is a limitation imposed by the loss of significant figures which results when large numbers of linear algebraic equations are solved numerically. It is also worth noting that the values of these coefficients decrease rapidly with an increase in the number of points taken at the boundary.

(b) Unknown Coefficients for the Velocity Equation

An approximate solution for the velocity in circular ducts with diametrically opposite flat sides is obtained by applying equation (7) at a finite number of points along the boundary EFH (see Figure 1). The appropriate number of points on the straight part of the boundary EF and the circular part FH were obtained by arbitrarily choosing a number of points, on the circular part of the boundary and varying the number of equiangular spaced points

on the straight part of the boundary, or vice-versa. The numerical results for velocity and shear stress for ducts with different β's were evaluated for each such combination and were compared with the results of Carter and Oliphint [7] and Ōkubo [8]. The boundary errors were also calculated. Table 1 represents the best selection of points on both the circular and straight parts of the boundary. Because of the symmetry of the cross sections, equation (7) was applied to only one quarter of the cross-sectional area of the duct.

For regular polygonal ducts with a central circular hole, the boundary condition was satisfied exactly at the inner circular boundary. The boundary condition at the remaining regular polygonal boundary was satisfied at some equiangular points. For this shape, because of the N-fold symmetry, only one-2Nth of the outer boundary need be considered. Experience shows that a relatively greater boundary error exists around the corner point and that this can be reduced by selecting more points in the vicinity of the corner. To study the convergence of the solution from equation (11), 4-point, 6-point, 8-point and 10-point matchings were employed for various values of $\lambda = (a \cos \pi/N)/b$.

The unknown coefficients for equation (14), which represent the velocity distribution in circular ducts

with a central regular polygonal hole, can be evaluated by the point matching method at the inner regular polygonal boundary. The present form of equation (14) is based upon the condition that u = 0 at the outer circular boundary. Due to the symmetry of the cross section of the duct only one-2Nth of the inner boundary was considered. To check the accuracy of the results, 4-point and 6-point matchings were employed for various values of $\gamma = (\frac{c}{a \cos \pi/N})$. Since the computations are rather extensive, the numerical results for the unknown coefficients for the aforementioned cases are not listed in this thesis.

Reference [4] presents the numerical values of the unknown coefficients A_j for velocity equation (16) for regular polygonal ducts. These values were also evaluated with equiangular intervals along a one-2Nth portion of the boundary.

Table 1 Number of Points Matched on Two Boundaries in Circular Ducts with Diametrically Opposite Flat Sides

β°	No. of Points Matched on Straight Boundary	No. of Points Matched on Curved Boundary
5	4	69
10	7	61
20	13	49
30	15	41

β^0	No. of Points Matched on Straight Boundary	No. of Points Matched on Curved Boundary
40	17	35
50	15	31
60	17	27
70	21	23
80	30	12
85	30	6

(b) Unknown Coefficients for the Temperature Equation

Having found the coefficients A_j and B_j for their respective equations (7,11,14,16), one can proceed further to evaluate the second set of coefficients A'_j and B'_j from the temperature equations (21,26,29,30). For circular ducts with diametrically opposite flat sides, equation (21) can be satisfied at the same points as selected in evaluating the best possible values for the unknown coefficients of the velocity equation (7). For regular polygonal ducts with a central circular hole numerical results are obtained for the unknown coefficients for 4-point, 6-point, 8-point and 10-point matching for various values of $\lambda = (a \cos \pi/N)/b$, by satisfying the temperature equation (26) on the regular polygonal boundary of the duct. The boundary condition on the circular boundary is satisfied exactly.

For circular ducts with a concentric regular polygonal hole the unknown coefficients B_o' and A_j' for 4-point and 6-point matchings are obtained for various values of $\gamma = \frac{c}{a \cos \pi/N}$ by satisfying equation (29) at the same points on the inner regular polygonal boundary as for velocity equation (14). Due to the rather extensive numerical results, the values of the unknown coefficients are not presented in this thesis.

With the case (b) type boundary condition, for regular polygonal ducts, the heat flux $\left(\frac{d\theta'}{dn}\right)$ is constant on the boundary. This makes it more difficult to evaluate the unknown coefficients A_j' for temperature equation (30). The following procedure was utilized to evaluate the constant A_j' for different sets of point matchings on the regular polygonal boundary.

The temperature gradient normal to the duct boundary can be found from

$$\frac{\partial\theta'}{\partial n} = \cos\phi \frac{\partial\theta'}{\partial r} - (\sin\phi/r) \frac{\partial\theta'}{\partial\phi} \quad \text{for } (r/a) = (\cos \pi/N)/\cos\phi .$$

The normal temperature gradient is

$$\frac{\partial\theta'}{\partial n} = \left(\frac{a^3 c_1 c_2}{\mu\alpha}\right)\left[\frac{r^3}{16}\cos\phi - \sum_{j=0,1,2}^{\infty} \frac{A_j}{4jN+4} r^{jN+1} \left\{ 2\cos\phi \cos jN\phi + (jN)\cos(jN-1)\phi \right\} + \sum_{j=1,2,3}^{\infty} A_j' (jN) r^{jN-1} \cos(jN-1)\phi\right] \tag{31}$$

For fully developed flow with uniform heat input per unit length, the axial temperature gradient ($\partial t/\partial z$) is constant. Noting the following relationships [5],

$$\frac{\partial t}{\partial z} = \frac{Q}{\rho A u_m c_p} \quad , \quad \left(\frac{d\theta'}{dn}\right)_{wall} = \frac{Q}{kS} \quad \text{and}$$

$$u_m = - \frac{M c_1 a^2}{\mu} \quad ,$$

it can be shown that

$$\frac{c_1 c_2 a^3}{\mu\alpha} = - \frac{Qa}{AMk} \quad \text{and} \quad \left(\frac{d\theta'}{dn}\right)_{wall} \Big/ \left(\frac{c_1 c_2 a^3}{\mu\alpha}\right) = - \left(\frac{AM}{Sa}\right) \tag{32}$$

Substituting equations (32) into equation (31), the following dimensionless equation can be written

$$\sum_{j=1,2,3}^{\infty} A_j \, (jN) \, r^{jN-1} \cos (jN-1)\phi = - \left(\frac{AM}{Sa}\right) - \frac{r^3}{16} \cos \phi$$

$$+ \sum_{j=0,1,2}^{\infty} \frac{A_j}{4jN + 4} \cdot r^{jN+1} \left[2 \cos \phi \cos jN\phi \right.$$

$$\left. + (jN) \cos (jN-1)\phi \right] \tag{33}$$

In practice, of course, the finite series is truncated and the boundary condition is satisfied at a finite number of suitably selected points as discussed before. The convergence of the solution can be demonstrated by gradually increasing the number of unknown coefficients.

The leading term of the homogeneous solution for temperature, A'_o (= constant), may be found from the requirement that

$$\int\int_A \theta' r dr d\phi = 0 \tag{34}$$

Incidentally, the above method leads readily to the exact solutions for circular ducts. The results are,

$$u = \left(\frac{a^2 c_1}{4\mu}\right)\left[r^2 - 1\right] \tag{35}$$

$$\theta' = \left(\frac{a^4 c_1 c_2}{\mu\alpha}\right)\left(\frac{r^4}{64} - \frac{r^2}{16} + \frac{5}{192}\right) \tag{36}$$

The unknown coefficients A'_o for various regular polygons were obtained by numerical integration. For a square duct the result checks excellently with exact integration using Chebyshev polynomials for cos jNΦ in the integration of the following form,

$$\int_o^{\pi/N} (\cos jN\phi / \cos^{jN+i}\phi)\, d\phi \tag{37}$$

The solution to the above integral, for $i > 2$, is presented in the appendix whereas for $i = 2$, the above integral can be integrated exactly. The formula is

$$\int \cos^{j-1}\phi \cos(j+1)\phi\, d\phi = \frac{1}{j}\cos^j\phi \sin j\phi \tag{38}$$

Tables 2 and 3 show the numerical values of coefficients

Table 2 Coefficients A_j for Regular Polygonal Ducts $\left[a^{2-jN}\right]$

N	A_0	A_1	A_2	A_3
3	0.833333×10^{-1}	-0.166667	0.343873×10^{-15}	0.466933×10^{-15}
4	0.147396	-0.915117×10^{-1}	0.838082×10^{-2}	-0.271102×10^{-2}
5	0.182372	-0.564904×10^{-1}	0.801765×10^{-2}	-0.312033×10^{-2}
6	0.202566	-0.380356×10^{-1}	0.666125×10^{-2}	-0.273692×10^{-2}
7	0.215065	-0.272529×10^{-1}	0.541605×10^{-2}	-0.226553×10^{-2}
8	0.223272	-0.204455×10^{-1}	0.442328×10^{-2}	-0.185886×10^{-2}
9	0.228925	-0.158869×10^{-1}	0.365351×10^{-2}	-0.153408×10^{-2}
10	0.232974	-0.126907×10^{-1}	0.305603×10^{-2}	-0.127912×10^{-2}
20	0.245838	-0.296296×10^{-2}	0.854921×10^{-3}	-0.344408×10^{-3}

Table 3 Coefficients A'_j for Regular Polygonal Ducts $\left[a^{4-jN}\right]$

N	A'_0	A'_1	A'_2	A'_3
3	0.416312×10^{-2}	$-0.141921 \times 10^{-10}$	0.208333×10^{-2}	0.718499×10^{-10}
4	0.100517×10^{-1}	-0.203463×10^{-4}	0.616696×10^{-3}	-0.125392×10^{-3}
5	0.144642×10^{-1}	-0.297913×10^{-4}	0.243563×10^{-3}	-0.729675×10^{-4}
6	0.174854×10^{-1}	-0.306135×10^{-4}	0.117337×10^{-3}	-0.360874×10^{-4}
7	0.195707×10^{-1}	-0.288462×10^{-4}	0.646885×10^{-4}	-0.163910×10^{-4}
8	0.209334×10^{-1}	-0.264676×10^{-4}	0.392210×10^{-4}	-0.615695×10^{-5}
9	0.219456×10^{-1}	-0.240728×10^{-4}	0.254991×10^{-4}	-0.812108×10^{-6}
10	0.226908×10^{-1}	-0.218439×10^{-4}	0.174816×10^{-4}	0.197804×10^{-5}
20	0.251777×10^{-1}	-0.925630×10^{-5}	0.166311×10^{-5}	0.326394×10^{-5}

A_j and A'_j for regular polygonal ducts of N = 3 to 10 inclusive and N = 20. These coefficients were obtained using 4-point matching. The numerical results of computation for 4-point, 8-point and 12-point matching indicate that the leading coefficients, A_o and A'_o for velocity and temperature, respectively, change very little. This suggests that even the results from 4-point matching are quite close to the exact values. These leading coefficients, for equilateral triangular ducts, do not change at all from 3 to 12-point matching. This indicates that the 3-point matching solution for equilateral triangular ducts is very close to the exact solution.

2.5 Analysis by the Variational Method

The variational method, as a tool for the solution of laminar heat transfer problems with various boundary conditions, is discussed fully by Sparrow and Siegel [5]. In this thesis, only the circular ducts with diametrically opposite flat sides are subjected to this method in order to evaluate the heat transfer characteristics using case (a) type boundary conditions.

(a) Velocity Solution for Circular Ducts with Diametrically Opposite Flat Sides

In solving the velocity problem, we are able to benefit from the knowledge accumulated in the theory of elasticity. There is a direct connection between equation (1) and the differential equation for the stress function in the Saint-Venant torsion problem. Thus, from the results given by Timoshenko [6], one can write a first approximation to the laminar velocity distribution in the circular duct with diametrically opposite flat sides (see Figure 1) as follows,

$$u = \left(-\frac{c_1}{2\mu}\right)\left(x^2 - b^2\right)\left(x^2 + y^2 - a^2\right) A_o \tag{39}$$

where the boundary of the duct is given by the equations $x = \pm b$, $x^2 + y^2 = a^2$, and the function $(x^2 - b^2)$ $(x^2 + y^2 - a^2)$ assures that each of the two terms satisfies the condition of zero velocity at the boundary. The unknown constant A_o is to be determined by the well-known Ritz method for minimizing a variational integral. Equation (39) is introduced into the following variational integral [5].

$$I = \int_o^{+b} \int_o^{\sqrt{a^2-x^2}} \left[\left(u_x^2 + u_y^2\right) + \frac{2c_1 u}{\mu}\right] dx\, dy \tag{40}$$

(A) Velocity Equation for Complex Force with Dissipation Expressed Also Below -

The minimizing process is carried out by differentiating with respect to the unknown constant A_o and by setting the resulting equation to zero, obtaining for $\beta = 60°$,

$$A_o = \frac{1.01}{a^2} \tag{41}$$

To test the accuracy of this expression, a comparison with the velocity solution from equation (7) is made in Figure 15 for $\beta = 60°$. Profiles are plotted along the two coordinate axes. The agreement is generally very good, except for deviation near the corner and the centre.

With the thought of improving the approximation, the variational method was re-applied using an expression of slightly greater complexity than equation (39). The steps in the calculation will be shown in some detail, so that future calculations which proceed in the same manner may be described only in outline form. The profile chosen for the improved approximation is

$$u = \left(-\frac{c_1}{2\mu}\right)\left(x^2-b^2\right)\left(x^2+y^2-a^2\right)\left(A_o + A_1x^2 + A_2y^2\right) \tag{42}$$

The factors (x^2-b^2) and $(x^2+y^2-a^2)$ again assure that each of the three terms satisfies the condition of zero velocity at the boundary described by $x = \pm b$ and $y = \pm \sqrt{a^2-x^2}$. The constants A_o, A_1, and A_2 remain to be determined.

Substitution of equation (42) into the variational

integral (40), leads to a result which can be further differentiated with respect to each of the A's to give us the values of A_o, A_1 and A_2 which will minimize the value of I. This operation yields,

$$\frac{\partial I}{\partial A_o} = 0; \quad 0.204\, A_o a^2 + 0.00573\, A_1 a^4 + 0.03105\, A_2 a^4 + 0.206 = 0$$

$$\frac{\partial I}{\partial A_1} = 0; \quad 0.00573\, A_o a^2 + 0.008038\, A_1 a^4 - 0.004889\, A_2 a^4 + 0.00939 = 0$$

$$\frac{\partial I}{\partial A_2} = 0; \quad 0.03726\, A_o a^2 + 0.000724\, A_1 a^4 + 0.02004\, A_2 a^4 + 0.03932 = 0 \qquad (43)$$

Simultaneous solution of this group of linear algebraic equations provides the following values for $\beta = 60°$

$$A_o = \frac{0.97466}{a^2}, \quad A_1 = \frac{0.5527}{a^4}, \quad A_2 = \frac{0.13016}{a^4} \qquad (44)$$

After substituting into the equation (42),

$$u = \left(-\frac{c_1}{2\mu}\right)\left(x^2-b^2\right)\left(x^2+y^2-a^2\right)\left(\frac{0.97466}{a^2} + \frac{0.5527\, x^2}{a^4} + \frac{0.13016\, y^2}{a^4}\right) \qquad (45)$$

The mass flow rate evaluated from equation (45) and expressed in terms of K is compared with that obtained from point matching, in Figure 2. The agreement is generally very good. The exact solution is approached more and

more closely as more terms are added to the approximating polynomial for u. But this process of increasing the number of terms requires a tremendous amount of time to solve the variational integral (40) as the terms increase to their square power. The other improved expression for the velocity profile is as follows,

$$u = \left(-\frac{c_1}{2\mu}\right)\left(x^2-b^2\right)\left(x^2+y^2-a^2\right)\left(A_o+A_1x^2+A^2y^2+A_3x^2y^2+A_4x^4+A_5y^4\right) \qquad (46)$$

The results obtained for K from the above equation are compared in Figure 2 with the value of K obtained from both the three constants and point matching. The agreement is found to be very good.

(b) Temperature Solution for Circular Ducts with Diametrically Opposite Flat Sides

Consider the situation of uniform temperature around each cross section, with the heat transfer per unit length in the axial direction constant. Under these conditions, it is clear that the wall temperature will increase from section to section along the length of the passage.

For this situation one may use the variational method [5],

$$I = \int_o^b \int_o^{\sqrt{a^2-x^2}} \left(\theta_x^2 + \theta_y^2 + 2c_2\,\frac{\theta u}{\alpha}\right) dx\, dy \qquad (47)$$

where the boundary condition for the duct is that $\theta = 0$.

Table 4 Coefficients A_j for Circular Ducts with Diametrically Opposite Flat Sides-Variational Method

β^0	$A_0 \cdot a^2$	$A_1 \cdot a^4$	$A_2 \cdot a^4$	$A_3 \cdot a^6$	$A_4 \cdot a^6$	$A_5 \cdot a^6$
5	0.50538	0.22564	0.21397 x 10^{-2}	0.11914	0.15067 x 10	-0.49341 x 10^{-2}
10	0.51600	0.22769	0.27976 x 10^{-2}	0.14525	0.16010 x 10	-0.59354 x 10^{-2}
20	0.55787	0.24930	0.73911 x 10^{-2}	0.30133	0.19271 x 10	-0.11600 x 10^{-1}
30	0.62392	0.32394	0.24400 x 10^{-1}	0.72995	0.22579 x 10	-0.24715 x 10^{-1}
40	0.70962	0.44805	0.71912 x 10^{-1}	0.15651 x 10	0.24437 x 10	-0.40107 x 10^{-1}
50	0.80983	0.56756	0.17678	0.28637 x 10	0.25513 x 10	-0.32353 x 10^{-1}
60	0.91082	0.62272	0.37045	0.47234 x 10	0.26958 x 10	0.67895 x 10^{-1}
70	0.98568	0.52398	0.63934	0.75964 x 10	0.29655 x 10	0.50685
80	1.0211	0.08094	0.47216	0.12757 x 10^2	0.34725 x 10	0.24920 x 10
85	1.0509	-0.3078	-0.33026	0.16394 x 10^2	0.38020 x 10	0.49344 x 10

Table 5 Coefficients A'_j for Circular Ducts with Diametrically Opposite Flat Sides - Variational Method

β^0	$A'_0 \cdot a^2$	$A'_1 \cdot a^4$	$A'_2 \cdot a^4$	$A'_3 \cdot a^6$	$A'_4 \cdot a^6$	$A'_5 \cdot a^6$
5	0.4660 x 10^{-1}	0.1462 x 10^{-1}	-0.1489 x 10^{-1}	-0.1477 x 10	0.8328 x 10^{-1}	-0.5272 x 10^{-3}
10	0.4745 x 10^{-1}	0.1487 x 10^{-1}	-0.1509 x 10^{-1}	-0.1393 x 10	0.9406 x 10^{-1}	-0.6395 x 10^{-3}
20	0.5045 x 10^{-1}	0.1647 x 10^{-1}	-0.1562 x 10^{-1}	-0.7097 x 10^{-1}	0.1123 x 10^{-2}	-0.1289 x 10^{-2}
30	0.5370 x 10^{-1}	0.2026 x 10^{-1}	-0.1532 x 10^{-1}	0.1428 x 10^{-1}	0.1222 x 10^{-2}	-0.2900 x 10^{-2}
40	0.5470 x 10^{-1}	0.2308 x 10^{-1}	-0.1257 x 10^{-2}	0.5023 x 10^{-1}	0.1088 x 10^{-2}	-0.5369 x 10^{-2}
50	0.5083 x 10^{-1}	0.1857 x 10^{-1}	-0.6297 x 10^{-2}	0.8413 x 10^{-1}	0.7611 x 10^{-1}	-0.7144 x 10^{-2}
60	0.3990 x 10^{-1}	0.3475 x 10^{-1}	0.2945 x 10^{-1}	0.9350 x 10^{-1}	0.3228 x 10^{-1}	-0.8775 x 10^{-2}
70	0.2267 x 10^{-1}	-0.1902 x 10^{-2}	0.1103 x 10^{-1}	0.6415 x 10^{-1}	-0.1571 x 10^{-1}	-0.6662 x 10^{-2}
80	0.6264 x 10^{-2}	-0.3619 x 10^{-1}	0.6371 x 10^{-1}	-0.1641 x 10^{-1}	-0.5899 x 10^{-1}	0.3619 x 10^{-2}
85	0.1622 x 10^{-2}	-0.3762 x 10^{-1}	0.4506 x 10^{-1}	-0.7503 x 10^{-1}	-0.7490 x 10^{-1}	0.5397 x 10^{-2}

Since the temperature around the boundary is uniform, the temperature distribution across the section would be expected to have a shape not too different from that obtained for the velocity. Selecting a polynomial for θ having a form similar to equation (46), we have,

$$\theta = \left(\frac{c_1 c_2 a^2}{\mu\alpha}\right)\left(x^2-b^2\right)\left(x^2+y^2-a^2\right)\left(A_o'+A_1'x^2+A_2'y^2+A_3'x^2y^2 + A_4'x^4+A_5'y^4\right) \tag{48}$$

Introducing the above expression for θ into the variational integral (47) along with the velocity expression from equation (46) and carrying out the integration and minimizing the resultant expression by differentiating with respect to each unknown constant A_j', yields six linear algebraic equations which can be solved to obtain the unknowns A_o', A_1', A_2' ... A_5' for the temperature equation. The unknown coefficients A_o, A_1, A_2 ... A_5 for the velocity equation are presented in Table 4 and the corresponding coefficients A_o', A_1', A_2' ... A_5' for the temperature equation are presented in Table 5.

CHAPTER III

RESULTS OF ANALYSIS

3.1 Circular Ducts with Diametrically Opposite Flat Sides

(a) Flow Characteristics

The relationship between the rate of flow and the pressure drop, which in dimensionless terms may be presented as a relationship between the friction factor and Reynolds number, is of great engineering interest. The mass flow rate, w, through the cross section of the duct can be calculated from

$$w = 4\rho \int_0^b \int_0^{\sqrt{a^2-x^2}} u \, dx \, dy \qquad (49)$$

This can be further subdivided into two parts. By considering polar coordinates (r,ϕ) the mass flow rate, w, becomes,

$$w = 4\rho a^2 \left[\int_0^{\beta} \int_0^{\frac{\cos\beta}{\cos\phi}} urdrd\phi + \int_{\frac{\pi}{2}-\beta}^{\frac{\pi}{2}} \int_0^{1} urdrd\phi \right] \qquad (50)$$

or $w = \rho K \left(-\frac{1}{\mu}\frac{dp}{dz}\right) a^4$, where a is the radius of the circumscribing circle and K is a constant. The values of K for different opening angles β obtained from both the point

matching and variational methods are tabulated in Table 8, together with results for rectangular ducts [6] (exact) and work by Carter [7]. Figure 2 represents a comparison of the constant K evaluated by the variational method, using three and six coefficients, with values obtained by point matching.

The friction factor-Reynolds number relationship is defined by the following equation

$$f \cdot Re = \frac{1}{2}\left(-\frac{1}{\mu}\frac{dp}{dz}\right)\frac{D_e^2}{u_m} \tag{51}$$

where D_e is the equivalent hydraulic diameter and u_m ($= w/\rho A$) is the average velocity. The results obtained from equation (51) are given in Table 9 and are graphically represented in Figure 14.

For Newtonian fluids, the wall shear stress is defined by $\tau = \mu\left(\frac{\partial u}{\partial n}\right)$. The shear stress results (from equation (7)) for the straight boundary are given by the equation

$$\tau = (-ac_1)\left[\frac{r\cos\phi}{2} - \sum_{j=0,1,2}^{\infty} A_j\,(2j)\,r^{2j-1}\cos(2j-1)\phi\right] \tag{52}$$

and for the curved boundary by

$$\tau = (-ac_1)\left[+\frac{r}{2} - \sum_{j=0,1,2}^{\infty} A_j\,(2j)\,r^{2j-1}\cos 2j\phi\right] \tag{53}$$

Table 6 Maximum Velocity for Circular Ducts with Diametrically Opposite Flat Sides

$$\left[u/\left(-\frac{a^2 c_1}{\mu}\right)\right] \times 10$$

β^0	Variational Method	Point Matching	Exact	
0	-	-	2.5	(circle)
5	2.508	2.499	-	
10	2.502	2.494	-	
20	2.463	2.448	-	
30	2.340	2.318	-	
40	2.082	2.063	-	
50	1.673	1.659	-	
60	1.139	1.130	1.139	(rectangle)
70	0.577	0.572	0.573	(")
80	0.1540	0.1507	0.1508	(")
85	0.0399	0.0380	0.0380	(")

Table 7 Maximum Shear Stress for Circular Ducts with Diametrically Opposite Flat Sides

$$\left[\tau/\left(-ac_1\right)\right] \times 10$$

β^0	Variational Method		Point Matching		Results from * Literature	Exact	
0	-		-		-	5.0	(circle)
5	4.988	CUR**	5.259	VER***	-	-	
10	4.974	"	5.485	"	-	-	
20	4.889	"	5.808	"	-	-	
28.95	4.706	"	5.937	"	5.863	-	
30	4.677	"	5.941	"	-	-	
40	5.742	VER***	5.837	"	-	-	
41.40	5.788	"	5.802	"	5.888	-	
50	5.582	"	5.428	"	-	-	
51.30	5.492	"	5.348	"	5.346	-	
60	4.631	"	4.624	"	4.650	4.448	(rectangle)
70	3.285	"	3.362	"	-	3.226	(rectangle)
80	1.732	"	1.732	"	-	1.666	(rectangle)
85	0.9071	"	0.8667	"	-	0.7895	(rectangle)

* Carter's Results. ** On curved boundary. *** On straight boundary.

Table 6 Maximum Velocity for Circular Pools with Dimensionless Opening Size Ratio

$$\left[\ln\left(-\frac{\lambda_1}{\alpha}\right)\right] = \ln$$

α	Maximum Velocity	Opening Ratio	Beam
0	-	-	-
5	1,000	-	-
10	2,302	2,194	-
20	3,903	3,884	-
30	5,940	5,810	-
40	7,983	7,983	-
50	9,911	9,859	-
60	11,911	11,910	-
70	13,913	13,913	-
80	15,914	15,914	-
90	17,915	17,915	-

Table 7 Maximum Elastic Energy for Circular Pools with Dimensionless Impulse Plate Ratios

$$\left[\ln\left(-\frac{\lambda_1}{\alpha}\right)\right] = \ln$$

α	Maximum Velocity	Opening Ratio	Beam
0	-	-	-
5	1,000	-	-
10	2,302	-	-
20	3,903	-	-
30	5,940	-	-
40	7,983	-	-
50	9,911	-	-
60	11,911	-	-
70	13,913	-	-
80	15,914	-	-
90	17,915	-	-

Table 8 Constant K for Circular Ducts with Diametrically Opposite Flat Sides

β^0	Variational Method	Point Matching	Results from * Literature	Exact	
0	-	-	-	$\pi/0.8$	(circle)
5	3.838	3.925	-	-	
10	3.818	3.908	-	-	
20	3.699	3.773	-	-	
28.95	3.424	3.466	3.393	-	
30	3.377	3.416	-	-	
40	2.779	2.797	-	-	
41.40	2.675	2.691	2.69	-	
50	1.963	1.969	-	-	
51.30	1.848	1.854	1.833	-	
60	1.098	1.101	1.095	1.143	(rectangle)
70	0.4119	0.4125	-	0.4185	(")
80	0.06189	0.06194	-	0.06217	(")
85	0.00829	0.00834	-	0.00834	(")

Table 9 Values of f · Re for Circular Ducts with Diametrically Opposite Flat Sides

β^0	Variational Method	Point Matching	Exact	
0	-	-	16	(circle)
5	16.360	15.998	-	
10	16.365	15.980	-	
20	16.247	15.933	-	
30	16.047	15.862	-	
40	15.944	15.842	-	
50	16.043	15.986	-	
60	16.508	16.475	15.548	(rectangle)
70	17.623	17.603	16.987	(")
80	19.839	19.822	19.565	(")
85	21.699	21.551	21.486	(")

* Carter's Results [7].

The results from the variational method, for the curved and the straight boundaries, respectively, using equation (46) are,

$$\tau = c_1 \left(x^2+y^2\right)^{\frac{1}{2}} \left(x^2-b^2\right)\left(A_o+A_1x^2+A_2y^2+A_3x^2y^2+A_4x^4+A_5y^4\right) \qquad (54)$$

and

$$\tau = \left(bc_1\right)\left(b^2+y^2-a^2\right)\left(A_o+A_1b^2+A_2y^2+A_3b^2y^2+A_4b^4+A_5y^4\right) \qquad (55)$$

The shear stress distribution along both the straight and the curved parts of the boundary is presented graphically in Figures 3 and 4. Table 7 gives the values of local maximum shear stress on the boundary for different opening angles β. Figures 5, 6 and 7 represent the velocity distributions along three different directions using the point matching and variational methods as indicated on the respective figures. The velocity distribution calculated by the variational method is smaller in magnitude than the point matching values in the vicinity of the boundary and is therefore not presented in Figures 6 and 7.

(b) Heat Transfer Characteristics

With the velocity and temperature fields known, various heat transfer characteristics can be computed

The velocity from the variational method, for the curves and the ellipse boundaries, respectively, have values (48) and

$$v = \sqrt{\left(\frac{n^2\pi^2}{a^2}\right)\left(\frac{n^2\pi^2}{b^2}\right)\left(\frac{n^2\pi^2}{a^2}+\frac{n^2\pi^2}{b^2}\right)} \qquad (48)$$

and

$$v = \left(\frac{n^2\pi^2}{a^2}\right)\left(\frac{n^2\pi^2}{a^2}+\frac{n^2\pi^2}{b^2}\right) \qquad (49)$$

The above curves distribution along both the straight and curved plate of the boundary is presented graphically in Figures 1 and 2. Table 1 gives the values of latest maximum wave curves on the boundary for different central angles θ. Figures 3, 4 and 5 represent the velocity distributions along three different directions using the point matching and variational methods in between a the respective figures. The velocity distribution obtained by the variational method is smaller in magnitude than the point matching values in the vicinity of the boundary and is illustrated and discussed in Figures 4 and 5.

(b) Semi-Elliptic Cylinder

With the velocity and temperature fields known, various heat transfer characteristics can be computed

readily. The limiting Nusselt number (Nu) based on the bulk temperature can be evaluated [4] by,

$$(Nu)_{lim} = \frac{hD_e}{k} = -(D_e/S\alpha)(\partial t/\partial z)\left[\int\int_A ur'dr'd\phi\right]^2 / \left[\int\int_A u\theta\, r'dr'd\phi\right] \tag{56}$$

The temperature distribution using the point matching method in all three directions $\phi = 0$, $\phi = \beta$ and $\phi = \pi/2$ are plotted in Figures 8, 9 and 10 respectively. The results using the variational method are also plotted for comparison. Figure 16 shows a comparison of the temperature distributions along the same aforementioned three directions for a duct with an opening angle of $\beta = 60°$.

The use of the variational method again results in only minor differences (in the vicinity of the duct boundary) with the temperature obtained from point matching. The dimensionless temperature gradients normal to the straight part of the boundary obtained from equation (21) can be expressed as follows,

$$\left(\frac{\partial\theta}{\partial n}\right)\Big/\left(\frac{a^3 c_1 c_2}{\mu\alpha}\right) = -\frac{r^3 \cos\phi}{16} + \sum_{j=0,1,2}^{\infty} \frac{A_j r^{2j+1}}{8j+4} \left[2\cos\phi\cos 2j\phi + (2j)\cos(2j-1)\phi\right] - \sum_{j=0,1,2}^{\infty} A_j' (2j)\, r^{2j-1}\cos(2j-1)\phi\ . \tag{57}$$

and from equation (48) it can be expressed as,

$$\left(\frac{\partial\theta}{\partial n}\right)\Big/\left(\frac{2ba^2\, c_1 c_2}{\mu\alpha}\right) = \left(b^2-y^2+a^2\right)\left(A_o'+A_1'b^2+A_2'y^2+A_3'b^2y^2 + A_4'b^4+A_5'y^4\right) \tag{58}$$

The above results for various values of β are presented in Figures 11 and 12. The results from the variational method generally agree with those of the point matching method except for ducts with β less than 30 degrees. This is because the series is truncated to six coefficients in the case of the variational method. It is of some interest to note how the local temperature gradient at the curved boundary approaches that expected for a circular duct, as β approaches 5 degrees.

With the velocity field given in the form of equations (7) or (46) the limiting Nusselt number can be evaluated by using equation (56). Exact integration can be performed using equations (46) and (48) for velocity and temperature respectively, as found by the variational method; whereas in equations (7) and (21) for velocity and temperature as evaluated by the point matching method it was found that the integral $\int\int_A u\theta r'\, dr'd\phi$ is very difficult to evaluate exactly over the whole area. It can only be applied exactly over the area HOF (see Figure 1) so numerical integration has to be applied for the rest of

and then equation (60) is then be represented as,

$$\left(\frac{\partial \theta}{\partial n}\right)\left(\frac{\partial \theta_{new}^{k} - \theta_{old}^{k}}{\omega_k}\right) = \left(\theta_{i-1}^{k} - 2\theta_{i}^{k} + \theta_{i+1}^{k}\right) + \left(\theta_{j-1}^{k} - 2\theta_{j}^{k} + \theta_{j+1}^{k}\right) + \left(\theta_{k-1}^{k} - 2\theta_{k}^{k} + \theta_{k+1}^{k}\right)$$

(61)

The above results the various values of θ are determined in Figures 11 and 12. The results from the variational method numerically agrees with order of the finite method of method accept for small with I take time to compare. This is because due setting Ia iteration to six iterations in the case of the variational method. It is to some confirm in note how the local temperature gradient at the current boundary elsewhere that computed for a cylinder both at 5 seconds and 7 seconds.

With the velocity field given to the form of equation (7) or (76) the Jacobian matrix could be evaluated by using equation (64). Newton Iteration can be performed using equations (62) and (63) for velocity and temperature respectively, as found by the variational method. Equations in equations (7) and (61) the velocity and temperature are evaluated by the point matching method to note found that the integral $\int_{0}^{1}$ [illegible] to evaluate accurately over the whole area. It can only be applied exactly over the area for [illegible] it is important to determine how it be applied that that must be

the area, EFO (see Figure 1). For this purpose the area EFO of the cross section was divided into square grids with width (or base) and height no greater than $\left((1/50)\ a \cos \beta\right)$ for ducts with $\beta < 60°$, and with width (or base) and height no greater than $\left((1/100)\ a \cos \beta\right)$ for ducts with $\beta > 60°$.

It was found difficult to evaluate the limiting Nusselt number for ducts with $\beta = 85°$, using the point matching method, due to the fact that the boundary error involved was much higher than for the remaining cases where $\beta < 85°$. The resulting Nusselt numbers using the two methods are shown in Figure 13 and the results are listed in Table 11. The maximum temperature difference θ in the centre of the cross section is also tabulated for various β's in Table 10.

A comparison can be made between the results evaluated using the variational method and the results evaluated using the point matching method. In the case of the variational method, the functions $(x^2 - b^2)$ and $(x^2 + y^2 - a^2)$ actually satisfied the boundary condition $u = \theta = 0$. Whereas in point matching there always exists some boundary error which ultimately effects the flow and heat transfer results. The comparison of the results from one, three and six constant A's indicates that an increase in the number of constants using the variational method will

Table 10 Maximum Temperature for Circular Ducts with Diametrically Oppoiste Flat Sides

$$\left[\theta/\left(\frac{a^4 c_1 c_2}{\mu\alpha}\right)\right] \times 10^2$$

β^0	Variational Method	Point Matching	Exact	
0	-	-	4.6875	(circle)
5	4.625	4.685	-	
10	4.602	4.665	-	
20	4.455	4.496	-	
30	4.027	4.034	-	
40	3.210	3.205	-	
50	2.100	2.0955	-	
60	0.998	0.9968	1.013	(rectangle)
70	0.2652	0.2652	0.266	(")
80	0.01889	0.01892	0.0189	(")
85	0.00123	0.00121	0.0012	(")

Table 11 Limiting Nusselt numbers for Circular Ducts with Diametrically Opposite Flat Sides

β^0	Variational Method	Point Matching	Exact	
0	-	-	4.364	(circle)
5	4.354	4.363	-	
10	4.351	4.359	-	
20	4.326	4.335	-	
30	4.283	4.296	-	
40	4.254	4.269	-	
50	4.289	4.303	3.824	(rectangle)
60	4.475	4.483	4.123	(")
70	4.974	4.991	4.748	(")
80	6.062	6.020	5.981	(")
85	6.880	-	6.946	(")
90	-	-	8.24	(parallel plates)

not improve the results significantly, compared with the amount of work involved. Hence it appears that the results obtained with the six constants, using the variational method, are better than the results obtained by point matching.

3.2 Regular Polygonal Ducts with a Central Circular Hole

(a) Flow Characteristics

The mass flow rate through regular polygonal ducts with a central circular hole can be calculated from the following equation,

$$w = 2N\rho\, a^2 \int_0^{\beta} \int_{\frac{\cos\beta}{\lambda}}^{\frac{\cos\beta}{\cos\phi}} urdrd\phi \qquad (59)$$

The result of integration after substituting the velocity equation (11) is

$$w = (2N\rho)\left(-\frac{a^4}{\mu}\frac{dp}{dz}\right)\left[-\frac{\cos^4\beta}{16}\left(\frac{\sin\beta}{3\cos^3\beta} + \frac{2}{3}\frac{\sin\beta}{\cos\beta} - \frac{\beta}{\lambda^4}\right)\right.$$

$$- \frac{\eta^2\cos^2\beta}{4\ln\eta}\left\{\frac{\beta}{2\lambda^2}\ln\left(\frac{\cos\beta}{\lambda}\right) - \beta\left(\frac{1}{4\lambda^2} + \frac{1}{2}\right) + \frac{3}{4}\tan\beta\right\}$$

$$\left. + A_o\left\{\frac{\cos^2\beta}{2}\left(\tan\beta - \frac{\beta}{\lambda^2}\right) - \frac{\cos^2\beta}{\ln\eta}\left(\beta\left(\frac{1}{2} + \frac{1}{4\lambda^2}\right) - \frac{3}{4}\tan\beta\right.\right.\right.$$

$$- \frac{\beta}{2\lambda^2} \ln \left(\frac{\cos \beta}{\lambda}\right)\Bigg\} + \sum_{j=1,2,3}^{\infty} A_j \left\{ \frac{\cos \beta \sin(jN+1)\beta}{(jN+1)(jN+2)} \right.$$

$$- \frac{\cos^{jN+2} \beta \sin j\pi}{(jN)(jN+2)\ \lambda^{jN+2}} + \frac{\eta^{2jN} \sin(jN-1)\beta \cos \beta}{(jN-1)(jN-2)}$$

$$\left. - \frac{\eta^{2jN} \sin j\pi}{(jN)(jN-2)\ \cos^{jN-2} \beta\ \lambda^{-jN+2}} \right\} \Bigg] \qquad (60)$$

A constant K is defined in the following manner,

$$w = \rho K \left(- \frac{a^4}{\mu} \frac{dp}{dz}\right) \qquad (61)$$

The value of K for various values of λ were determined by matching 4, 6, 8 and 10 points at the boundary. On comparison with the results obtained by Gaydon and Nuttall [11] for the upper and lower bounds of K for square and hexagonal ducts with a central circular hole, it was found that the above calculated values lie in between the two bounds. The results of 10-point matching very closely approximate upper bound values thus demonstrating the accuracy of the results. The results for square and hexagonal ducts together with those for upper and lower bounds are tabulated in Tables 12 and 13. Also, tabulated in Table 14 for λ = 1.1, 20 and 1 to 10 inclusive are the results for the constant K from 10-point matching, for various regular polygonal ducts with a central circular

$$\frac{\partial}{\partial x_k} \ln \left\{ \cos \beta_i \right\} = \sum_{j=1}^{n} \left\{ \frac{\partial}{\partial x_k} \ln \left\{ \cos \beta_j \right\} \right\}$$

$$\frac{\partial}{\partial x_k} \ln \left\{ \cos \beta_i \right\} = \frac{\sin \beta_i}{\cos \beta_i} \frac{\partial \beta_i}{\partial x_k}$$

$$\frac{\partial \beta_i}{\partial x_k} = \frac{\cos \beta_i}{\sin \beta_i} \left\{ \frac{\partial}{\partial x_k} \ln \left\{ \cos \beta_i \right\} \right\}$$

A constant C is defined in the following manner,

$$C = \exp\left(-\frac{\alpha}{\beta} \frac{\partial \beta}{\partial \alpha}\right)$$

The value of C for various values of α were determined by evaluating β, β_1 and β_2 points on the boundary. A comparison with the results obtained by Pogorski and Carroll [11] for the upper and lower bounds of a disc sector and rectangular duct with a central circular insert, it was found that the above calculated values lie at between the two bounds. The results of Pogorski and Carroll closely approximate upper bound values for small values of the eccentricity of the annulus. The results are usually more accurate where the annulus more closely approximates a disc sector [8]. Also, since there is only a slight variation of β with α, β_1 and β_2 are the values of β for various values of α, a constant C

Table 12 Values of the Constant K for a Square Duct with a Central Circular Hole

λ	Lower Bound	4-point	6-point	8-point	10-point	Upper Bound
2	0.02355	0.02443	0.02432	0.02430	0.02430	0.02435
3	0.04322	0.04423	0.04410	0.04408	0.04408	0.04410
6	0.06992	0.07102	0.07089	0.07087	0.07086	0.07088
10	0.08320	0.08434	0.08421	0.08419	0.08419	0.08420
20	0.09538	0.09652	0.09638	0.09636	0.09635	0.09638
∞	0.13957	-	-	-	-	0.14060

Table 13 Values of the Constant K for a Hexagonal Duct with a Central Circular Hole

λ	Lower Bound	4-point	6-point	8-point	10-point	Upper Bound
2	0.03566	0.03709	0.03693	0.03690	0.03689	0.0369
3	0.07211	0.07399	0.07379	0.07375	0.07374	0.07374
6	0.12313	0.12544	0.12518	0.12513	0.12511	0.12516
10	0.14878	0.15124	0.15094	0.15089	0.15087	0.15092
20	0.17224	0.17480	0.17448	0.17442	0.1744	0.17443
10^3	0.21948	0.2223	0.2219	0.2218	0.2218	0.22185
10^6	0.23788	0.2408	0.2404	0.2403	0.2403	0.24036
∞	0.25622	-	-	-	-	0.25892

hole. The graphical results are shown in Figure 18.

The results for K using $\lambda = 1$ cannot be obtained from equation (11) since the solution is only good for a geometry with N-fold symmetry. However the case of $\lambda = 1.1$ was considered.

With the velocity distributions represented by equation (11) in the form of finite series, wall shear stress distributions can be computed readily. In the case of Newtonian fluids the shear stress is calculated from $\tau = \mu(\partial u/\partial n)$ and $\partial u/\partial n = (\sin \phi)/r \cdot \partial u/\partial \phi - \cos \phi \, \partial u/\partial r$, which in turn gives

$$\tau = \left(-ac_1 \right) \left[\left(\frac{1}{2} r - \frac{\eta^2}{4r \ln \eta} \right) \cos \phi + \frac{A_0 \cos \phi}{r \ln \eta} \right.$$

$$- \sum_{j=1,2,3}^{\infty} A_j (jN) \, r^{jN-1} \cos (jN-1)\phi - \sum_{j=1,2,3}^{\infty}$$

$$\left. \frac{A_j(jN) \, \eta^{2jN}}{r^{jN+1}} \cdot \cos (jN + 1)\phi \right] \qquad (62)$$

Shear stress distributions at the outer boundary for $N = 4$ are shown graphically in Figure 19. It was found that the shear stress distributions along the inner circular boundary are fairly uniform for most of the cases and are therefore not presented.

A friction factor-Reynolds number relationship can also be defined for regular polygonal ducts with a central

Table 14 Values of the Constant K for Regular Polygonal Ducts with a Central Circular Hole, 10-point Matching

$\left[K \times 10^2\right]$

λ	N = 3	N = 4	N = 5	N = 6	N = 7	N = 8	N = 9	N = 10	N = 20	N = ∞ (exact)
1.1	0.3138	0.2057	0.1334	0.0962	0.0764	0.0650	0.0580	0.0534	0.0409	-
2	1.187	2.430	3.204	3.690	4.005	4.219	4.370	4.479	4.833	4.947
3	1.842	4.408	6.203	7.374	8.151	8.683	9.060	9.336	10.241	10.542
4	2.238	5.653	8.120	9.750	10.838	11.586	12.738	12.506	13.789	14.220
5	2.500	6.488	9.413	11.356	12.657	13.553	14.190	14.657	16.200	16.720
6	2.686	7.086	10.341	12.511	13.966	14.969	15.683	16.206	17.939	18.523
7	2.827	7.538	11.043	13.384	14.955	16.040	16.813	17.379	19.254	19.888
8	2.937	7.893	11.594	14.070	15.734	16.882	17.701	18.301	20.288	20.961
9	3.026	8.180	12.040	14.626	16.368	17.564	18.419	19.047	21.126	21.830
10	3.100	8.419	12.411	15.087	16.886	18.130	19.016	19.666	21.821	22.551
20	3.478	9.635	14.302	17.440	19.554	21.016	22.059	22.825	25.364	26.227

Table 15 Values of f · Re, for Regular Polygonal Ducts with a Central Circular Hole, 10-point Matching

λ	N = 3	N = 4	N = 5	N = 6	N = 7	N = 8	N = 9	N = 10	N = 20	N = ∞ (exact)
1.1	10.797	14.304	16.980	19.135	20.681	21.730	22.428	22.891	23.906	-
2	19.728	22.026	22.793	23.119	23.289	23.394	23.466	23.519	23.716	23.813
3	19.821	21.669	22.329	22.658	22.858	22.992	23.088	23.160	23.427	23.546
4	19.512	21.255	21.934	22.295	22.521	22.675	22.786	22.869	23.172	23.308
5	19.215	20.922	21.624	22.009	22.252	22.418	22.537	22.627	22.952	23.088
6	18.965	20.654	21.374	21.775	22.028	22.203	22.329	22.423	22.761	22.901
7	18.755	20.433	21.165	21.577	21.839	22.020	22.149	22.246	22.594	22.737
8	18.578	20.247	20.987	21.407	21.675	21.860	21.993	22.092	22.446	22.591
9	18.425	20.086	20.833	21.259	21.532	21.719	21.854	21.955	22.314	22.461
10	18.293	19.945	20.698	21.128	21.404	21.593	21.730	21.832	22.195	22.343
20	17.514	19.104	19.866	20.310	20.596	20.793	20.935	21.041	21.417	21.567

Cuadro 10 - Distribución porcentual de la población económicamente activa de 10 años y más, según rama de actividad económica y sexo, por departamento, 1973

(Continúa)

Departamento y rama de actividad económica	Total	Hombres	Mujeres
Total	100.0	100.0	100.0
Agricultura, caza, silvicultura y pesca	57.1	57.1	57.1
Explotación de minas y canteras	0.1	0.1	0.1
Industrias manufactureras	11.2	11.2	11.2
Electricidad, gas y agua	0.1	0.1	0.1
Construcción	3.1	3.1	3.1
Comercio	10.1	10.1	10.1
Transporte, almacenamiento y comunicaciones	2.1	2.1	2.1
Servicios	15.2	15.2	15.2
Actividades no bien especificadas	1.0	1.0	1.0
Alta Verapaz	100.0	100.0	100.0
Agricultura, caza, silvicultura y pesca	71.1	71.1	71.1
Explotación de minas y canteras	0.1	0.1	0.1
Industrias manufactureras	7.1	7.1	7.1
Electricidad, gas y agua	0.1	0.1	0.1
Construcción	2.1	2.1	2.1
Comercio	6.1	6.1	6.1
Transporte, almacenamiento y comunicaciones	1.1	1.1	1.1
Servicios	11.2	11.2	11.2
Actividades no bien especificadas	1.0	1.0	1.0
Baja Verapaz	100.0	100.0	100.0
Agricultura, caza, silvicultura y pesca	61.1	61.1	61.1
Explotación de minas y canteras	0.1	0.1	0.1
Industrias manufactureras	9.1	9.1	9.1
Electricidad, gas y agua	0.1	0.1	0.1
Construcción	2.1	2.1	2.1
Comercio	8.1	8.1	8.1
Transporte, almacenamiento y comunicaciones	1.1	1.1	1.1
Servicios	13.2	13.2	13.2
Actividades no bien especificadas	1.0	1.0	1.0
El Progreso	100.0	100.0	100.0
Agricultura, caza, silvicultura y pesca	57.1	57.1	57.1
Explotación de minas y canteras	0.1	0.1	0.1
Industrias manufactureras	11.2	11.2	11.2
Electricidad, gas y agua	0.1	0.1	0.1
Construcción	3.1	3.1	3.1
Comercio	10.1	10.1	10.1
Transporte, almacenamiento y comunicaciones	2.1	2.1	2.1
Servicios	15.2	15.2	15.2
Actividades no bien especificadas	1.0	1.0	1.0
Chimaltenango	100.0	100.0	100.0
Agricultura, caza, silvicultura y pesca	57.1	57.1	57.1
Explotación de minas y canteras	0.1	0.1	0.1
Industrias manufactureras	11.2	11.2	11.2
Electricidad, gas y agua	0.1	0.1	0.1
Construcción	3.1	3.1	3.1
Comercio	10.1	10.1	10.1
Transporte, almacenamiento y comunicaciones	2.1	2.1	2.1
Servicios	15.2	15.2	15.2
Actividades no bien especificadas	1.0	1.0	1.0
Chiquimula	100.0	100.0	100.0
Agricultura, caza, silvicultura y pesca	57.1	57.1	57.1
Explotación de minas y canteras	0.1	0.1	0.1
Industrias manufactureras	11.2	11.2	11.2
Electricidad, gas y agua	0.1	0.1	0.1
Construcción	3.1	3.1	3.1
Comercio	10.1	10.1	10.1
Transporte, almacenamiento y comunicaciones	2.1	2.1	2.1
Servicios	15.2	15.2	15.2
Actividades no bien especificadas	1.0	1.0	1.0
Petén	100.0	100.0	100.0
Agricultura, caza, silvicultura y pesca	57.1	57.1	57.1
Explotación de minas y canteras	0.1	0.1	0.1
Industrias manufactureras	11.2	11.2	11.2
Electricidad, gas y agua	0.1	0.1	0.1
Construcción	3.1	3.1	3.1
Comercio	10.1	10.1	10.1
Transporte, almacenamiento y comunicaciones	2.1	2.1	2.1
Servicios	15.2	15.2	15.2
Actividades no bien especificadas	1.0	1.0	1.0
Quetzaltenango	100.0	100.0	100.0
Agricultura, caza, silvicultura y pesca	57.1	57.1	57.1
Explotación de minas y canteras	0.1	0.1	0.1
Industrias manufactureras	11.2	11.2	11.2
Electricidad, gas y agua	0.1	0.1	0.1
Construcción	3.1	3.1	3.1
Comercio	10.1	10.1	10.1
Transporte, almacenamiento y comunicaciones	2.1	2.1	2.1
Servicios	15.2	15.2	15.2
Actividades no bien especificadas	1.0	1.0	1.0
Quiché	100.0	100.0	100.0
Agricultura, caza, silvicultura y pesca	57.1	57.1	57.1
Explotación de minas y canteras	0.1	0.1	0.1
Industrias manufactureras	11.2	11.2	11.2
Electricidad, gas y agua	0.1	0.1	0.1
Construcción	3.1	3.1	3.1
Comercio	10.1	10.1	10.1
Transporte, almacenamiento y comunicaciones	2.1	2.1	2.1
Servicios	15.2	15.2	15.2
Actividades no bien especificadas	1.0	1.0	1.0
Retalhuleu	100.0	100.0	100.0
Agricultura, caza, silvicultura y pesca	57.1	57.1	57.1
Explotación de minas y canteras	0.1	0.1	0.1
Industrias manufactureras	11.2	11.2	11.2
Electricidad, gas y agua	0.1	0.1	0.1
Construcción	3.1	3.1	3.1
Comercio	10.1	10.1	10.1
Transporte, almacenamiento y comunicaciones	2.1	2.1	2.1
Servicios	15.2	15.2	15.2
Actividades no bien especificadas	1.0	1.0	1.0
Sacatepéquez	100.0	100.0	100.0
Agricultura, caza, silvicultura y pesca	57.1	57.1	57.1
Explotación de minas y canteras	0.1	0.1	0.1
Industrias manufactureras	11.2	11.2	11.2
Electricidad, gas y agua	0.1	0.1	0.1
Construcción	3.1	3.1	3.1
Comercio	10.1	10.1	10.1
Transporte, almacenamiento y comunicaciones	2.1	2.1	2.1
Servicios	15.2	15.2	15.2
Actividades no bien especificadas	1.0	1.0	1.0
San Marcos	100.0	100.0	100.0
Agricultura, caza, silvicultura y pesca	57.1	57.1	57.1
Explotación de minas y canteras	0.1	0.1	0.1
Industrias manufactureras	11.2	11.2	11.2
Electricidad, gas y agua	0.1	0.1	0.1
Construcción	3.1	3.1	3.1
Comercio	10.1	10.1	10.1
Transporte, almacenamiento y comunicaciones	2.1	2.1	2.1
Servicios	15.2	15.2	15.2
Actividades no bien especificadas	1.0	1.0	1.0
Santa Rosa	100.0	100.0	100.0
Agricultura, caza, silvicultura y pesca	57.1	57.1	57.1
Explotación de minas y canteras	0.1	0.1	0.1
Industrias manufactureras	11.2	11.2	11.2
Electricidad, gas y agua	0.1	0.1	0.1
Construcción	3.1	3.1	3.1
Comercio	10.1	10.1	10.1
Transporte, almacenamiento y comunicaciones	2.1	2.1	2.1
Servicios	15.2	15.2	15.2
Actividades no bien especificadas	1.0	1.0	1.0
Sololá	100.0	100.0	100.0
Agricultura, caza, silvicultura y pesca	57.1	57.1	57.1
Explotación de minas y canteras	0.1	0.1	0.1
Industrias manufactureras	11.2	11.2	11.2
Electricidad, gas y agua	0.1	0.1	0.1
Construcción	3.1	3.1	3.1
Comercio	10.1	10.1	10.1
Transporte, almacenamiento y comunicaciones	2.1	2.1	2.1
Servicios	15.2	15.2	15.2
Actividades no bien especificadas	1.0	1.0	1.0
Suchitepéquez	100.0	100.0	100.0
Agricultura, caza, silvicultura y pesca	57.1	57.1	57.1
Explotación de minas y canteras	0.1	0.1	0.1
Industrias manufactureras	11.2	11.2	11.2
Electricidad, gas y agua	0.1	0.1	0.1
Construcción	3.1	3.1	3.1
Comercio	10.1	10.1	10.1
Transporte, almacenamiento y comunicaciones	2.1	2.1	2.1
Servicios	15.2	15.2	15.2
Actividades no bien especificadas	1.0	1.0	1.0
Totonicapán	100.0	100.0	100.0
Agricultura, caza, silvicultura y pesca	57.1	57.1	57.1
Explotación de minas y canteras	0.1	0.1	0.1
Industrias manufactureras	11.2	11.2	11.2
Electricidad, gas y agua	0.1	0.1	0.1
Construcción	3.1	3.1	3.1
Comercio	10.1	10.1	10.1
Transporte, almacenamiento y comunicaciones	2.1	2.1	2.1
Servicios	15.2	15.2	15.2
Actividades no bien especificadas	1.0	1.0	1.0
Zacapa	100.0	100.0	100.0
Agricultura, caza, silvicultura y pesca	57.1	57.1	57.1
Explotación de minas y canteras	0.1	0.1	0.1
Industrias manufactureras	11.2	11.2	11.2
Electricidad, gas y agua	0.1	0.1	0.1
Construcción	3.1	3.1	3.1
Comercio	10.1	10.1	10.1
Transporte, almacenamiento y comunicaciones	2.1	2.1	2.1
Servicios	15.2	15.2	15.2
Actividades no bien especificadas	1.0	1.0	1.0

circular hole by equation (51). The friction factor-Reynolds number, f · Re, is consistent with that for a simply connected duct; however it cannot be related to the wall shear stresses in a multiply connected duct. It is considered to be more useful if the friction factor for each closed independent boundary is defined by finding the location of maximum velocity from equation (11) for a given angular position. But this location cannot be found precisely and hence the job of obtaining a friction factor for each boundary is a difficult one and is not included in this study. The numerical values of f · Re from 10-point matching are listed in Table 15 for various cases. These graphical results are also shown in Figure 20.

(b) Heat Transfer Characteristics

The temperature gradient at the wall is of general practical interest. By considering the case (a) type boundary condition, the temperature gradient along the inner and outer boundary can be evaluated easily. The temperature gradient normal to the regular polygonal boundary can be expressed by using equation (26) as

$$\left(\frac{\partial\theta}{\partial n}\right)\Big/\left(\frac{a^3 c_1 c_2}{\mu\alpha}\right) = -\frac{1}{16} r^3 \cos\phi + \frac{\eta^2 r \cos\phi}{8 \ln\eta} (\ln r - 1)$$

$$\left(\frac{\partial \ln(\quad)}{\partial x}\right)$$

$$+ \frac{\eta^2 r \cos\phi}{16 \ln \eta} + A_0 \cos\phi \left[\frac{1}{2} r - \frac{r}{2 \ln \eta} (\ln r - 1) - \frac{r}{4 \ln \eta}\right] + \cos\phi \left[\frac{(Z)_{r=b}}{r \ln \eta} + \frac{A_0'}{r \ln \eta}\right] + \sum_{j=1,2,3}^{\infty} \frac{A_j r^{jN+1}}{4(jN+1)} \left[2 \cos\phi \cos jN\phi + (jN) \cos (jN-1)\phi\right]$$

$$+ \sum_{j=1,2,3}^{\infty} \frac{A_j \eta^{2jN} r^{-jN+1}}{4(jN-1)} \left[2 \cos\phi \cos jN\phi - (jN) \cos (jN+1)\phi\right] + \sum_{j=1,2,3}^{\infty} \frac{A_j (jN)^2 \eta^{2(jN+1)} r^{-(jN+1)}}{2\left[(jN)^2 - 1\right]}$$

$$\cos (jN+1)\phi - \sum_{j=1,2,3}^{\infty} A_j' (jN) r^{jN-1} \cos (jN-1)\phi - \sum_{j=1,2,3}^{\infty} A_j' (jN) \eta^{2jN} r^{-(jN+1)} \cos (jN+1)\phi \qquad (63)$$

The temperature gradient for various values of λ along the regular polygonal boundary are presented in Figure 21 for the case N = 4 only. The computed value for the temperature gradients at the circular boundary are found to be fairly uniform and are therefore not presented. For triangle and square the temperature gradient at the corner is zero. It is noted that the convergence of the heat transfer characteristics to the simply connected case ($\lambda = \infty$) is very slow.

Nusselt numbers for regular polygonal ducts with

a central circular hole can be evaluated by using the velocity and temperature equations (11) and (26).

The temperature and velocity distributions are presented graphically in Figures 22 to 29 inclusive by using 10-point matching along the two directions $\Phi = \pi/N$, and $\Phi = 0$ for square and 20-sided ducts.

Comparison is also made with the results from regular polygonal ducts with no central hole. The results from concentric annuli are presented in Figure 23. The velocity distribution along $\Phi = \pi/20$ for $N = 20$ and $\lambda = 2$ is compared with the corresponding one for an annulus in Figure 30. The agreement is quite good up to $(r' - b)/(a - b) = 0.35$; but from there on the velocity for the 20-sided regular polygon is slightly lower than for the annulus. This observation could have been anticipated, since one would not expect any effect from an outside regular polygonal boundary in the vicinity of an inner circular boundary for a reasonably large value of λ.

A heat transfer coefficient can be defined at each boundary by using the fluid bulk temperature of the flowing fluid between the respective boundary and a closed line of minimum temperature. By the trial and error method the location of the minimum temperature can be found from $\partial\theta/\partial r' = 0$ using equation (26) for a particular angular position. Numerical integration will

be required to evaluate the Nusselt number for each independent boundary.

An overall average coefficient may be defined in terms of the uniform wall temperature and the bulk fluid temperature for the total heat transfer rate from both walls. The Nusselt number can be evaluated in a manner similar to that used for the simply connected ducts [4], using the thermal boundary conditions presently under consideration. Therefore equation (56) is applied in this case to evaluate the limiting Nusselt number for various values of λ. The integral $\int\int_A ur'dr'd\phi$ was solved analytically, whereas the solution for the integral $\int\int_A u\theta r'dr'd\phi$ was found by numerical means. The results obtained from 8-point matching together with results for an annulus [10] are plotted in Figure 31 and the results obtained by the point matching method are tabulated in Table 16. Figure 31 reveals that the Nusselt number curve approaches that obtained by Dwyer [10] for higher values of λ. It is to be expected that the Nusselt number for the 20-sided regular polygonal duct with a central circular hole and $\lambda = \infty$ would be comparable to the Nusselt number of 4.36 obtained for a circular duct by classical analytical methods. Nusselt numbers are also calculated for N = 4 for very large values of λ. For $\lambda = 1000$ and $\lambda = 10^6$, the Nusselt numbers are

Table 16 Nusselt Number Results for Regular Polygonal Ducts with a Central Circular Hole

N	$\lambda = 2$	$\lambda = 3$	$\lambda = 4$	$\lambda = 5$	$\lambda = 6$	$\lambda = 7$	$\lambda = 8$	$\lambda = 9$	$\lambda = 10$	$\lambda = 20$
3	4.466	5.511	5.655	5.626	5.560	5.486	5.417	5.354	5.296	4.938
4	5.317	6.351	6.474	6.438	6.370	6.297	6.228	6.163	6.104	5.723
5	5.488	6.593	6.760	6.755	6.705	6.644	6.582	6.523	6.467	6.094
6	5.498	6.697	6.906	6.924	6.887	6.834	6.778	6.722	6.670	6.303
7	5.480	6.757	6.995	7.027	6.998	6.951	6.898	6.845	6.794	6.431
8	5.465	6.801	7.060	7.102	7.080	7.037	6.986	6.935	6.885	6.525
9	5.453	6.831	7.104	7.154	7.136	7.094	7.045	6.995	6.946	6.588
10	5.444	6.854	7.138	7.192	7.177	7.138	7.090	7.040	6.992	6.635
20	5.419	6.933	7.251	7.321	7.314	7.280	7.236	7.189	7.142	6.788

found to be 4.556 and 4.056 respectively. The Nusselt number for N = 4 with no inside circular hole is 3.608, which indicates that the above convergence is very slow.

3.3 Circular Ducts with a Central Regular Polygonal Hole

(a) Flow Characteristics

The mass flow rate can be calculated by using an equation similar to equation (59), which is

$$w = 2N\rho\, c^2 \int_0^{\beta} \int_{\frac{1}{\gamma \cos \Phi}}^{1} uR\, dR\, d\Phi \qquad (64)$$

After substitution of u from equation (14) and on integrating, we get

$$w = (2N\rho)\left(-\frac{c^4}{\mu}\frac{dp}{dz}\right)\left[\frac{1}{16\gamma^4}\left(\frac{\sin\beta}{3\cos^3\beta}+\frac{2}{3}\tan\beta\right)+\frac{\beta}{16}\right.$$

$$-\frac{\sin\beta}{8\gamma^2\cos\beta}+B_0\left\{-\frac{\beta}{4}+\frac{1}{2\gamma^2}\left(\tan\beta\ \ln(\cos\beta)\right.\right.$$

$$\left.\left.+\ln\gamma\tan\beta+\frac{3}{2}\tan\beta-\beta\right)\right\}+\sum_{j=1,2,3}^{\infty}\frac{A_j}{(Nj+2)}$$

$$\left\{\frac{\sin Nj\beta}{(Nj)}-\frac{\sin(Nj+1)\beta}{\gamma^{Nj+2}(Nj+1)\cos^{Nj+1}\beta}\right\}-\sum_{j=1,2,3}^{\infty}$$

$$\left.\frac{A_j}{(-Nj+2)}\left\{\frac{\sin Nj\beta}{(Nj)}-\frac{1}{\gamma^{-Nj+2}}\frac{\cos^{Nj-1}\beta\sin(Nj-1)\beta}{(Nj-1)}\right\}\right] \qquad (65)$$

Defining a constant L in the same manner as in equation (61) we get,

$$w = \rho L \left(- \frac{c^4}{\mu} \frac{dp}{dz} \right) \tag{66}$$

The results obtained for L from the above equation for N = 20 with various $\gamma = \frac{c}{a \cos \pi/N}$, closely approximate those obtained for concentric cylinders. This serves to demonstrate the accuracy of the results. The numerical results for constant L with various values of γ using 4-point and 6-point matchings for various circular ducts with a central regular polygonal hole are given in Tables 17 and 18; the graphical results for 6-point matching are plotted in Figure 33.

The shear stress at the inner regular polygonal boundary can be represented using equation (14),

$$\tau = \left(- c \frac{dp}{dz} \right) \left[\frac{B_0 \cos \phi}{R} - \frac{R \cos \phi}{2} + \sum_{j=1,2,3}^{\infty} A_j (jN) R^{jN-1} \right.$$
$$\left. \cos (jN - 1)\phi + \sum_{j=1,2,3}^{\infty} A_j (jN) R^{-jN-1} \cos (jN+1)\phi \right] \tag{67}$$

Graphical results for the shear stress distribution at the inner boundary are shown for $\gamma = 2$ only, in Figure 34. The graphs show a large fluctuation which might be suspected due to the large boundary error at the inner regular polygonal boundary for lower values of N. With the

Obtaining a solution to the flow under the influence of the equation (B1) we get,

$$u = -\rho_0 \left(\frac{r}{\mu}\right) \frac{\partial p}{\partial z} \qquad (B2)$$

The velocity obtained for a flow via power series solution for $N = 20$ with various $\gamma = \frac{\beta}{\mu}$ closely approximates those obtained for concentric cylinders. This serves to demonstrate the accuracy of the results. The numerical results for comparing a Bird Metzner medium at γ equal to unity and n-octane materials for which a constant tensile strength have been given in Tables II and III. The graphical results for n-octane according are plotted in figure 1).

The shear stress of the power series polynomial [illegible] can be represented using equation (A2).

$$\tau = \left(-\frac{dp}{dz}\right)\left[\frac{\beta r \cos\theta}{2}\right] \cdot \sum_{j=1}^{\infty} \frac{\gamma^{2j-1}}{2j-1} \cdot \sum_{k=1}^{j} A_k \cos\theta^{2k-1}$$

$$\cos(2n-1)\theta = \sum_{k=1}^{n} K_k \cos\theta^{2k-1} \cos^{(n-1)}\theta \qquad (B3)$$

Graphical results for the flow curves illustrating at the lower boundary are shown for $\gamma = 1$ unity in figure 2). The results show a large discrepancy using models by comparing due to the large curvature which at the lower wall [illegible] comments for lower values of γ. This is

Table 17 Values of the Constant L for Circular Ducts with a Central Regular Polygonal Hole, 4-point Matching

$\left[L \times 10 \right]$

γ	N = 3	N = 4	N = 5	N = 6	N = 7	N = 8	N = 9	N = 10	N = 20	N = ∞ (exact)
2	0.2404	0.3102	0.3749	0.4131	0.4361	0.4508	0.4606	0.4675	0.4884	0.495
3	0.577	0.814	0.915	0.964	0.991	1.007	1.018	1.026	1.048	1.054
4	0.937	1.194	1.294	1.340	1.365	1.380	1.390	1.397	1.416	1.422
5	1.174	1.465	1.558	1.599	1.622	1.635	1.644	1.649	1.671	1.672
6	1.388	1.665	1.750	1.787	1.807	1.819	1.827	1.832	1.854	1.854
7	1.558	1.818	1.896	1.930	1.948	1.959	1.966	1.971	1.988	1.989
8	1.697	1.939	2.011	2.042	2.059	2.069	2.075	2.080	2.096	2.096
9	1.810	2.038	2.104	2.133	2.149	2.158	2.164	2.168	2.183	2.183

| | | |

Table 18 Values of the Constant L for Circular Ducts with a Central Regular Polygonal Hole, 6-point Matching

$\left[L \times 10\right]$

γ	N = 3	N = 4	N = 5	N = 6	N = 7	N = 8	N = 9	N = 10	N = 20	N = ∞ (exact)
2	0.2433	0.3194	0.3812	0.4174	0.4391	0.4530	0.4623	0.4688	0.4887	0.495
3	0.615	0.830	0.924	0.969	0.995	1.010	1.020	1.027	1.049	1.054
4	0.951	1.210	1.303	1.345	1.368	1.382	1.392	1.398	1.420	1.422
5	1.220	1.480	1.565	1.604	1.625	1.637	1.645	1.651	1.674	1.072
6	1.432	1.679	1.757	1.791	1.810	1.821	1.828	1.833	1.854	1.852
7	1.599	1.831	1.902	1.934	1.951	1.961	1.967	1.974	1.991	1.989
8	1.734	1.951	2.017	2.046	2.061	2.071	2.079	2.083	2.098	2.096
9	1.845	2.049	2.109	2.136	2.151	2.159	2.169	2.171	2.185	2.183

Table 19 Values of f · Re for Circular Ducts with a Central Regular Polygonal Hole, 6-point Matching

γ	N = 3	N = 4	N = 5	N = 6	N = 7	N = 8	N = 9	N = 10	N = 20	N = ∞ (exact)
2	15.609	23.268	23.776	23.770	23.745	23.733	23.730	23.732	23.775	23.813
3	23.072	23.612	23.458	23.418	23.417	23.427	23.439	23.452	23.485	23.546
4	23.847	23.298	23.179	23.166	23.177	23.193	23.207	23.220	23.217	23.308
5	23.675	23.051	22.967	22.966	22.980	22.995	23.008	23.019	22.973	23.088
6	23.419	22.857	22.794	22.797	22.810	22.823	22.835	22.857	22.804	22.901
7	23.191	22.699	22.646	22.649	22.660	22.671	22.681	22.662	22.652	22.737
8	23.000	22.563	22.516	22.517	22.526	22.536	22.518	22.527	22.516	22.591
9	22.840	22.444	22.400	22.399	22.406	22.414	22.397	22.404	22.392	22.461

increase in the number of points at the boundary, the unknown coefficients for the velocity equation start diverging in absolute value which resulted in tremendously high values for the velocity distribution. The reason is unknown to the author.

It was found from equation (67) that the shear stress distributions along the outer boundary are fairly uniform for most of the cases and therefore not graphically presented.

Equation (51) was used to define the friction factor-Reynolds number relationship. In this case too it was physically more meaningful to define one friction factor for each independent boundary. But with the velocity field given by equation (14) it was found very difficult to establish a position for the maximum velocity for a particular angular position. Therefore no study was done for this type of friction factor. The numerical results for the friction factor-Reynolds number were computed for various circular ducts with a central regular polygonal hole for $\gamma = 1$ to 9 inclusive and are listed in Table 19, for 6-point matching. The graphical results are also presented in Figure 35.

(b) Heat Transfer Characteristics

The temperature gradient normal to the inner boundary,

increase in the number of points by one boundary, the
boundary quantities for the velocity equation start
diverging in another point called a transitional
high values for the velocity distribution. The reason
is unknown to the author.

It has found from equation (37) that the mean
stress distributions along the outer boundary are fairly
uniform for most of the cases and therefore are quanti-
tatively reasonable.

Equation (31) was used to solve the friction
factor Reynolds number relationship. It took more time
to get physically more meaningful to define the friction
factor for each independent condition. So as not any
velocity field given by equation (31) is very difficult
to encounter a position for the pressure satis-
fying for a particular velocity position. Therefore
we already see when the main core of mixture begins. The
numerical results for five position parameters are
real numbers presented by $\alpha_1 = 1.0$ & positive
and are listed in Table 1, for clear reading. The
physical results are also presented in Figure 2.

(b) Shear Stress Distribution

The temperature profile used in the heat transfer

with the thermal boundary condition of circumferentially uniform wall temperature at a given axial position and axially uniform but unequal heat fluxes from the inner and outer walls, can be obtained by using equation (29),

$$\left(\frac{\partial\theta}{\partial n}\right)\Big/\left(\frac{c^3\, c_1 c_2}{\mu\alpha}\right) = \cos\phi\left[\frac{R}{8} + \frac{B_0}{2}\, R(\ln R - 1) + \frac{B_0 R}{4}\right.$$

$$\left. - \frac{R^3}{16} - \frac{B_0'}{R}\right] + \sum_{j=1,2,3}^{\infty} \frac{A_j\, R^{jN+1}}{4jN + 4}\left[2\cos\phi\cos jN\phi\right.$$

$$\left. + (jN)\cos(jN-1)\phi\right] + \sum_{j=1,2,3}^{\infty} \frac{A_j\, R^{-jN+1}}{4jN - 4}$$

$$\left[2\cos\phi\cos jN\phi - (jN)\cos(jN+1)\phi\right] + \sum_{j=1,2,3}^{\infty}$$

$$\frac{A_j\, R^{-jN-1}\,(jN)^2}{2\left[(jN)^2 - 1\right]}\cos(jN+1)\phi - \sum_{j=1,2,3}^{\infty} A_j'\, R^{jN-1}$$

$$(jN)\cos(jN-1)\phi - \sum_{j=1,2,3}^{\infty} A_j'\, R^{-jN-1}\,(jN)\cos(jN+1)\phi \qquad (68)$$

The results from the above equation for the case of $\gamma = 2$ only, for various regular polygonal boundaries, are presented in Figure 36. The large fluctuation in the temperature gradient was expected due to a limited number of points matched at the inner regular polygonal boundary and also the effects from the large errors in velocity.

It was found that the temperature gradient for the circular boundary was fairly uniform for most of the cases. The velocity and temperature profiles along the two directions $\Phi = 0$ and $\Phi = \pi/N$ are shown in Figures 37 to 40 inclusive for N = 6 and 9 for various values of γ. Figures 41 and 42 represent the velocity distribution along $\Phi = 0$ and $\Phi = \pi/10$, respectively (for N = 10 only) for various values of γ. A comparison is also made with the results obtained for the circular cross-section. The temperature and velocity profiles in the other directions are bounded by the two profiles for $\Phi = 0$ and $\Phi = \pi/N$. The velocity distribution along $\Phi = \pi/20$ for N = 20 and $\gamma = 2$ is compared with the corresponding one for an annulus in Figure 43.

With the case (a) type boundary condition and an average heat transfer coefficient, which could be defined at each boundary by using the bulk fluid temperature of the fluid flowing between the respective boundary and a closed line of minimum temperature, the Nusselt number can be expressed by equation (56). It could be expected that numerical integration would be required for the calculation of the Nusselt number for each independent boundary.

The Nusselt number results which were computed by numerical integration for $\gamma = 2$ to 9 inclusive and for N = 4 to 9 inclusive are tabulated in Table 20 and some

Table 20 Nusselt Number Results for Circular Ducts with a Central Regular Polygonal Hole

γ	$\gamma = 2$	$\gamma = 3$	$\gamma = 4$	$\gamma = 5$	$\gamma = 6$	$\gamma = 7$	$\gamma = 8$	$\gamma = 9$
4	-	7.738	7.693	7.616	7.538	7.467	7.398	7.337
5	7.718	7.814	7.723	7.626	7.537	7.457	7.385	7.321
6	7.910	7.858	7.744	7.638	7.543	7.459	7.385	7.318
7	7.989	7.884	7.759	7.648	7.550	7.464	7.388	7.320
8	8.027	7.898	7.769	7.654	7.555	7.467	7.390	6.953
9	8.049	7.909	7.776	7.660	7.558	7.057	7.395	7.325

Table 20. Diagonal elements of the Clebsch-Gordan matrix

Coupling of identical spin-½ particles

$j_1 = j_2$	$J = 0$	$J = 1$	$J = 2$	$J = 3$	$J = 4$	$J = 5$	$J = 6$	$J = 7$
½	0.707	0.707						
1	0.577	0.577	0.577					
3/2	0.500	0.500	0.500	0.500				
2	0.447	0.447	0.447	0.447	0.447			
5/2	0.408	0.408	0.408	0.408	0.408	0.408		
3	0.378	0.378	0.378	0.378	0.378	0.378	0.378	
7/2	0.354	0.354	0.354	0.354	0.354	0.354	0.354	0.354

plotted in Figure 44. These results seem to be in good agreement with those of Dwyer [10] for annuli with large values of γ and N.

3.4 Regular Polygonal Ducts

(a) Flow Characteristics

The numerical results for fully developed laminar flow in regular polygonal ducts have been discussed by Cheng [4] using a series solution, so these will not be discussed here.

(b) Heat Transfer Characteristics

Using the temperature distribution defined by equation (16), the Nusselt number, average wall temperature, and bulk fluid temperature may be computed readily, and are defined as follows,

$$Nu = \frac{hD_e}{k}, \quad h = \frac{Q}{S(\theta_{wm} - \theta_b)} \tag{69}$$

$$\theta_b = \int\int_A u\theta' dA \Big/ \int\int_A u dA \tag{70}$$

$$\theta_{wm} = \int_0^{\pi/N} \theta_w \cdot d(a \cos \pi/N \tan \Phi)/a \sin \pi/N \tag{71}$$

The calculated results using 12-point matching for the average wall temperature, bulk fluid temperature, and normal temperature gradient at the wall are listed in Table 21 for various polygons. To check the convergence of the solution, 4-point, 8-point and 12-point matchings were employed for all computations involving the above heat transfer characteristics. The numerical results show that the differences among the above three kinds of matching are negligible; for example, the temperature gradients at the wall generally agree to four significant figures. This indicates that the boundary errors are very small and that the solution converges very quickly. The results for the Nusselt number and average wall temperature are tabulated in Tables 22 and 23 respectively. The numerical values for fluid bulk temperature show nearly the same trend as the values for average wall temperatures, as shown in Table 23. Temperature distributions from 12-point matching in two directions $\Phi = \pi/N$ and $\Phi = 0$ are plotted in Figures 47 and 48, respectively, for several representative polygons.

The question arises as to the accuracy of the Nusselt numbers calculated for different regular polygonal ducts. A comparison can be made between the results calculated by point matching and the results available in the literature. For instance the Nusselt number obtained for a

Table 21 Heat Transfer Results for Regular Polygonal Ducts with Uniform Peripheral Heat Flux

N	Average Wall Temp. $\left[\theta_{wm}/\frac{(-c_1c_2a^4)}{\mu\alpha}\right]\cdot 10^{+2}$	Bulk Temp. $\left[\theta_b/\frac{(-c_1c_2a^4)}{\mu\alpha}\right]\cdot 10^{+3}$	Temp. Gradient $\left[\left(\frac{\partial\theta'}{\partial n}\right)_w/\frac{(-c_1c_2a^3}{\mu\alpha}\right]\cdot 10^{+2}$
3	0.335	0.0781	0.9375
4	0.804	0.469	2.485
5	1.159	0.959	3.593
6	1.397	1.395	4.315
7	1.554	1.743	4.791
8	1.673	1.986	5.117
9	1.754	2.179	5.347
10	1.814	2.326	5.515
20	2.015	2.859	6.065
∞	2.083 (exact)	3.125 (exact)	6.25 (exact)

Table 22 Laminar-Flow Limiting Nusselt Number for Regular Polygonal Ducts with Uniform Peripheral Heat Flux

N	4-point	8-point	12-point
3	1.892	1.892	1.892
4	3.096	3.091	3.091
5	3.612	3.605	3.605
6	3.868	3.862	3.862
7	4.015	4.010	4.009
8	4.104	4.100	4.100
9	4.163	4.159	4.159
10	4.205	4.201	4.201
20	4.329	4.328	4.328
∞			4.364 (exact)

20-sided regular polygonal duct can be compared with that of a circle. An approximate 0.8 per cent difference between the two values indicates that they are in close agreement. Also, the Nusselt number obtained for a square duct is in close agreement with values calculated by Cheng [13] and Sparrow and Siegel [5].

The square duct with uniform peripheral heat flux was studied by Cheng [13] using separation of variables, and this led to rather involved results in the form of an infinite series. The Nusselt number of 3.82, computed by him, appears inconsistent with his results for rectangular ducts with a higher aspect ratio, and hence may be in error. The result from this investigation, 3.091, checks exactly with Sparrow and Siegel's [5] estimation, using the variational method, to three significant figures. All values for the Nusselt number for different regular polygonal ducts lie between 1.892 and 4.364, where the first value corresponds to an equilateral triangular duct and the latter value to a circular duct. The Nusselt number of 1.892 can be compared with that of 2.3691 as computed by Eckert, Irvine and Yen [14] for a circular sector duct with an apex angle of 60 degrees under case (b) type boundary conditions. Here the difference between Nusselt numbers is evident and is due to the circular boundary involved. The average

Table 23 Average Wall Temperature for Regular Polygonal Ducts with Uniform Peripheral Heat Flux

$$\left[\theta_{wm}\Big/\left(-\frac{c_1 c_2 a^4}{\mu\alpha}\right)\right] \times 10^2$$

N	4-point	8-point	12-point
3	0.335	0.335	0.335
4	0.804	0.804	0.804
5	1.160	1.158	1.159
6	1.398	1.397	1.397
7	1.556	1.554	1.554
8	1.675	1.673	1.673
9	1.756	1.754	1.754
10	1.816	1.814	1.814
20	2.016	2.015	2.015
∞	-	-	2.083

Nusselt numbers for uniform peripheral wall temperature and uniform peripheral heat flux are also presented in Figure 46 for comparison.

The locations of the "hot spots" in equilateral triangular ducts are indicated in Figure 49, which represents the temperature distribution along the sides of different regular polygonal ducts. The temperature difference, θ', is negative at the centers of the sides. This simply means that the temperatures at these points are lower than the average temperature, t_m, of the fluid. These effects are quite important in thermal stress analysis.

3.5 Concluding Remarks

General Remarks

1. The results of this analysis will apply only to fully developed flow. That is, the asymptotic forms of the Navier-Stokes and energy equations given by equations (1) and (2) are assumed valid. This will apply at points well downstream of the entrance.
2. The "hot spots" at the corners of the regular polygonal ducts with uniform peripheral heat flux are primarily caused by the rather low velocity field existing near the corner. In reality heat conduction along the boundary exists and this tends to decrease the temperature at the corners.
3. The results of computation show that higher boundary errors exist at the corners of the ducts. The exact reason for this is not known to the author. However these effects are limited to the corners only and have negligible effect on the overall flow or heat transfer characteristics.

Detailed Remarks

1. The present study indicates that both the point matching and variational methods, for the approximate solution of the stated boundary value problem, appear to

have advantages over the finite difference technique for the problems considered. In both the point matching and variational methods the accuracy of the result was found to depend upon the number of unknown coefficients selected.

Other techniques of satisfying boundary conditions such as least square method are not considered in this thesis.

2. A computer programme can be easily prepared to obtain results using the point matching technique, whereas with the variational method a great deal of work is involved in attaining the same degree of accuracy.

3. With the velocity field given in the form of series solutions (equation 5), the particular solution for the temperature can always be found using the point matching technique. The temperature distribution, using the variational method (for circular ducts with diametrically opposite flat sides), can also be defined in the same form as that of the velocity distribution.

4. The point matching method can be used for any compact section but elongated sections may give rise to divergent solutions or physically unreasonable results.

5. For geometrical configurations with both curvilinear and straight line parts forming the boundary, it was very

difficult to select the appropriate number of points on both boundaries to give the best possible heat transfer results coincident with a fairly small boundary error.

6. The point matching method can also be applied to regular polygonal ducts for fully developed laminar heat transfer with Neumann boundary conditions. The numerical results were found to converge quickly to the exact values. It is believed that the Nusselt number results obtained for this case are well within 0.5 percent of the exact values.

7. The question arises as to the accuracy of the various calculated results. The results for the mass flow rate shown in various tables are very close to the exact values. For example, the mass flow rate values for a 20-sided regular polygonal duct with a central circular hole or a circular duct with a central regular polygonal hole approach that of an annulus for the same values of λ or γ. For circular ducts with a central regular polygonal hole, the calculated values for the friction factor and the shear stress seem to differ significantly from the actual values, the reason being large errors in velocity and temperature at the boundary. The boundary errors calculated for velocity and temperature for circular ducts with diametrically opposite flat sides, regular polygonal ducts with a central circular hole and

regular polygonal ducts are found to be very small. The maximum error is estimated to be less than one percent of the maximum value of velocity or temperature in the duct.

8. It appears possible to extend the present method of point matching to cases with uniform heat sources and viscous-dissipation effects [17] for the shapes discussed, whereas the variational method [5] would be extremely cumbersome.

9. The variational method [5] can be applied to laminar flow problems in circular ducts with diametrically opposite flat sides with case (a) and (b) type boundary conditions.

10. The point matching technique may also be applied to the four geometrical shapes discussed with various other combinations of thermal boundary conditions [9].

regular polygonal decks are found to be very small. The maximum error is estimated to be less than one percent of the maximum value of velocity or momentum in the duct.

8. It appears possible to extend the present method of outer matching to cases with multiple base singularities whereas the matching method [3] must be increasingly complex.

9. The variational method [3] can be applied to various flow problems in elevated decks with dimensionally opposite flow edge into case (a) type boundary conditions.

10. The point matching technique may also be applied to the four semi-infinite plane diamond duct problem [5] other configurations of inward pointing conditions

REFERENCES

1. J. Barta, "On the Approximate Solution of a Two-Dimensional Elasticity Problem", Zeits. für Angew. Math Und Mechs., Vol. 17, 1937, pp. 184-185.
2. S.S. Sattinger and H.D. Conway, "The Solution of Certain Isosceles - Triangle and Rhombus Torsion and Plate Problems", International Journal of Mechanical Science, Vol. 7, 1965, pp. 221-228.
3. E.M. Sparrow, "Laminar Flow in Isosceles Triangular Ducts", AIChE Journal, Vol. 8, 1962, pp. 599-607.
4. K.C. Cheng, "Laminar Flow and Heat Transfer Characteristics in Regular Polygonal Ducts", Proceedings of the Third International Heat Transfer Conference, AIChE, Vol. 1, 1966, pp. 64-76.
5. E.M. Sparrow and R. Siegel, "A Variational Method for Fully Developed Laminar Heat Transfer in Ducts", Journal of Heat Transfer 81, 1959, pp. 157-167.
6. S. Timoshenko and J.N. Goodier, "Theory of Elasticity", Second Edition, McGraw-Hill Book Company, Inc., New York, N.Y., 1951, p. 280.
7. W.J. Carter and J.B. Oliphint, "Torsion of a Circular Shaft with Diametrically Opposite Flat Sides", Journal of Applied Mechanics, Vol. 19, 1952, pp. 249-251.

References

8. H. Ōkubo, "Torsion of a Circular Shaft with a Number of Longitudinal Notches", Journal of Applied Mechanics, Trans. ASME, Vol. 72, 1950, pp. 359-362.

9. R.E. Lundberg, P.A. McCuen, and W.C. Reynolds, "Heat Transfer in Annular Passages. Hydrodynamically Developed Laminar Flow with Arbitrarily Prescribed Wall Temperature or Heat Fluxes", International Journal of Heat and Mass Transfer, Vol. 6, 1963, pp. 495-529.

10. O.E. Dwyer, "Bilateral Heat Transfer in Annuli for Slug and Laminar Flow", Nuclear Science and Engineering, Vol. 19, 1964, pp. 48-57.

11. F.A. Gaydon and H. Nuttall, "Viscous Flow Through Tubes of Multiply Connected Cross Sections", Journal of Applied Mechanics, Vol. 26, Trans. ASME, Vol. 81, Series E, 1959, pp. 573-576.

12. K.C. Cheng and M. Jamil, "Laminar Flow and Heat Transfer in Ducts of Multiply Connected Cross Sections", To be presented at the Ninth National Heat Transfer Conference, Seattle, Washington, August 6-9, 1967.

13. H.M. Cheng, "Analytical Investigation of Fully Developed Laminar Flow Forced Convection Heat Transfer in Rectangular Ducts with Uniform Heat Flux", MS thesis, Massachusetts Institute of Technology, 1957.

14. E.R.G. Eckert, T.F. Irvine, J.R. and J.T. Yen, "Local Laminar Heat Transfer in Wedge-Shaped Passages", Trans. ASME, Vol. 80, 1958, pp. 1433-1438.

15. E.M. Sparrow and A. Haji-Sheikh, "Flow and Heat Transfer in Ducts of Arbitrary Shape with Arbitrary Thermal Boundary Conditions", Journal of Heat Transfer, Trans. ASME, Vol. 88, Series C, No. 4, pp. 351-358, 1966.

16. "Handbooks of Mathematical Functions with Formulas, Graphs, and Mathematical Tables", U.S. Department of Commerce, National Bureau of Standards, Applied Mathematic Series 55, 1965.

17. V.P. Tyagi, "Forced Convection of a Dissipative Liquid in a Channel with Neumann Conditions", Journal of Applied Mechanics, Vol. 33, No. 1, 1966, pp. 18-24.

14. E.E.O. Schatz, C.E. Izraine, W.K. and A.T. Tam, "Local Limiter Heat Transfer in Wedge-Shaped Passages", Trans. ASME, Vol. 80, 1958, pp. 1011-1030

15. E.M. Sparrow and A. Ohji-Ghadi, "Flow and Heat Transfer in Ducts of Arbitrary Shape with Arbitrary Thermal Boundary Conditions", Journal of Heat Transfer, Trans. ASME, Vol. 80, Series C, No. 4, pp. 131-358, 1958.

16. "Handbook of Mathematical Functions with Formulas, Graphs, and Mathematical Tables", U.S. Department of Commerce, National Bureau of Standards, Applied Mathematics Series 55, 1964.

17. W.M. Kays, "Forced Convection in a Rectangular Duct as a Conjugate Problem", Journal of Applied Mechanics, Vol. 41, No. 1, 1956, pp. 14-24

APPENDIX

Exact Integration using Chebyshev Polynomials

As there is no exact integration available for the following integral

$$\int_0^{\pi/N} \cos jN\phi / \cos^{jN+i} \phi \, d\phi \qquad (1)$$

where $i > 2$, it was difficult to evaluate the unknown coefficient A_0' by equation (34) for regular polygonal ducts with the case (b) type boundary condition. The solution to the above integral was attained using Chebyshev polynomials which changed the above integral into a simpler form, the solution to which exists in the literature. This simplified integral could then be evaluated using a digital computer.

The following conversion was adopted to evaluate the simpler form of the integral,

$$T_{Nj}(\cos \phi) = \cos Nj\phi = \frac{Nj}{2} \sum_{m=0}^{Nj/2} \frac{(-1)^m (Nj-m-1)!}{m!\ (Nj-2m)!} (2 \cos \phi)^{Nj-2m} \qquad (2)$$

Substituting in the above integral, one gets

$$\int_0^{\pi/N} \frac{Nj}{2} \sum_{m=0}^{Nj/2} \frac{(-1)^m (Nj-m-1)!}{m!\ (Nj-2m)!} \frac{2^{Nj-2m}}{\cos^{i+2m}\phi} \, d\phi \qquad (3)$$

which is the required form to be integrated exactly, the result evaluated via the digital computer.

APPENDIX

Exact Integration using Gaussian Quadrature

In there is no exact integration available for the following integral

$$\int_{0}^{\pi/2} \cos^{j}\theta(\cos^{2}\theta)^{n-1} \, d\theta \qquad (1)$$

where $j > 2$, it was difficult to evaluate the unknown coefficient g_n^j by equation (21) for angular polynomial ducts with the case (2) type boundary condition. The solution to the above integral was obtained using Chebyshev polynomials which changed the above integral into a simple form, the solution to which exists in literature. This simplified integral could then be evaluated using a digital computer.

The following computation was adopted to calculate the simpler form of the integral,

$$\cos^{j}\theta = \cos\theta\cdot\cos^{j-1}\theta = \frac{2}{\pi}\sum_{n=0}^{\infty}{}' \frac{(-1)^n \Gamma(j+n-\frac{1}{2})}{n!\,\Gamma(j+1+n)} (2\cos\theta)\,T_{2n}(\cos\theta) \qquad (2)$$

Substituting in the above integral, one gets

$$\int_{0}^{\pi/2} \frac{2}{\pi}\sum_{n=0}^{\infty}{}' \frac{(-1)^n \Gamma(j+n-\frac{1}{2})}{n!\,\Gamma(j+1+n)} \cos^{j-2n}\theta \, d\theta \qquad (3)$$

which is the required form to be integrated exactly, the result evaluated via the digital computer.

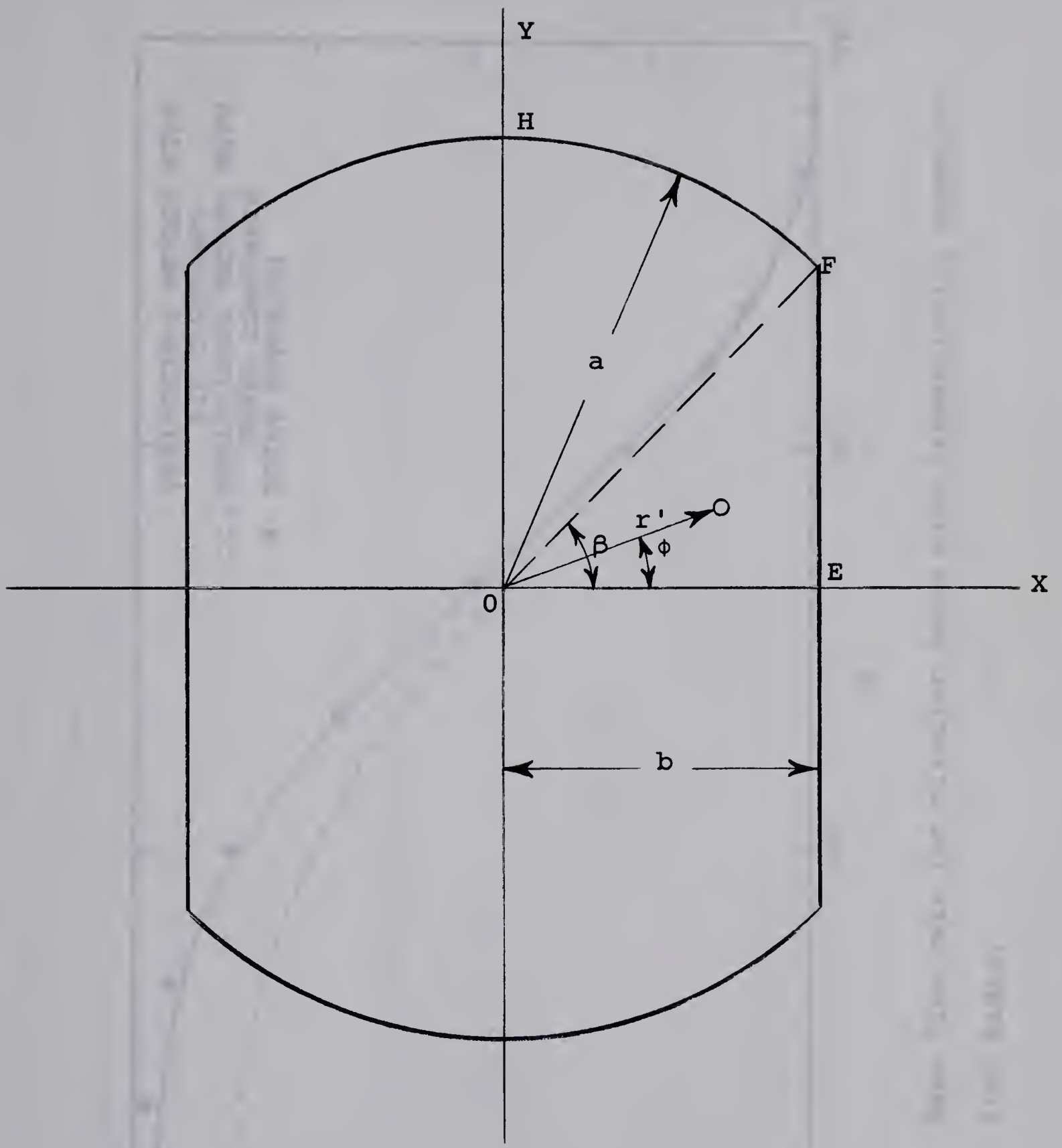

Fig. 1 Coordinate system for circular duct with diametrically opposite flat sides.


y
B
A
x
O

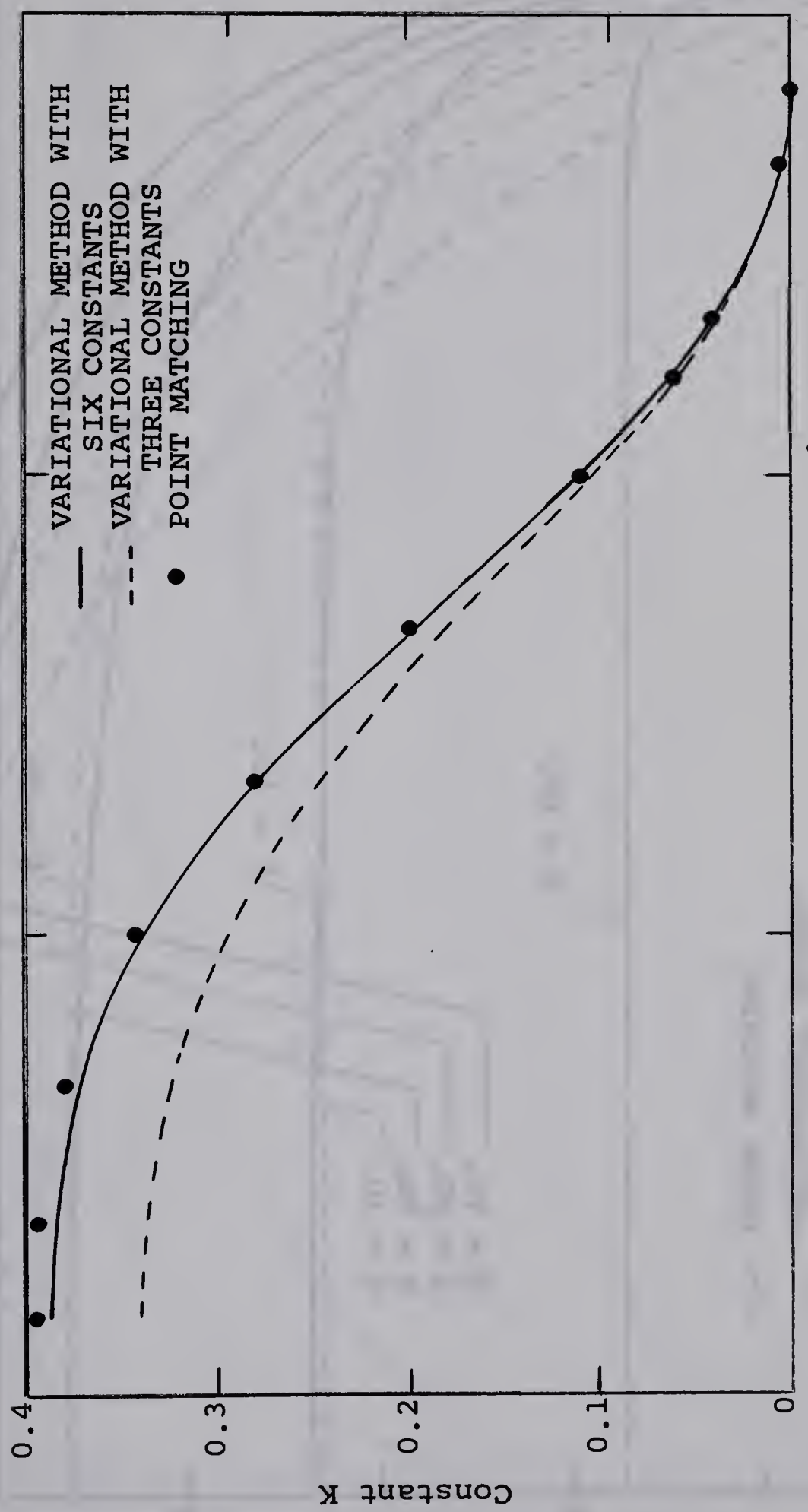

Fig. 2 Mass flow rate for circular ducts with diametrically opposite flat sides.

BRAIN TUMOR ARBITRARY
BRAIN TUMOR ARBITRARY SIDE CORRELATIONS
ESTIMATED TUMOR ARBITRARY SIDE CORRELATIONS
TOTAL ADJUSTING
80%
20%

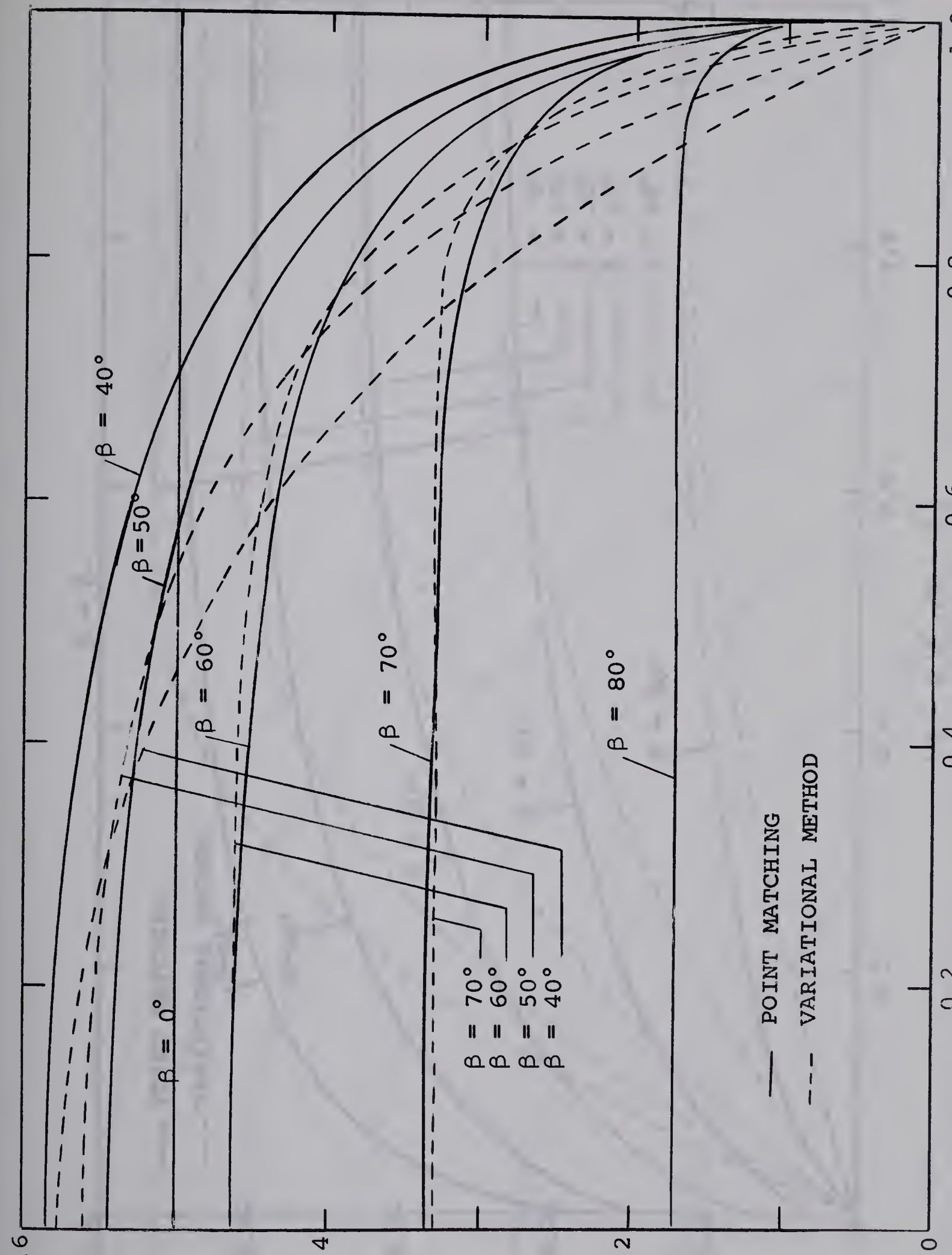

Fig. 3 Shear stress distribution along the straight wall of circular ducts with diametrically opposite flat sides.

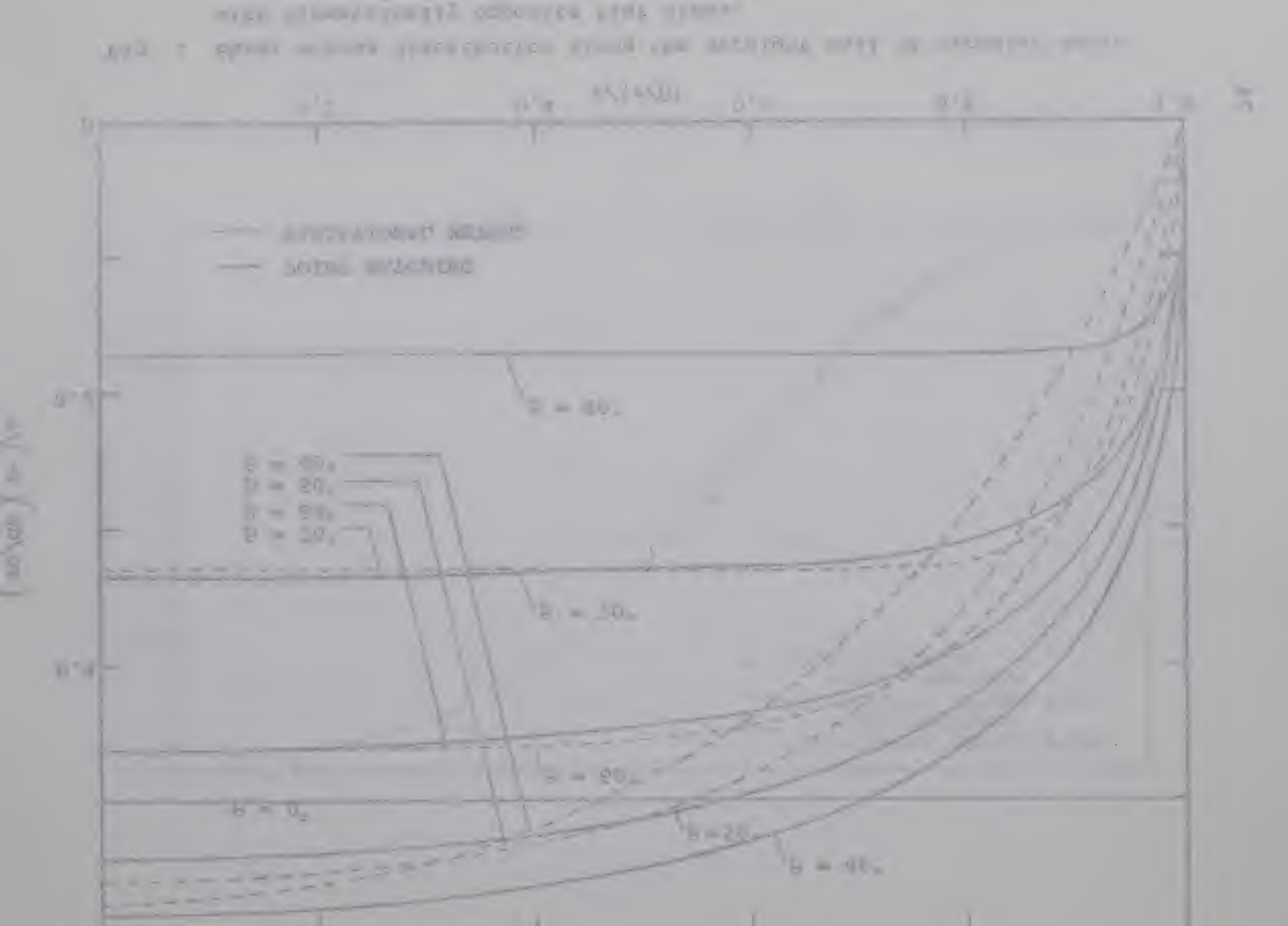

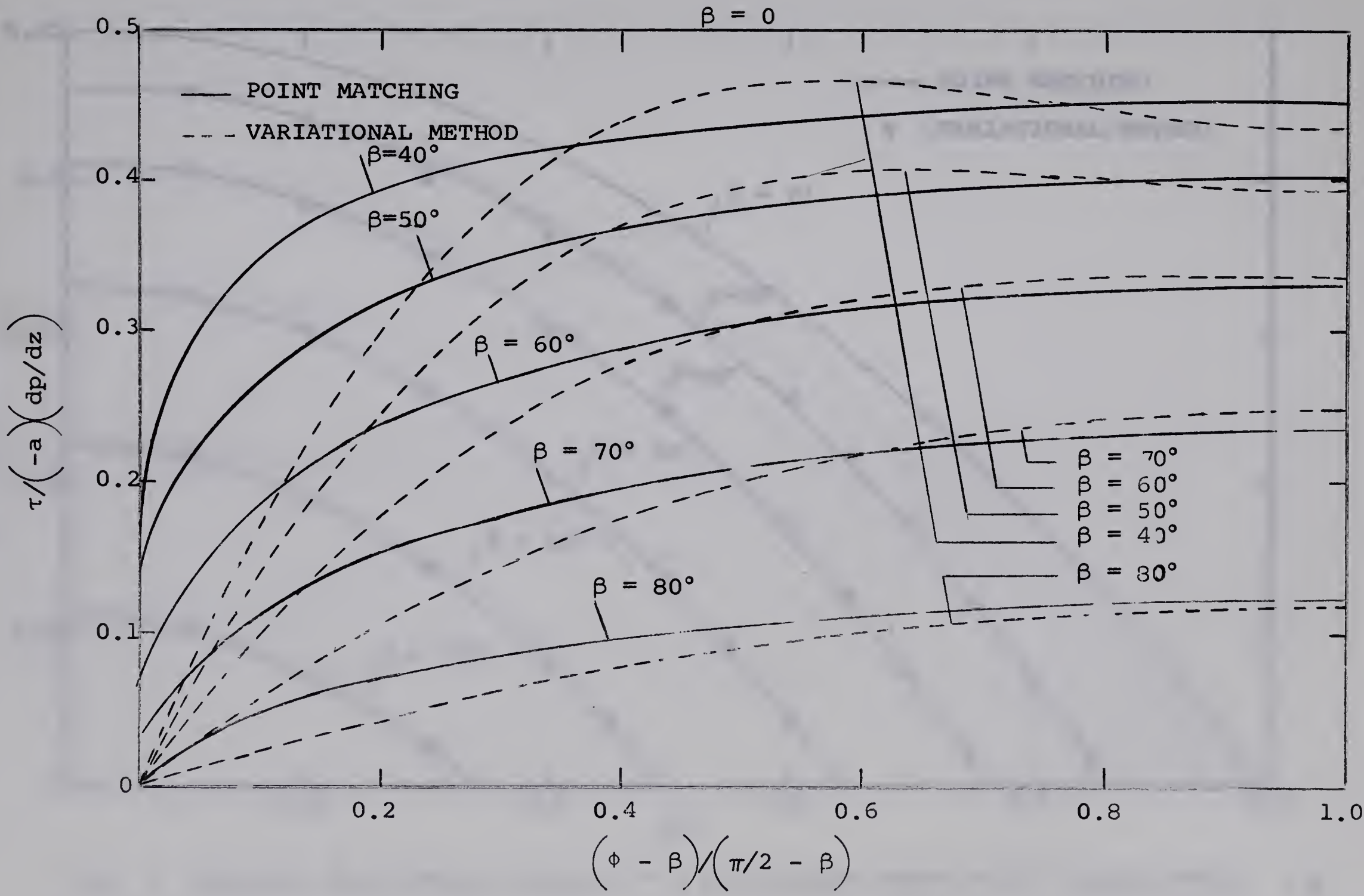

Fig. 4 Shear stress distribution along the curved wall of circular ducts with diametrically opposite flat sides.

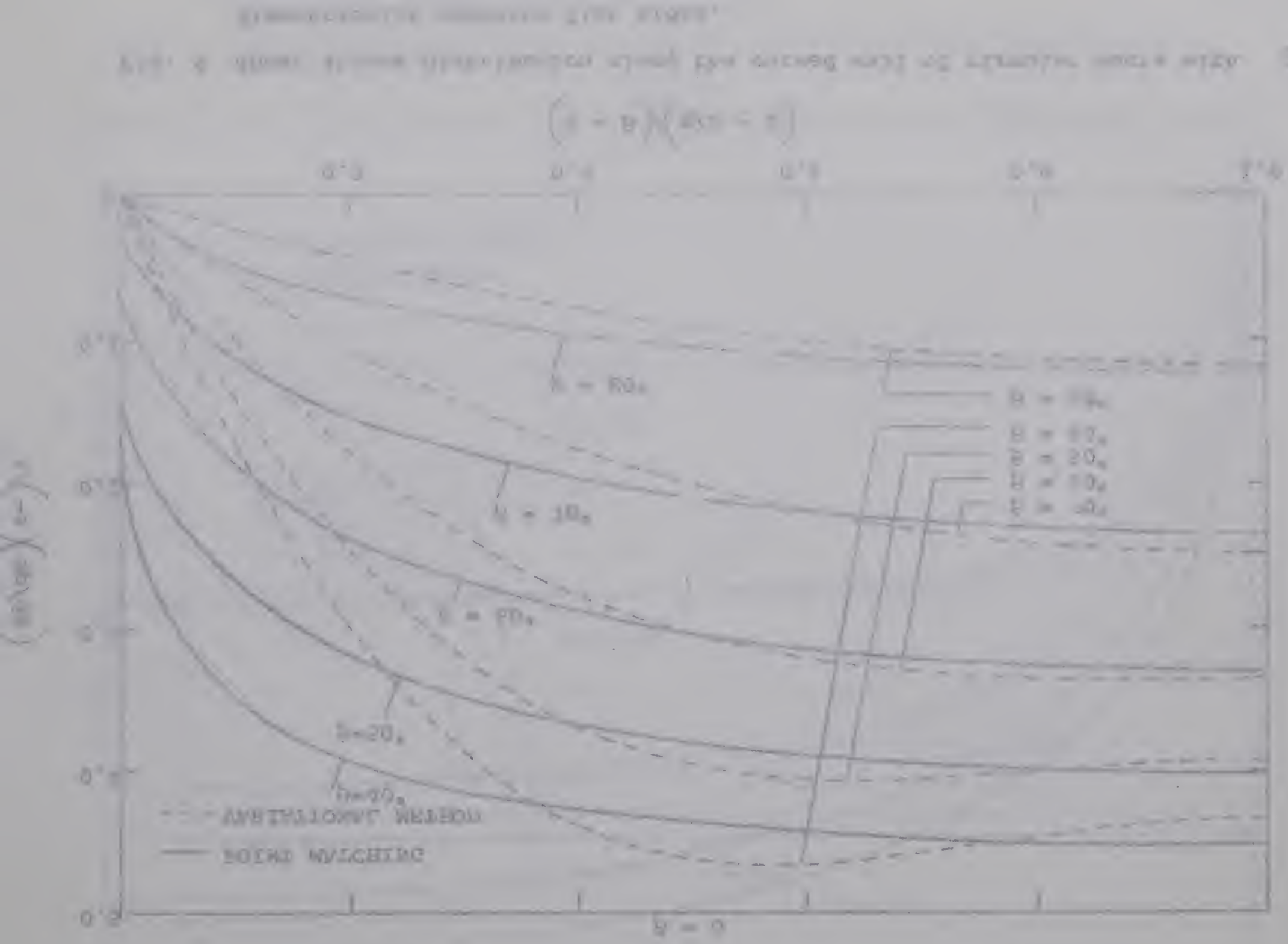
h = 80s
h = 40s
h = 30s
h = 20s
h = 10s
h = 5s
h=40s
h=20s
h=10s
CONSTANT VELOCITY METHOD
GOING NAVIGATING

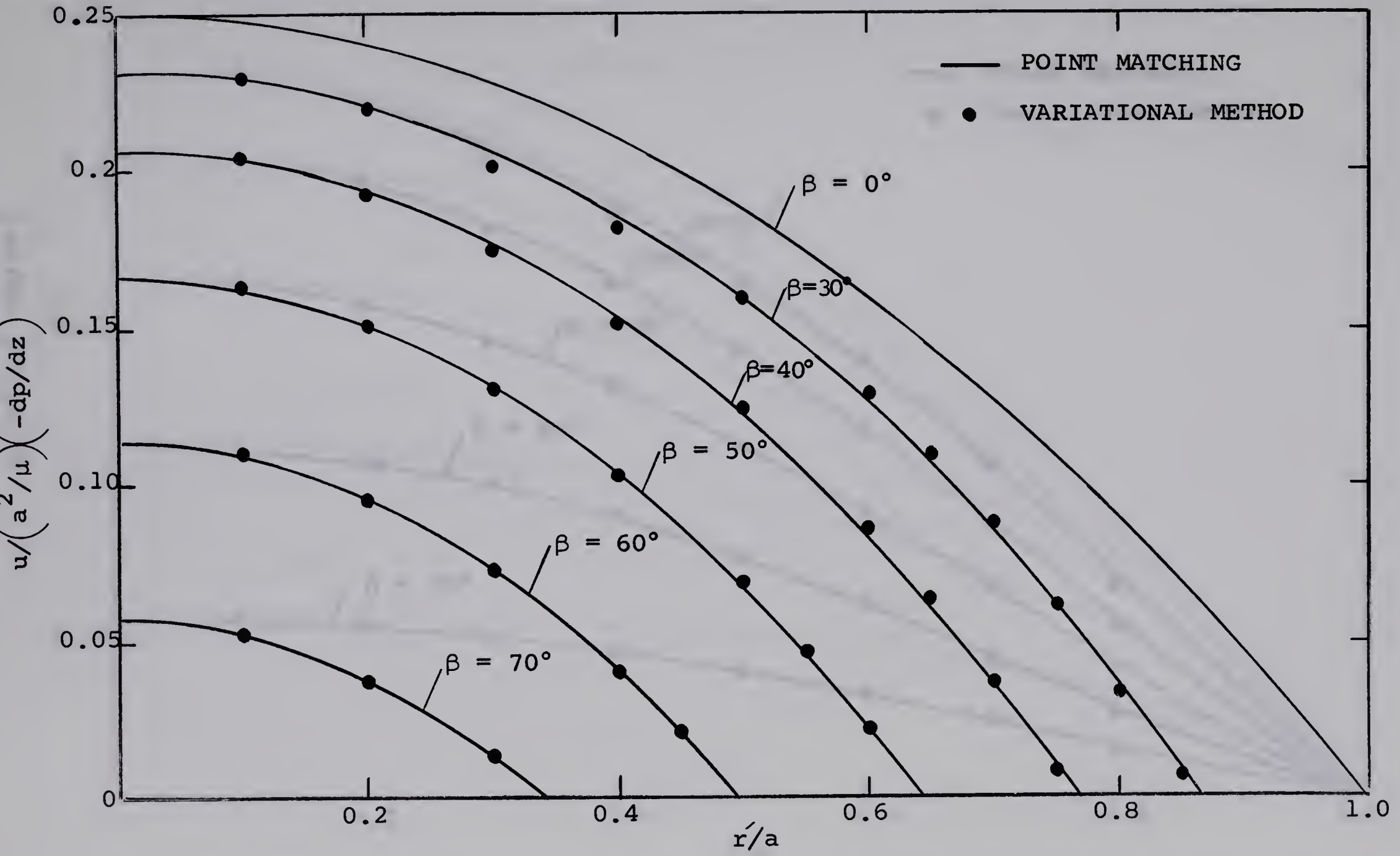

Fig. 5 Velocity distribution along $\phi = 0$ in circular ducts with diametrically opposite flat sides.

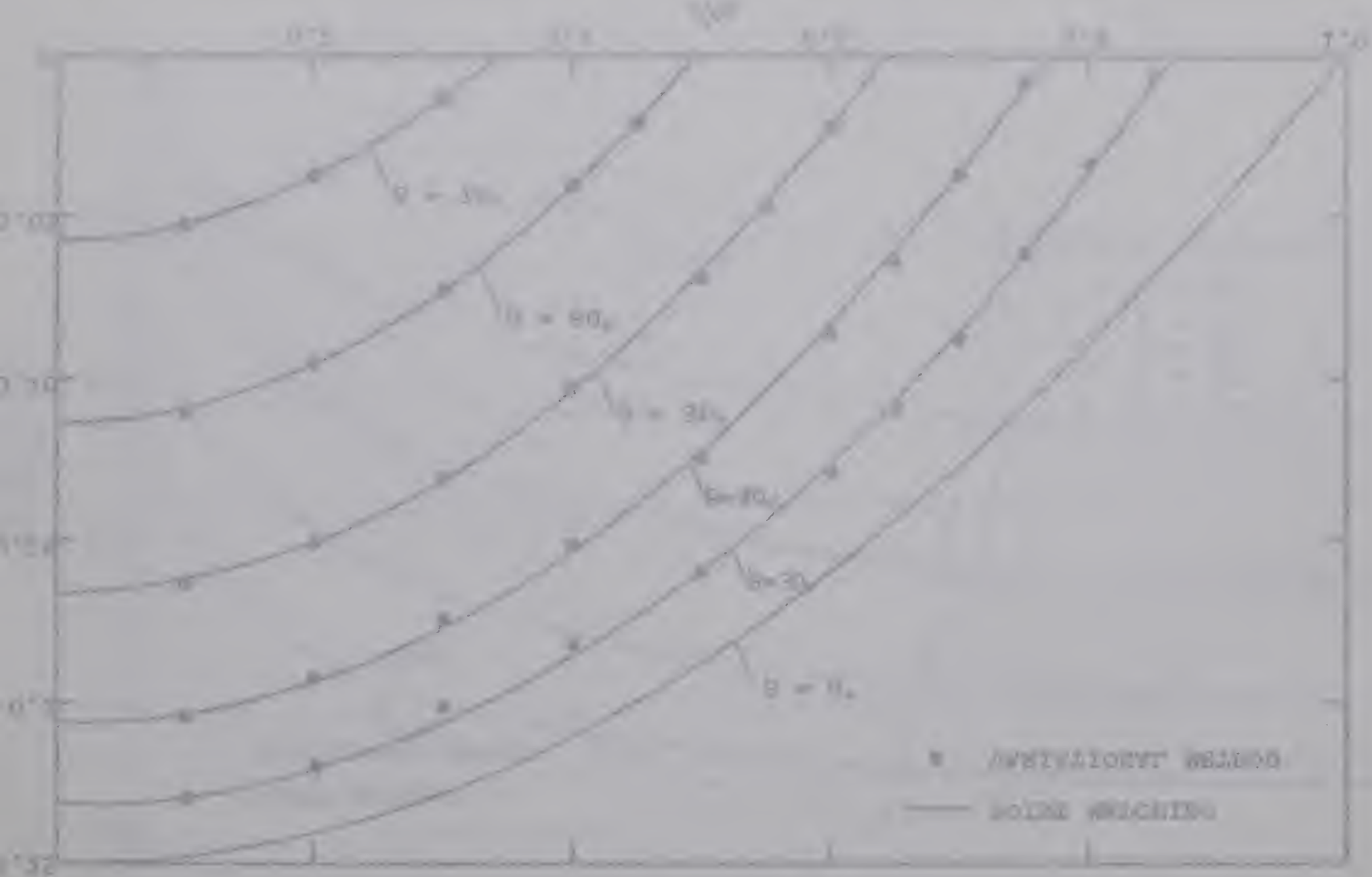

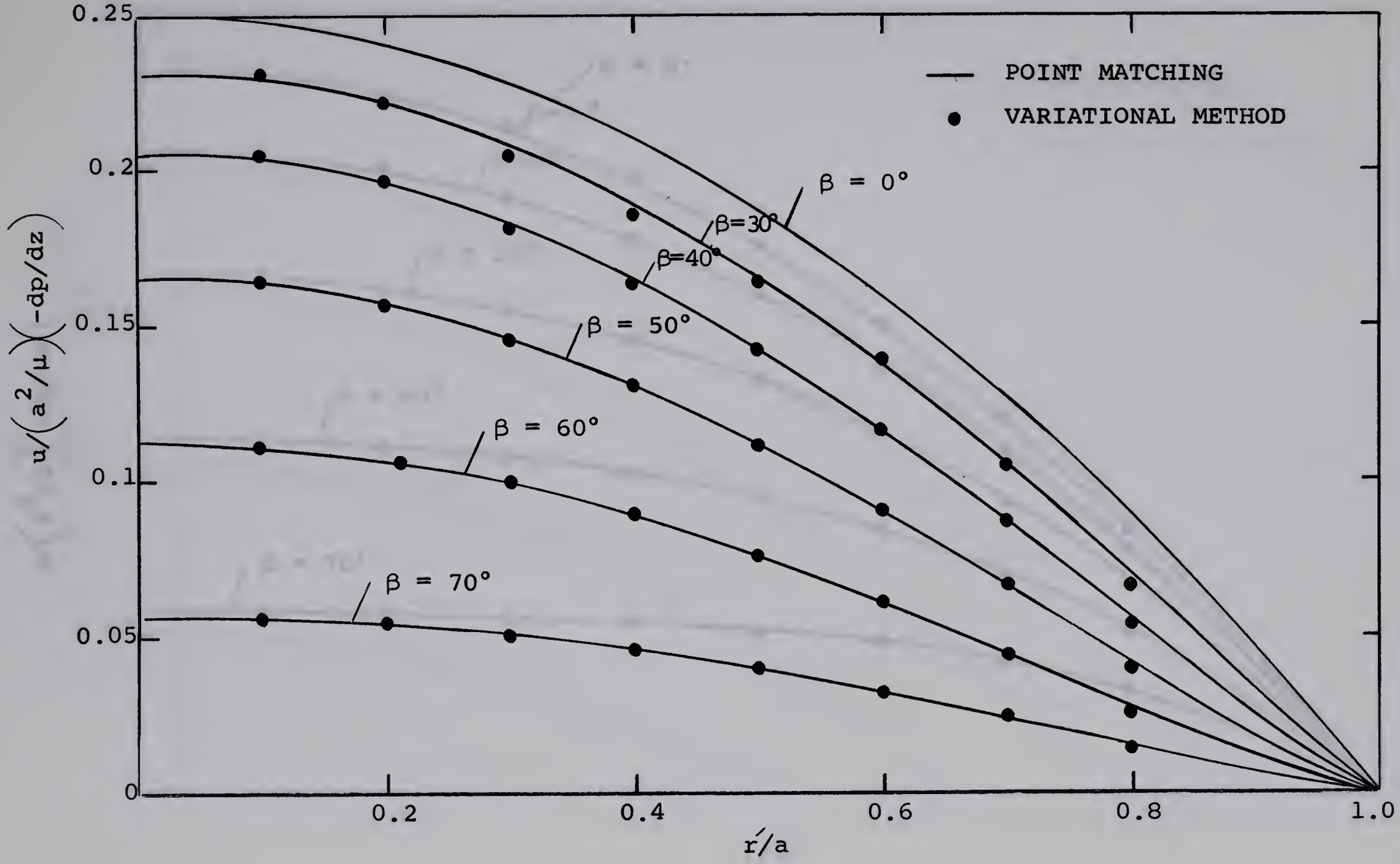

Fig. 6 Velocity distribution along $\Phi = \beta$ in circular ducts with diametrically opposite flat sides.

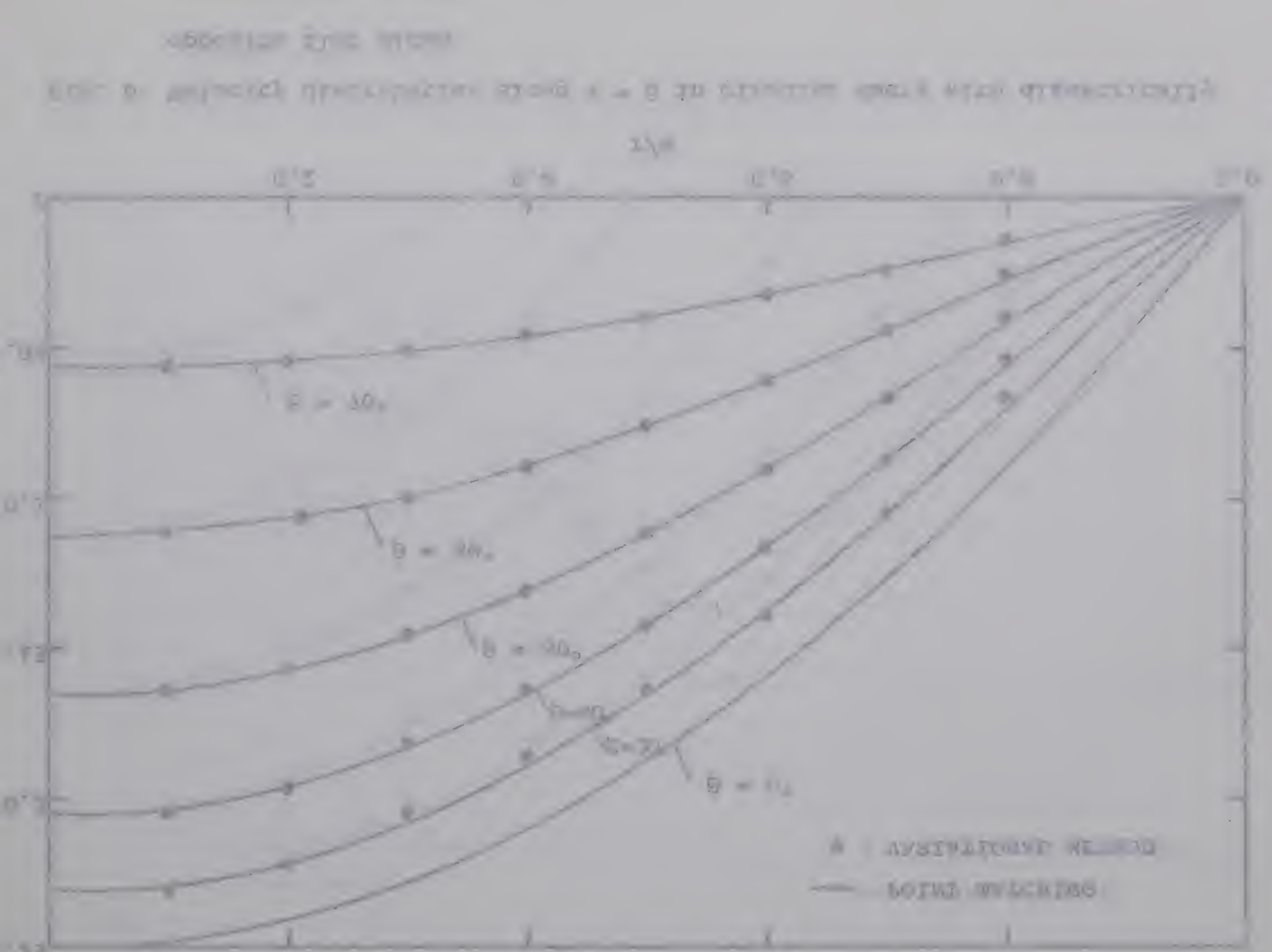
θ = 30°
θ = 45°
θ = 60°
θ = 75°
θ = 90°

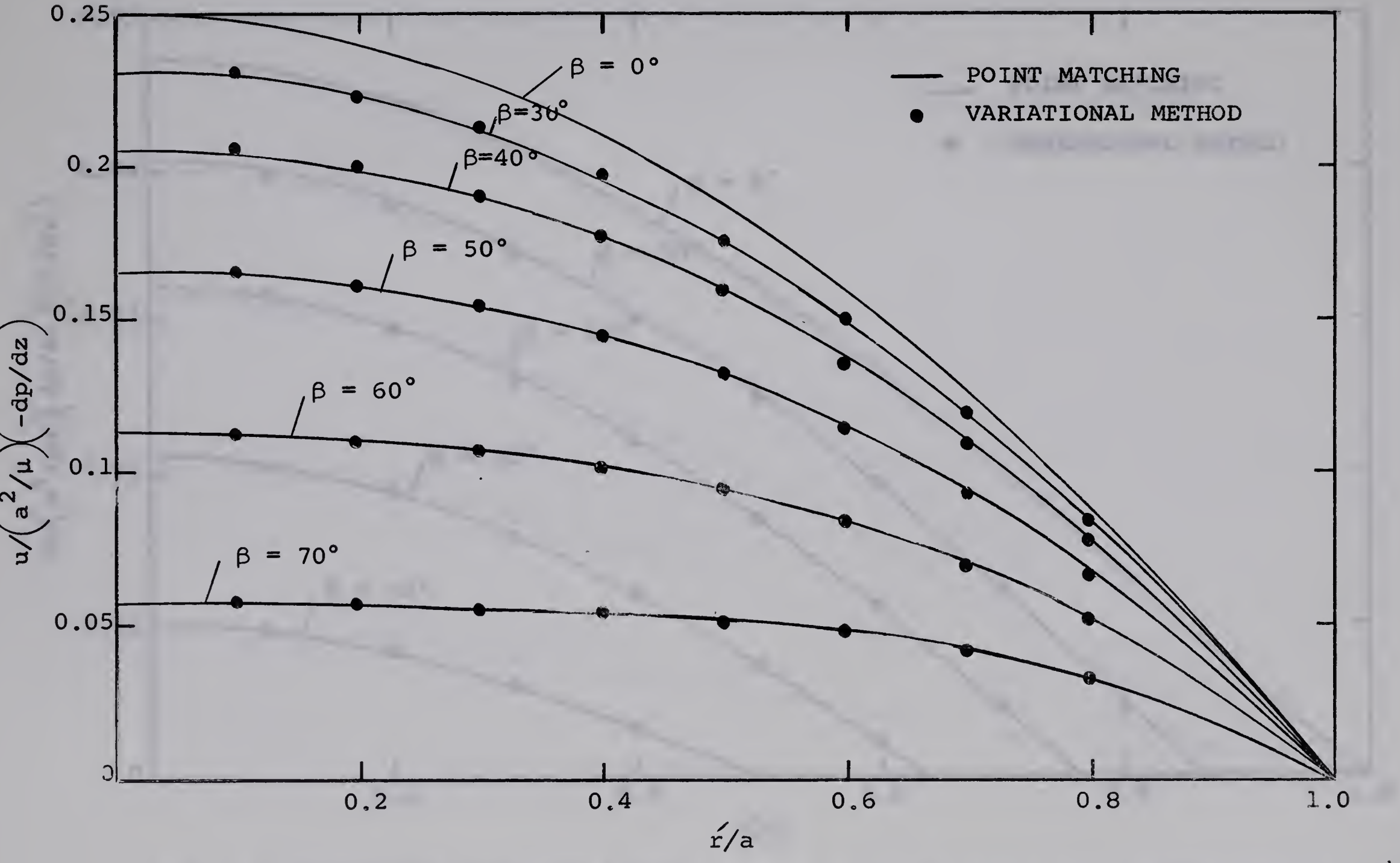

Fig. 7 Velocity distribution along $\Phi = \pi/2$ in circular ducts with diametrically opposite flat sides.

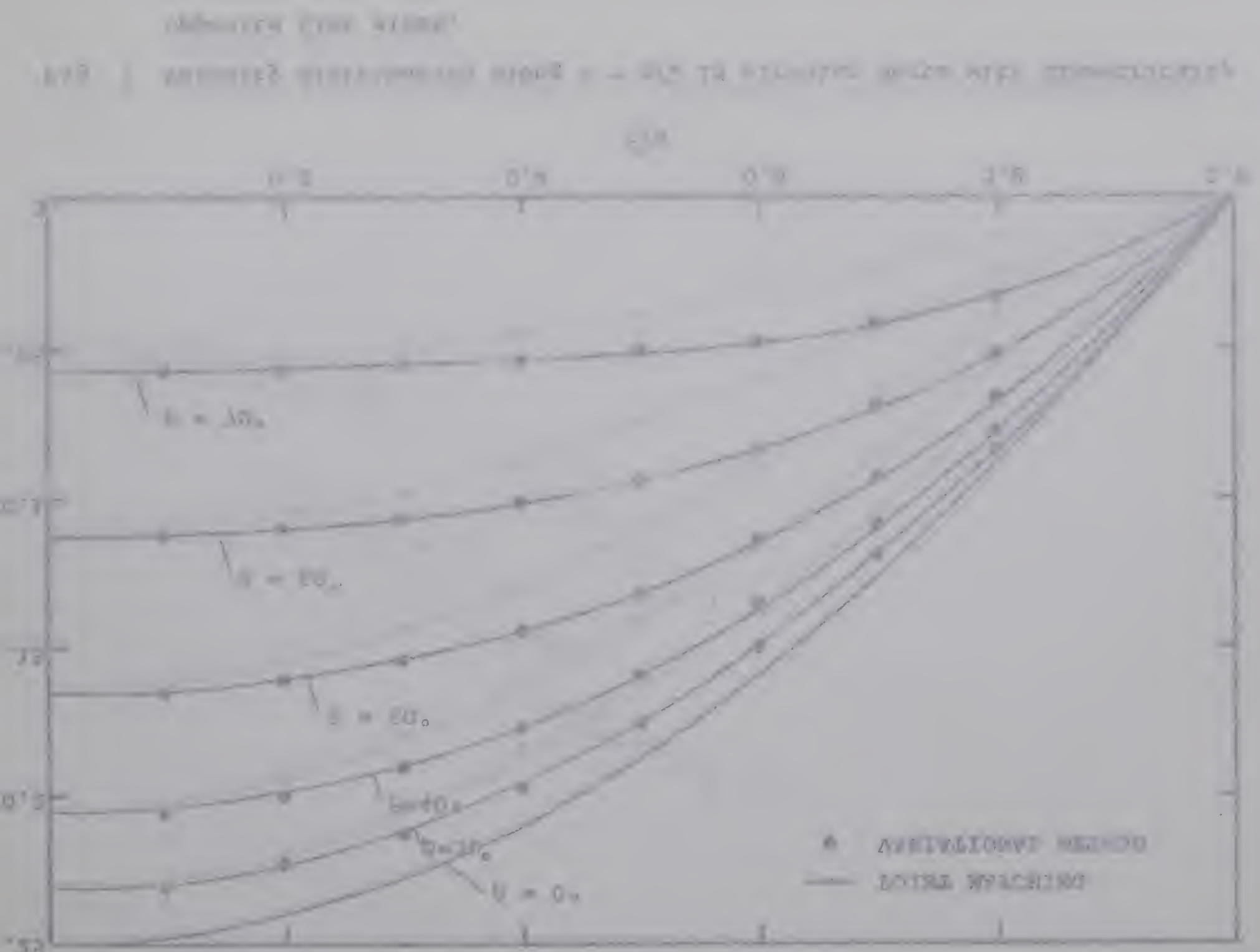
$\delta = \Delta\delta_0$
$\delta = 2\delta_0$
$\delta = 3\delta_0$
$\delta = 4\delta_0$
$\delta = 5\delta_0$
$\delta = 0$

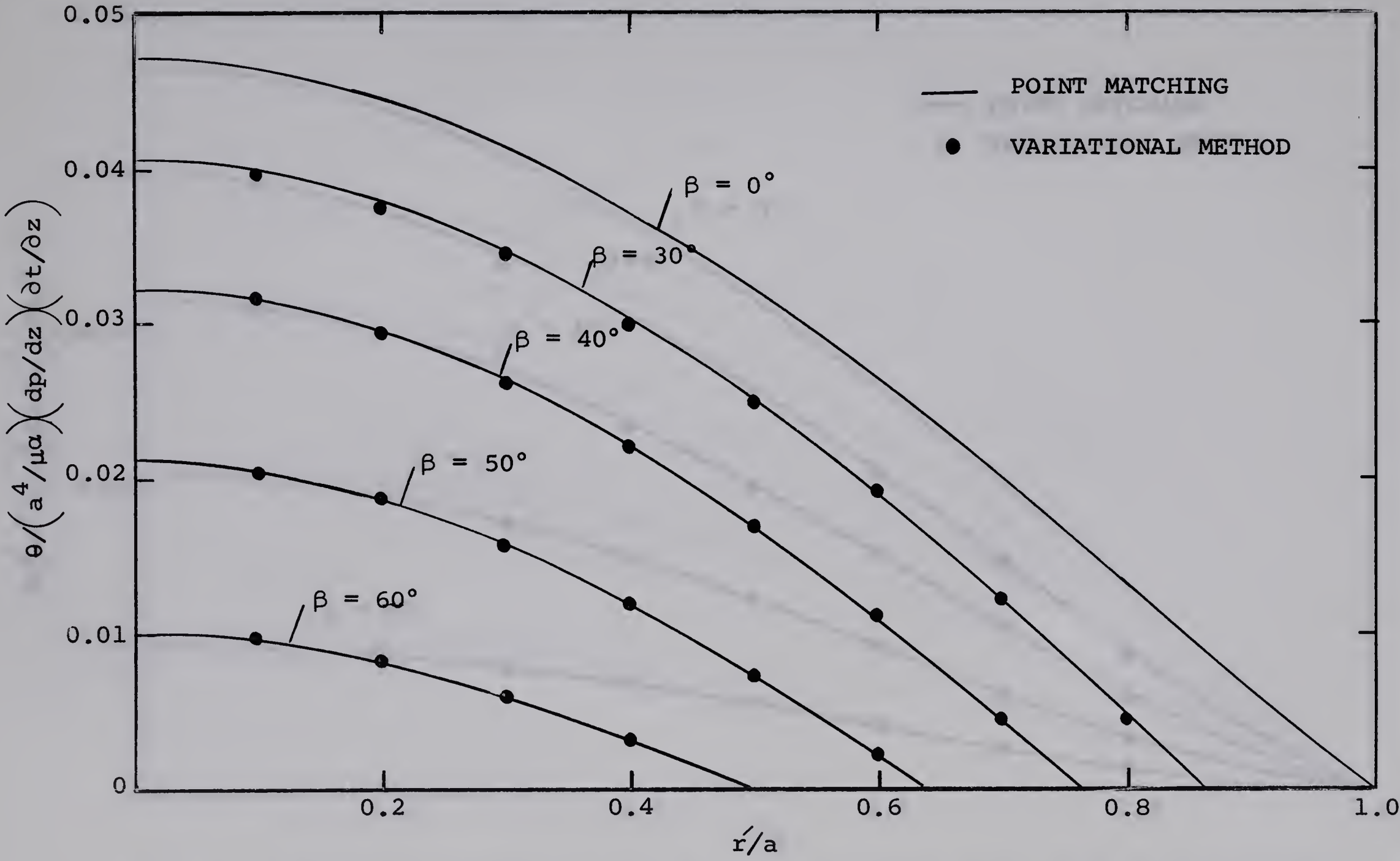

Fig. 8 Temperature profiles along $\phi = 0$ in circular ducts with diametrically opposite flat sides.

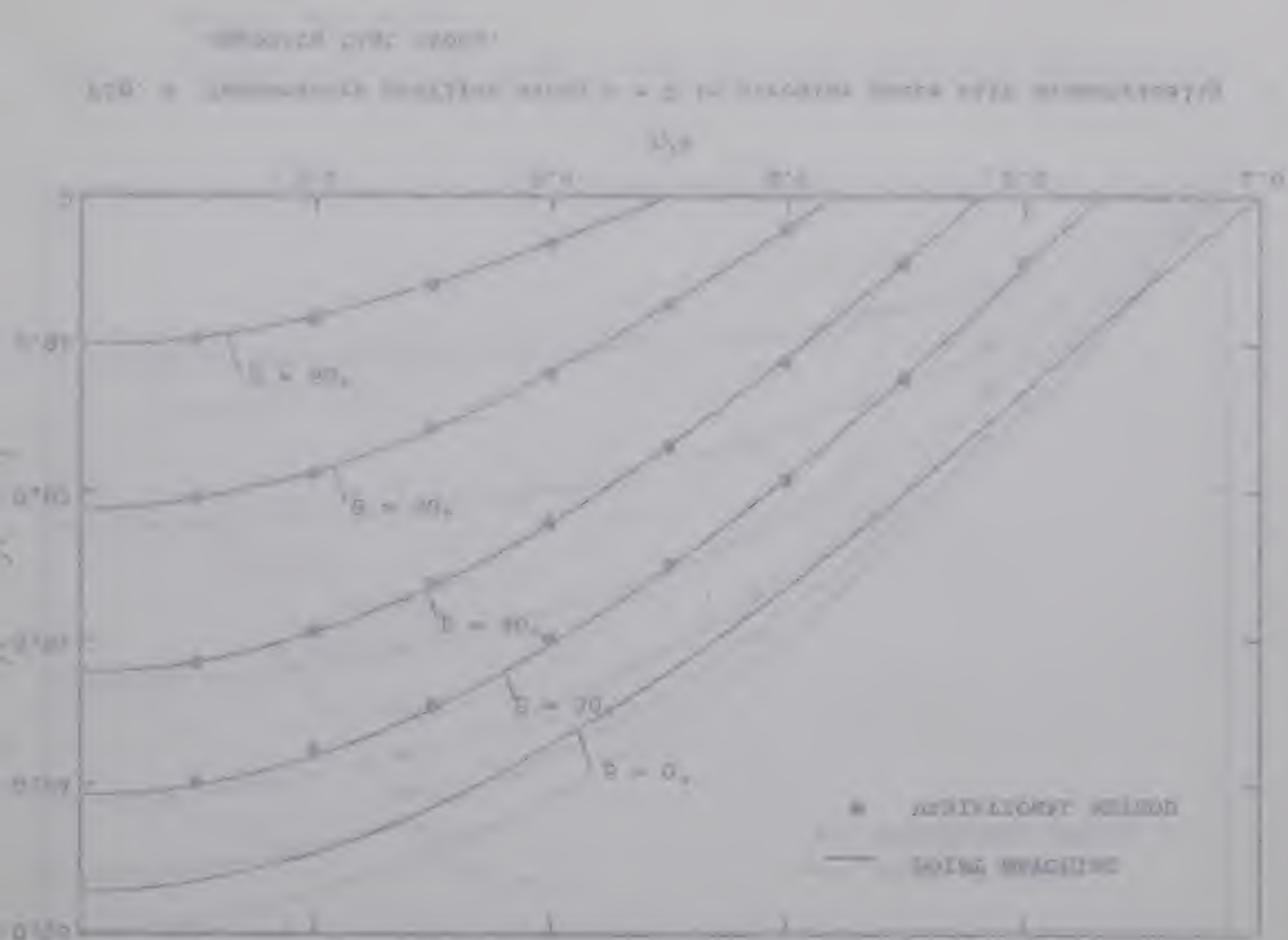
θ = 90°
θ = 80°
θ = 70°
θ = 0°
AERODYNAMIC REACTION
SWING BRACKETS

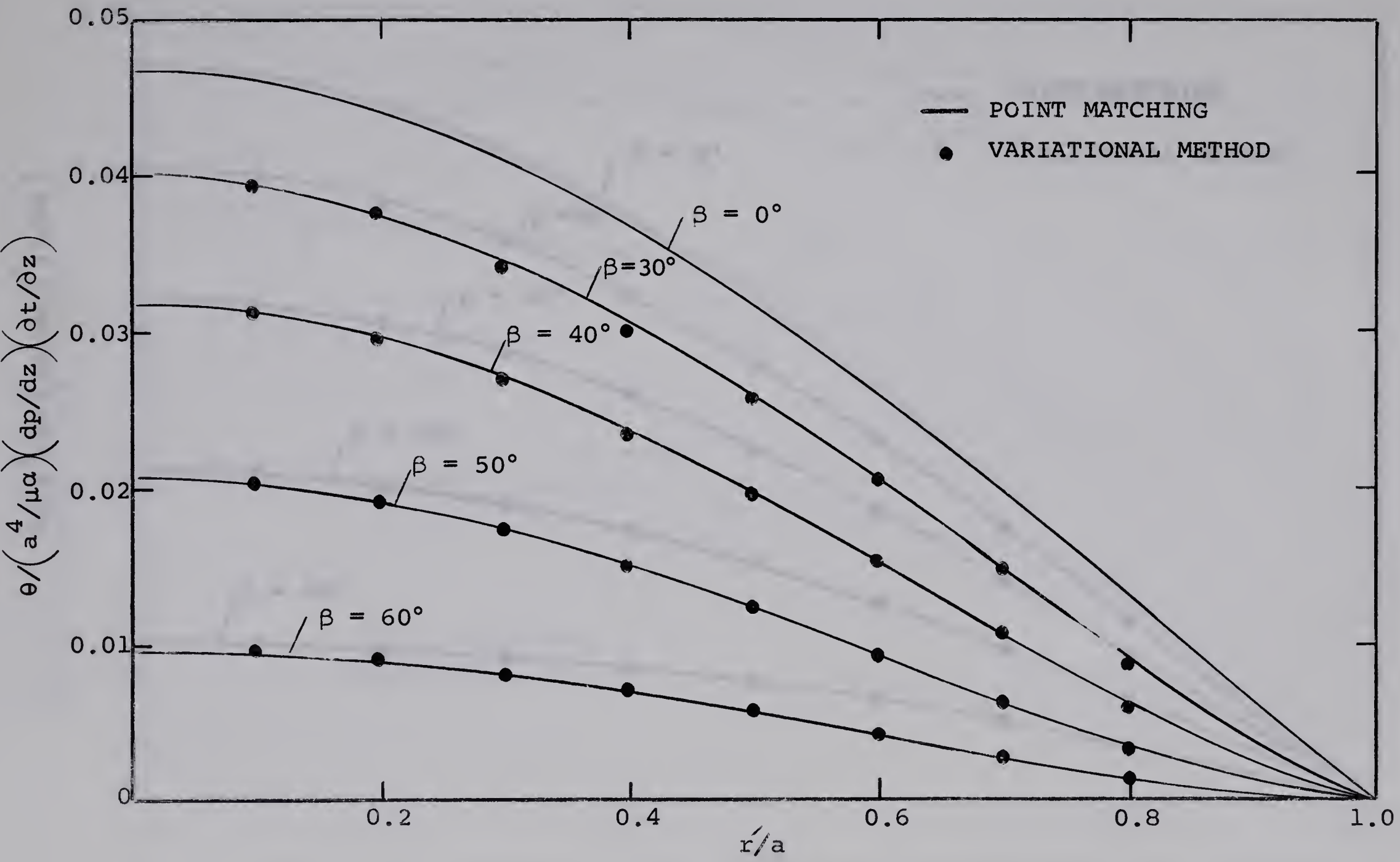

Fig. 9 Temperature profiles along $\Phi = \beta$ in circular ducts with diametrically opposite flat sides.

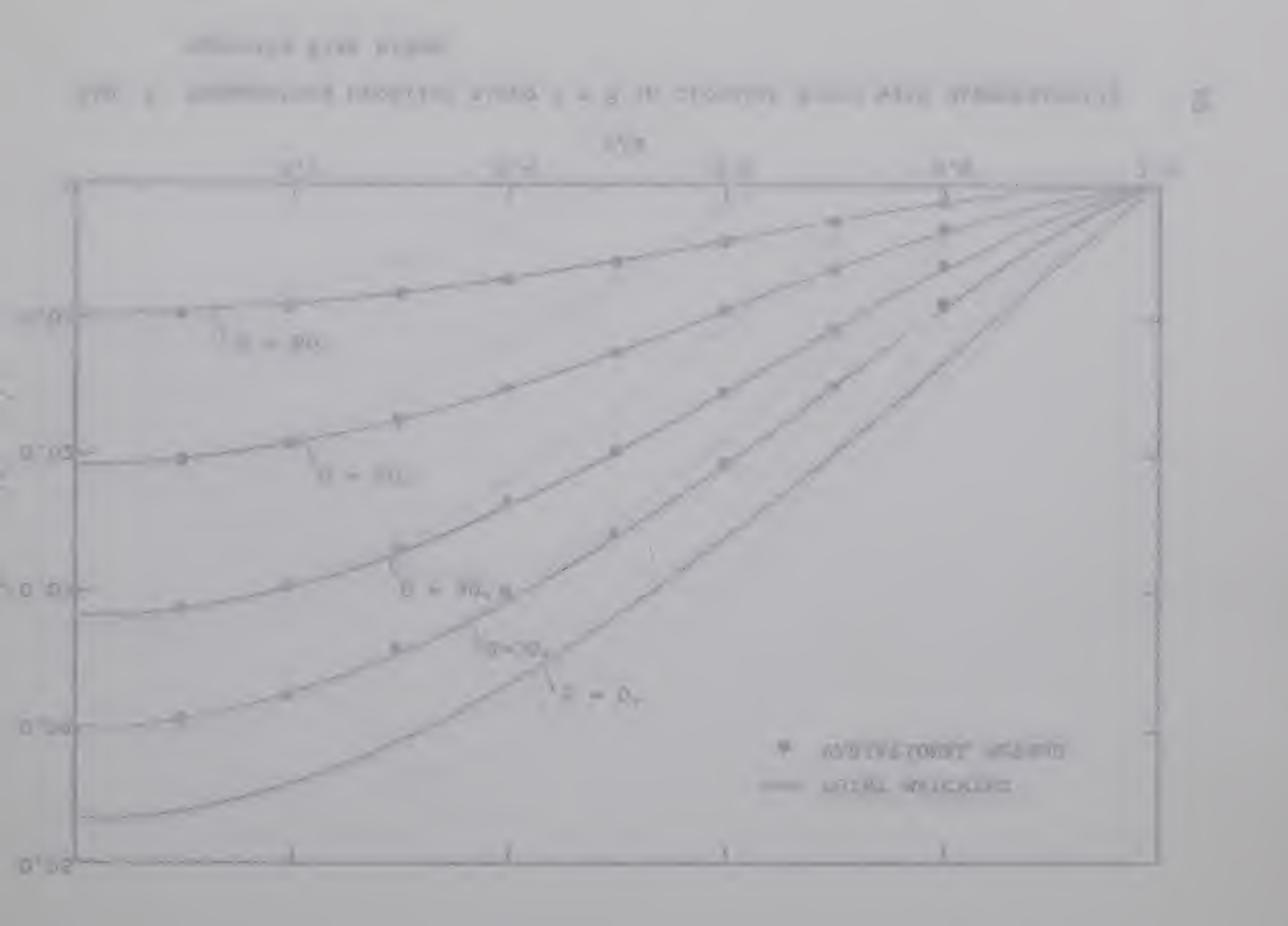

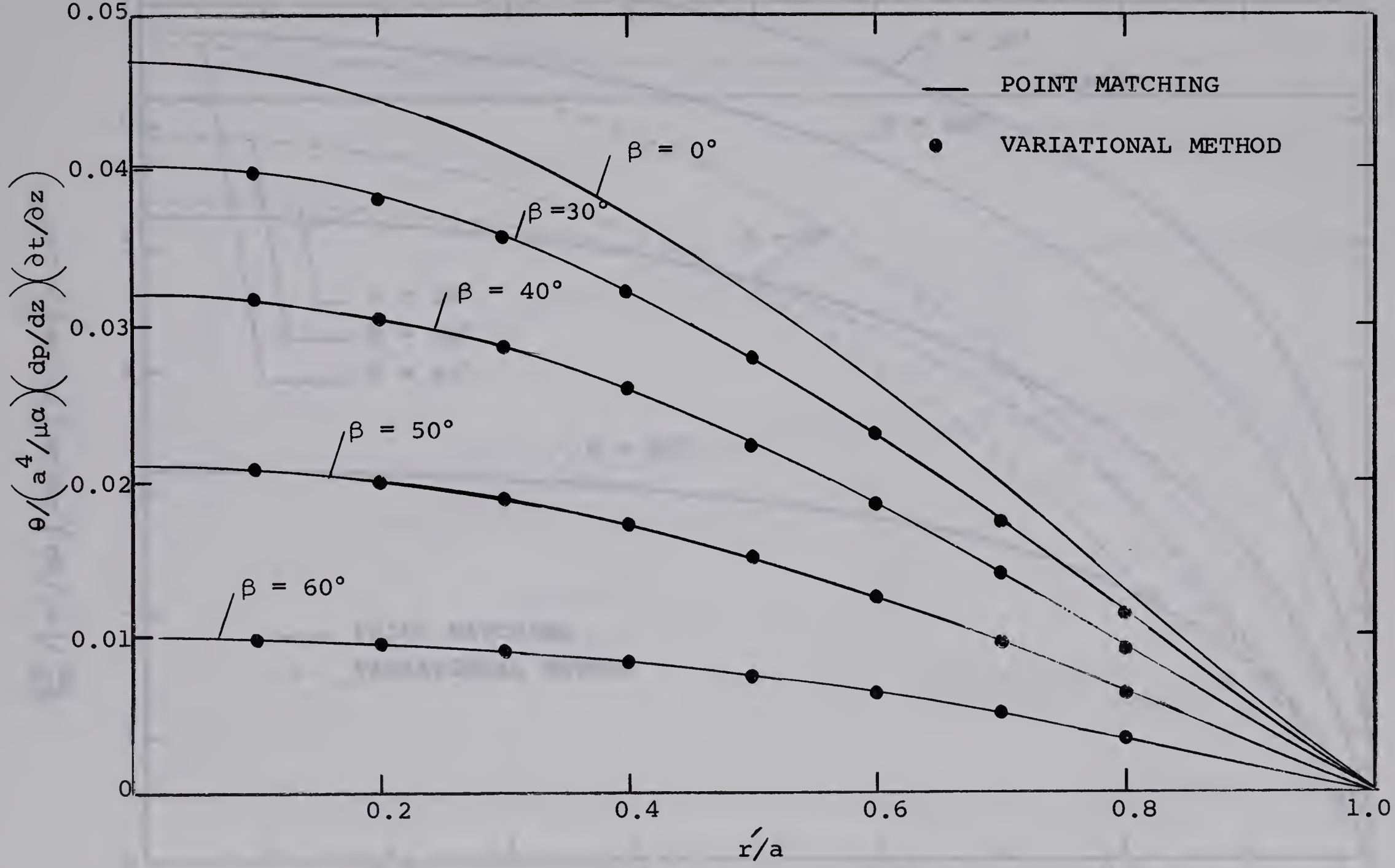

Fig. 10 Temperature profiles along $\Phi = \pi/2$ in circular ducts with diametrically opposite flat sides.

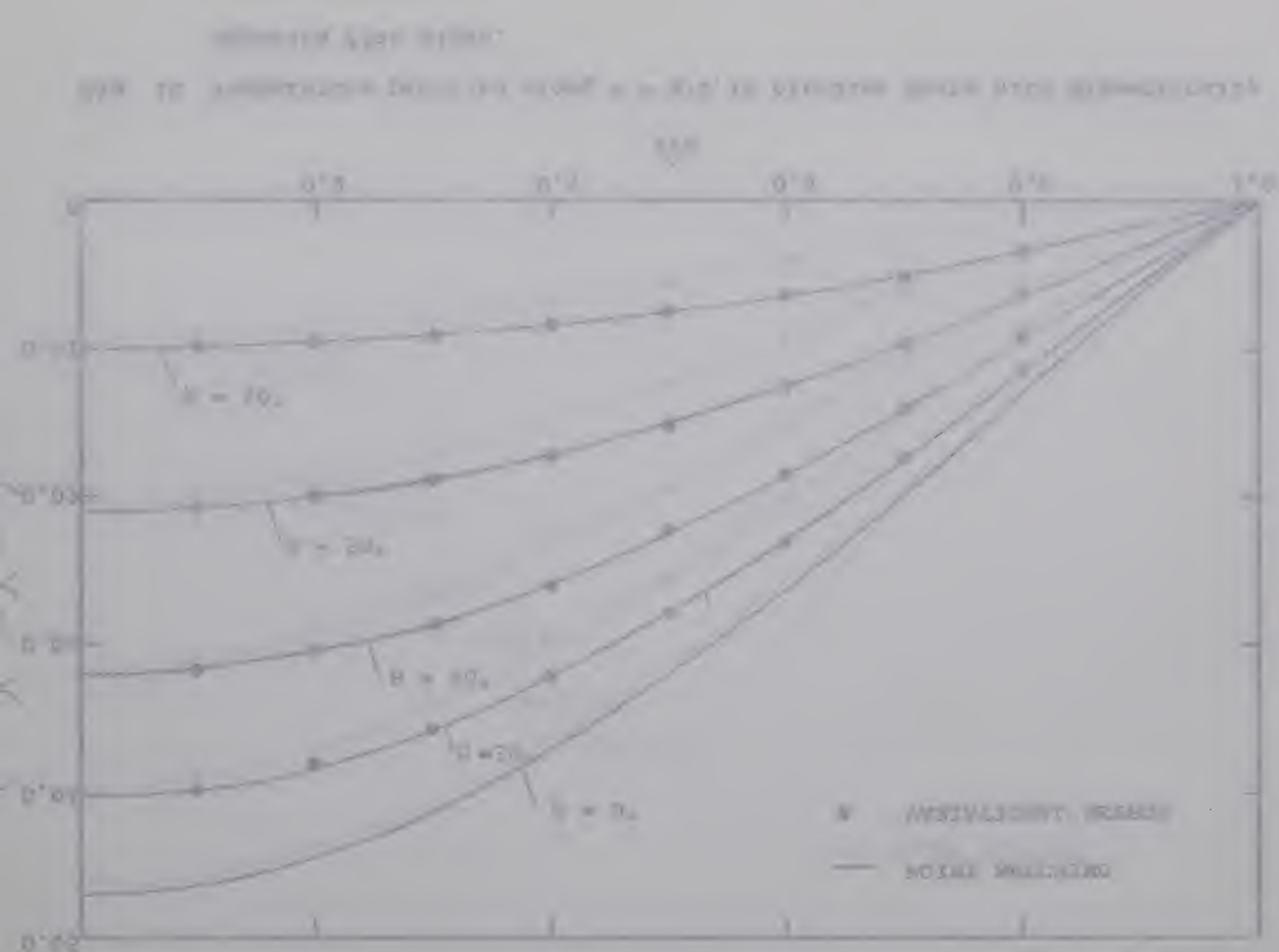
0·3
0·2
0·1
0·0
0·01
0·02
B = 10₀
B = 20₀
B = 30₀
B = 50₀
B = 70₀

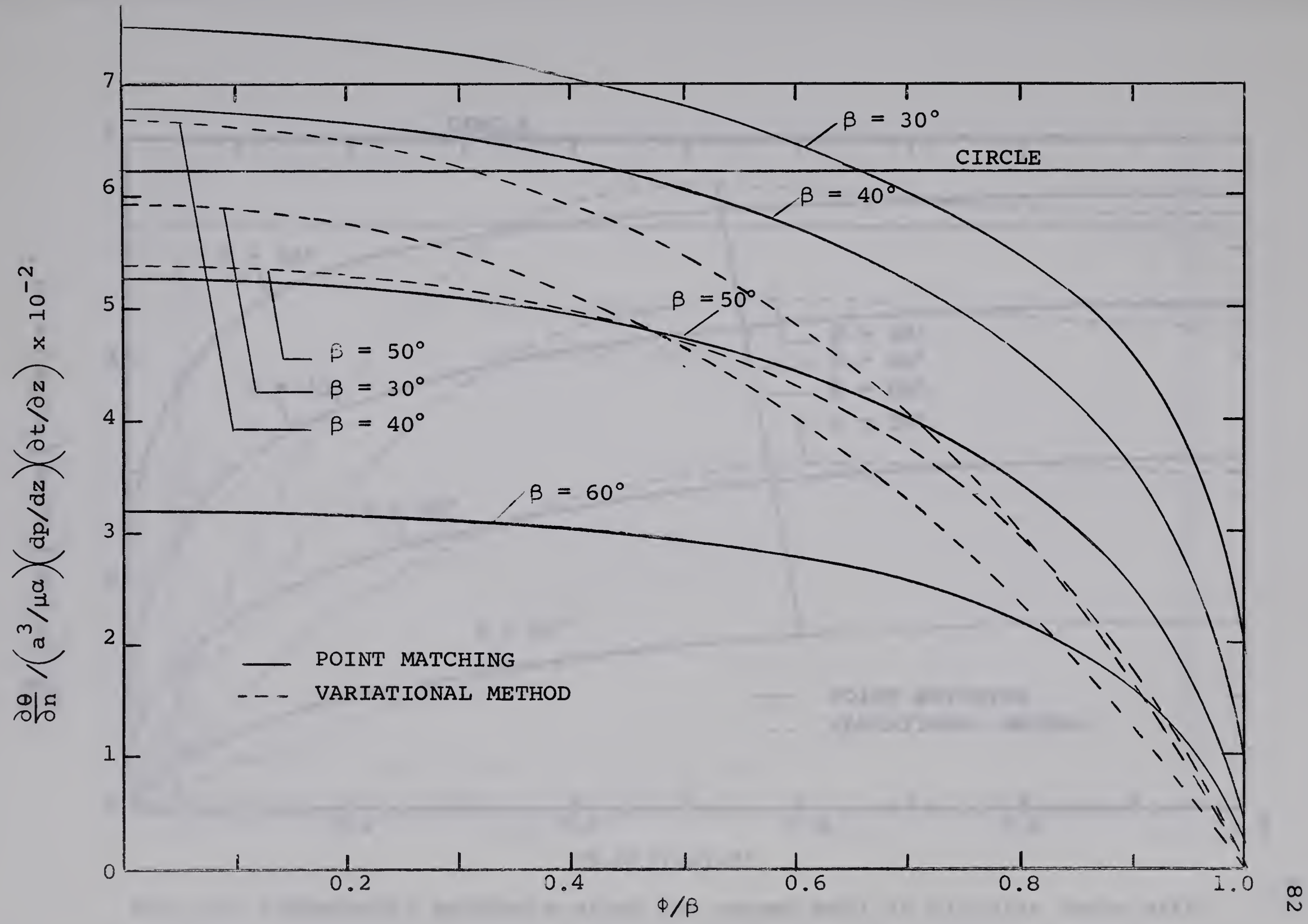

Fig. 11 Temperature gradients along the straight wall in circular ducts with diametrically opposite flat sides.

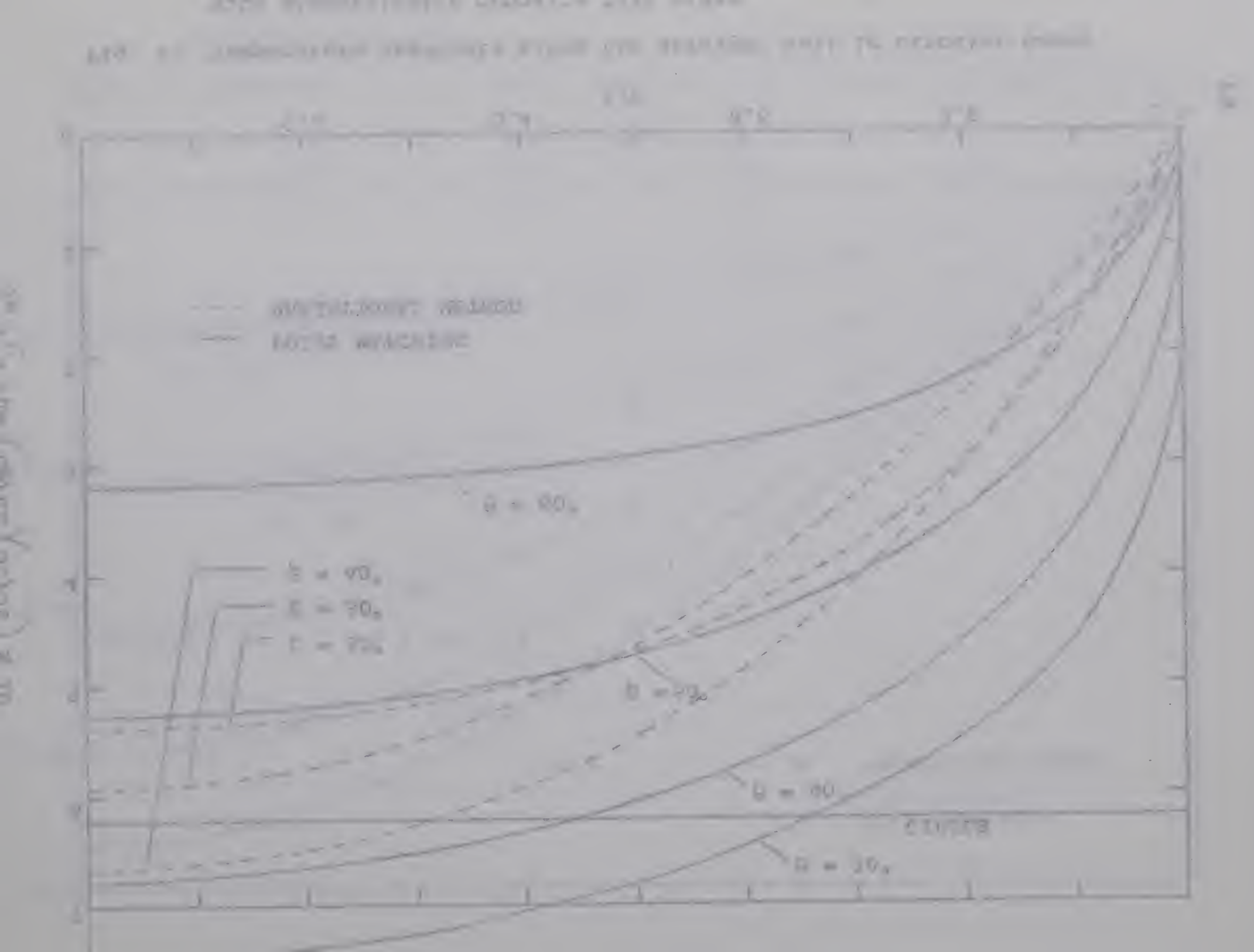
ANTISYMMETRIC MODES
MAIN MAGNETS
θ = 90°
θ = 70°
θ = 50°
θ = 30°
θ = 90
θ = 70
θ = 50
θ = 30

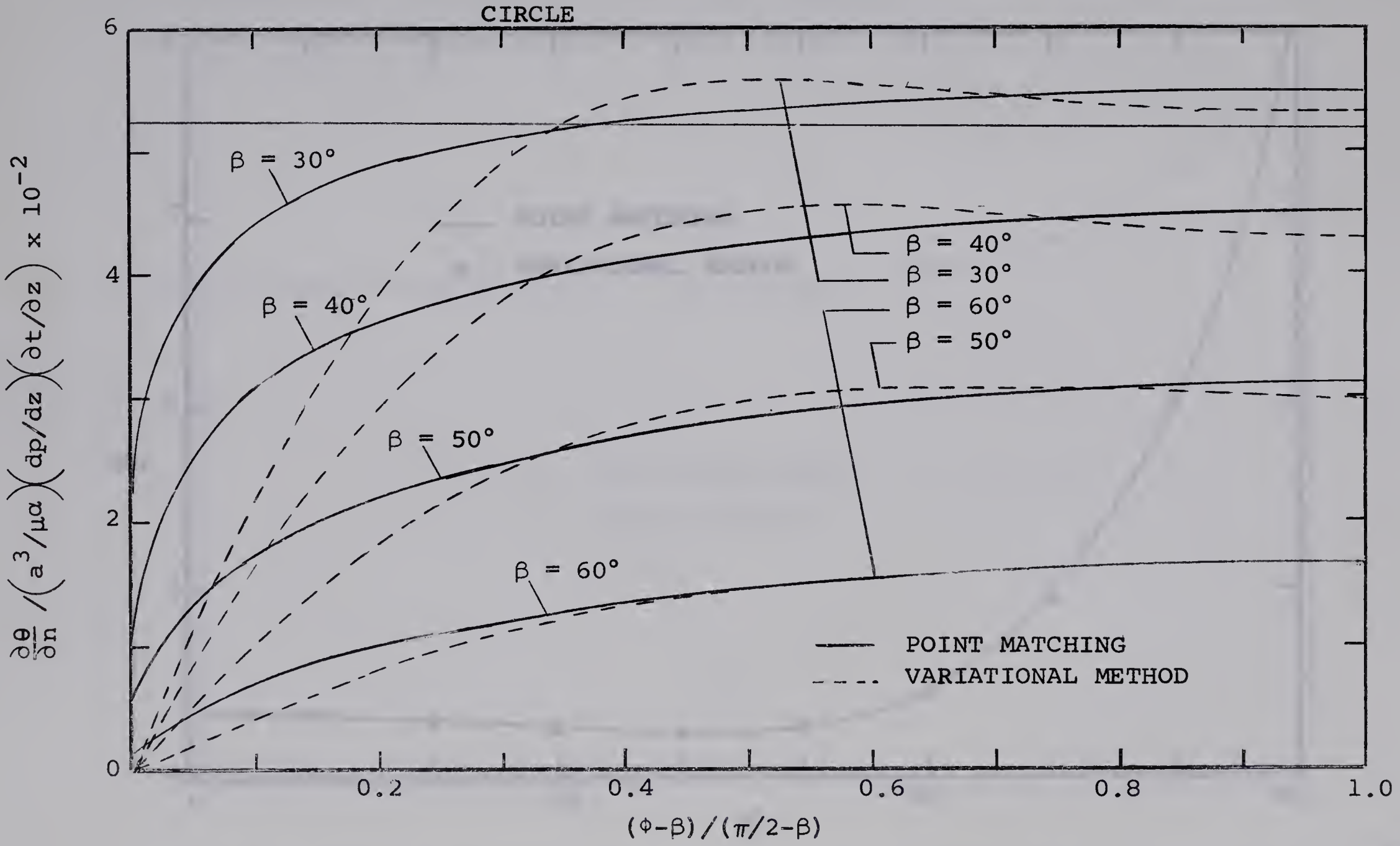

Fig. 12 Temperature gradients along the curved wall in circular ducts with diametrically opposite flat sides.


δ = 40°
δ = 20°
δ = 10°
δ = 30°
δ = 90°

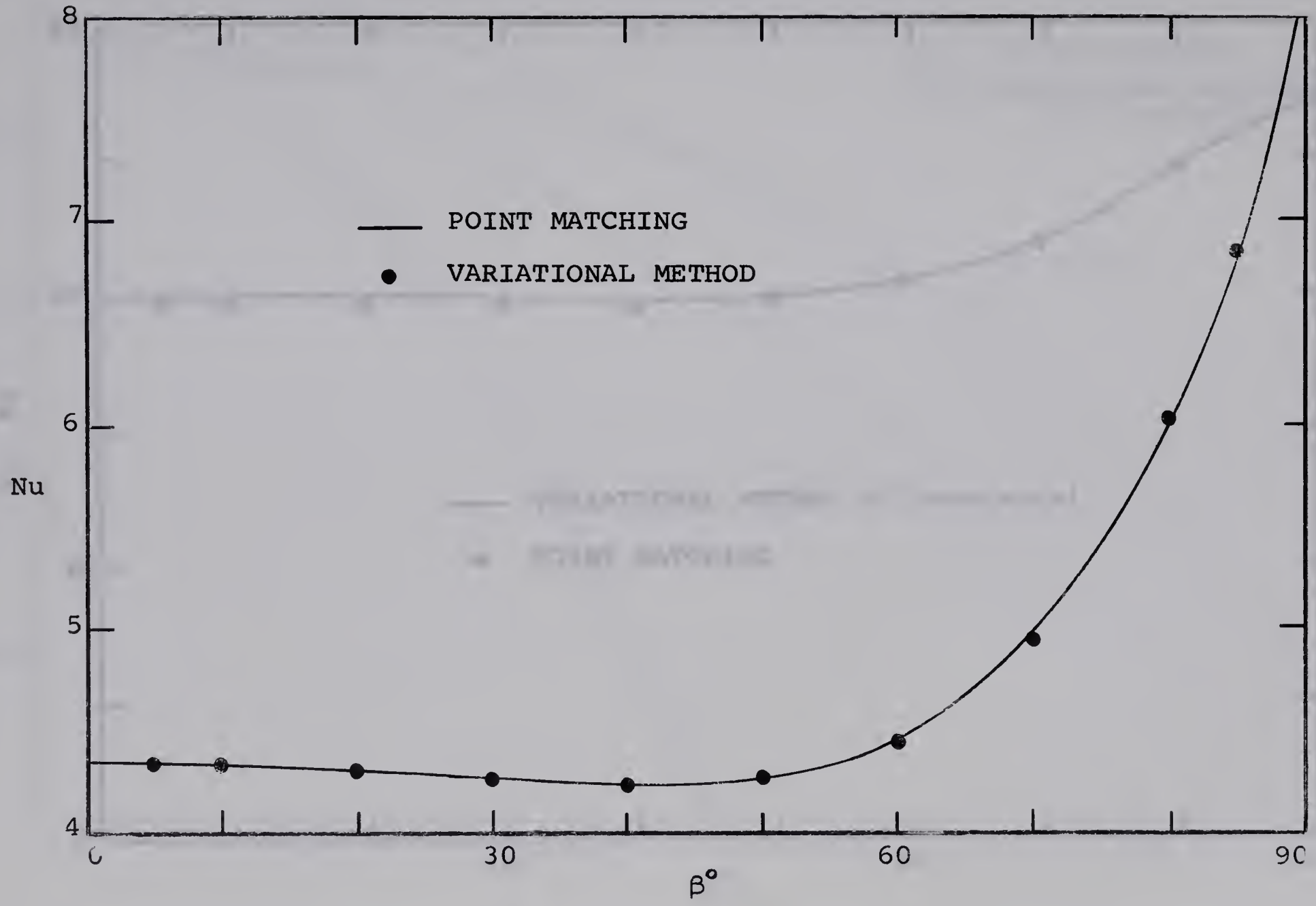

Fig. 13 Limiting Nusselt numbers for circular ducts with diametrically opposite flat sides.

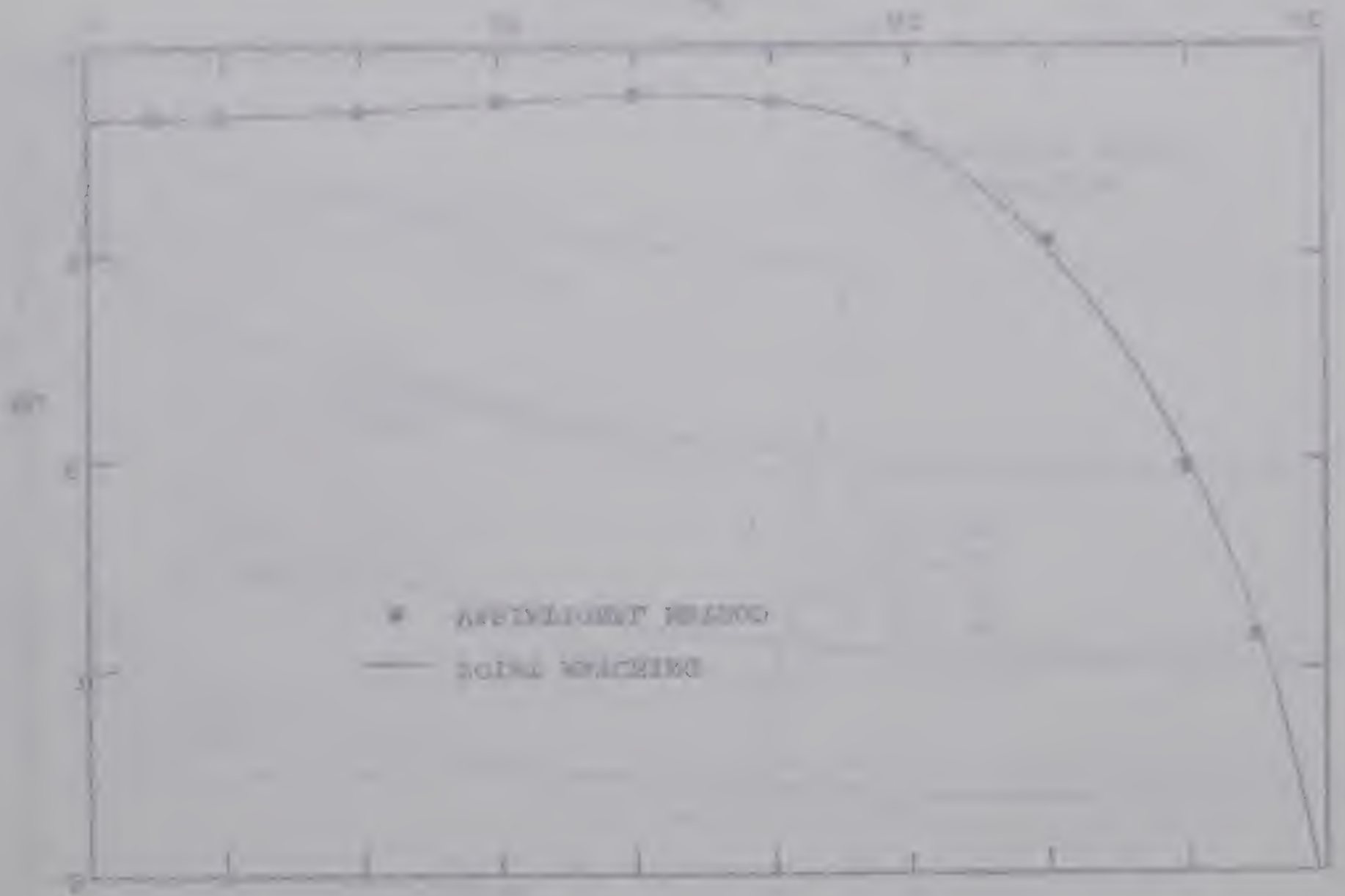

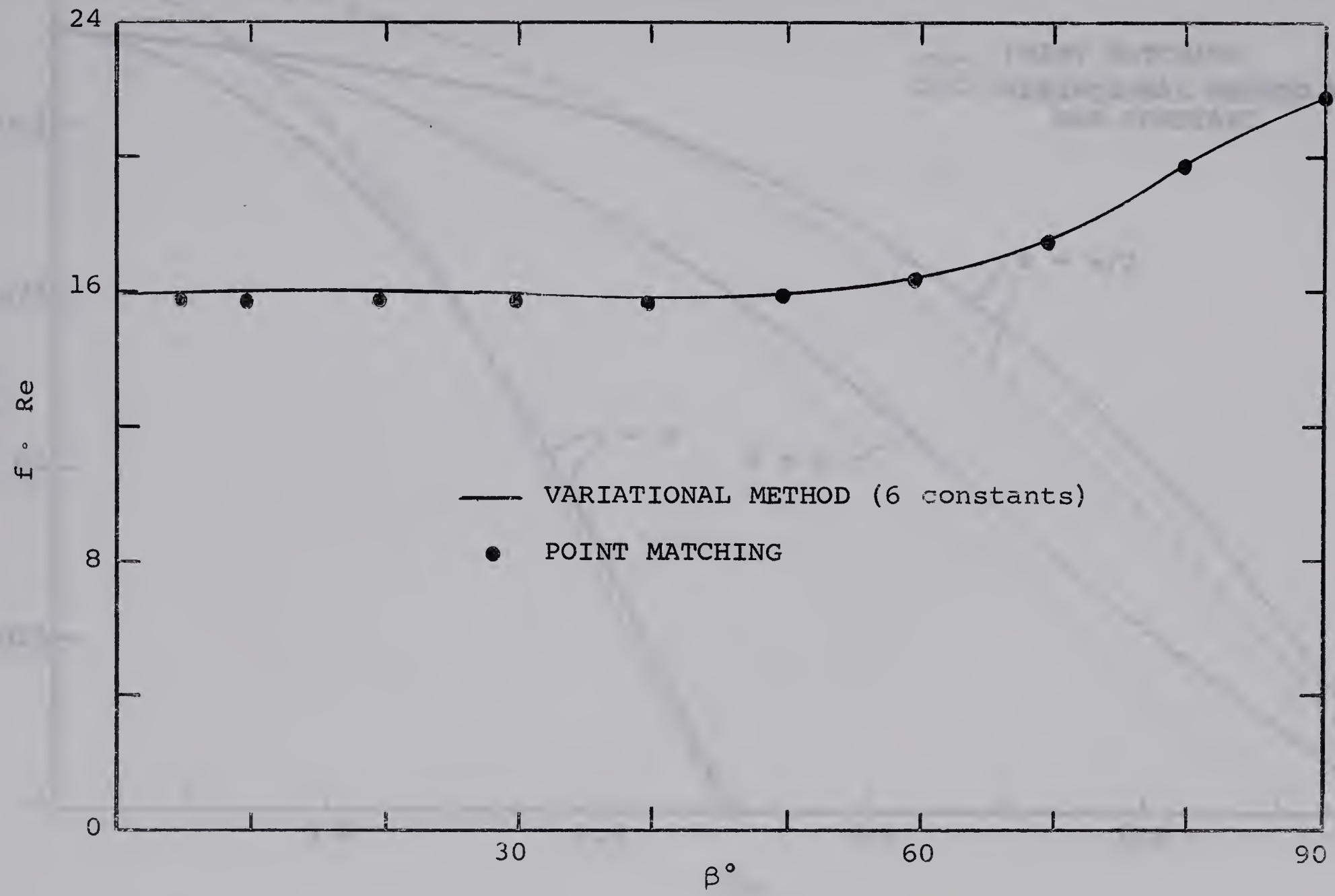

Fig. 14 Friction factor-Reynolds number results for circular ducts with diametrically opposite flat sides.

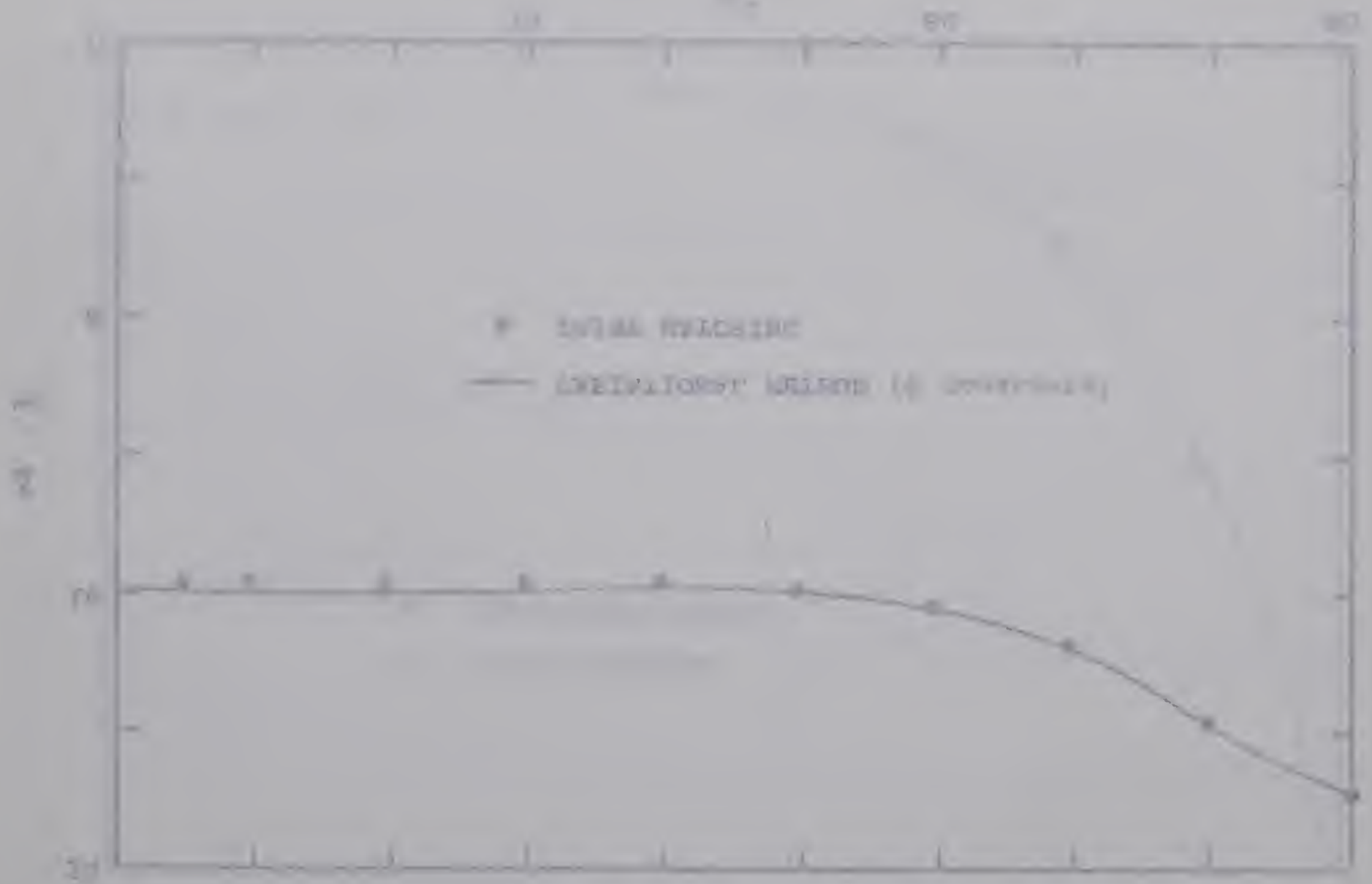

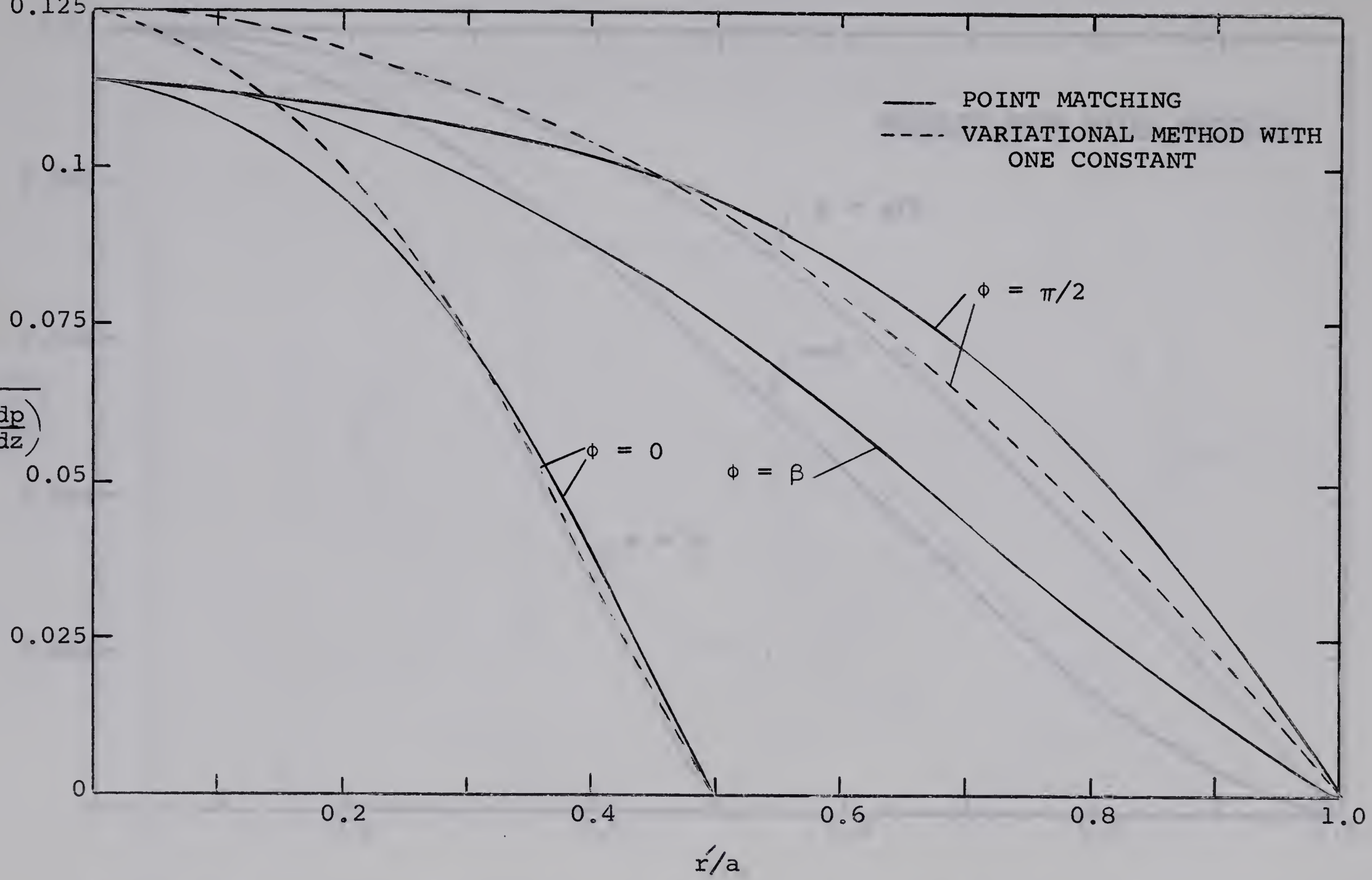

Fig. 15 Velocity distribution along $\phi = 0$, $\beta = \pi/3$ and $\phi = \pi/2$ in circular duct with diametrically opposite flat sides.

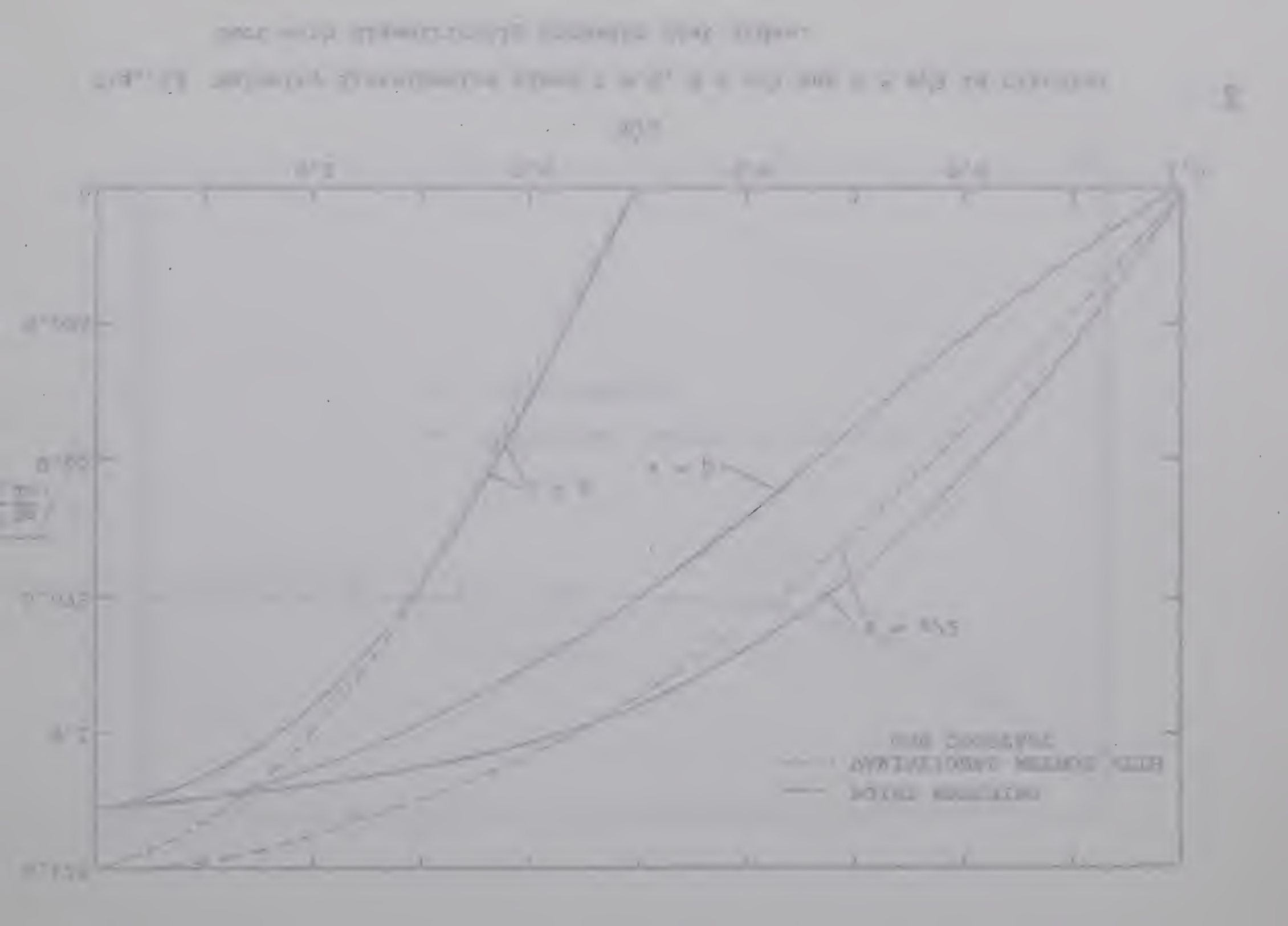

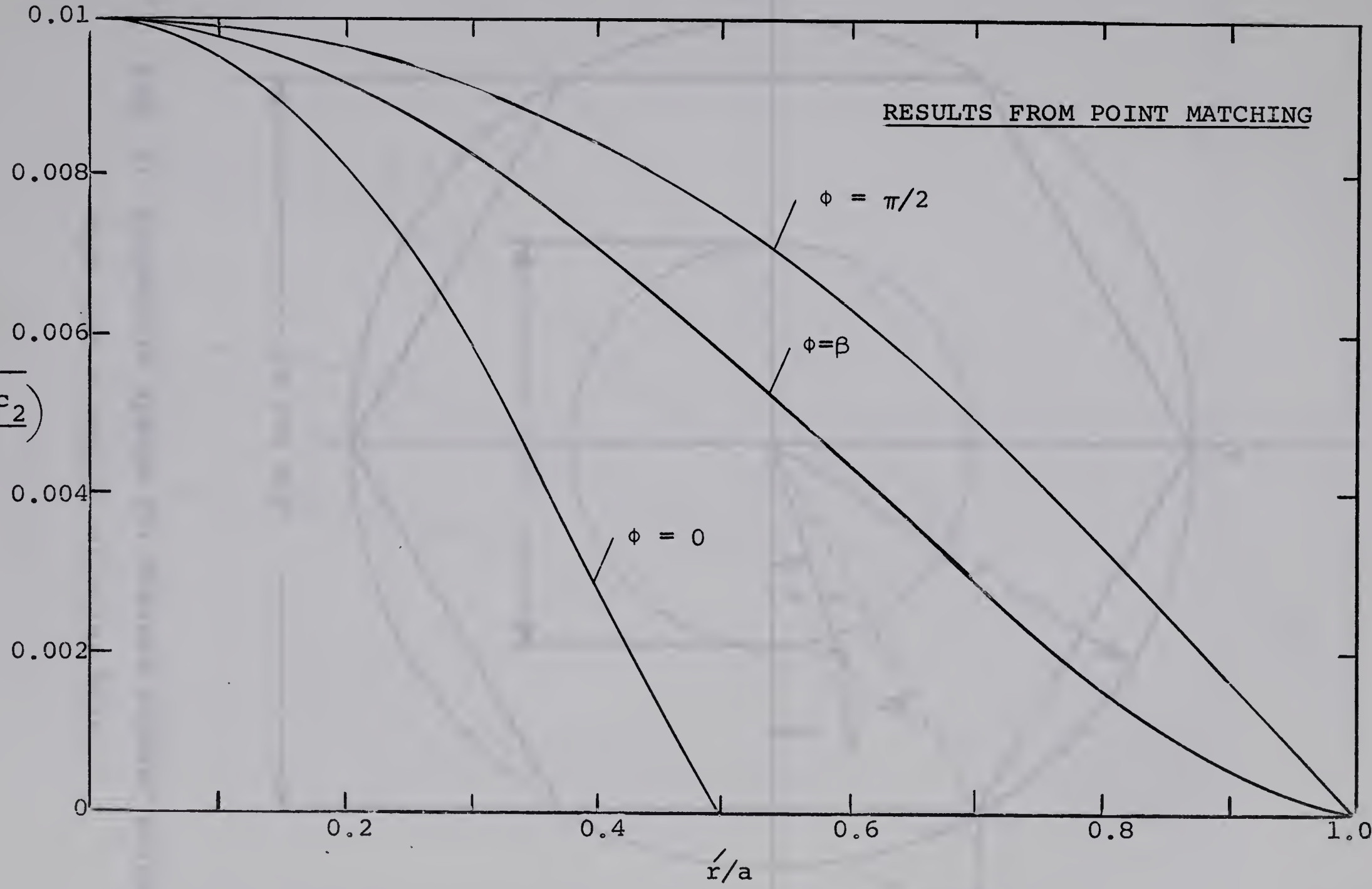

Fig. 16 Temperature profiles along $\phi = 0$, $\beta = \pi/3$ and $\phi = \pi/2$ in circular ducts with diametrically opposite flat sides.

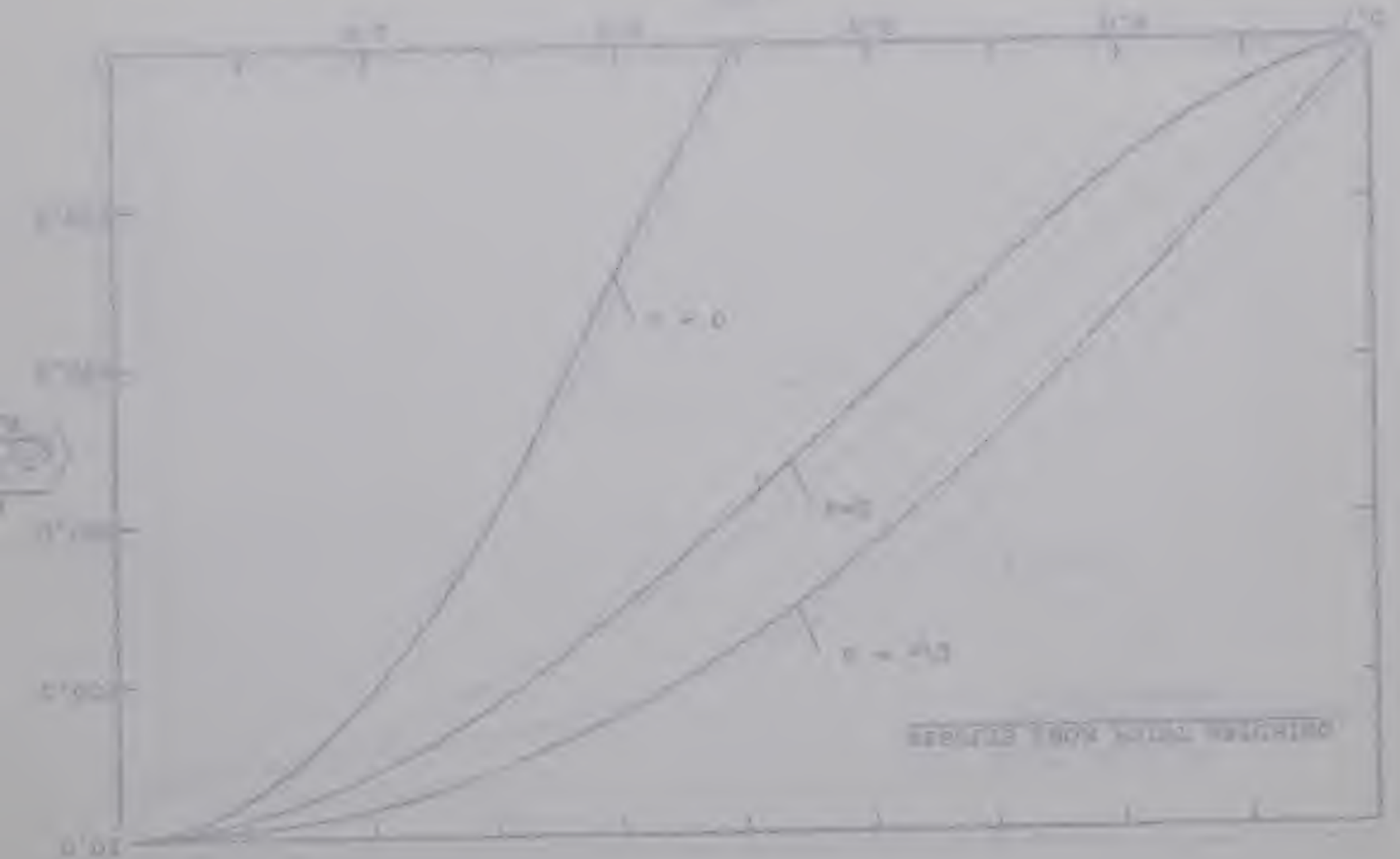
n = 0
n=1
n = 4/3

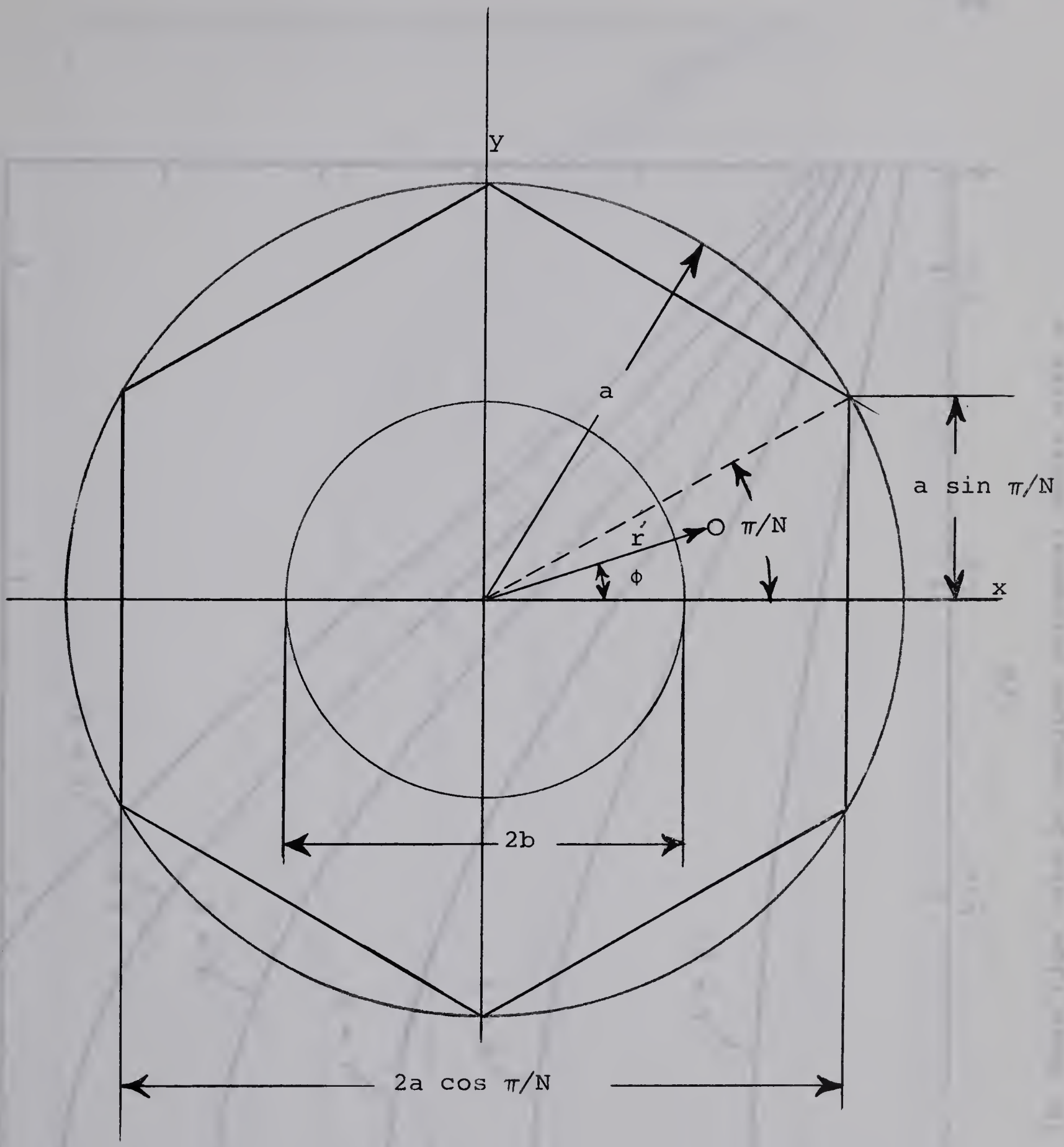

Fig. 17 Coordinate system for N-sided regular polygonal duct with a central circular hole.

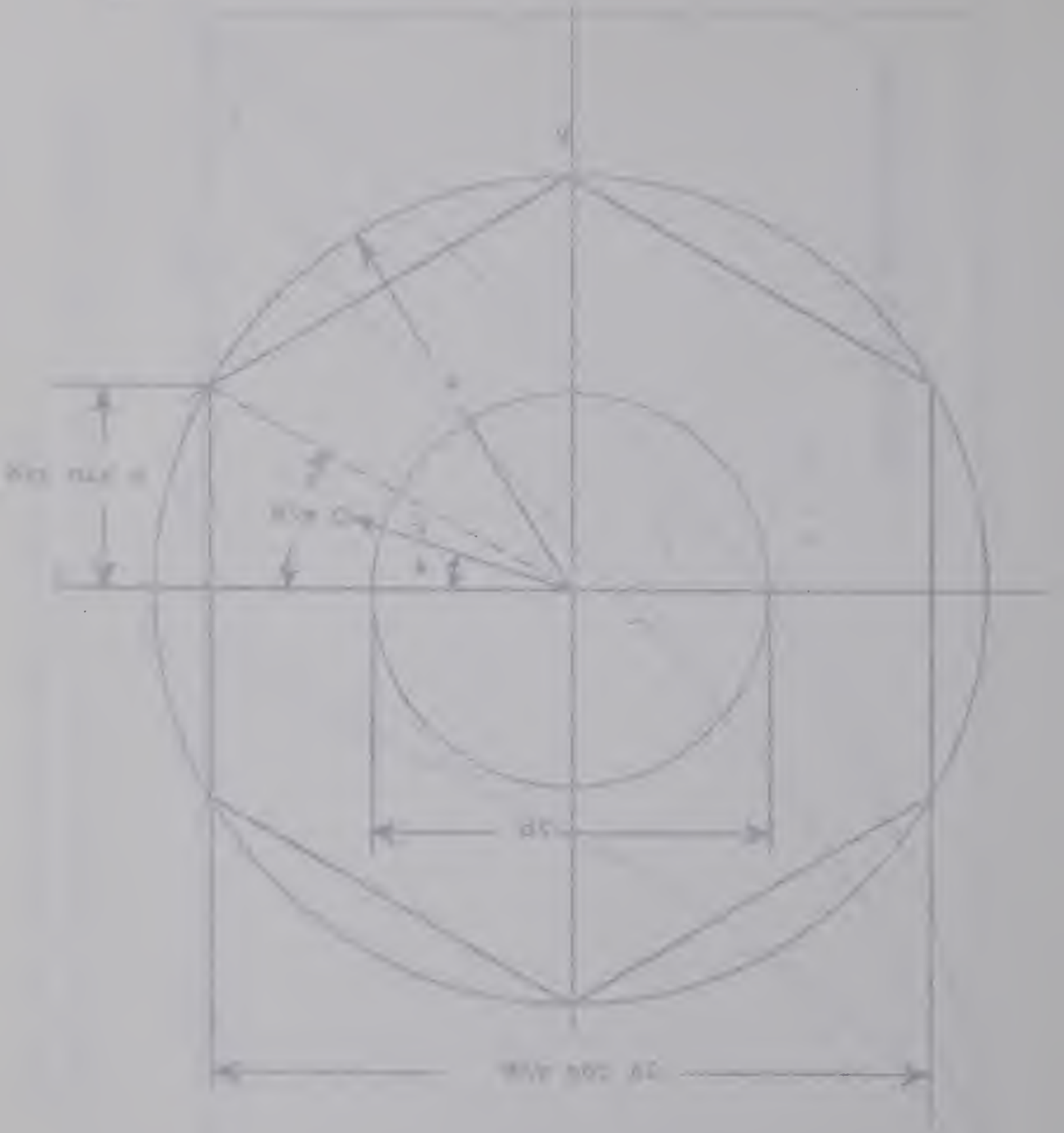

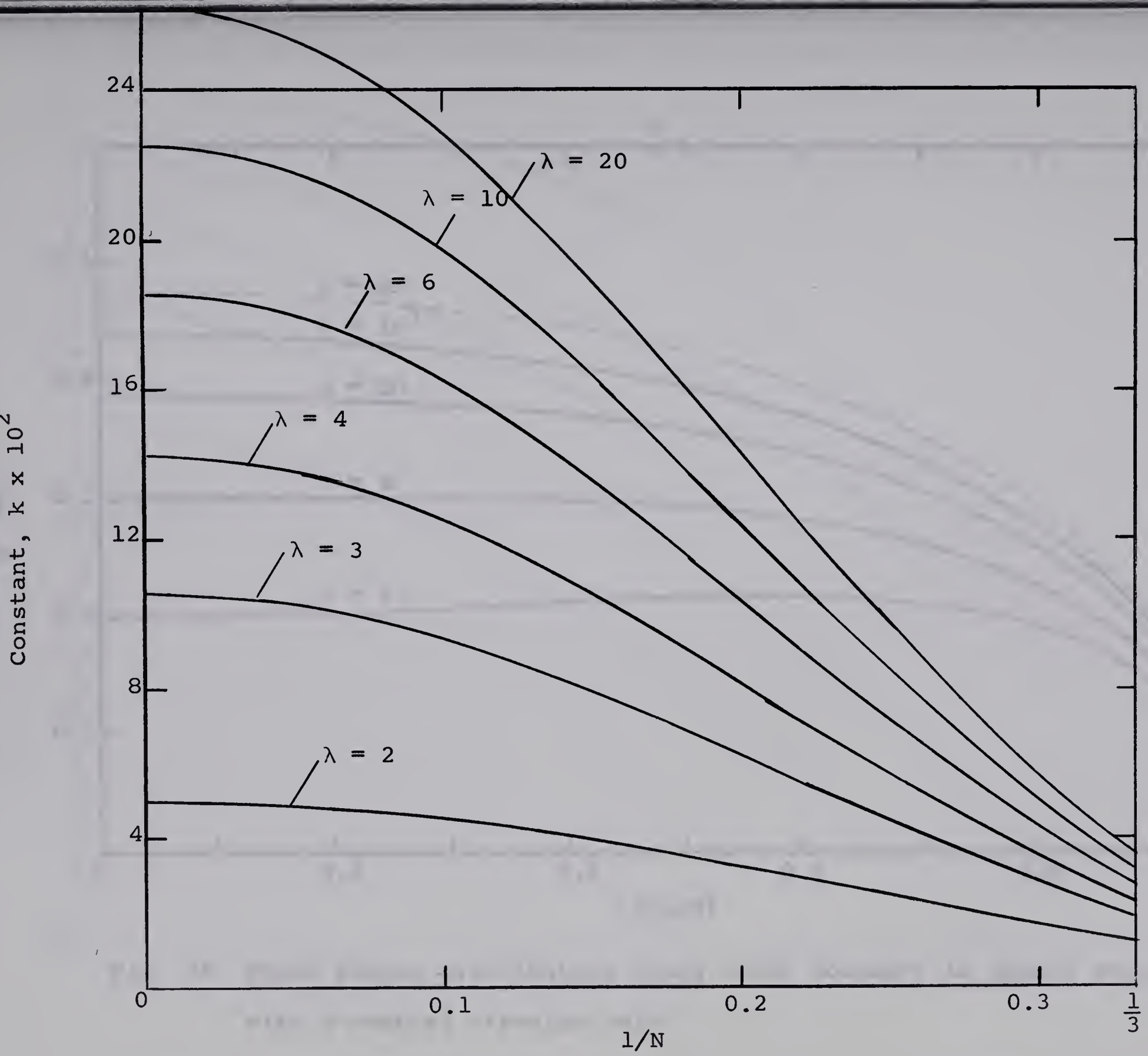

Fig. 18 Mass flow rate in regular polygonal ducts with a central circular hole.

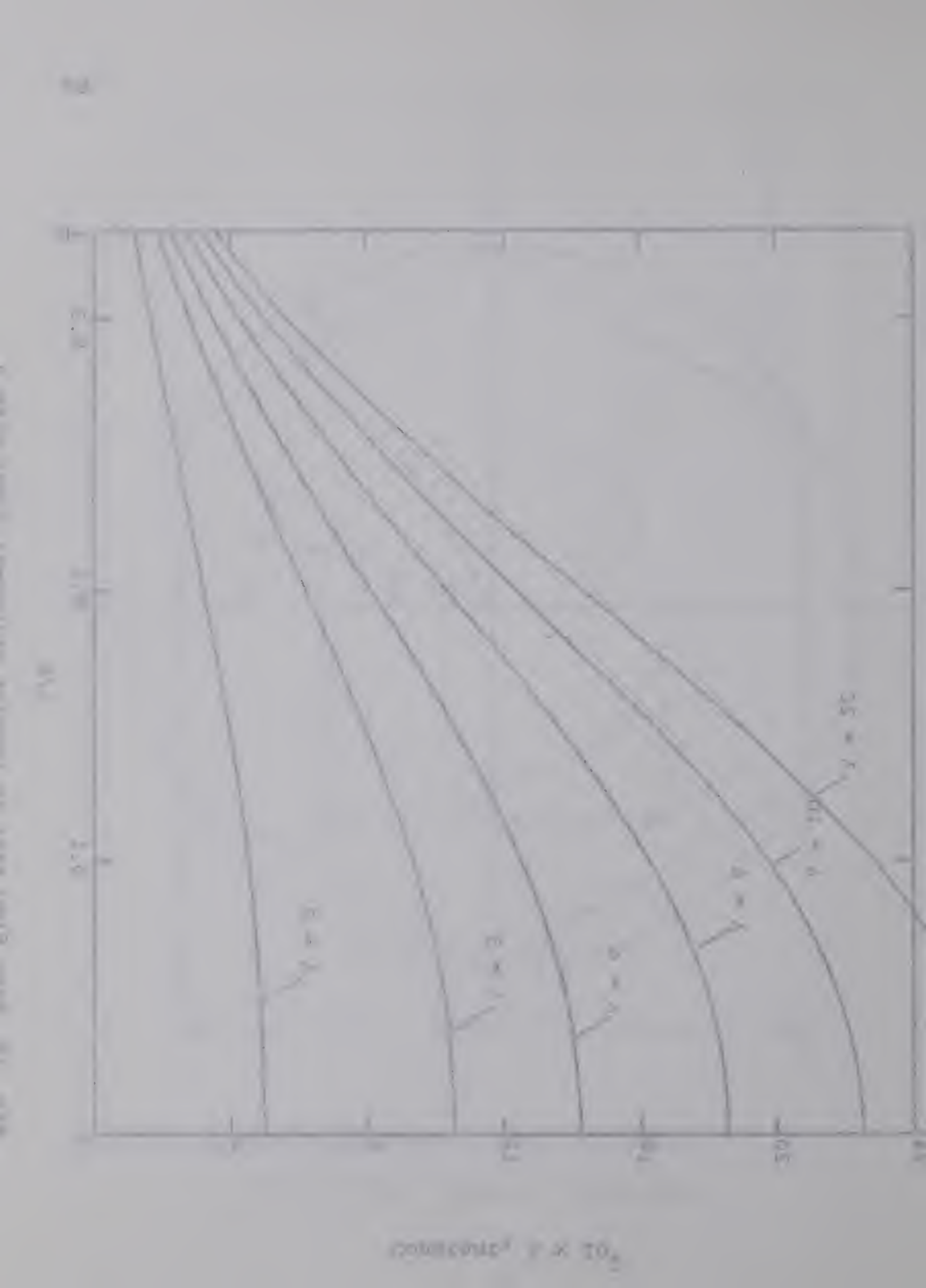

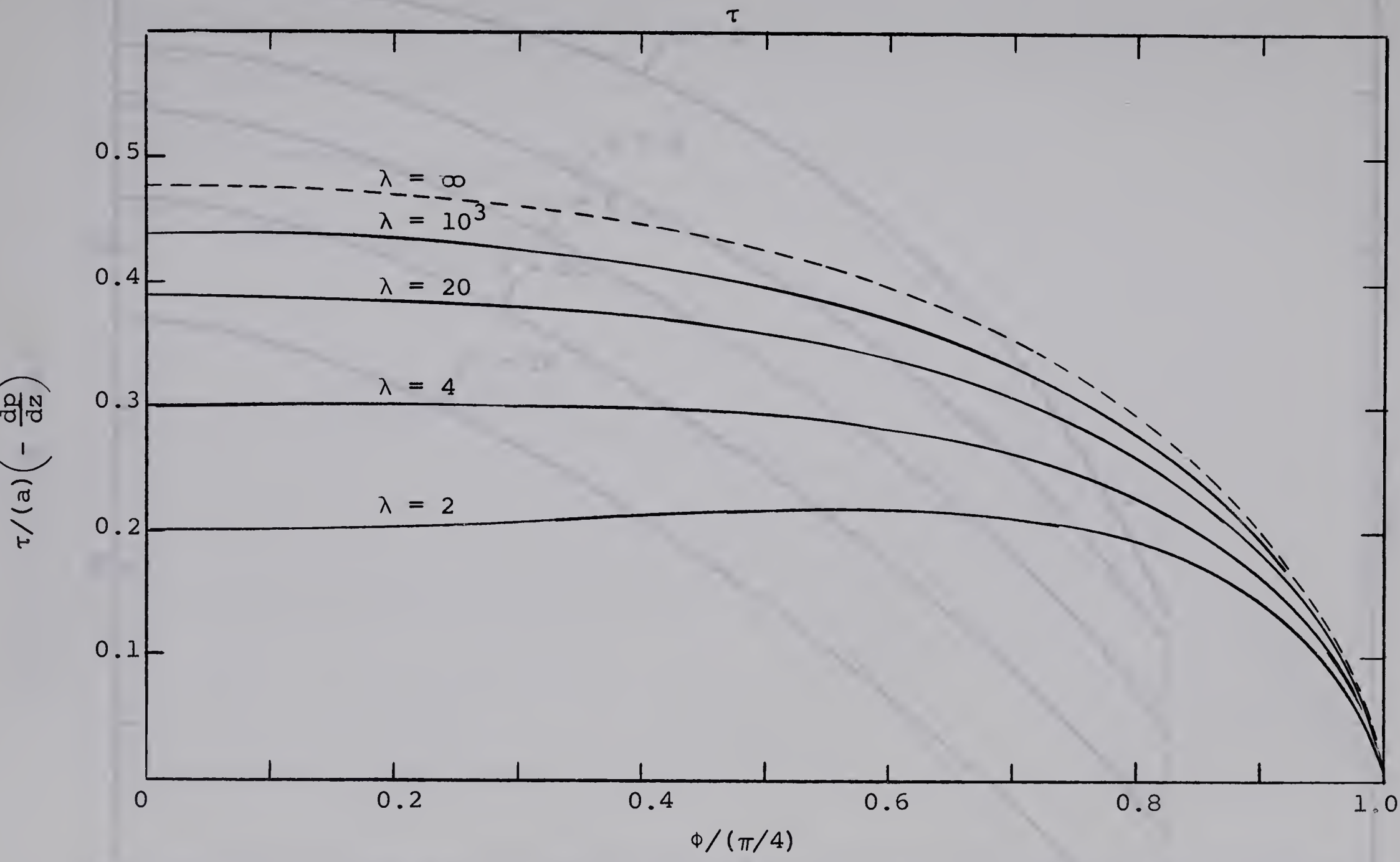

Fig. 19 Shear stress distribution along outer boundary in square ducts with a central circular hole.

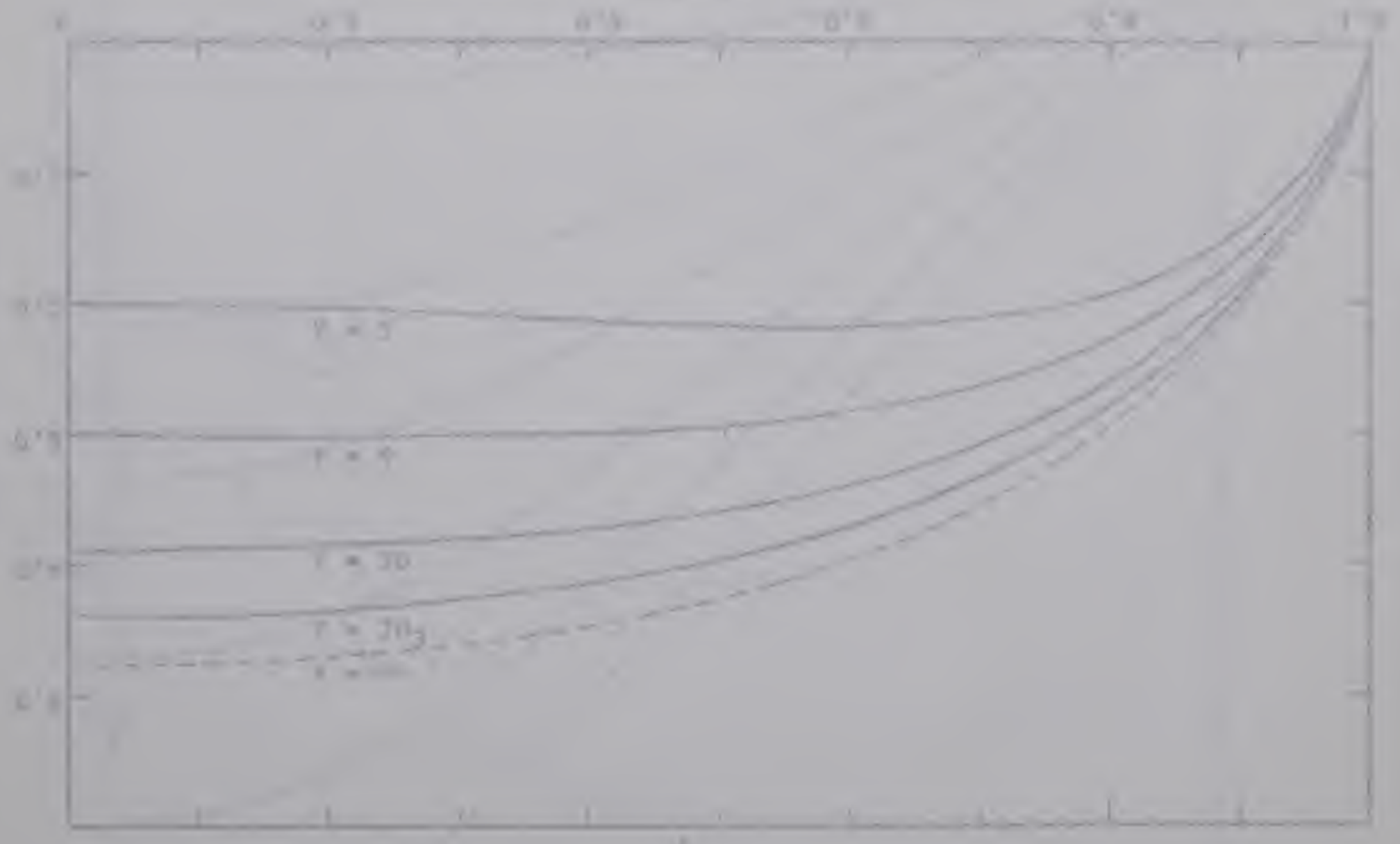
r = 5
r = 9
r = 20
r = 200

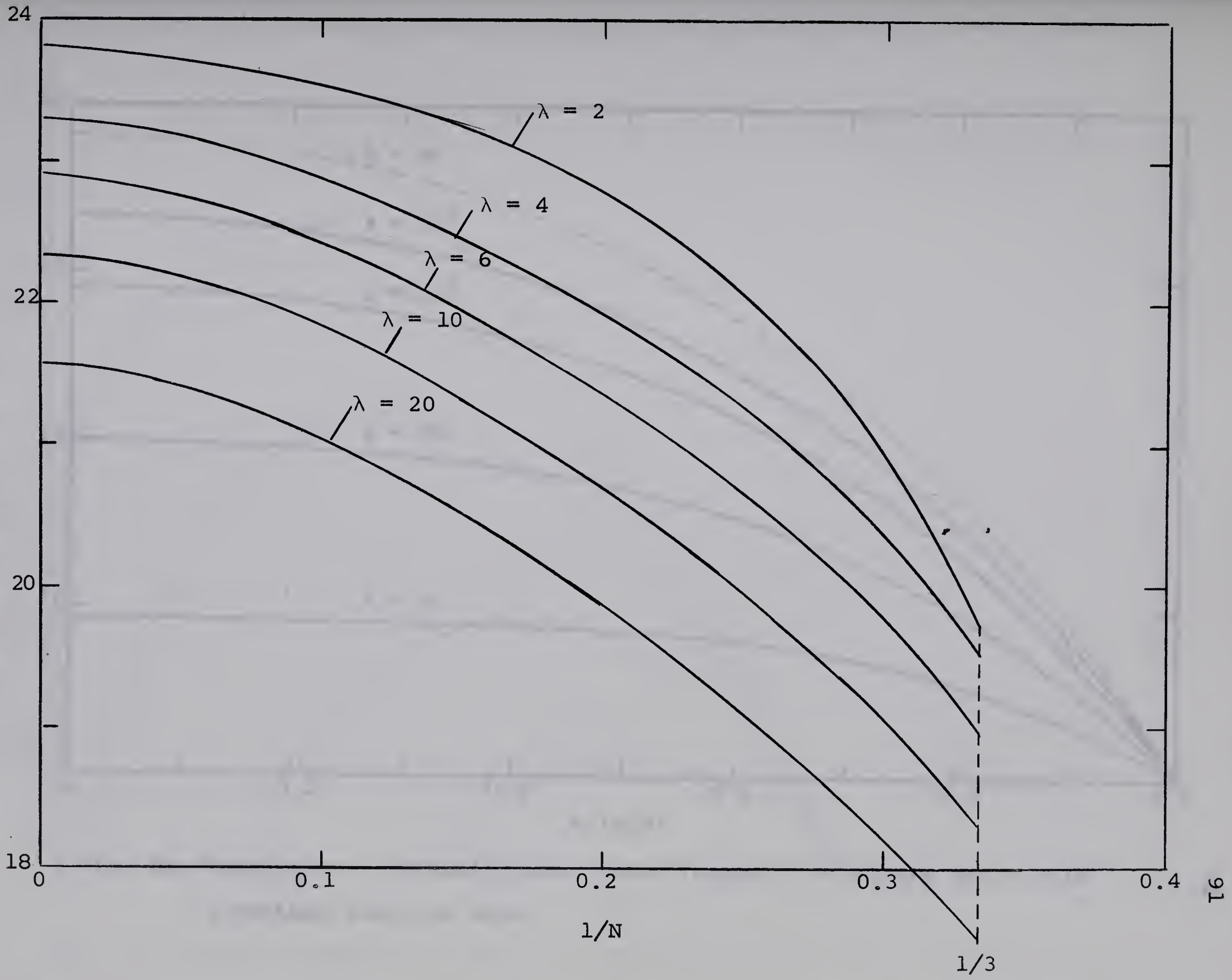

Fig. 20 Friction factor-Reynolds number results for regular polygonal ducts with a central circular hole.

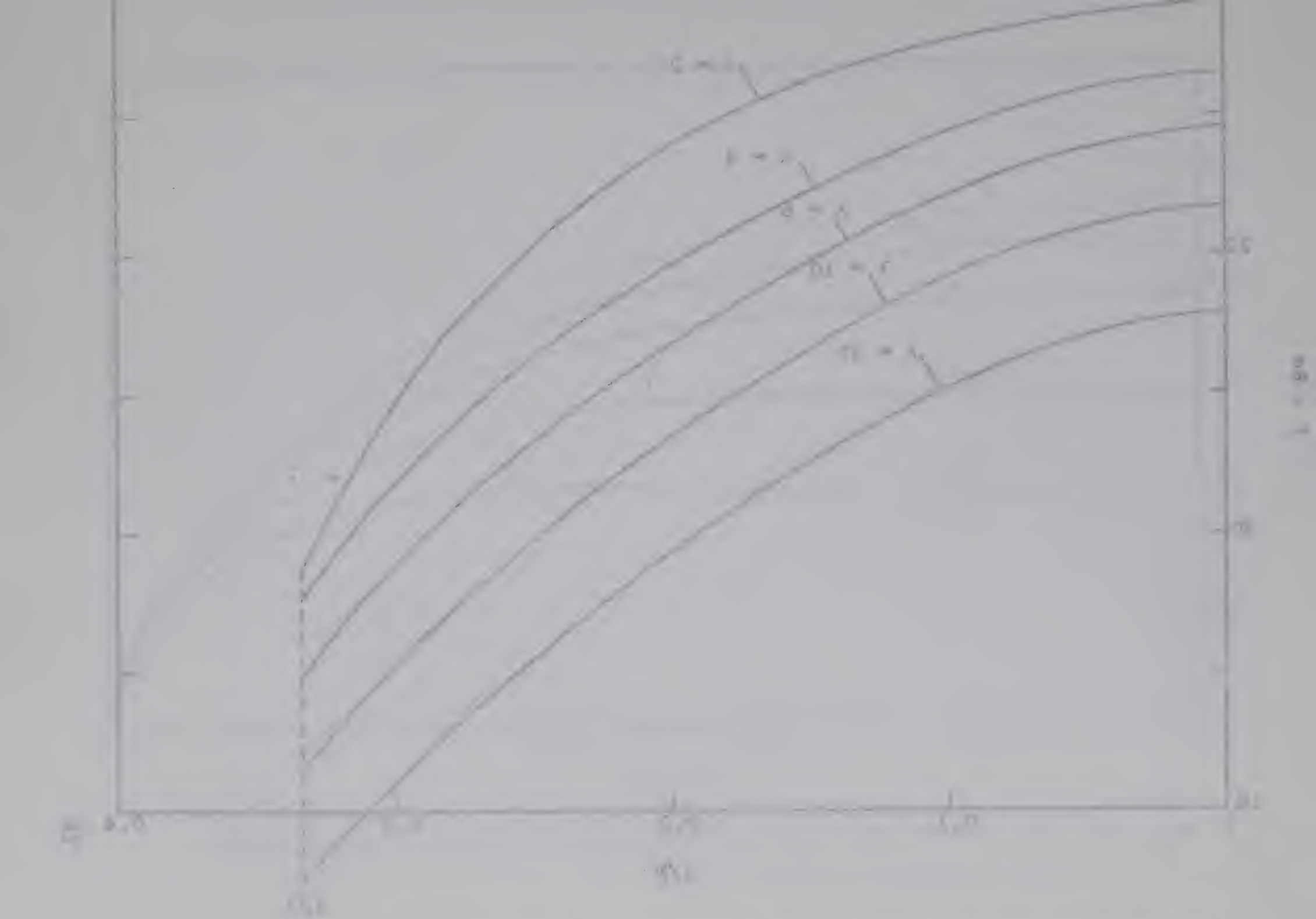

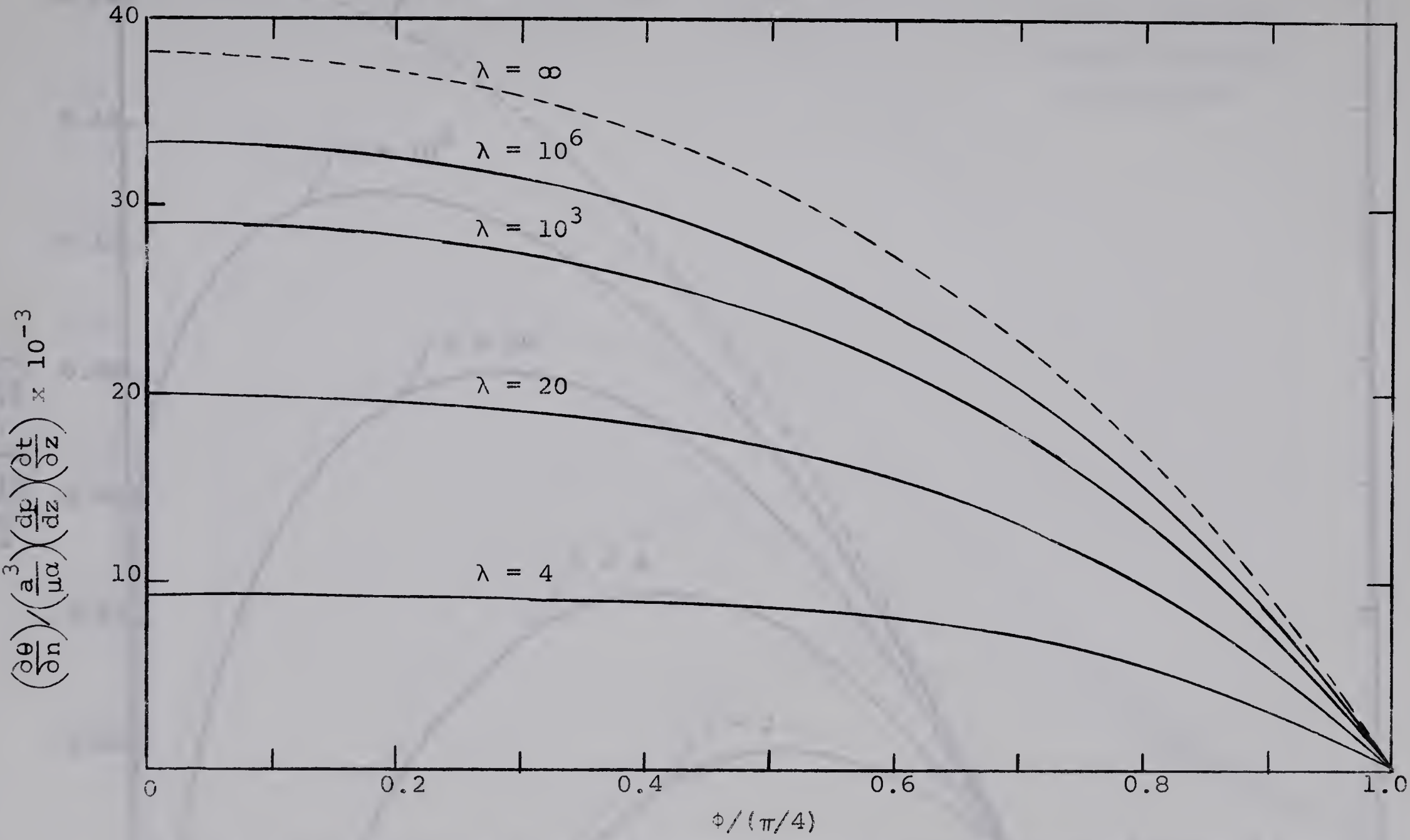

Fig. 21 Temperature gradients along outer boundary in square ducts with a central circular hole.

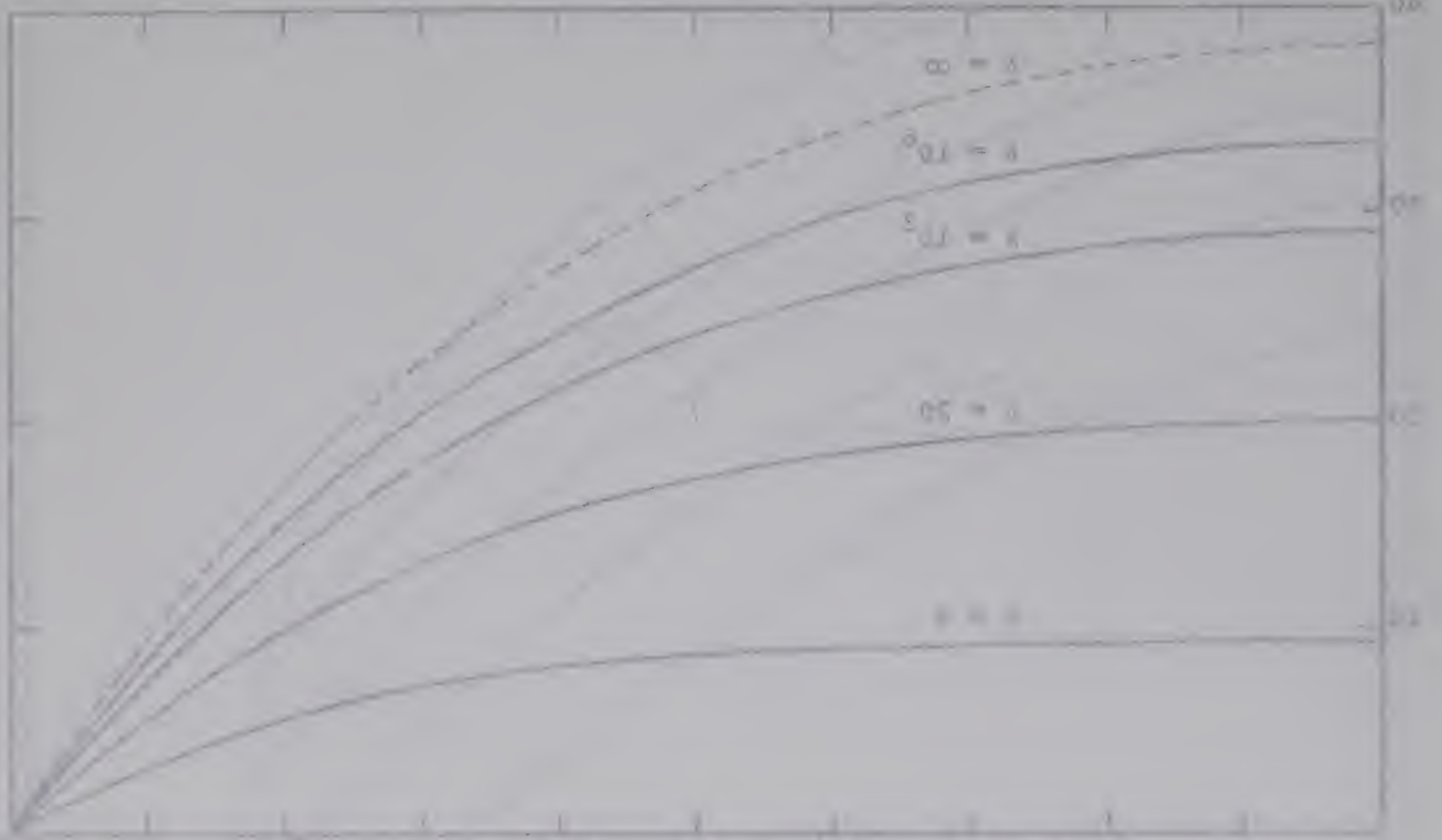
$\gamma = \infty$
$\gamma = 10$
$\gamma = 5$
$\gamma = 2$
$\gamma = 1$

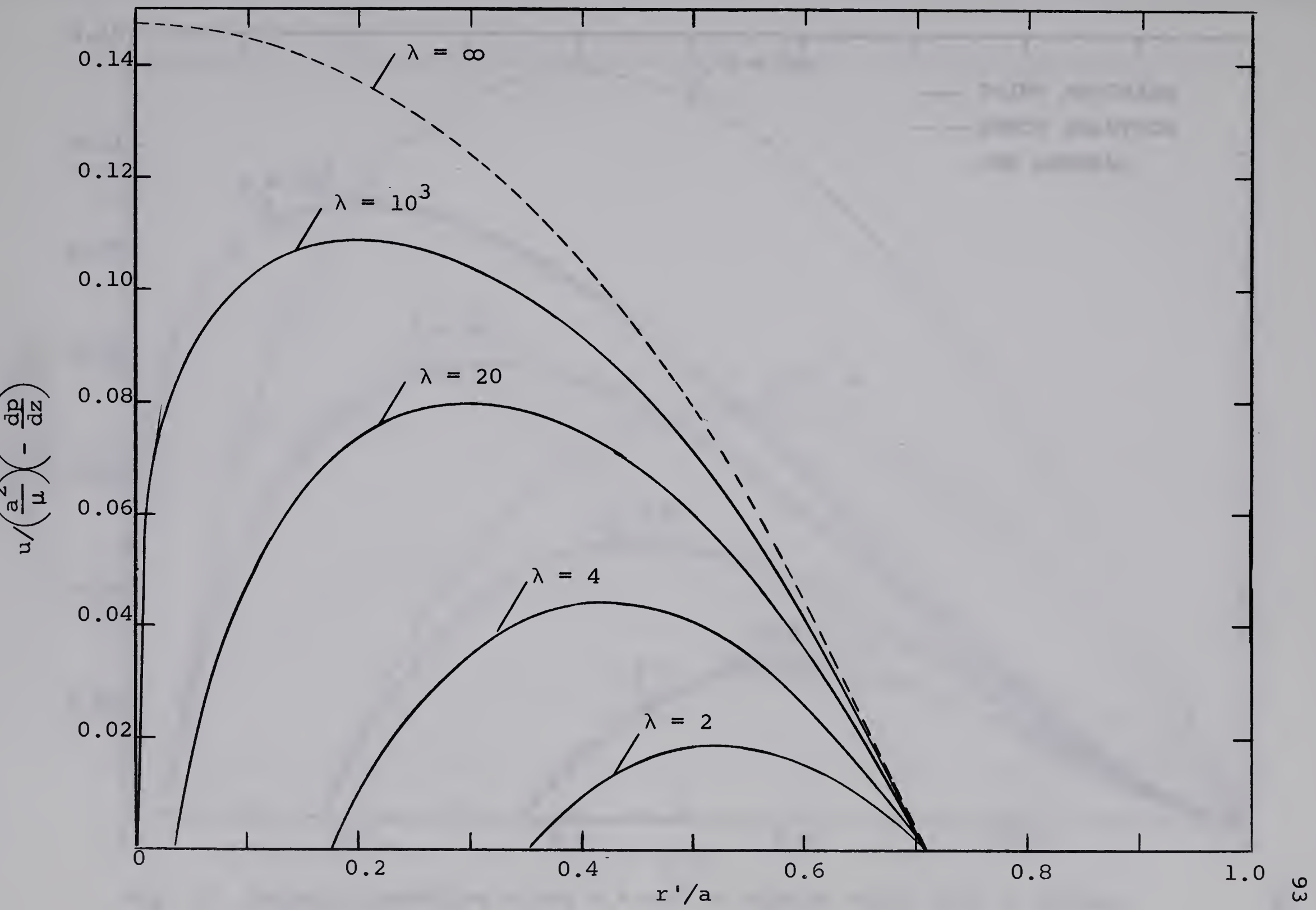

Fig. 22 Velocity profiles along $\phi = 0$ in square ducts with a central circular hole.

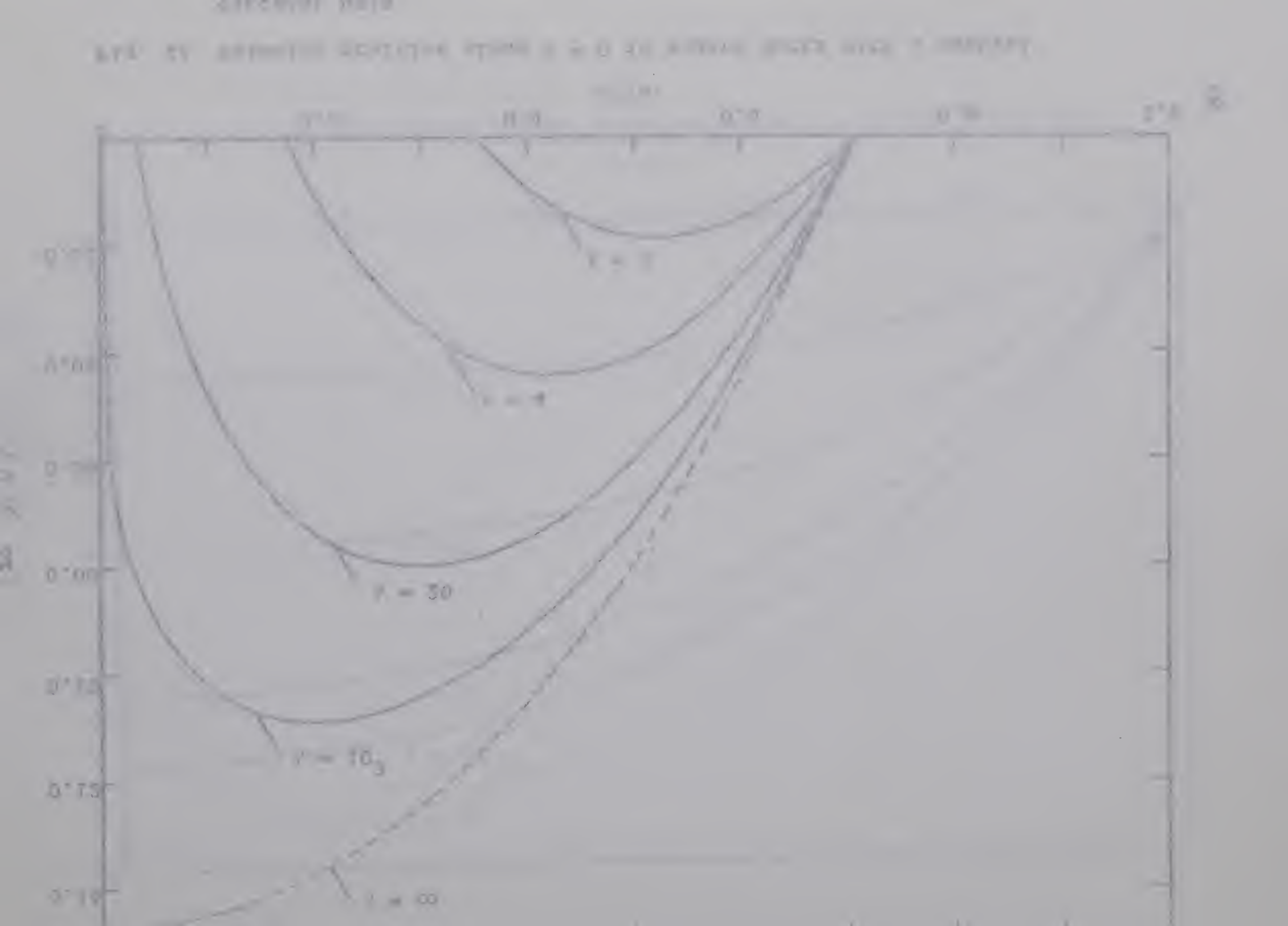
γ = 1
γ = 4
γ = 30
γ = 10₃
γ = ∞

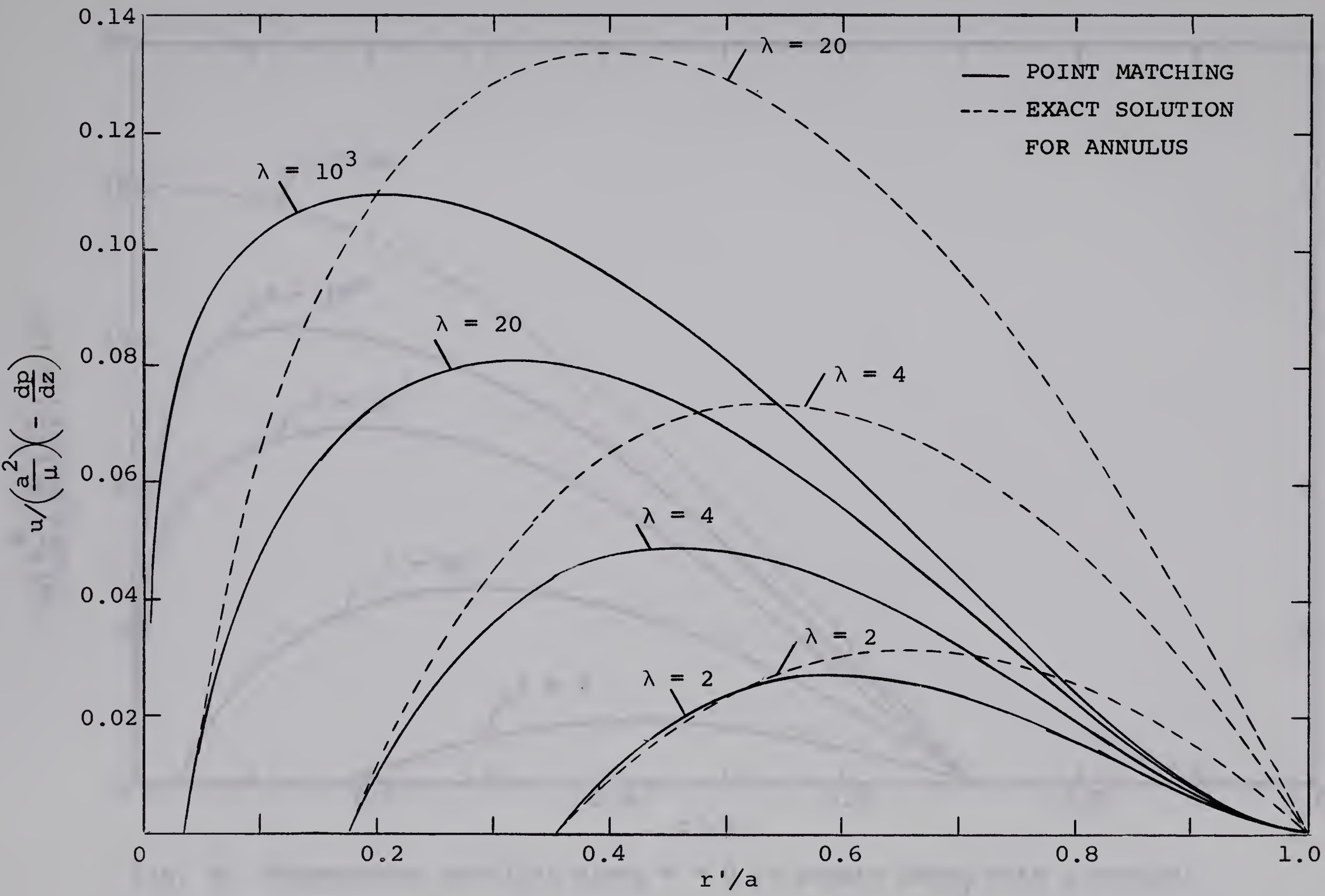

Fig. 23 Velocity profiles along $\Phi = \pi/4$ in square ducts with a central circular hole.

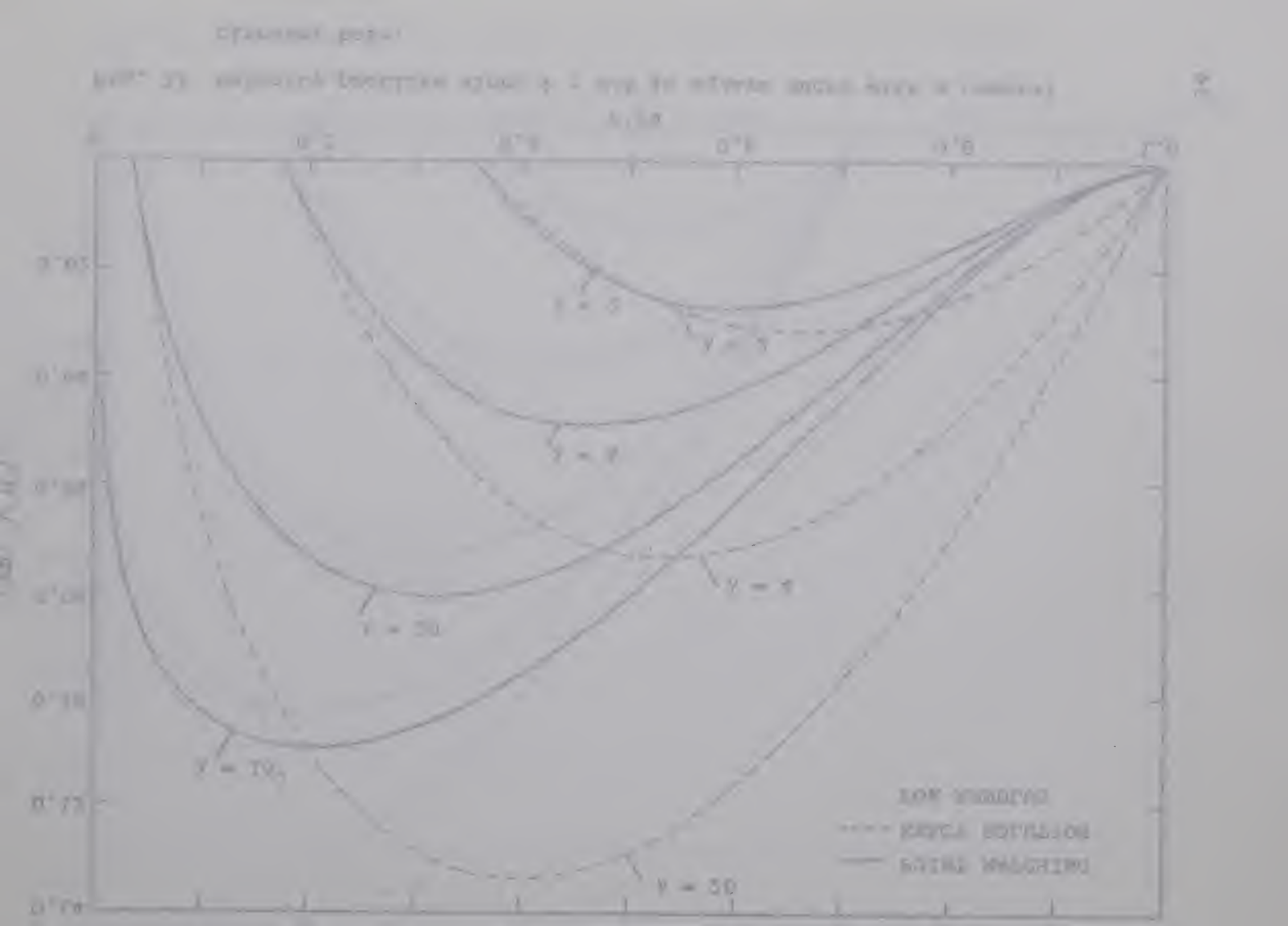
γ = 0
γ = 1
γ = 2
γ = 5
γ = 10
γ = 30

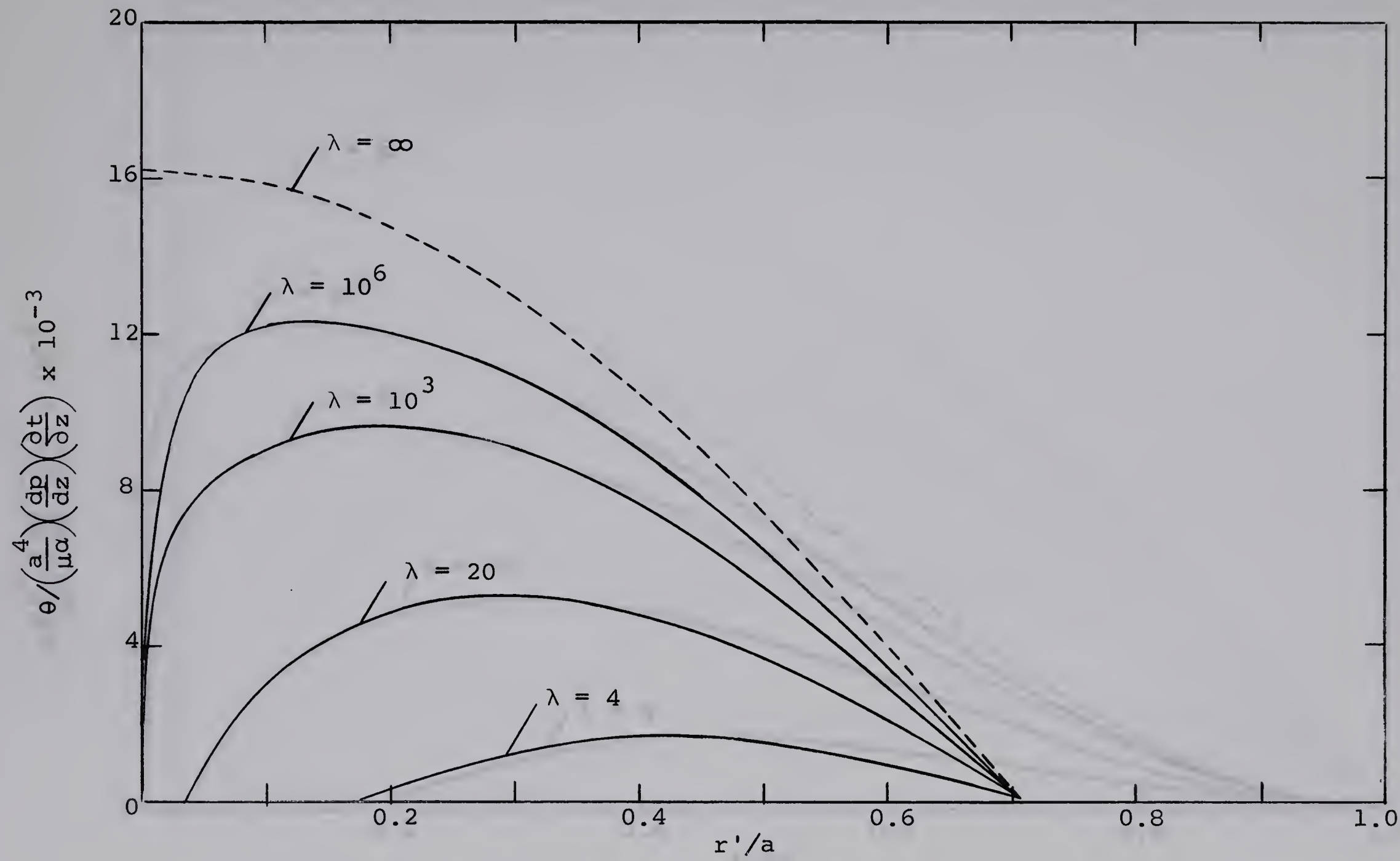

Fig. 24 Temperature profiles along $\phi = 0$ in square ducts with a central circular hole.

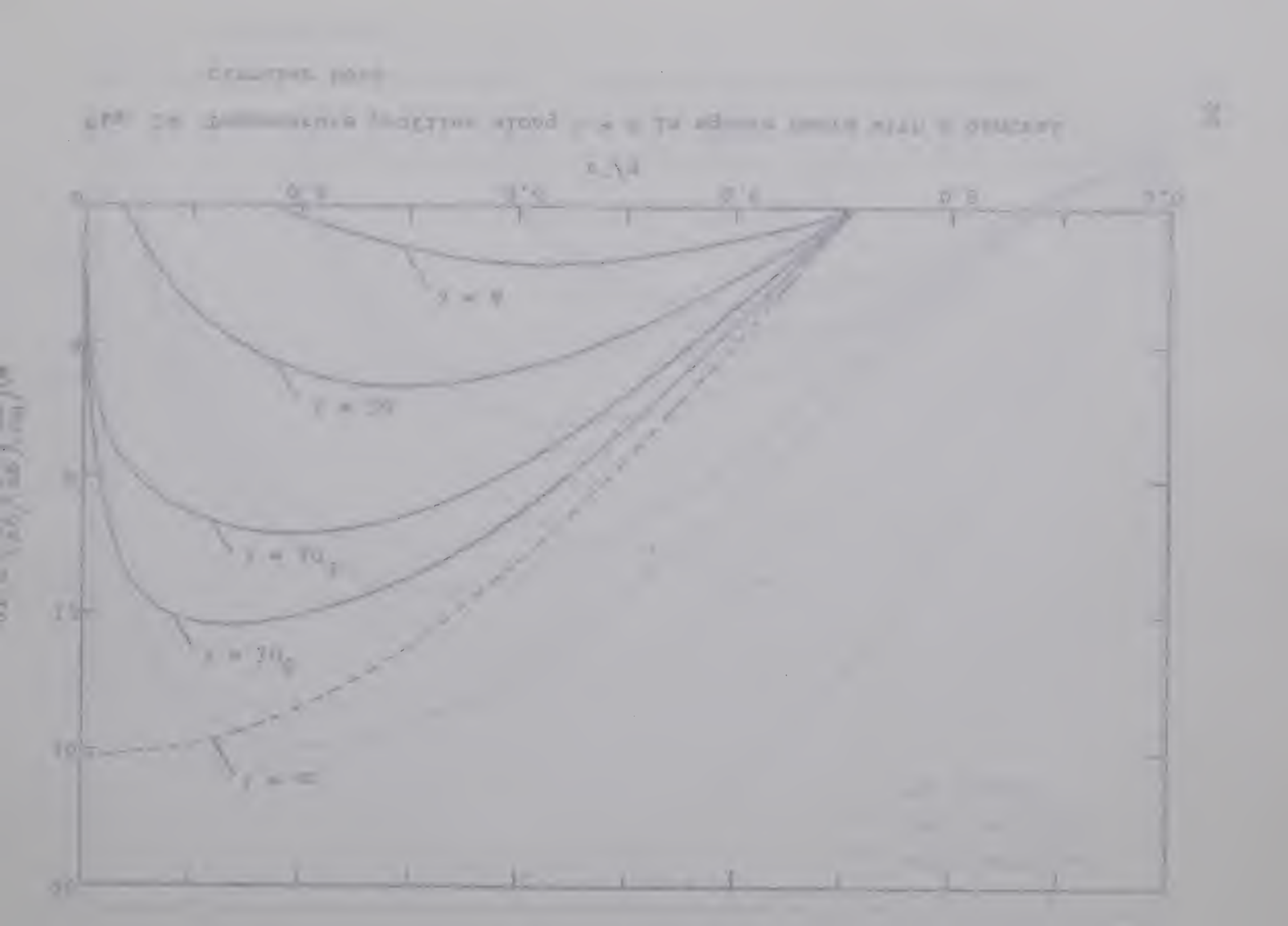
$\gamma = 0$
$\gamma = 20$
$\gamma = 10_1$
$\gamma = 10_2$
$\gamma = \infty$

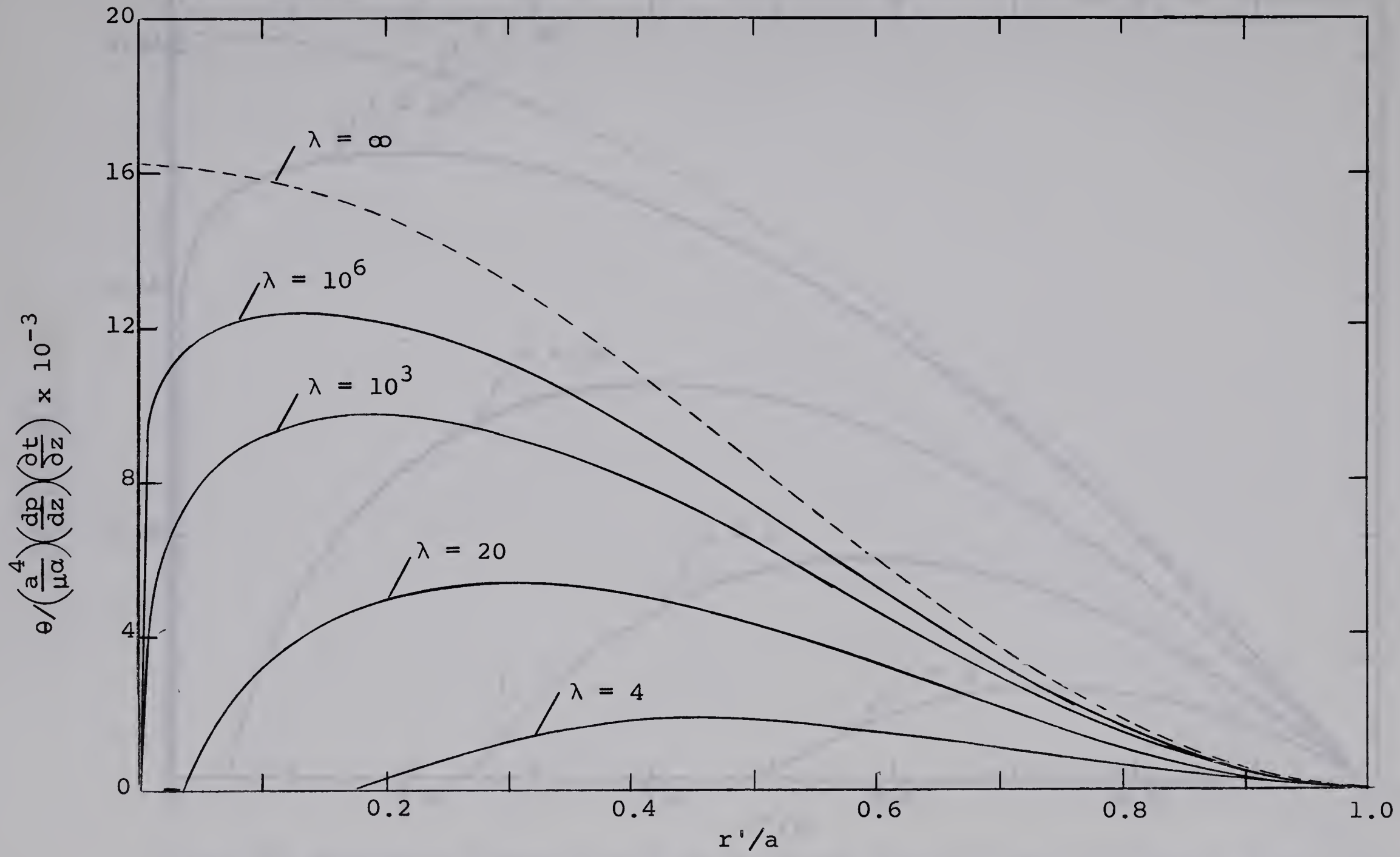

Fig. 25 Temperature profiles along $\Phi = \pi/4$ in square ducts with a central circular hole.

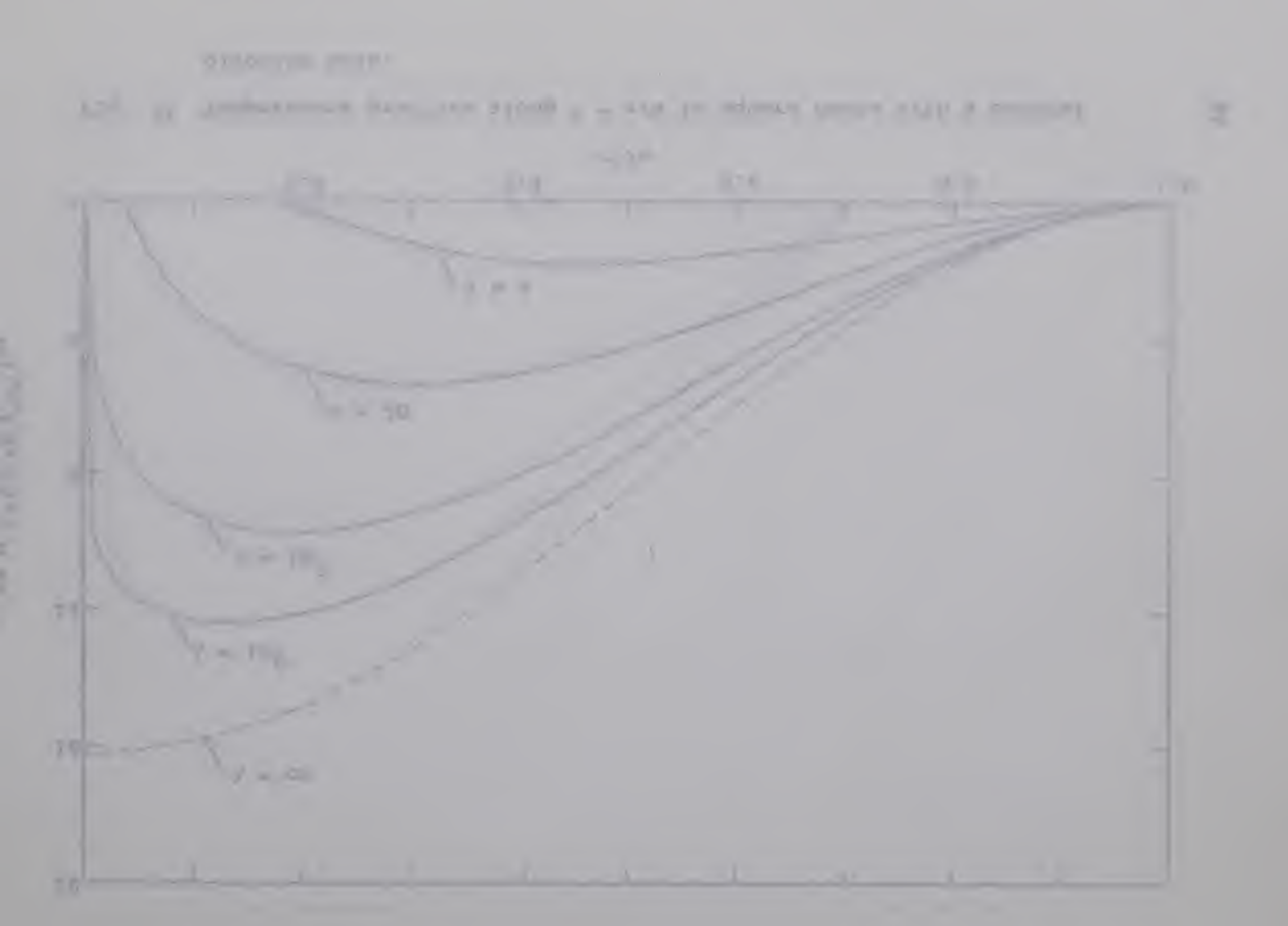

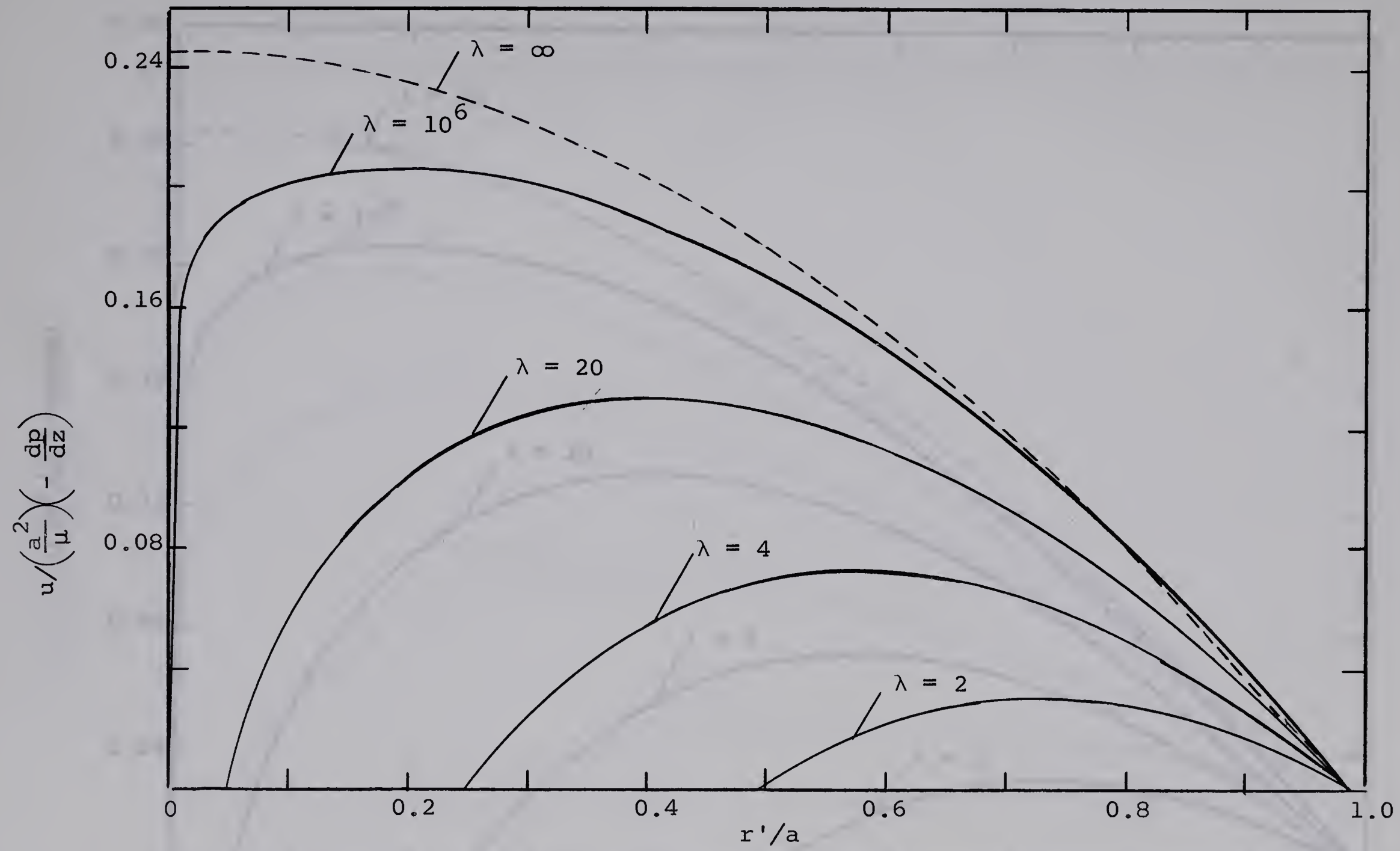

Fig. 26 Velocity profiles along $\Phi = 0$ in 20-sided regular polygonal ducts with a central circular hole.

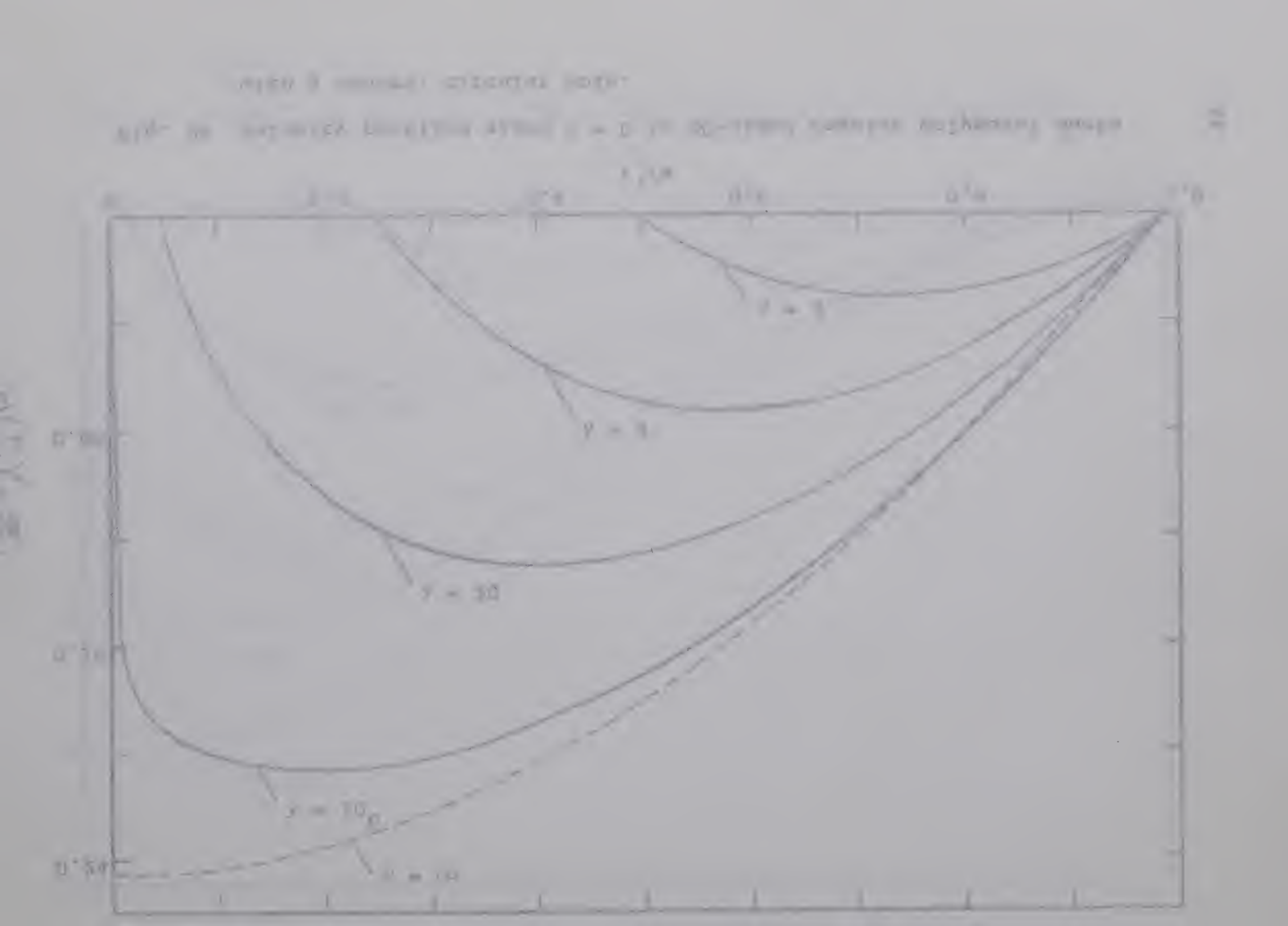
γ = 1
γ = 3
γ = 10
γ = 30
γ = 100
γ = ∞

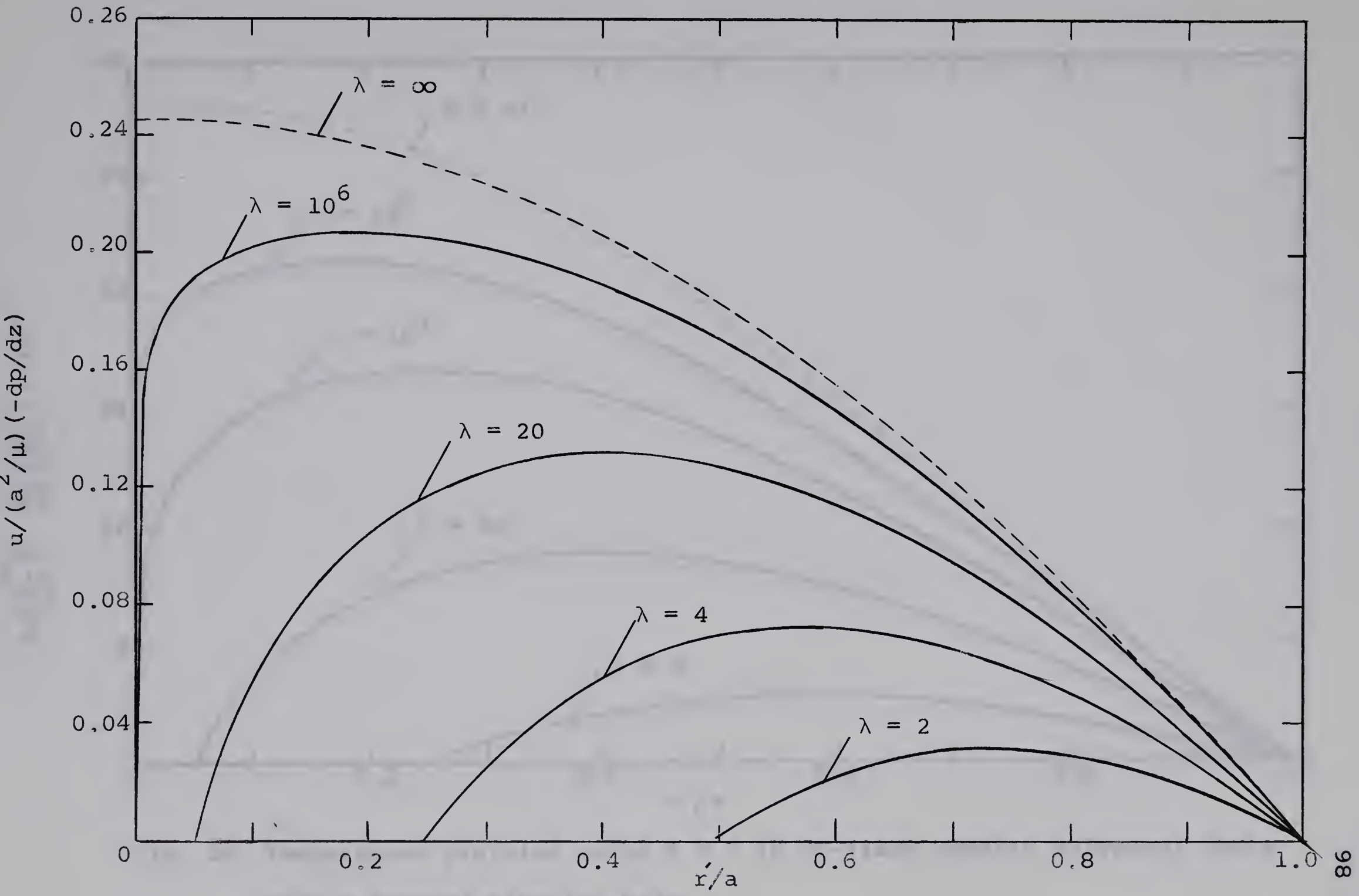

Fig. 27 Velocity profiles along $\phi = \pi/20$ in 20-sided regular polygonal ducts with a central circular hole.

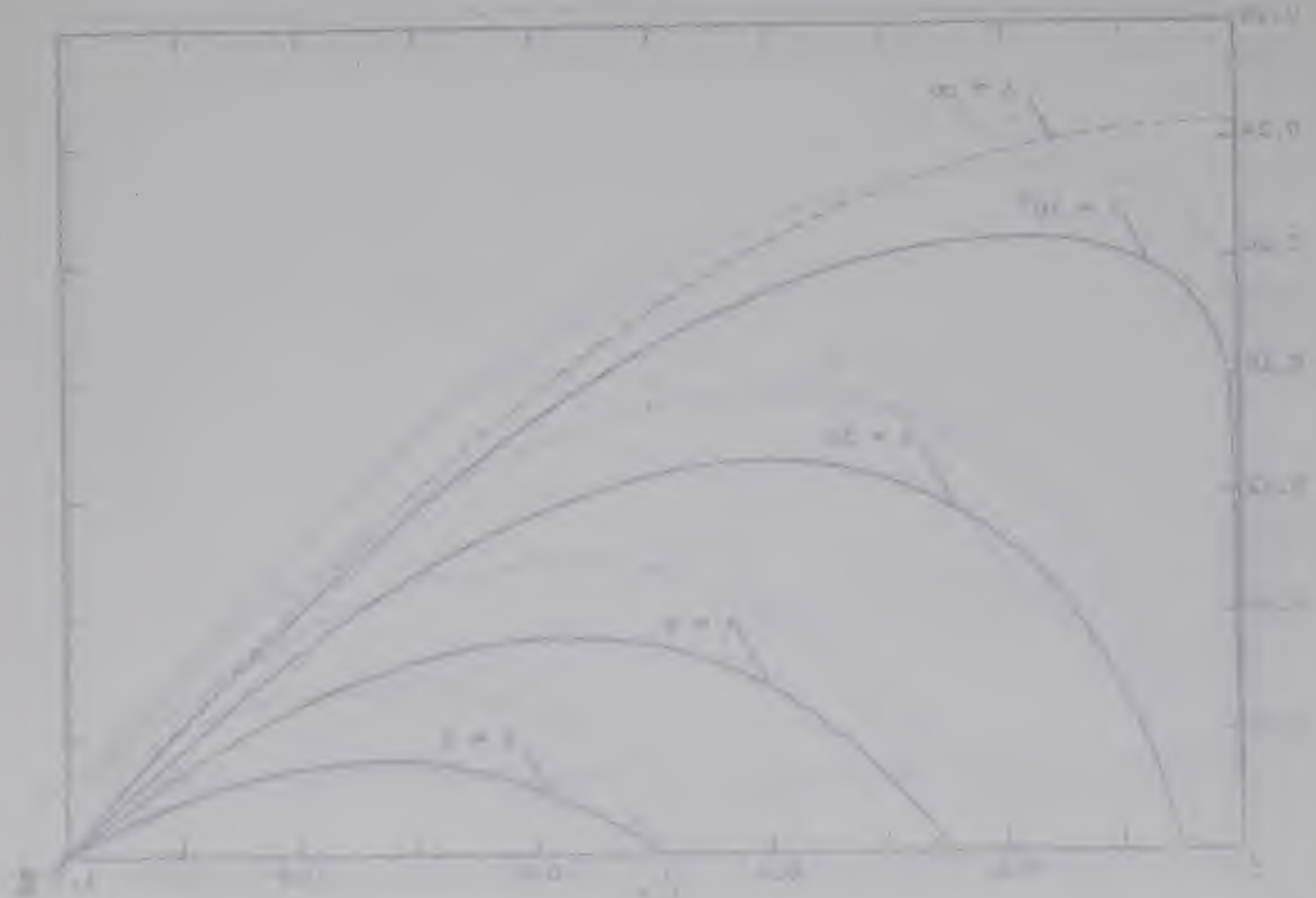

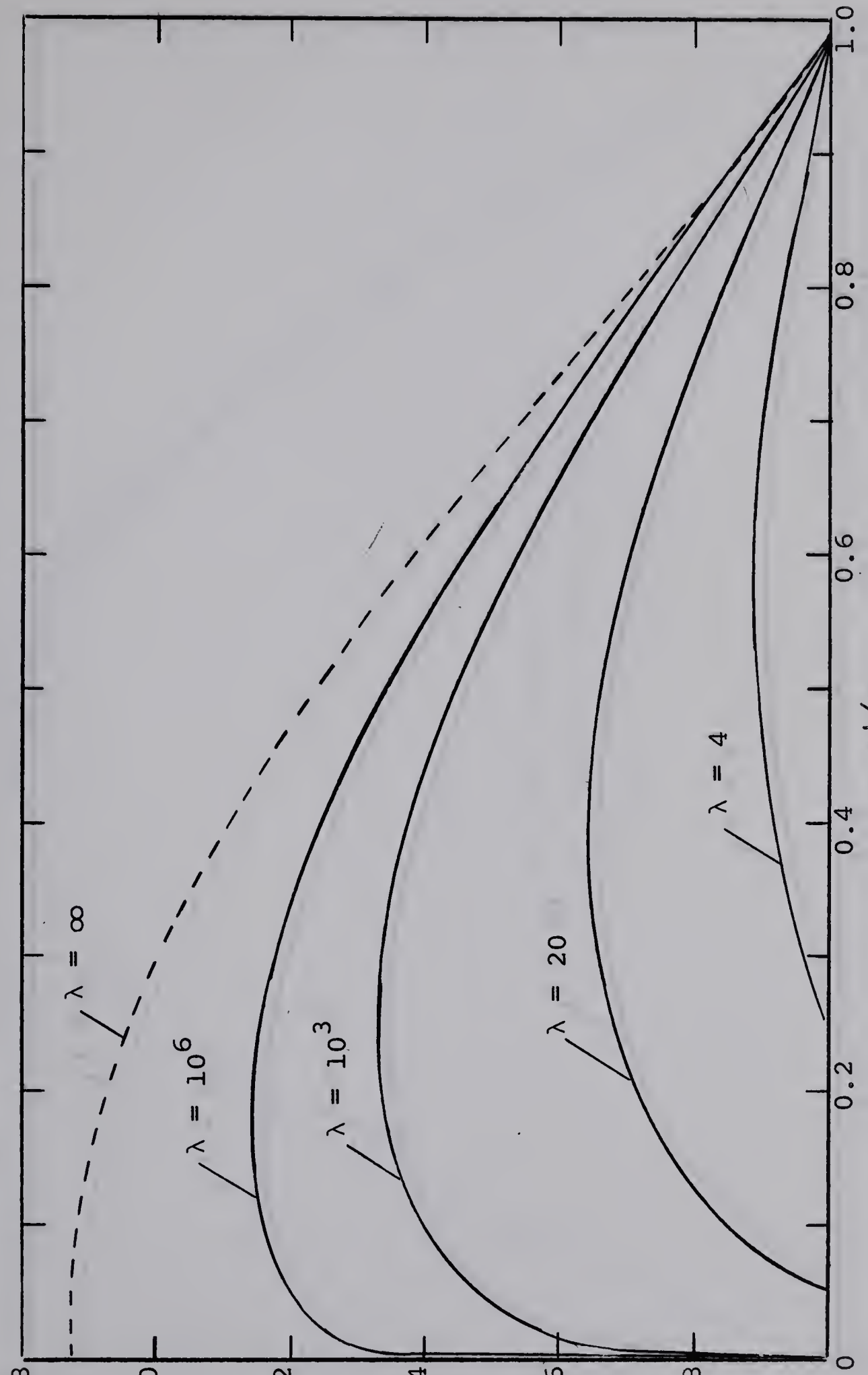

Fig. 28 Temperature profiles along $\phi = 0$ in 20-sided regular polygonal ducts with a central circular hole.

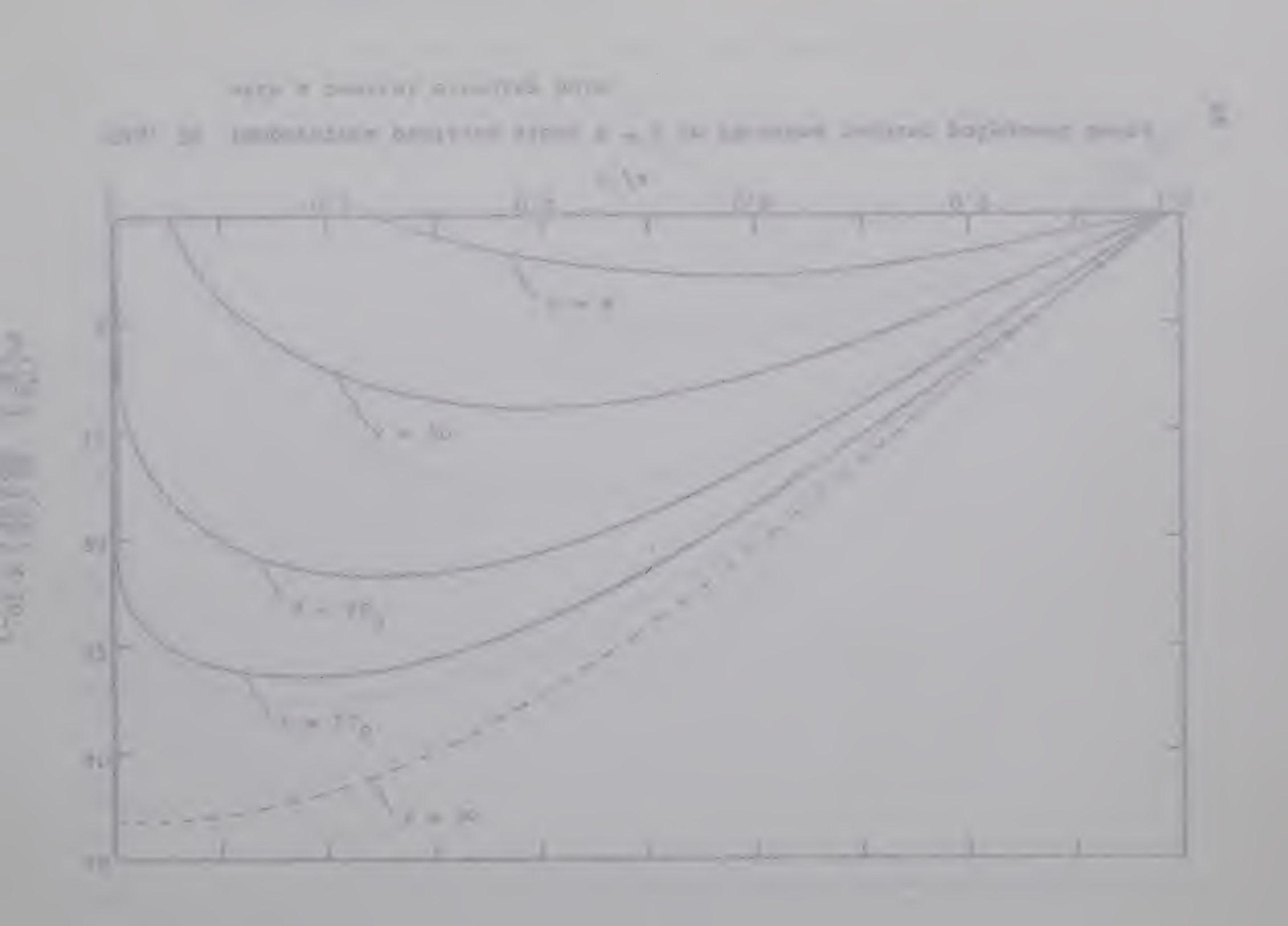

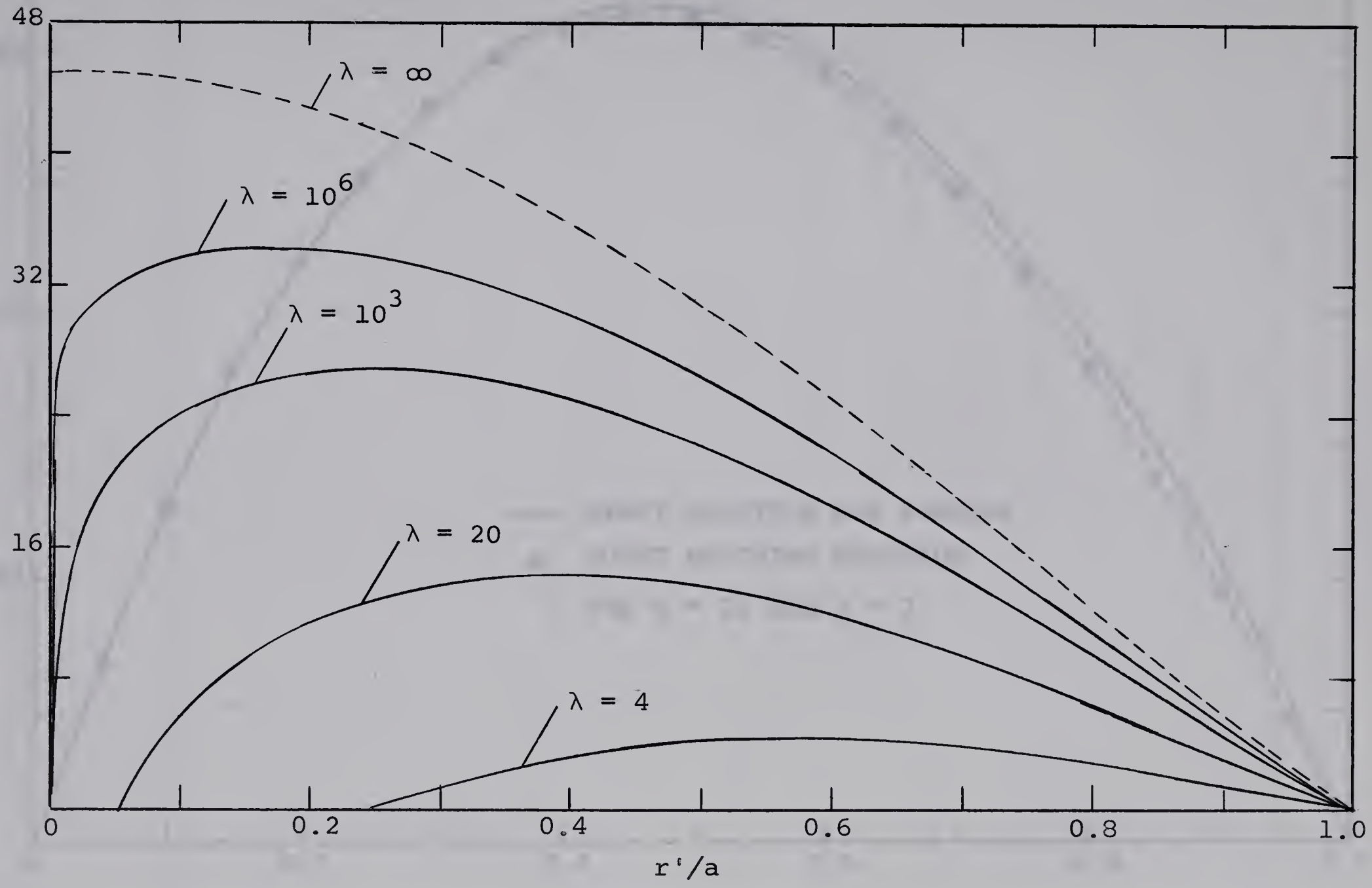

Fig. 29 Temperature profiles along $\Phi = \pi/20$ in 20-sided regular polygonal ducts with a central circular hole.

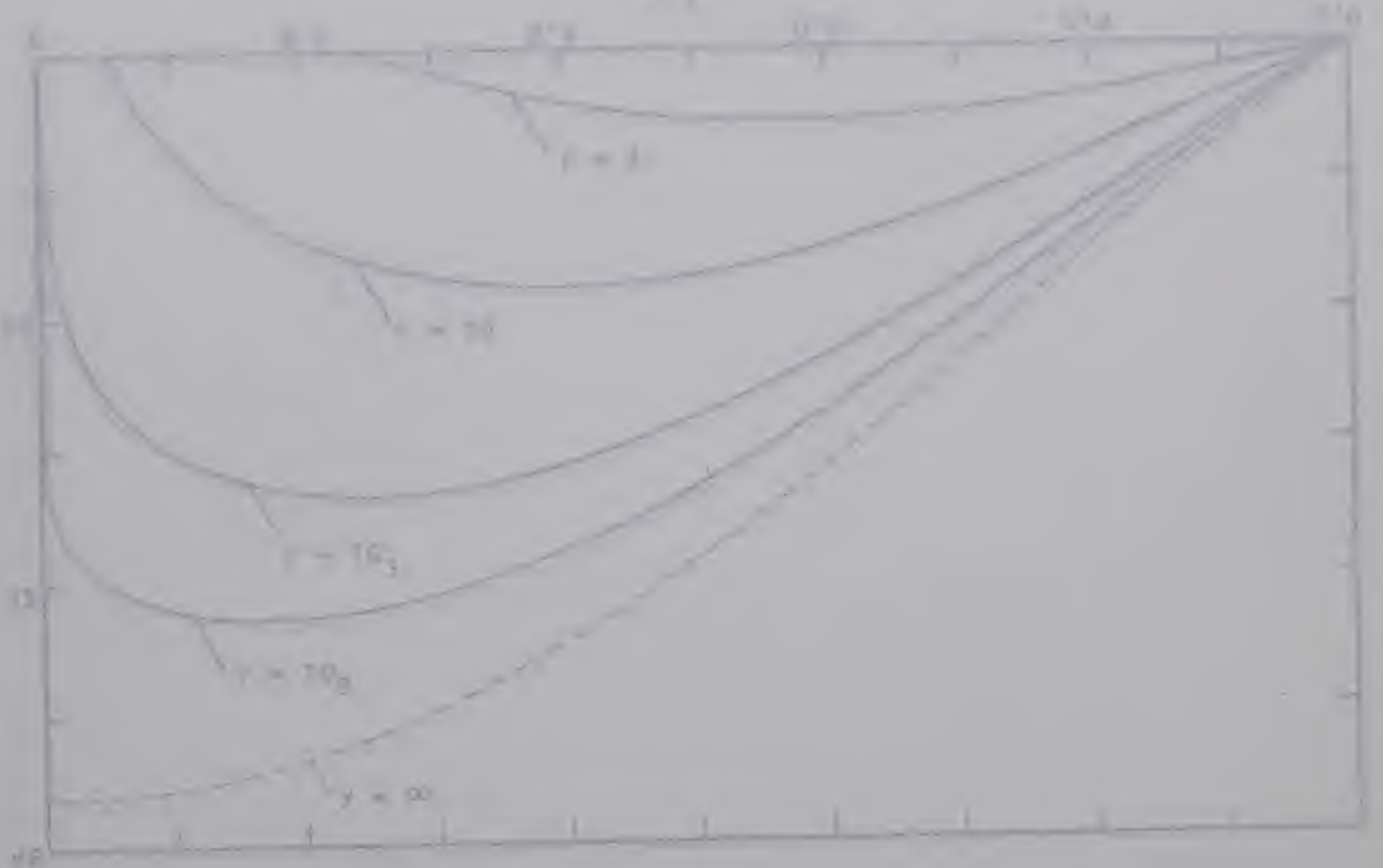
$\gamma = \infty$
$\gamma = 10_3$
$\gamma = 10_2$

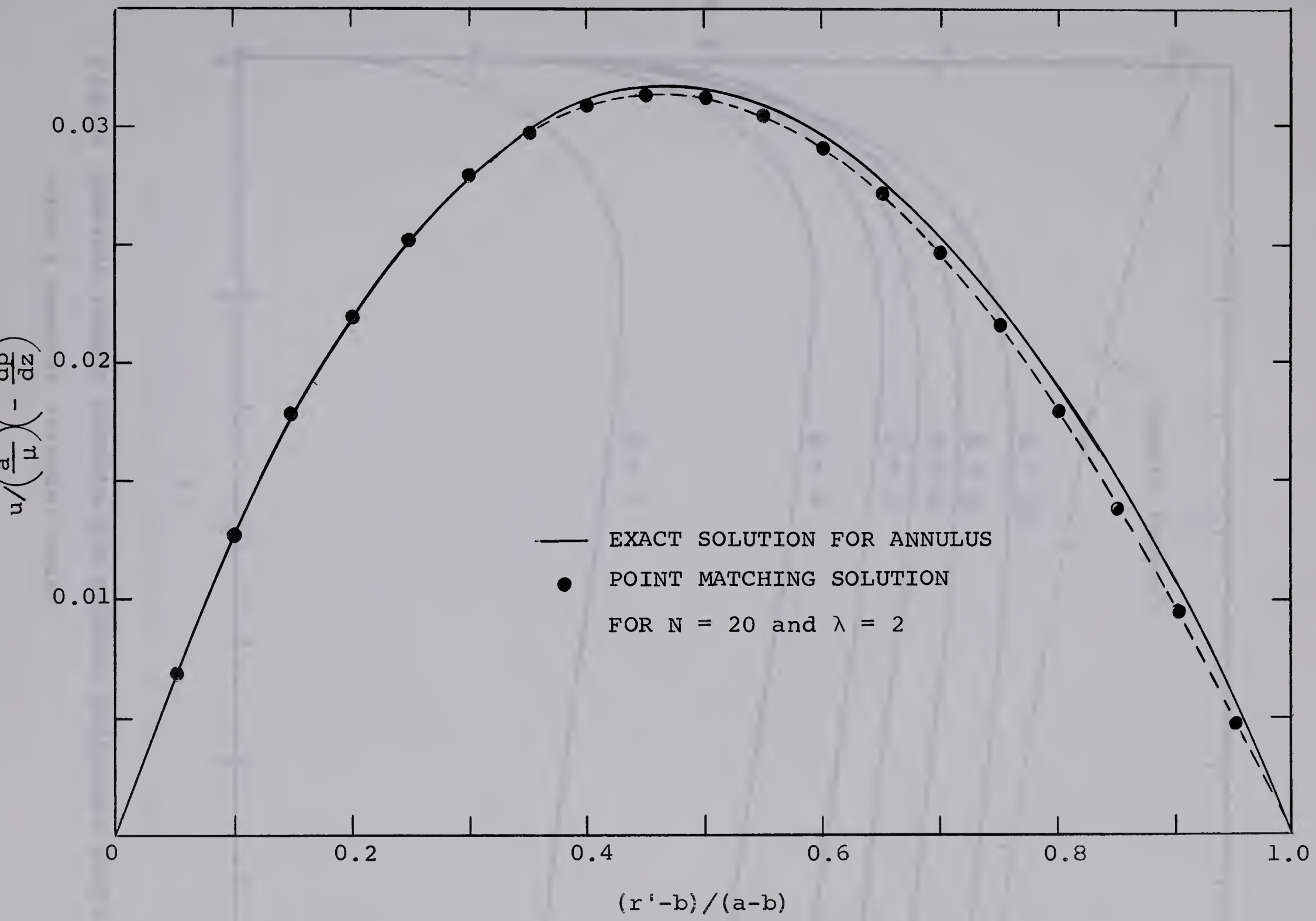

Fig. 30 Velocity distribution along $\Phi = \pi/20$ in 20-sided regular polygonal ducts with a central circular hole.

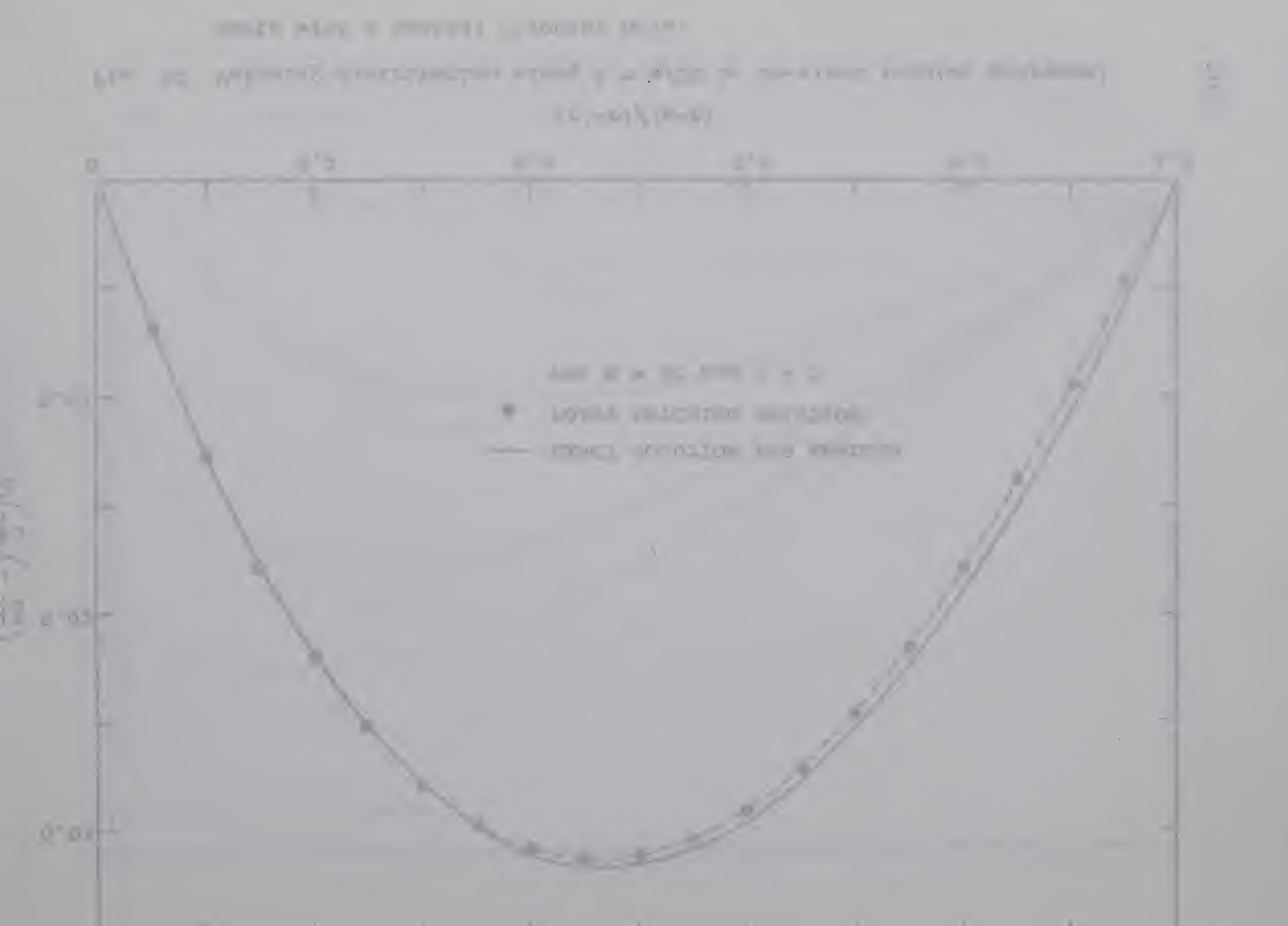

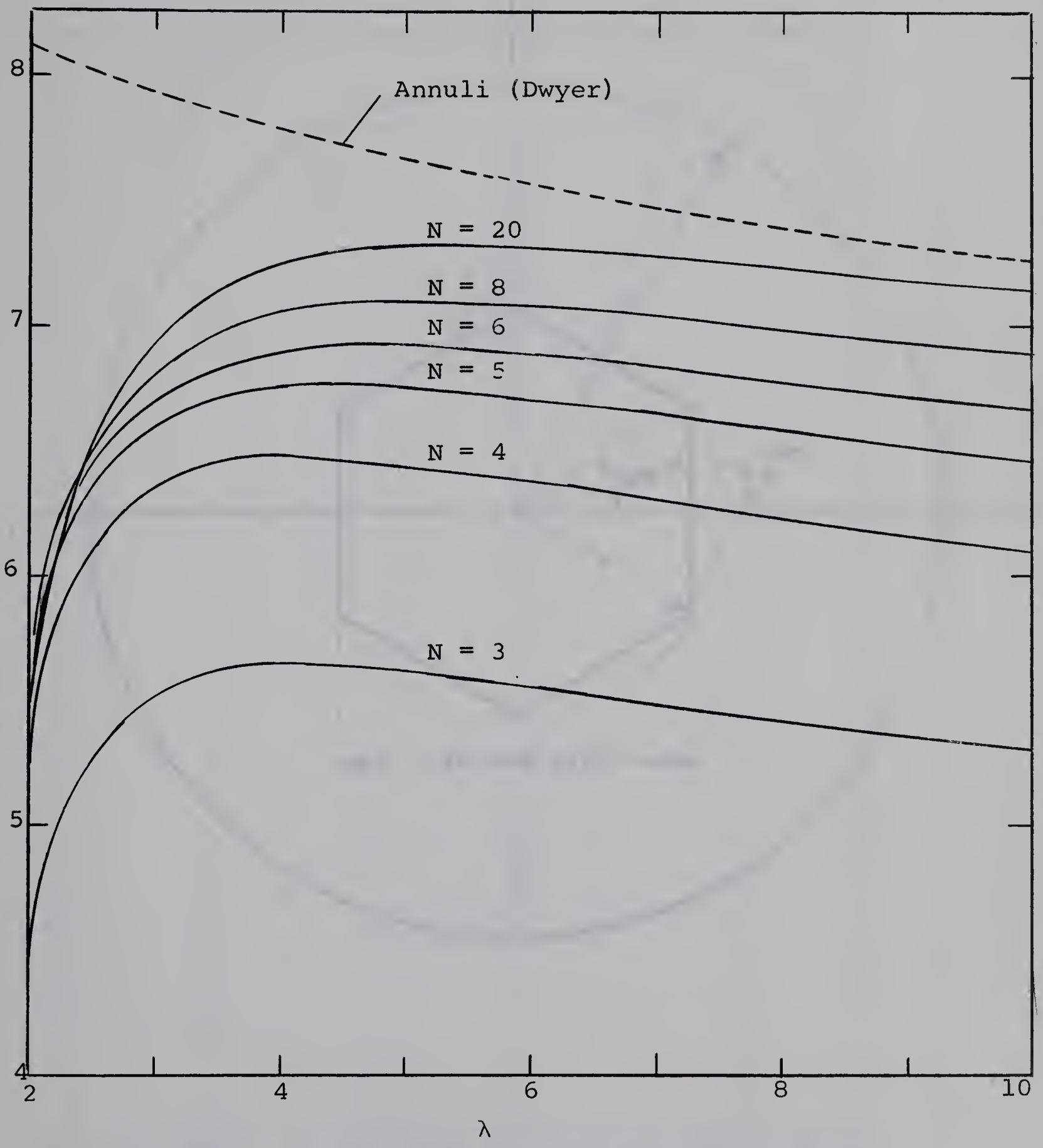

Fig.31 Nusselt number results for regular polygonal ducts with a central circular hole.

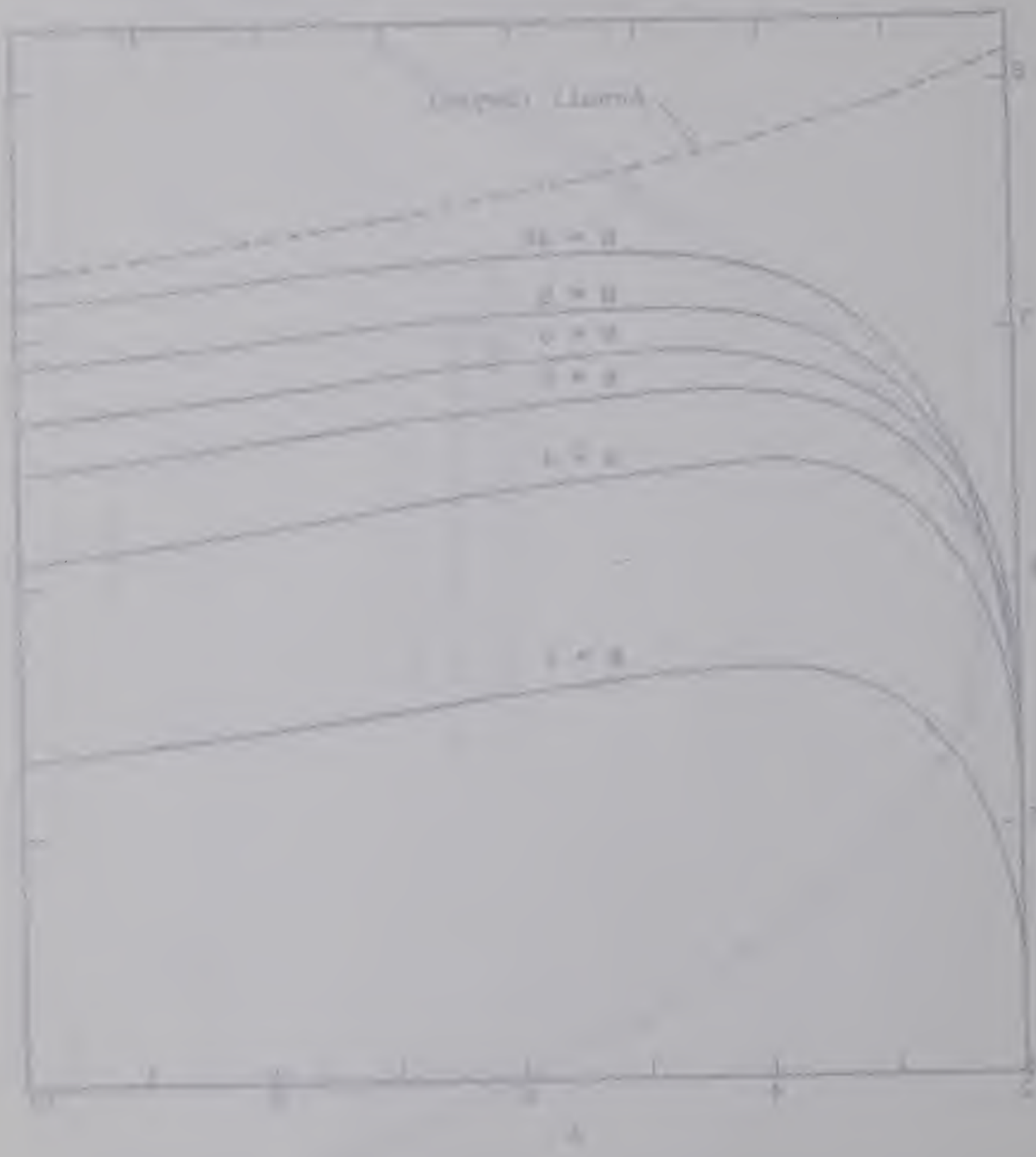

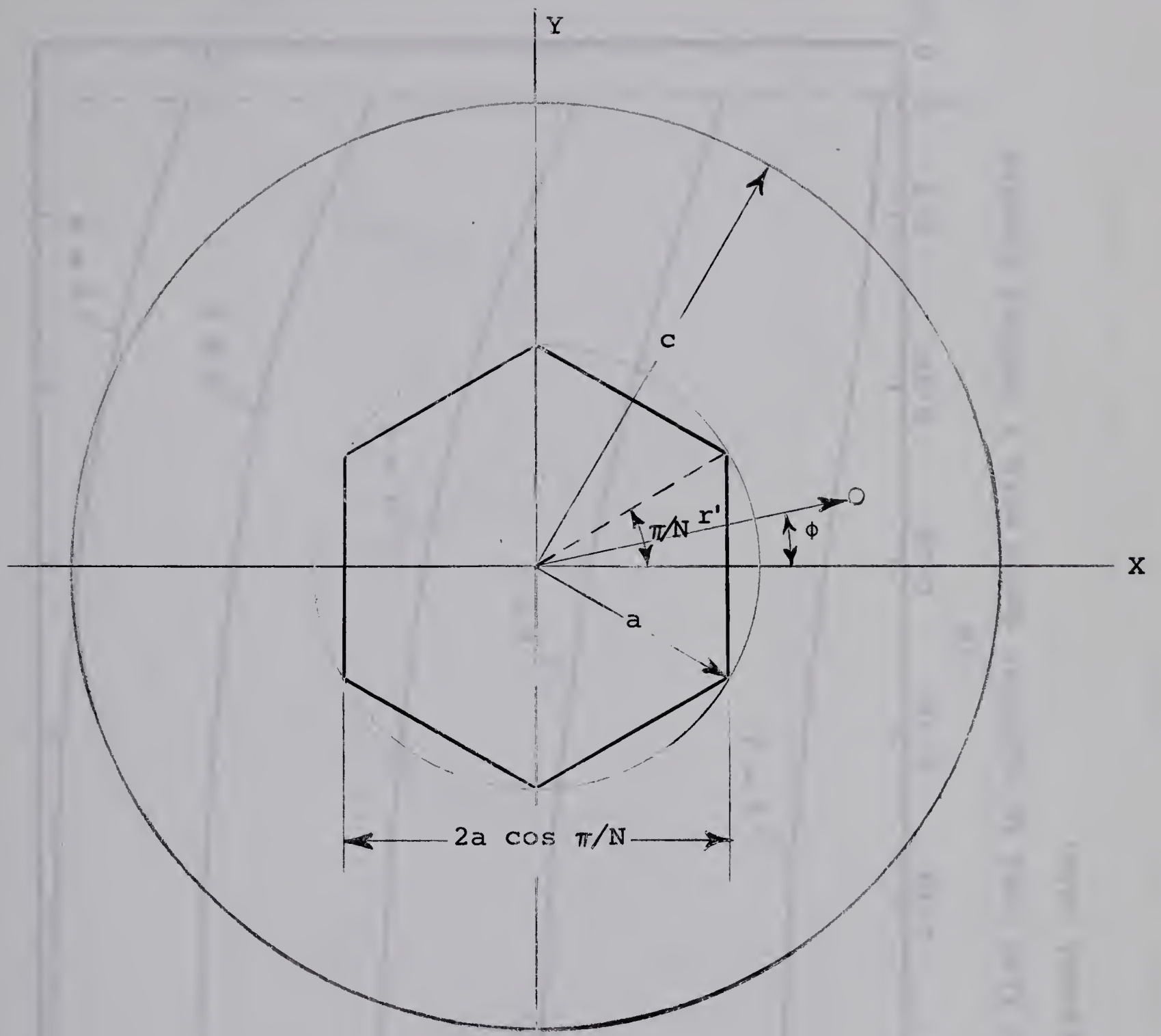

Fig. 32 Coordinate system for circular duct with a central regular polygonal hole.

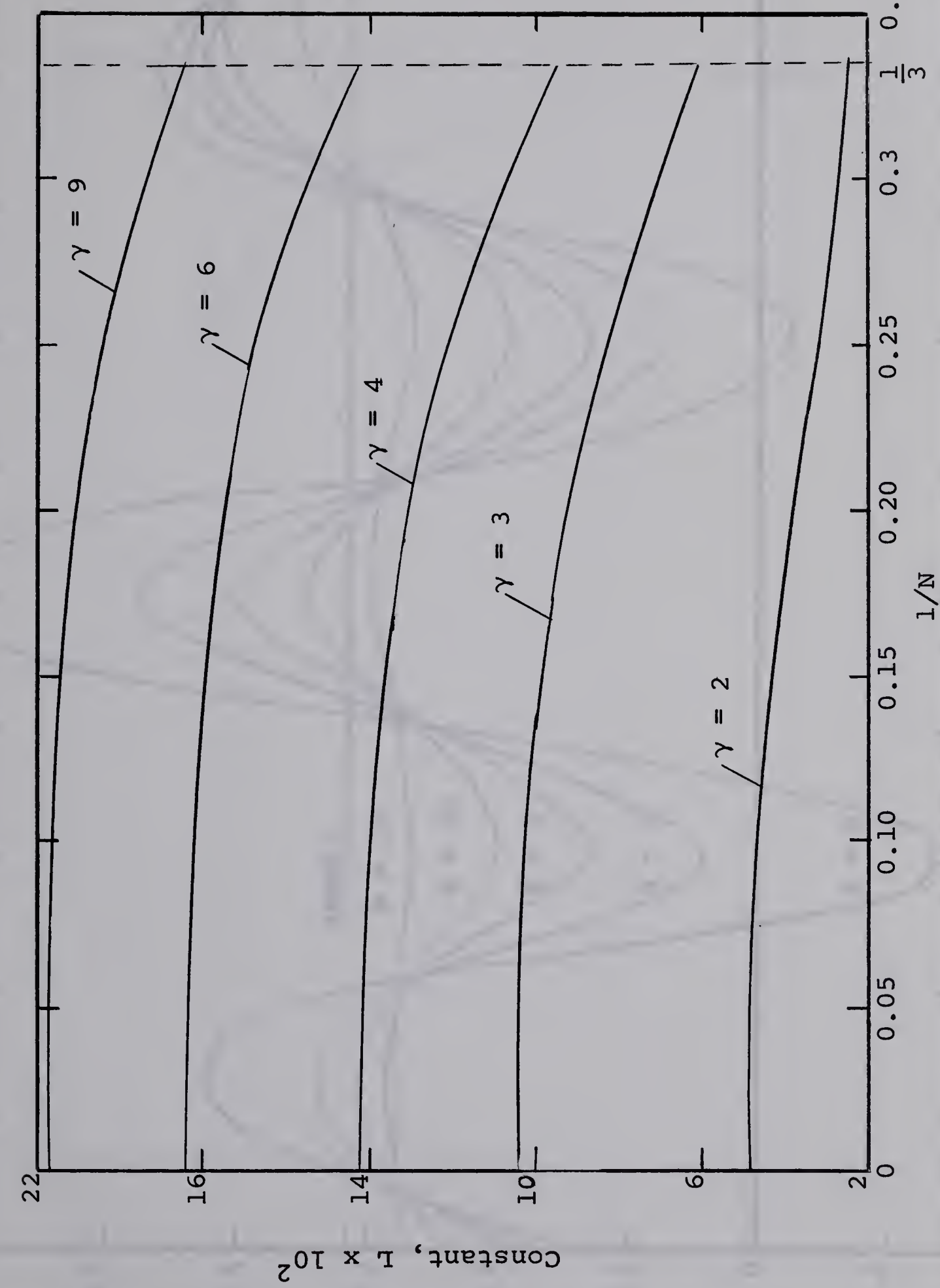

Fig. 33 Mass flow rate in circular ducts with a central regular polygonal hole.

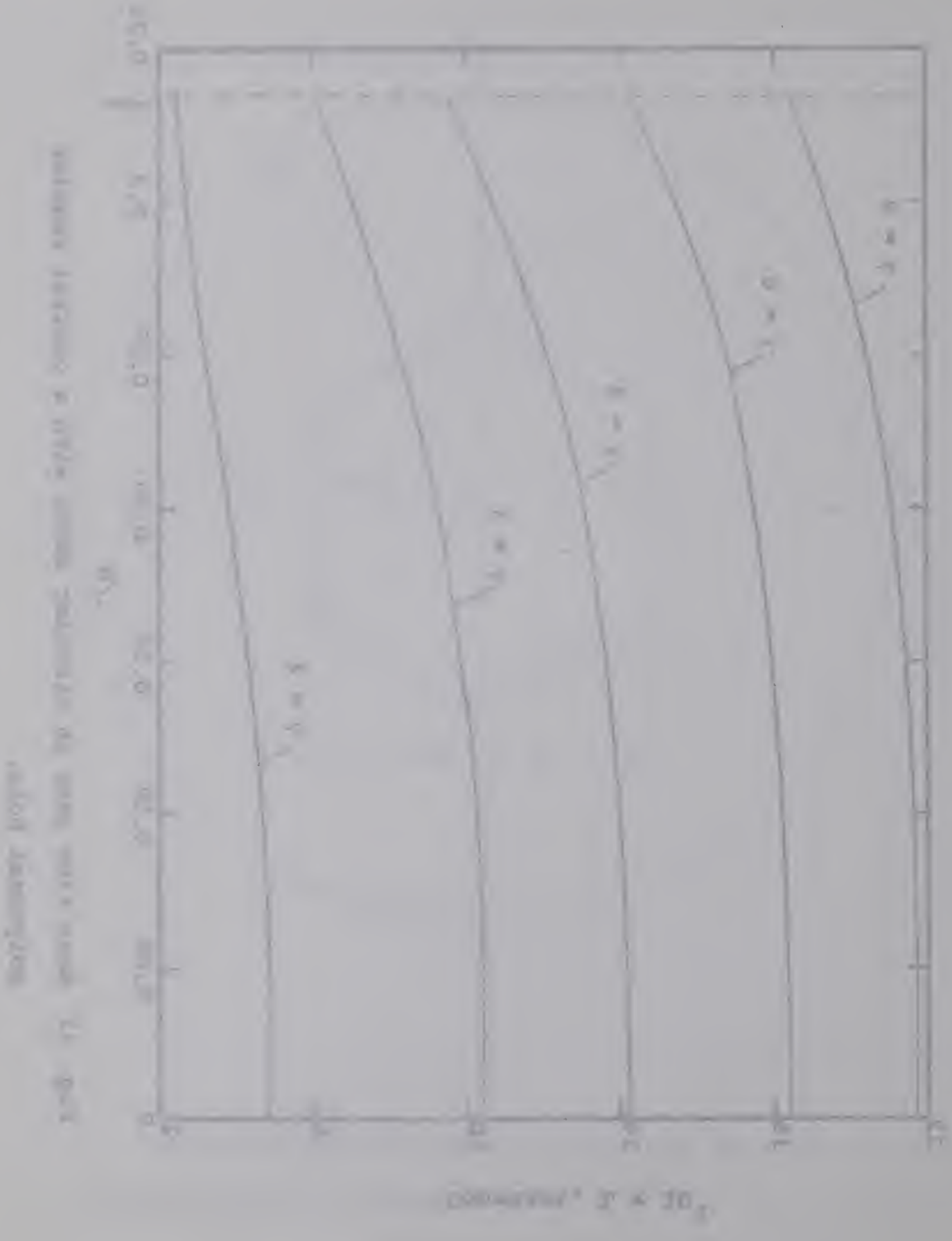

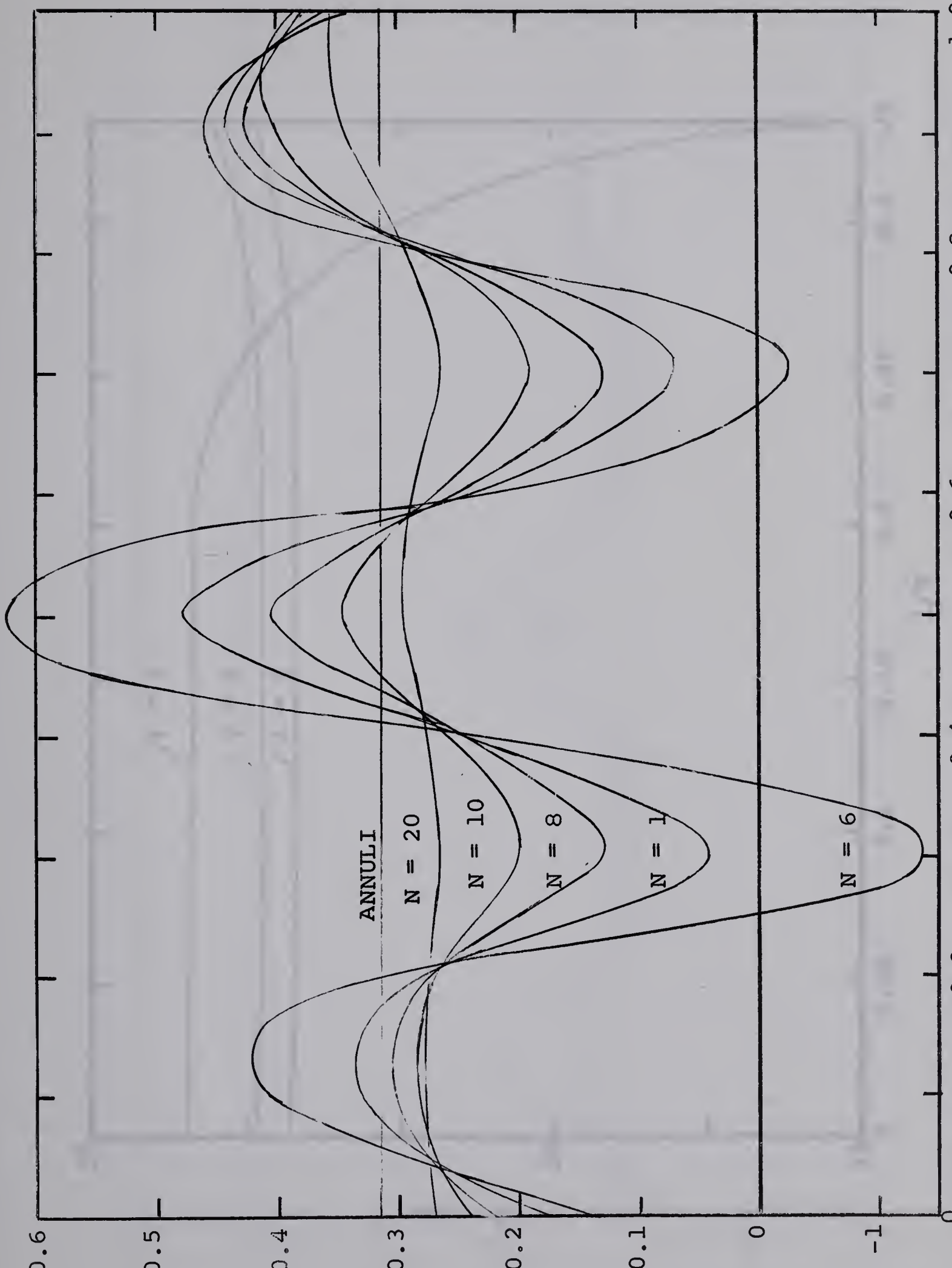

Fig. 34 Shear stress distribution along inner boundary in circular ducts with a central regular polygonal hole for $\gamma = 2$.

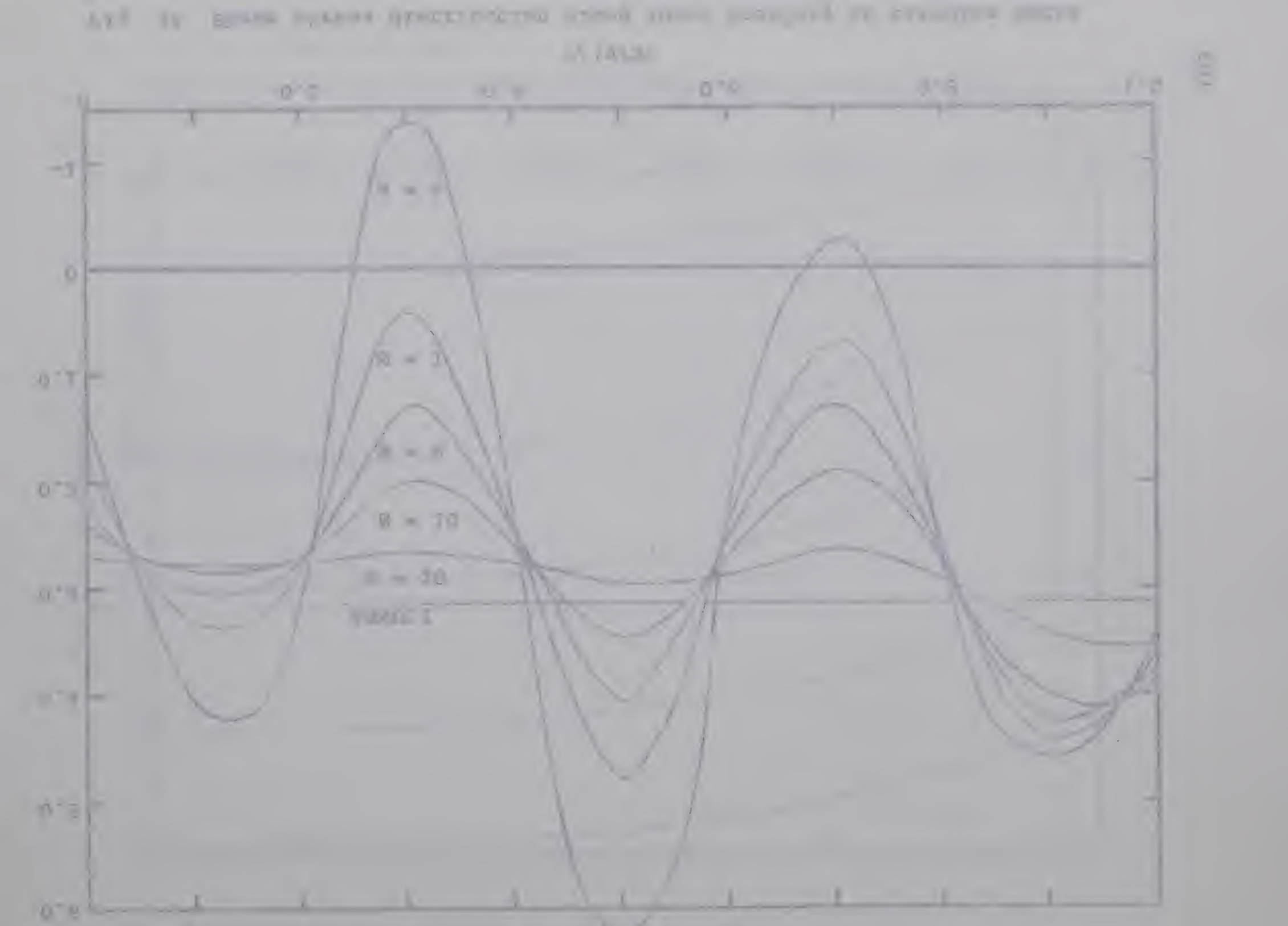
0
-1
n = 1
n = 3
n = 6
n = 10
n = 30

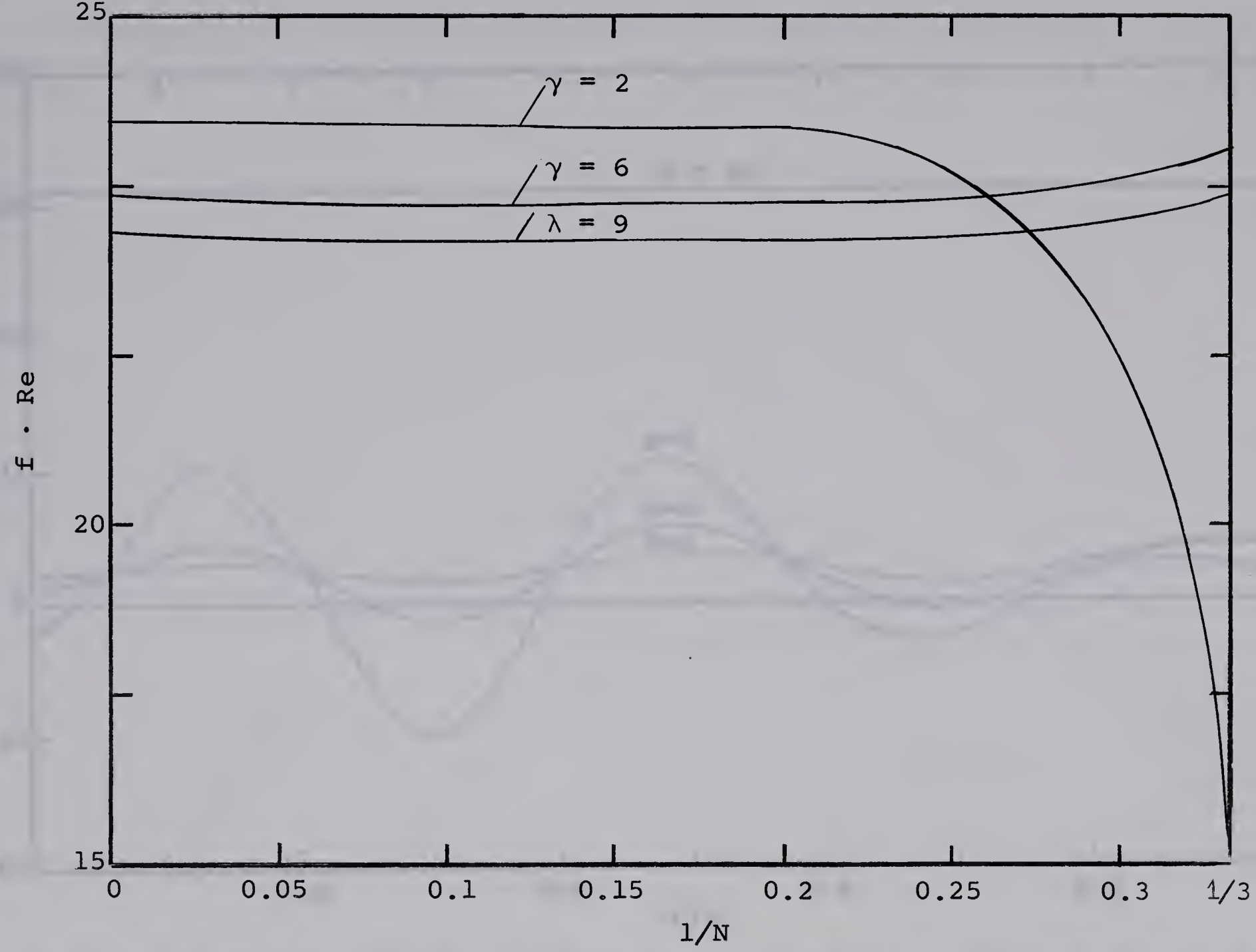

Fig. 35 Friction factor-Reynolds number results for circular ducts with a central regular polygonal hole.

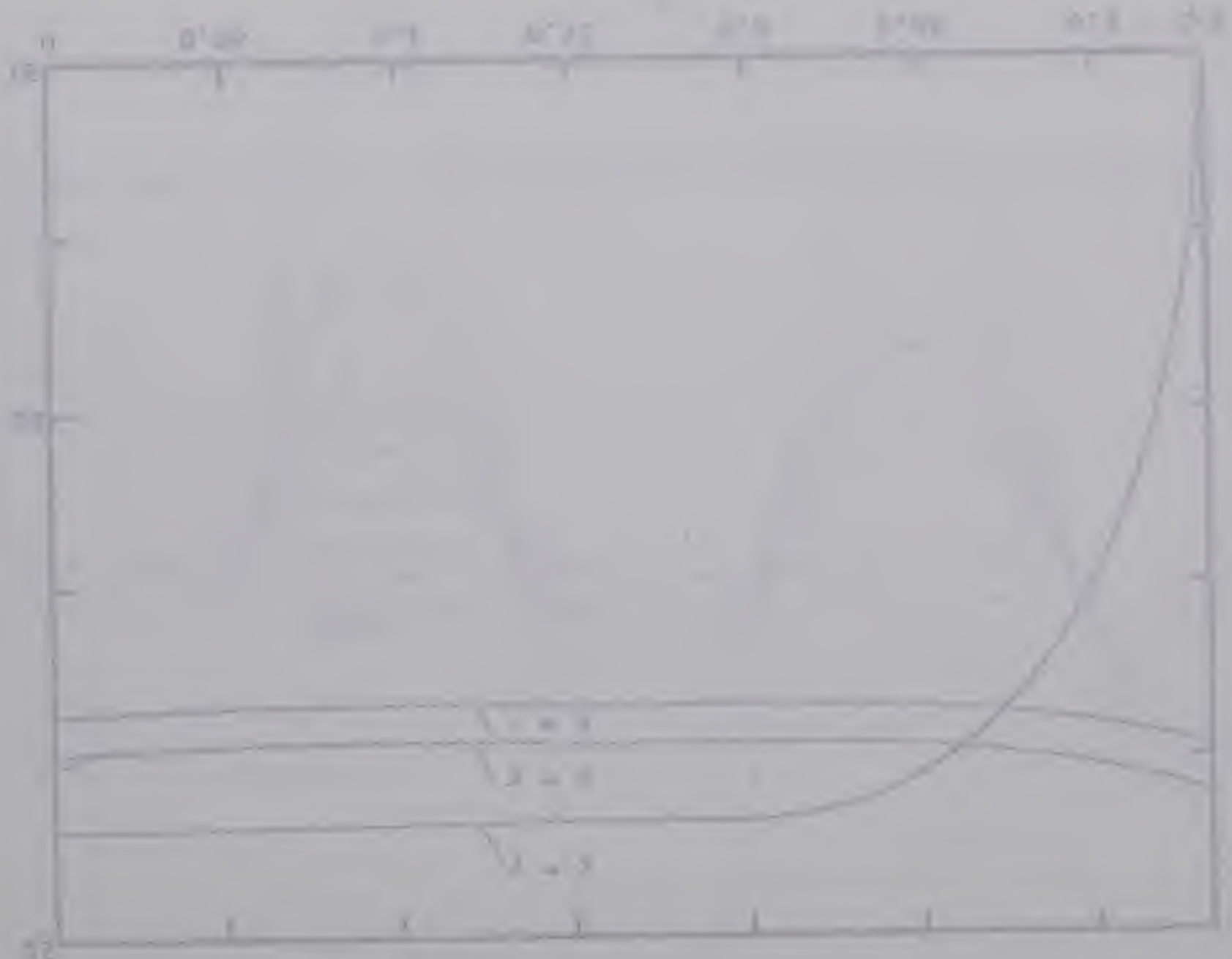

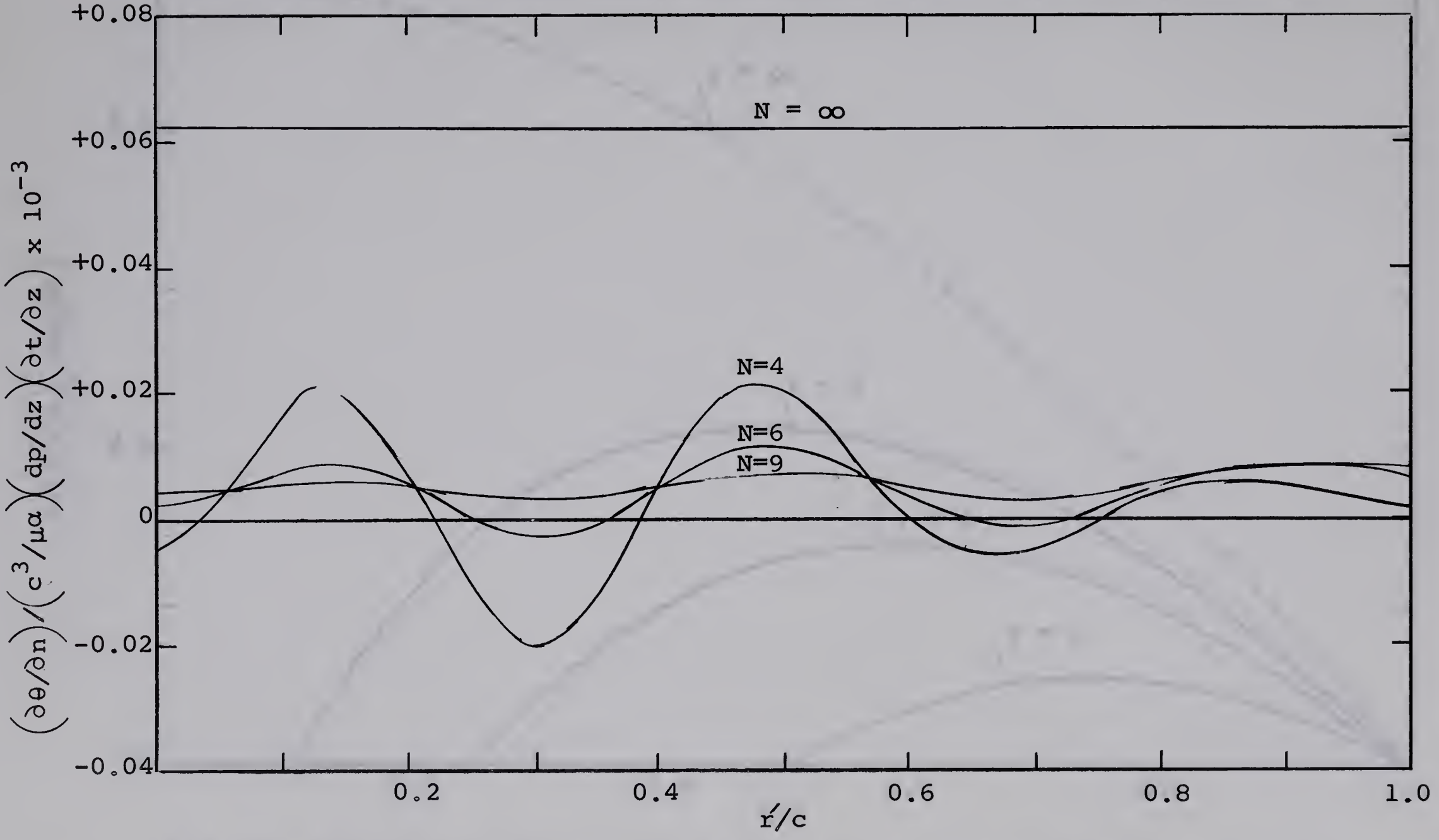

Fig. 36 Temperature gradients along inner boundary in circular duct with a central regular polygonal hole for $\gamma = 2$.

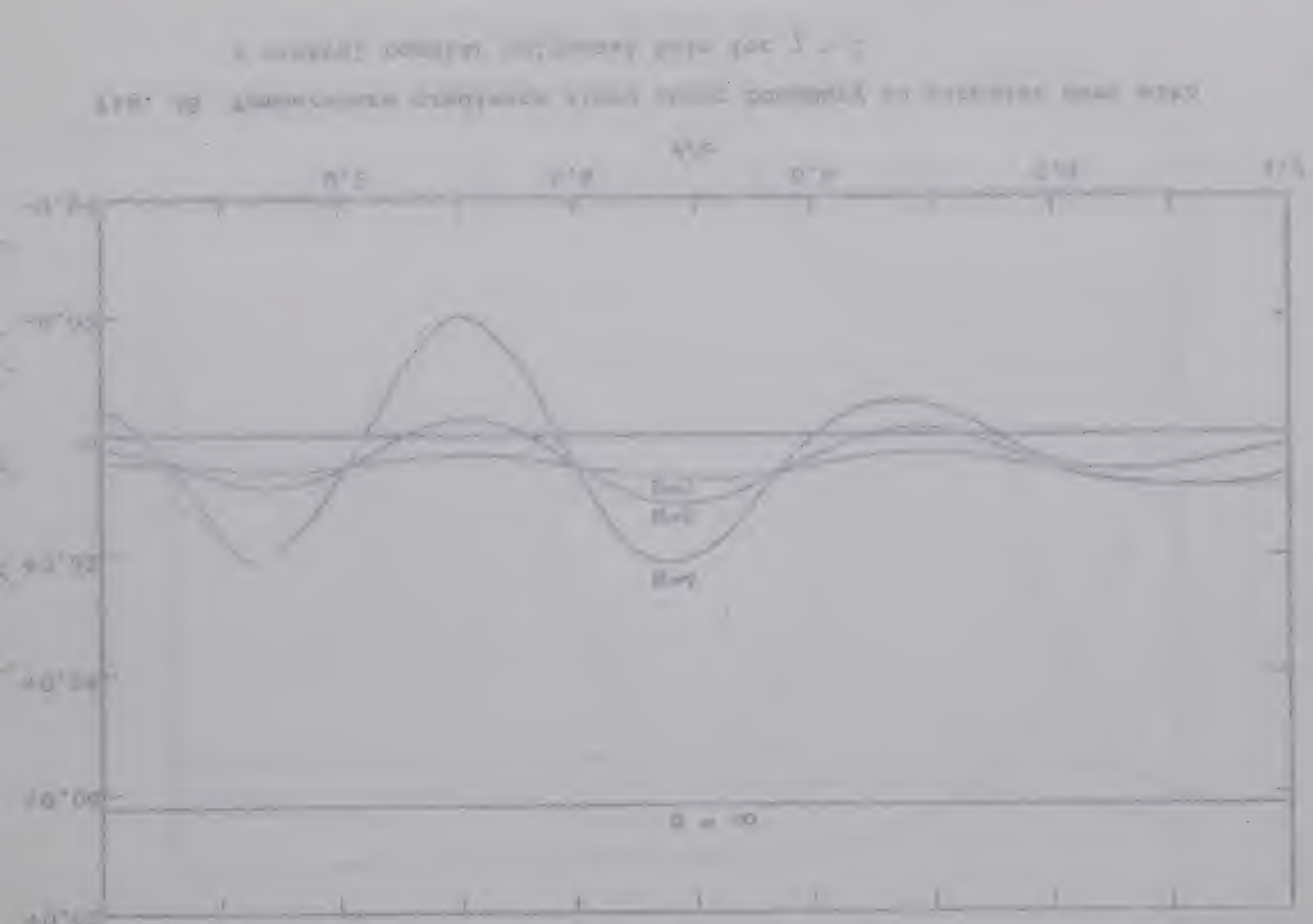

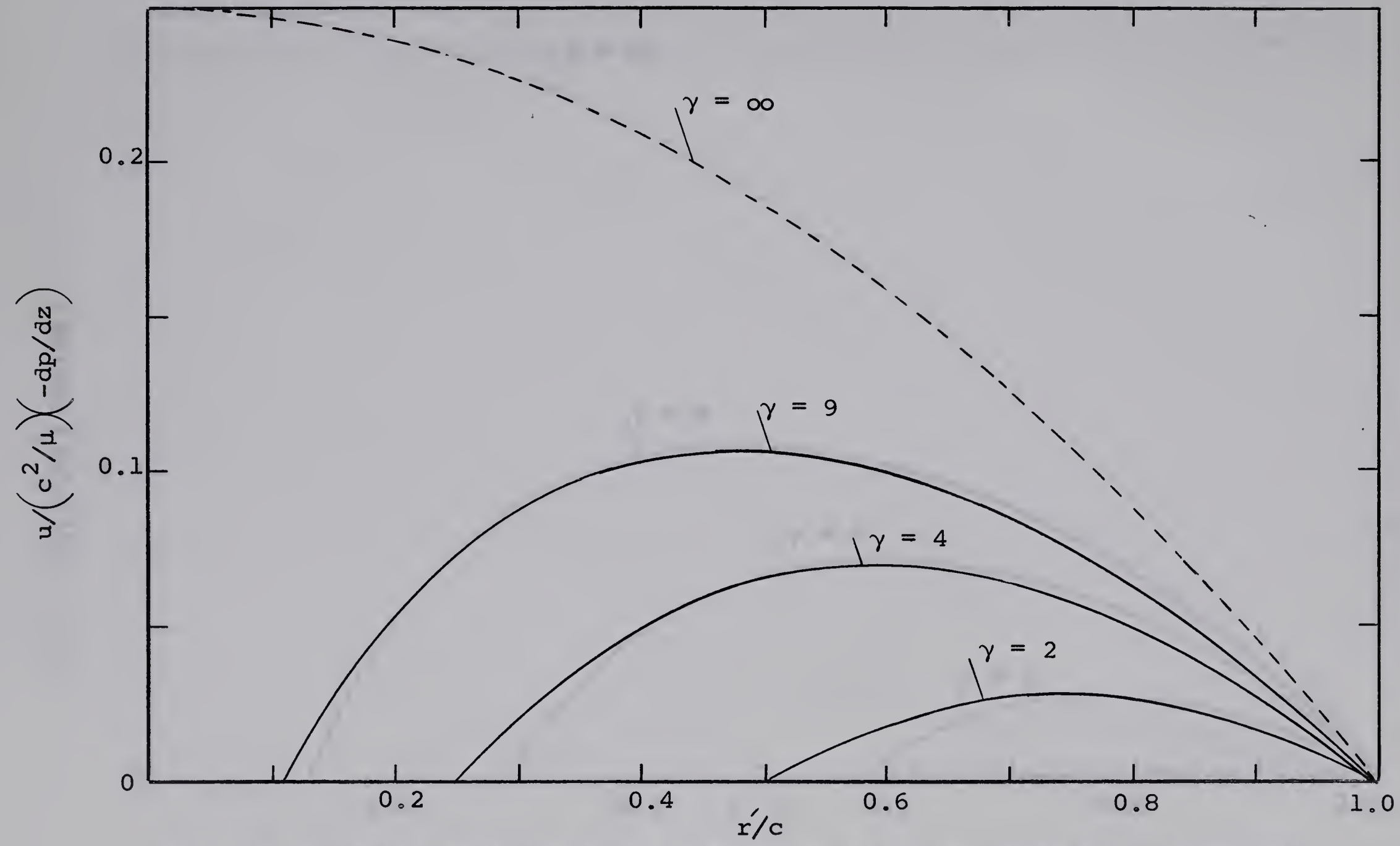

Fig. 37 Velocity profiles along $\phi = 0$ in circular ducts with a central hexagonal hole.

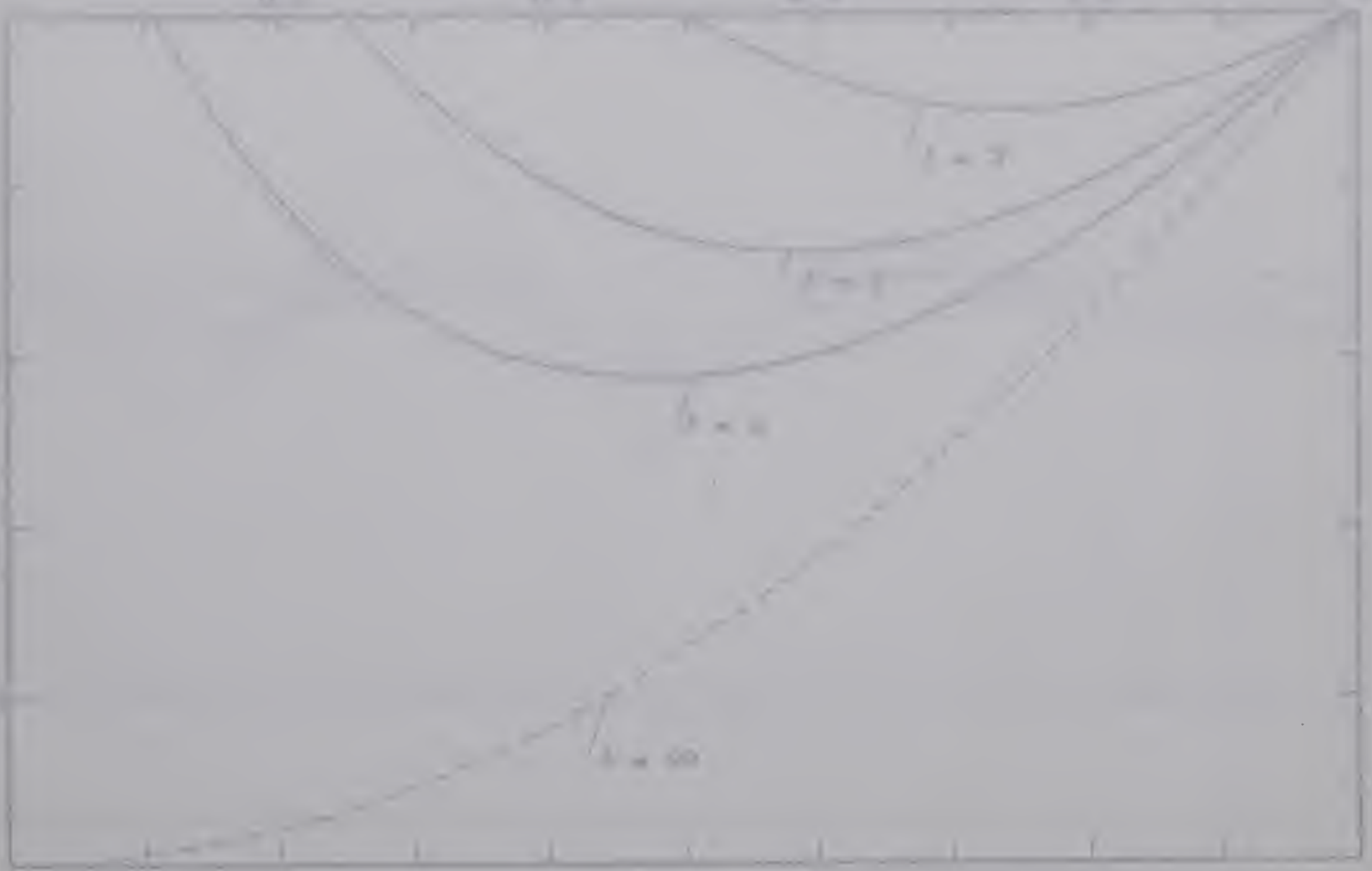
λ = 3
λ = 1
λ = 0
λ = ∞

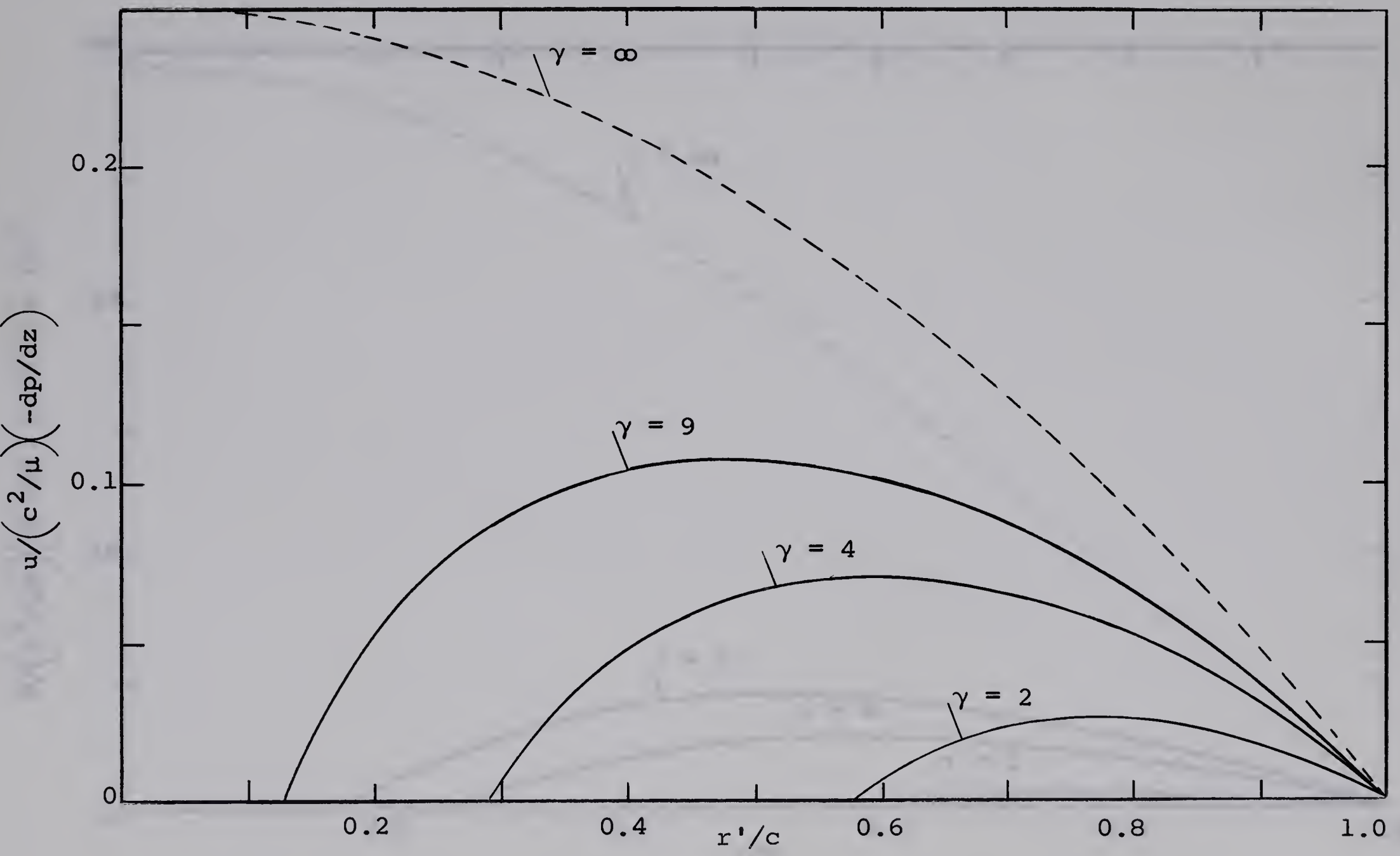

Fig. 38 Velocity profiles along $\Phi = \pi/6$ in circular ducts with a central hexagonal hole.

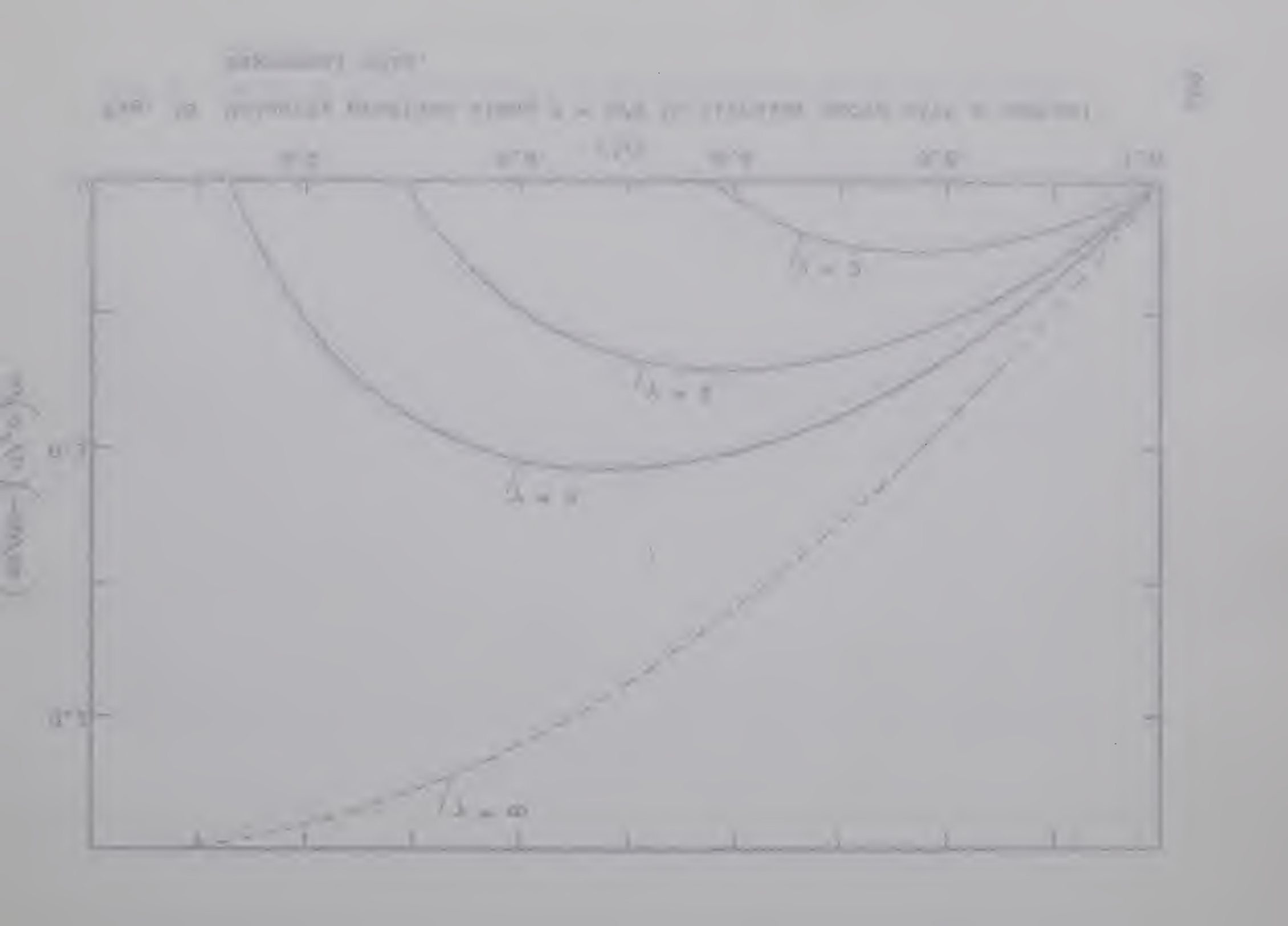
λ = 3
λ = 2
λ = 1
λ = ∞

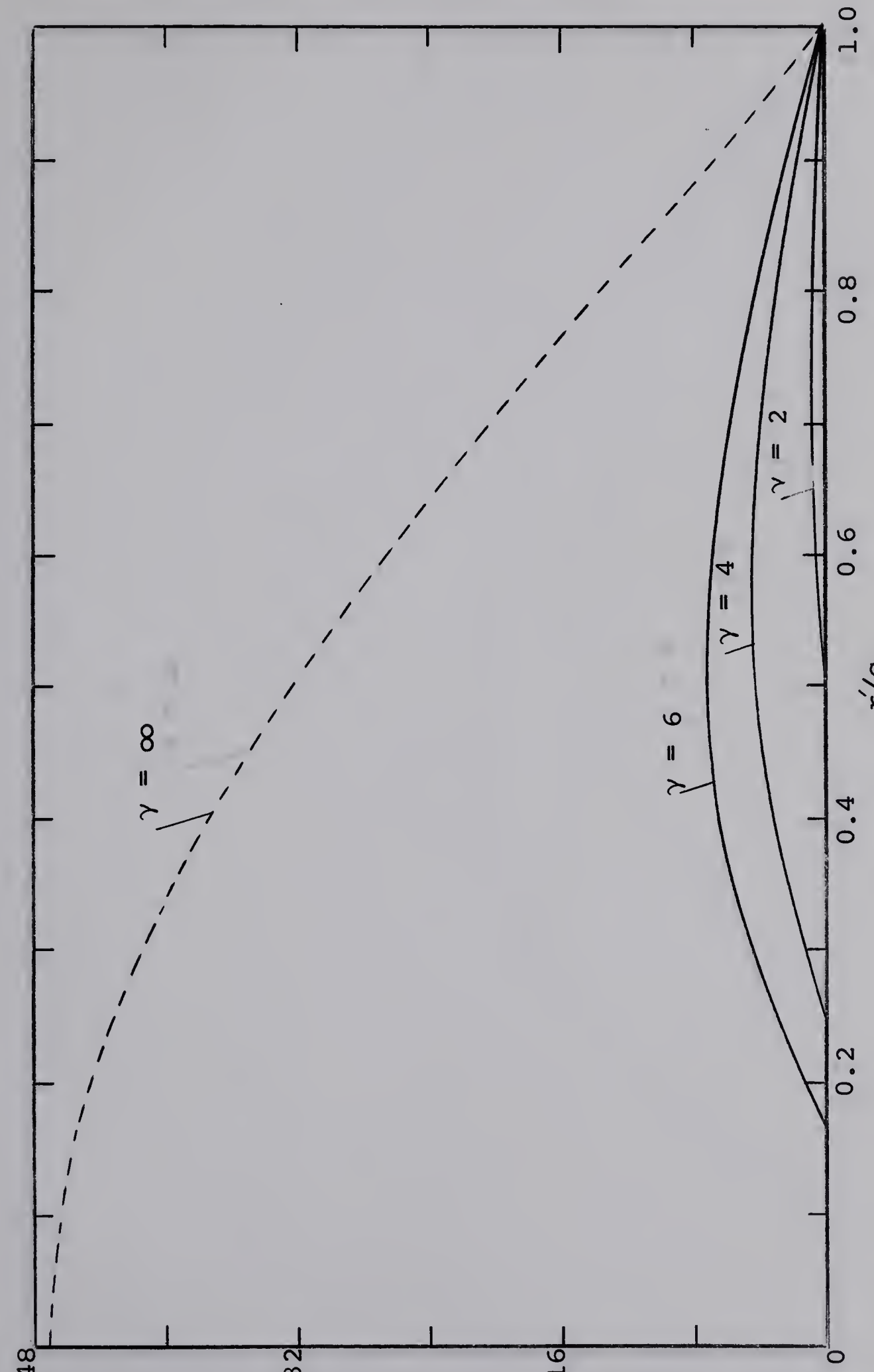

Fig. 39 Temperature profiles along $\phi = 0$ in circular ducts with a central 9-sided regular polygonal hole.

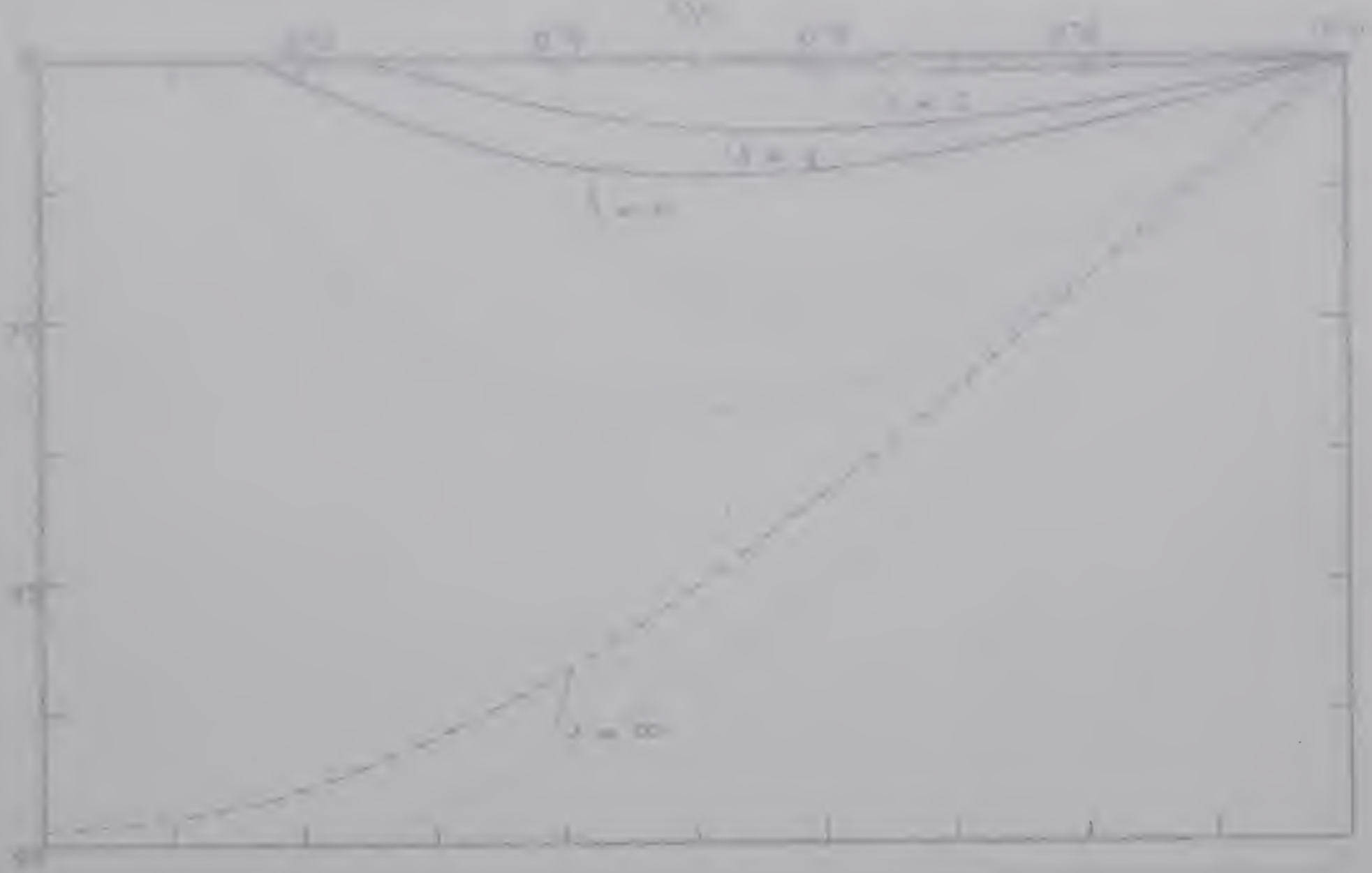

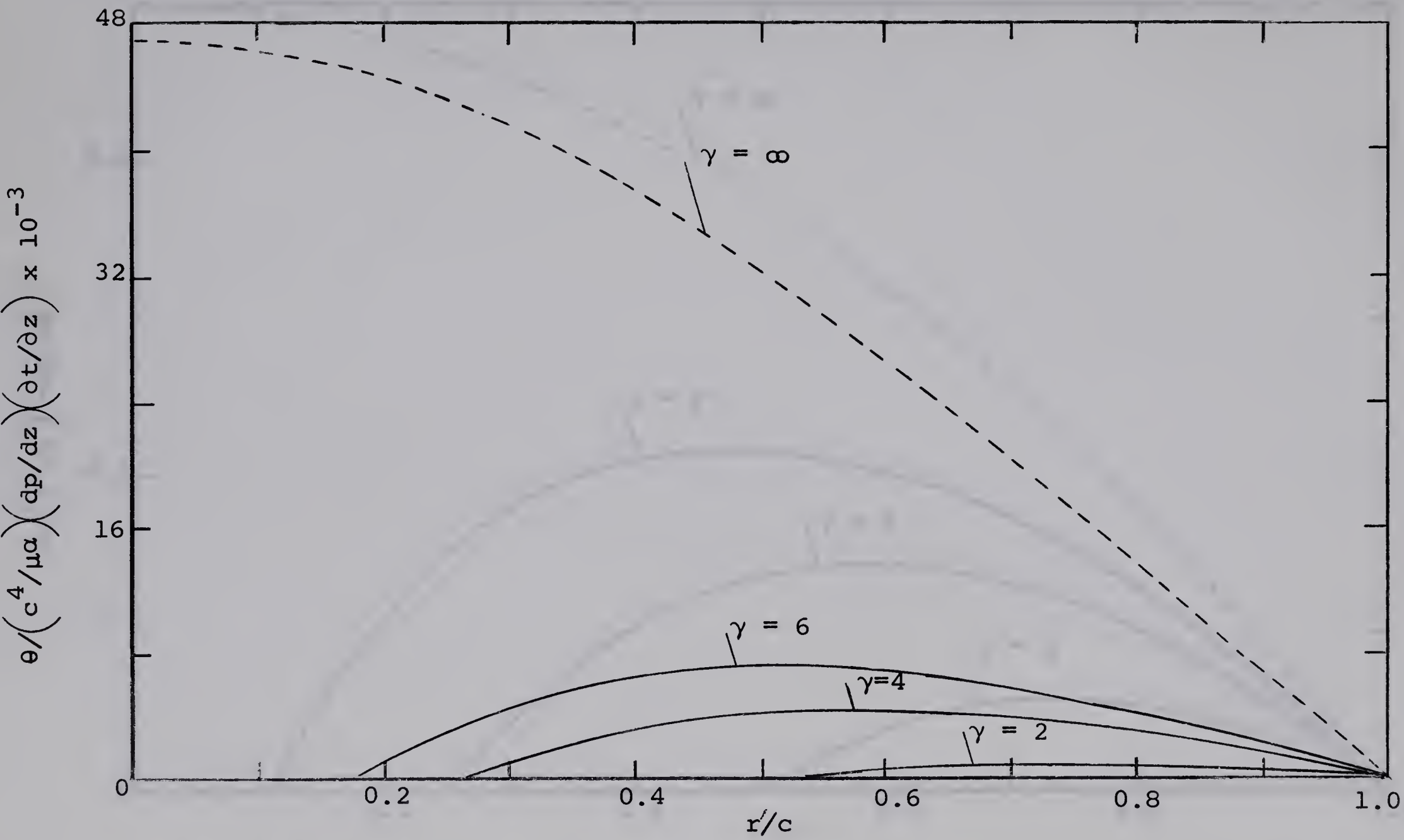

Fig. 40 Temperature profiles along $\Phi = \pi/9$ in circular ducts with a central 9-sided regular polygonal hole.

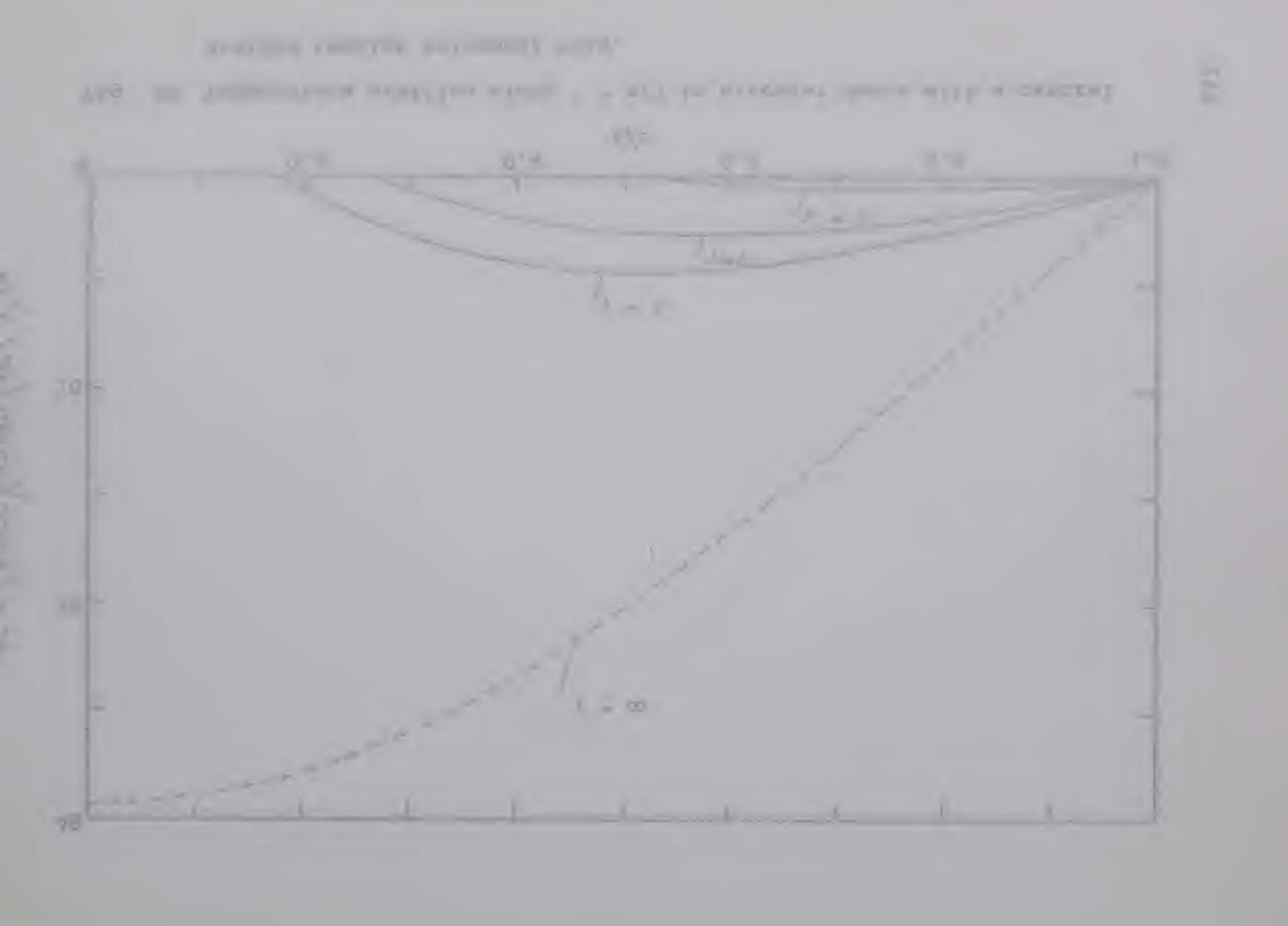
$\lambda = \infty$

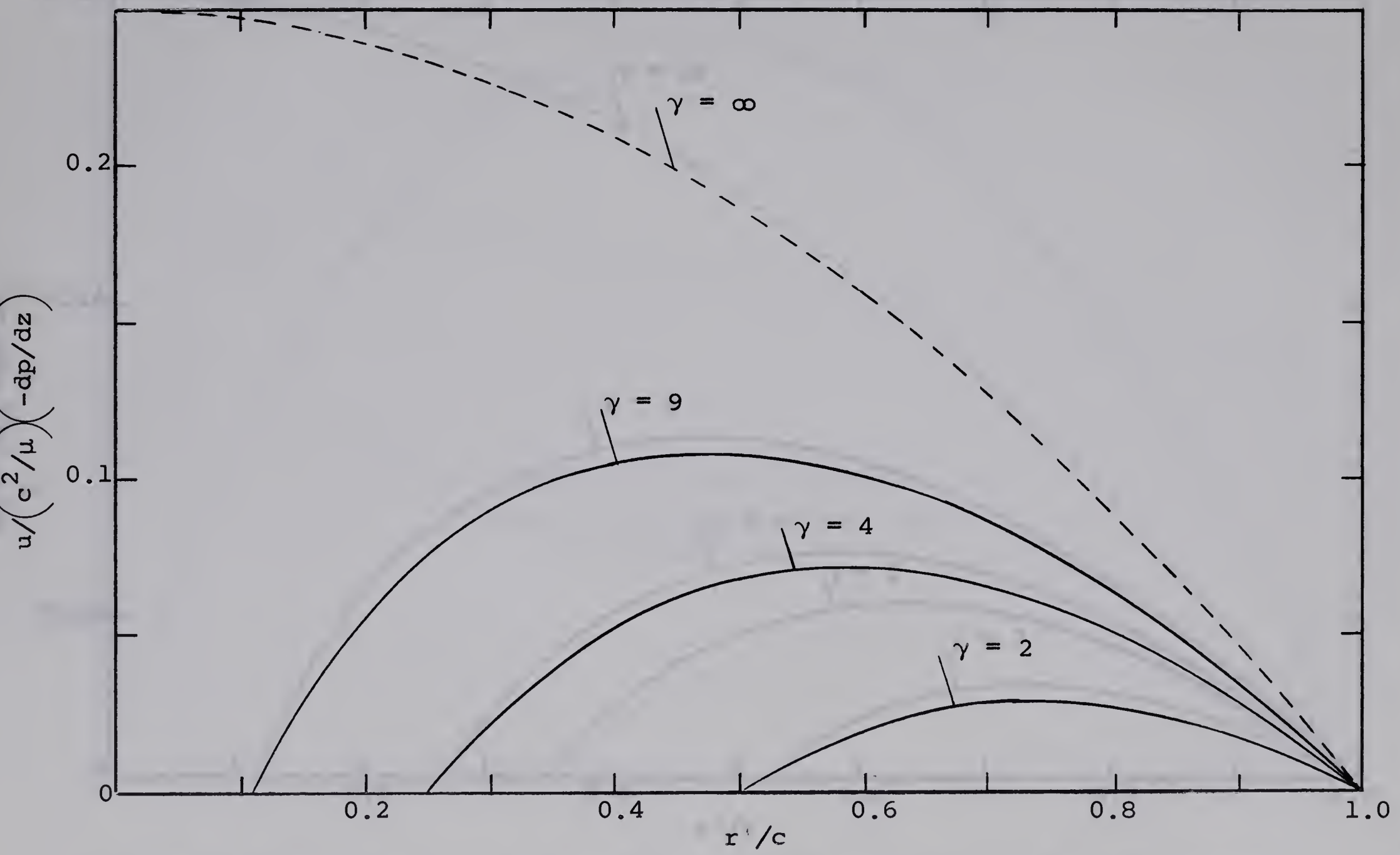

Fig. 41 Velocity profiles along $\Phi = 0$ in circular ducts with a central 10-sided regular polygonal hole.

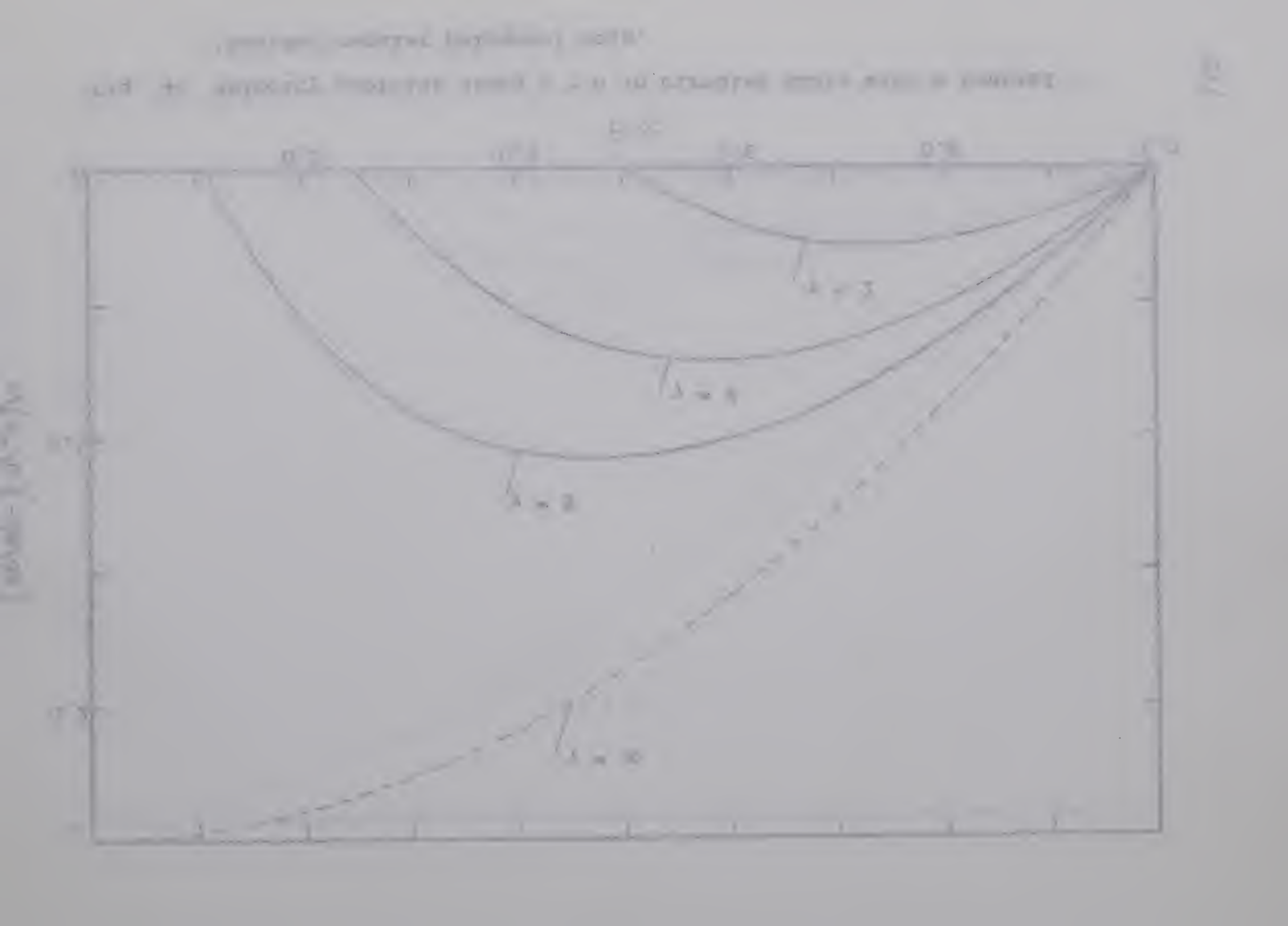
λ = 3
λ = 6
λ = 8
λ = 10

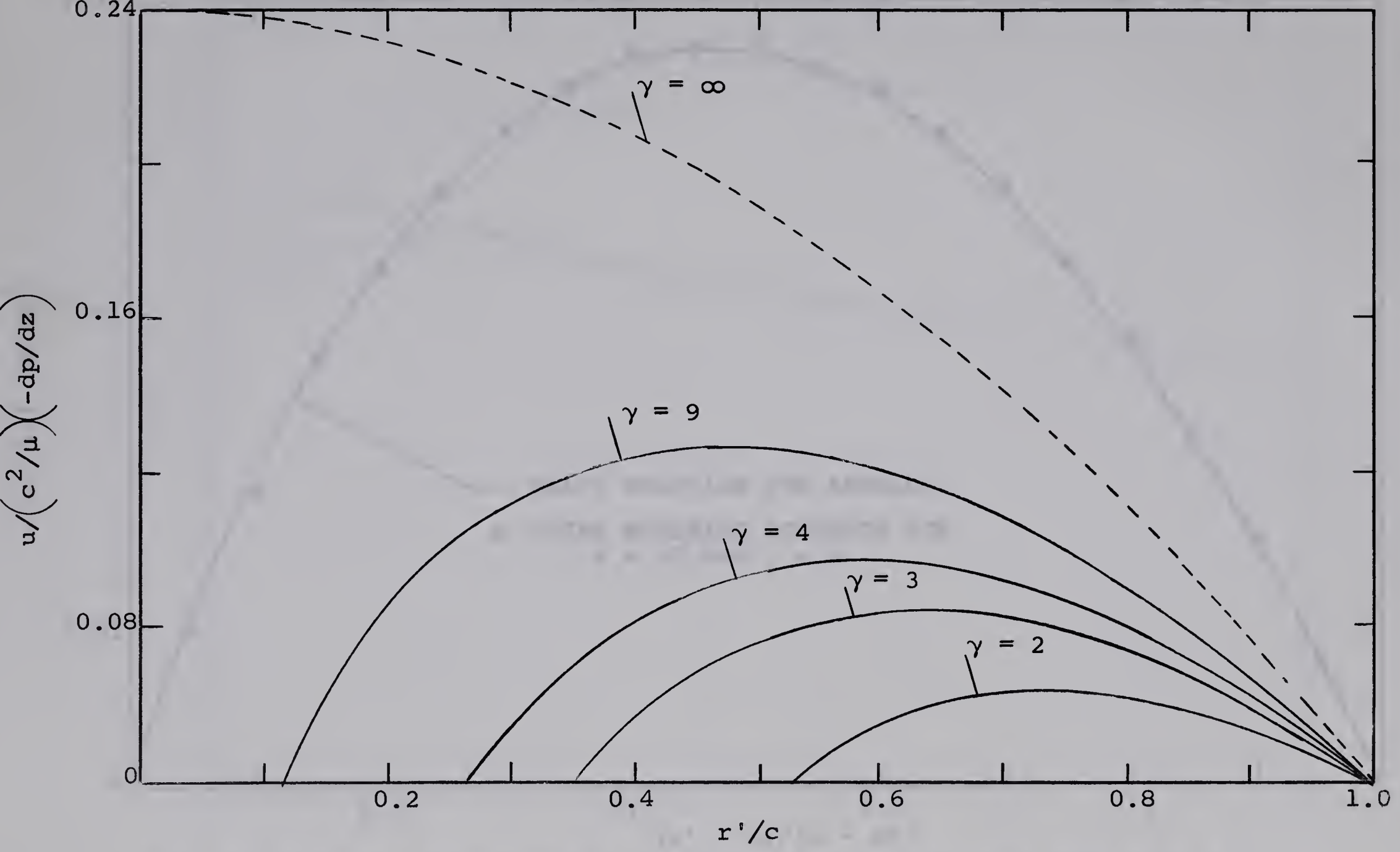

Fig. 42 Velocity profiles along $\Phi = \pi/10$ in circular ducts with a central 10-sided polygonal hole.

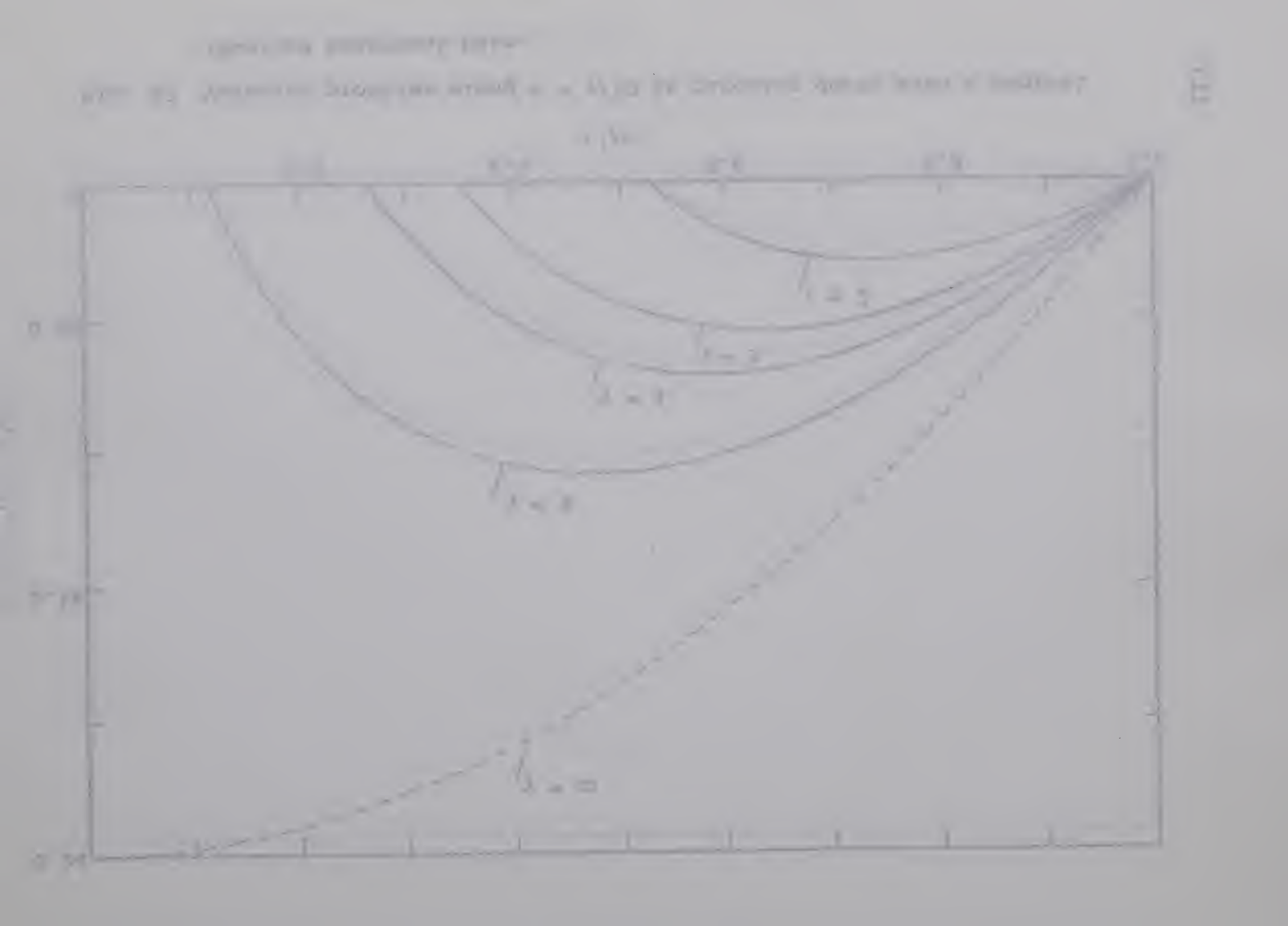

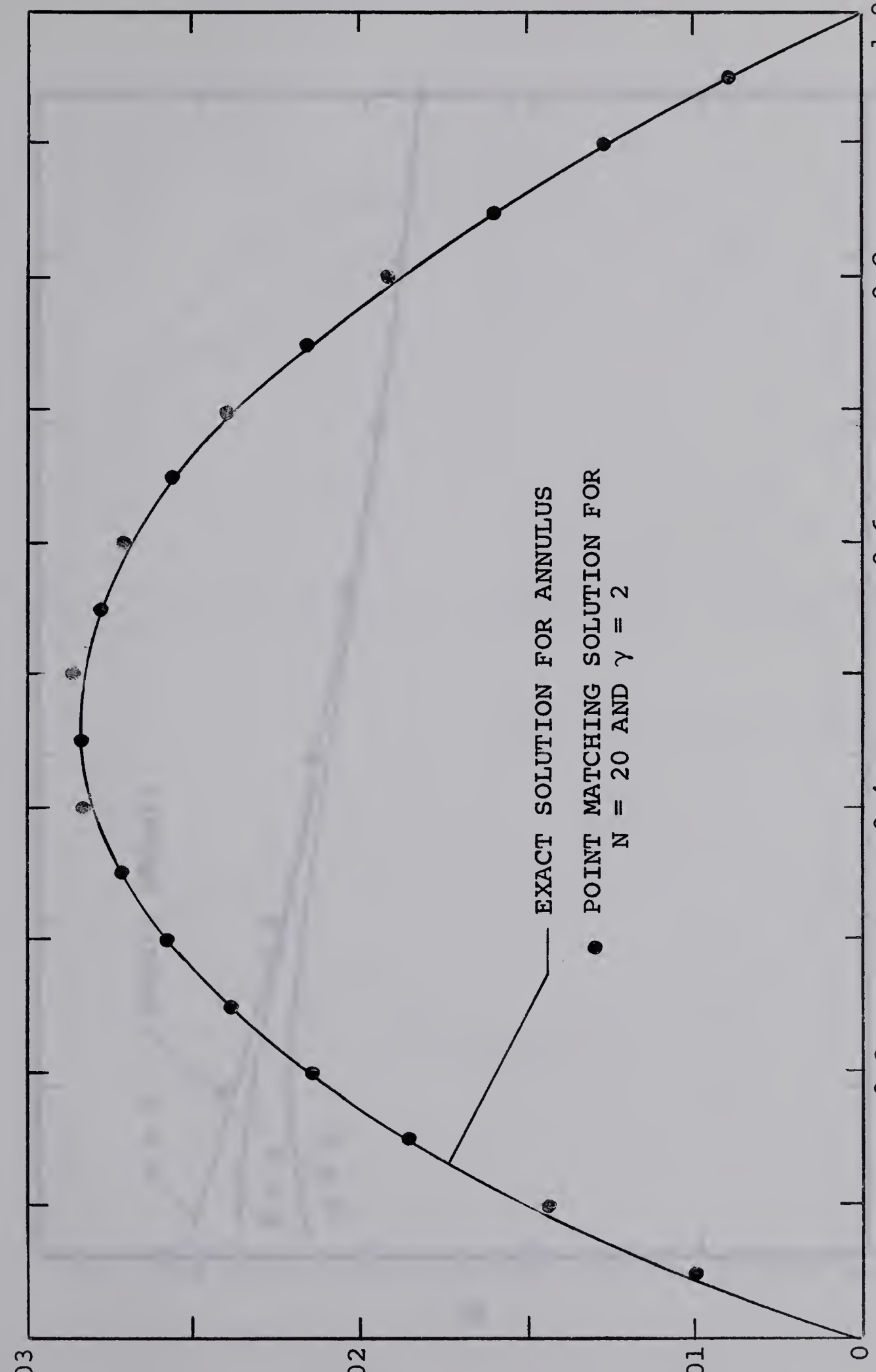

Fig. 43 Velocity distribution along $(r' - a)/(c - a)$ for $\alpha = \pi/20$ in circular duct with a central 20-sided regular polygonal hole.

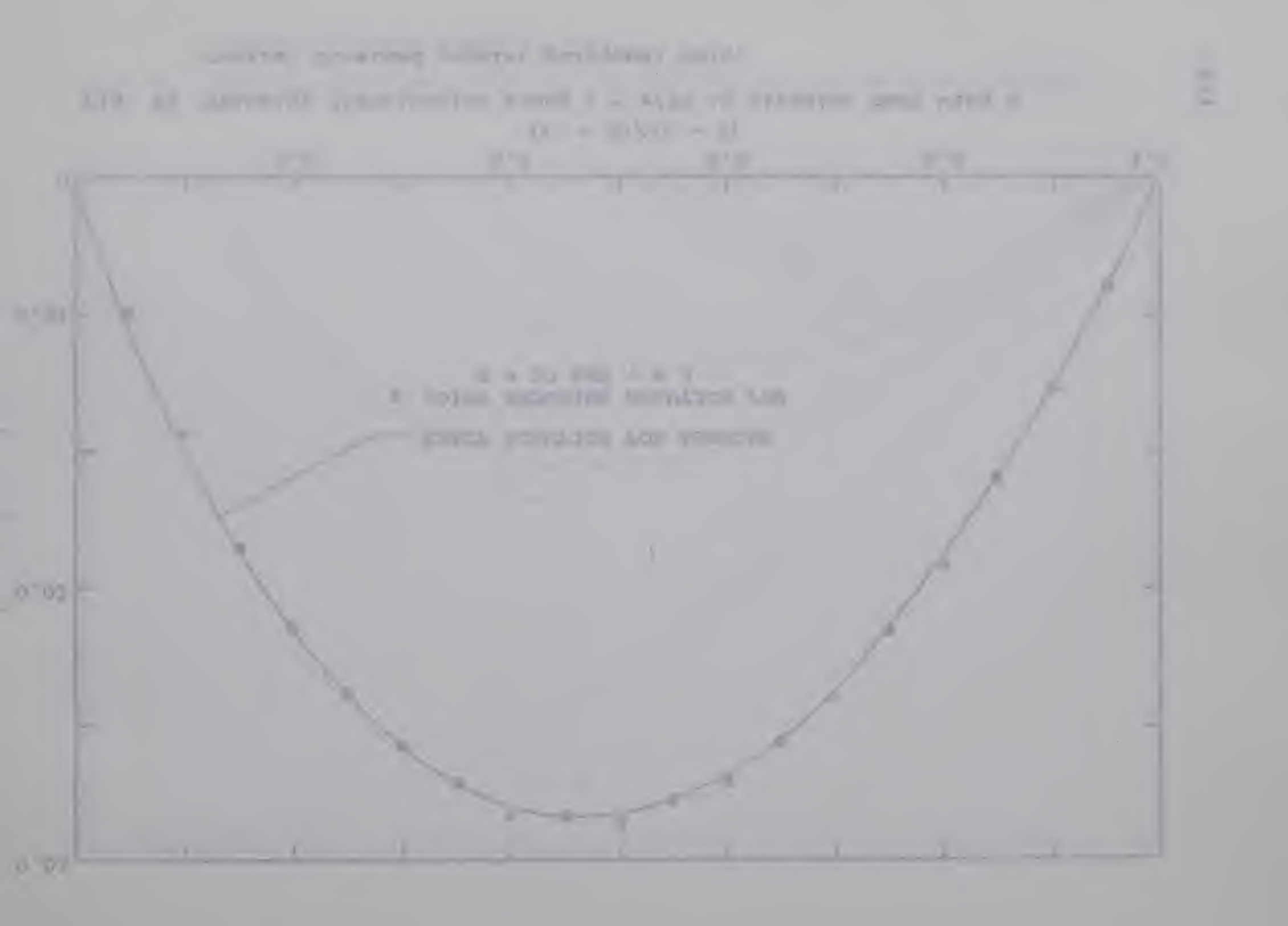

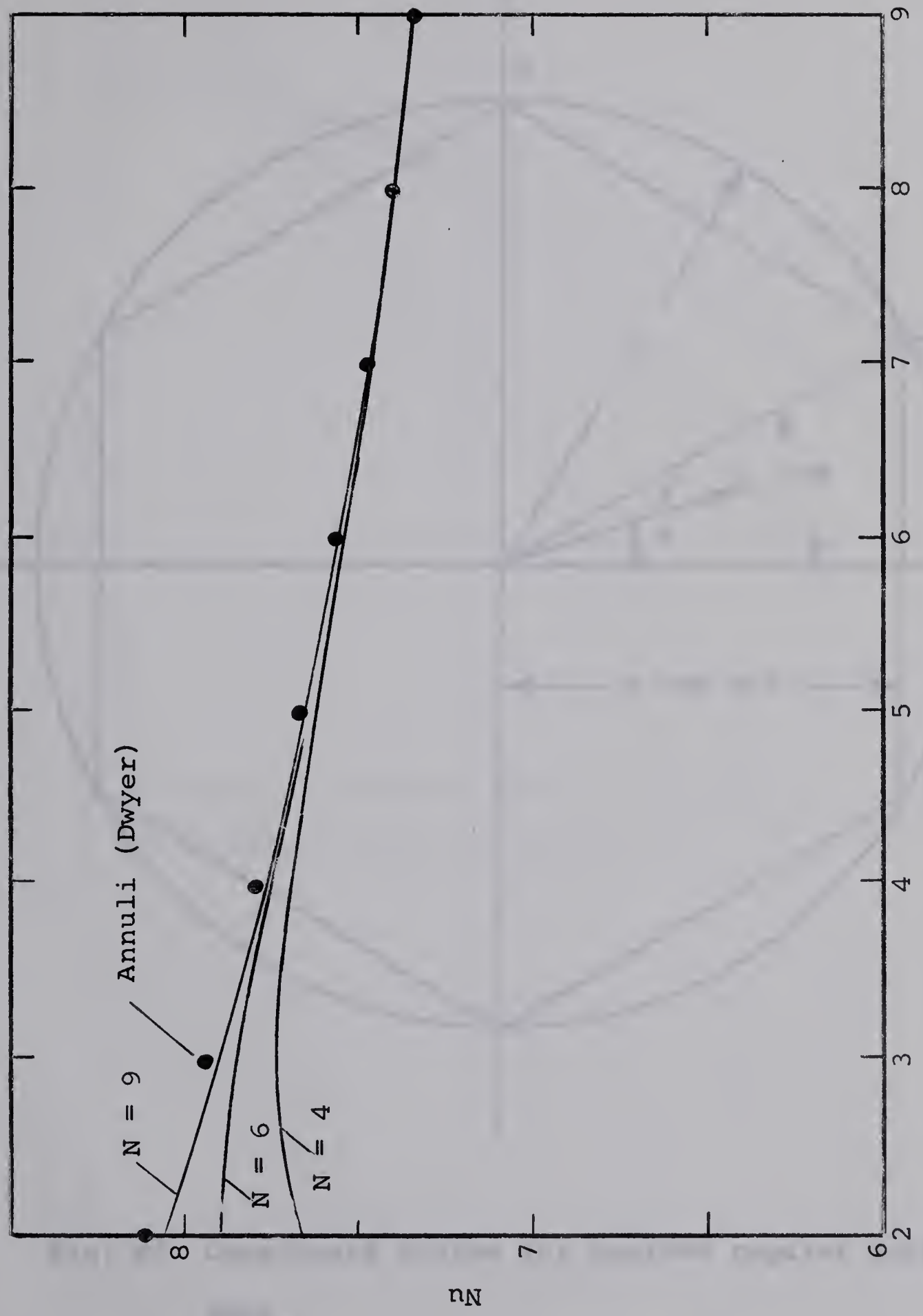

Fig. 44 Nusselt number results for circular ducts with a central regular polygonal hole.

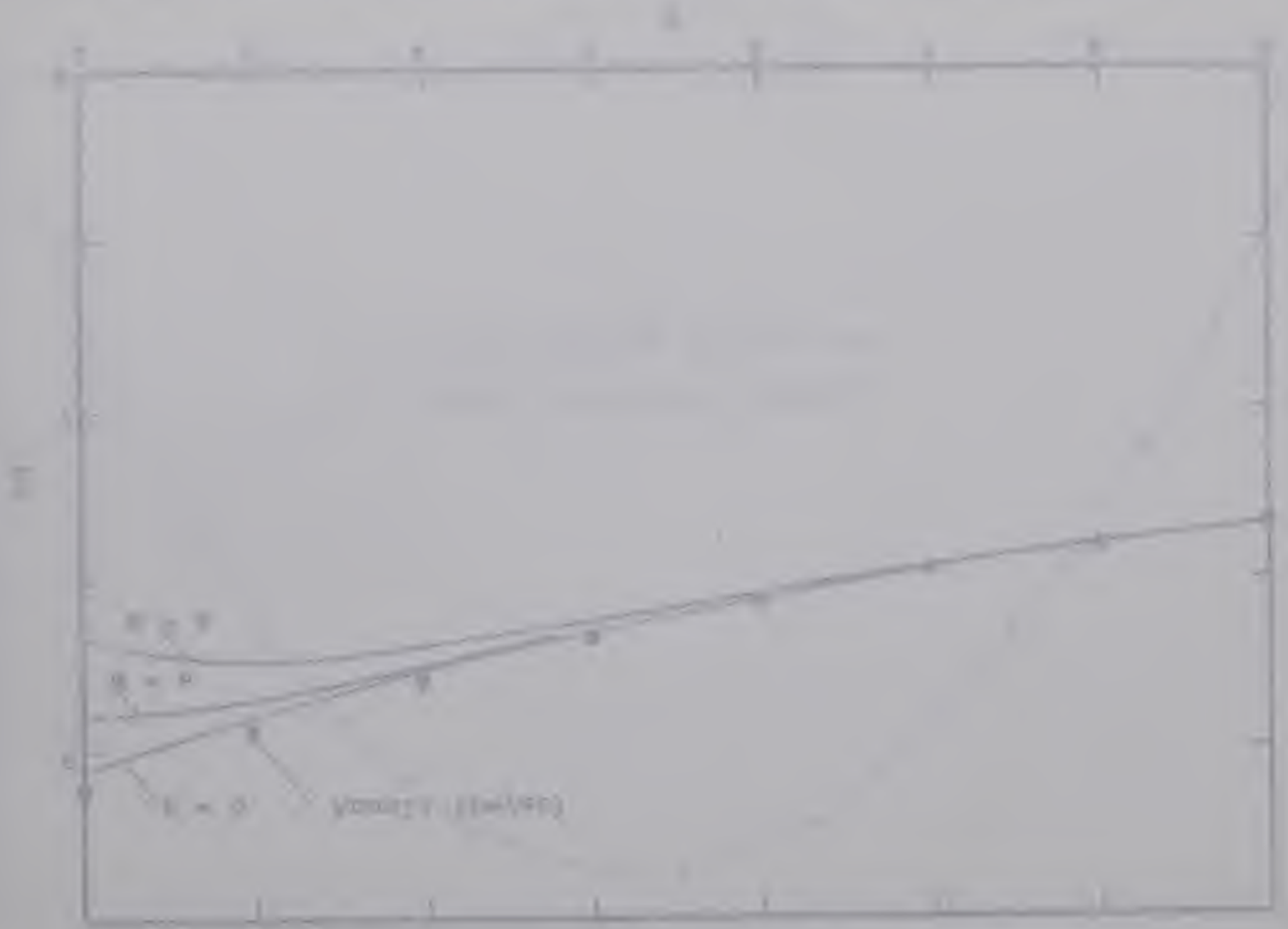

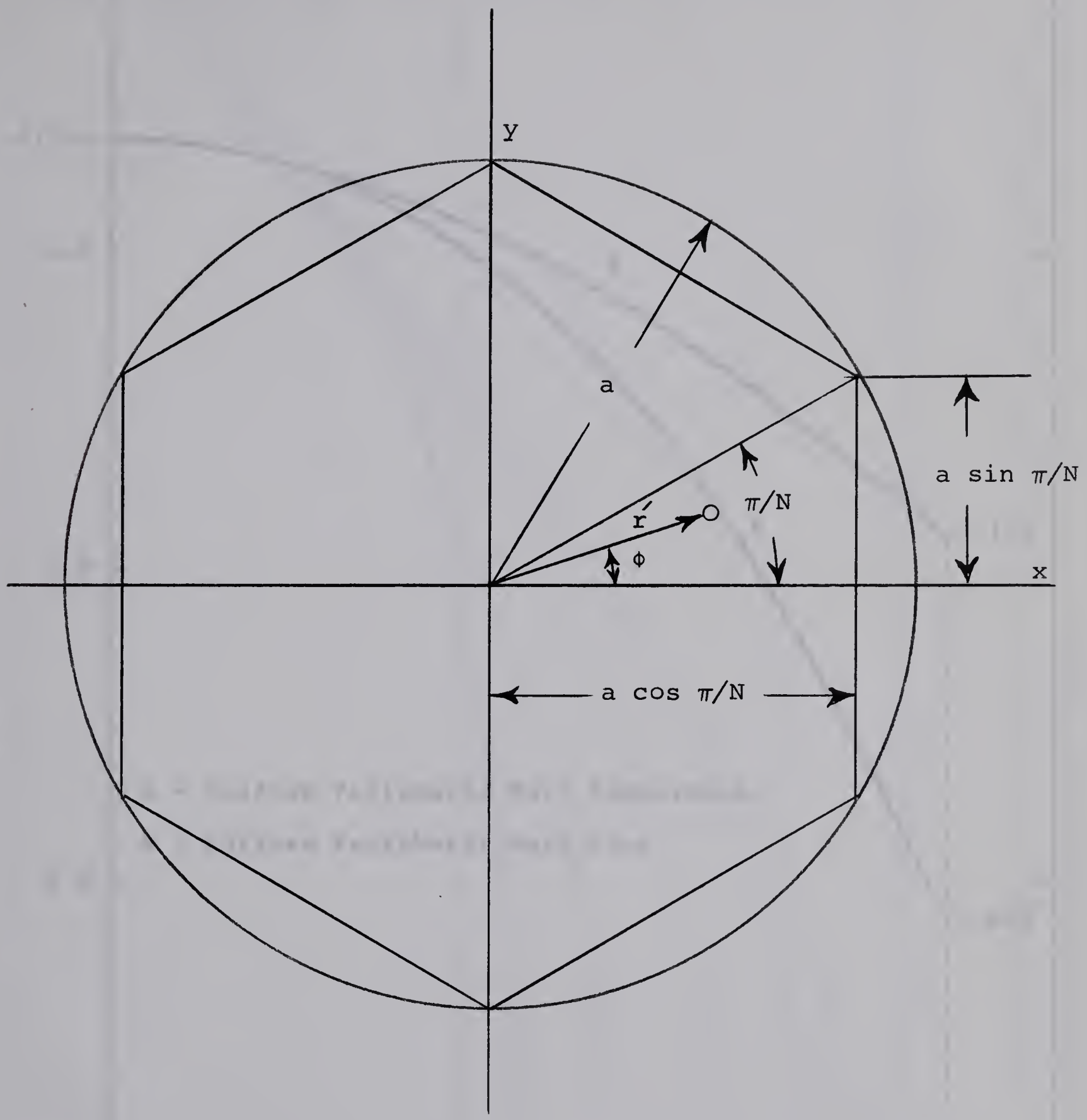

Fig. 45 Coordinate system for N-sided regular polygonal duct.

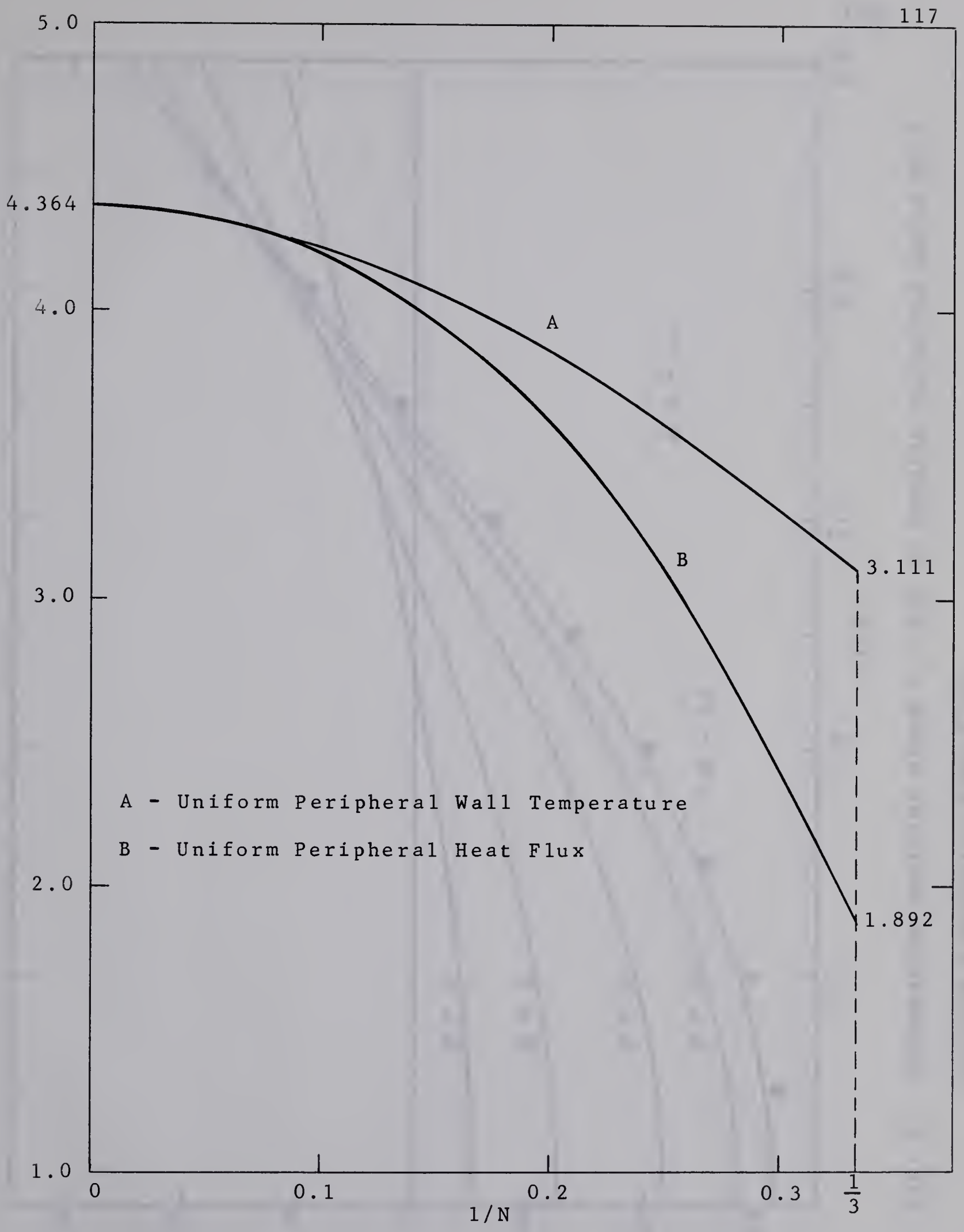

Fig. 46 Average Nusselt numbers for hydrodynamically and thermally developed laminar flow in regular polygonal ducts.

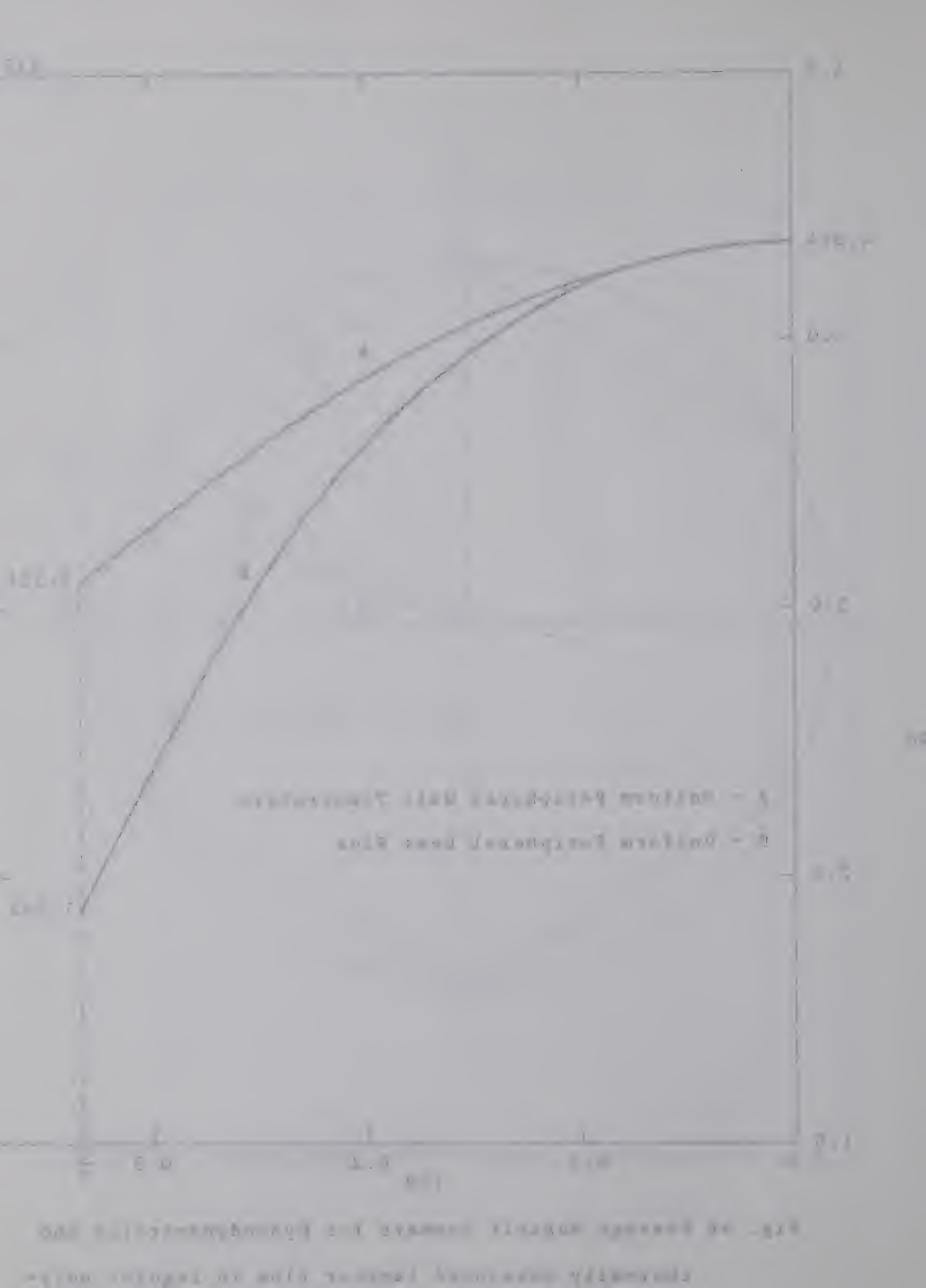

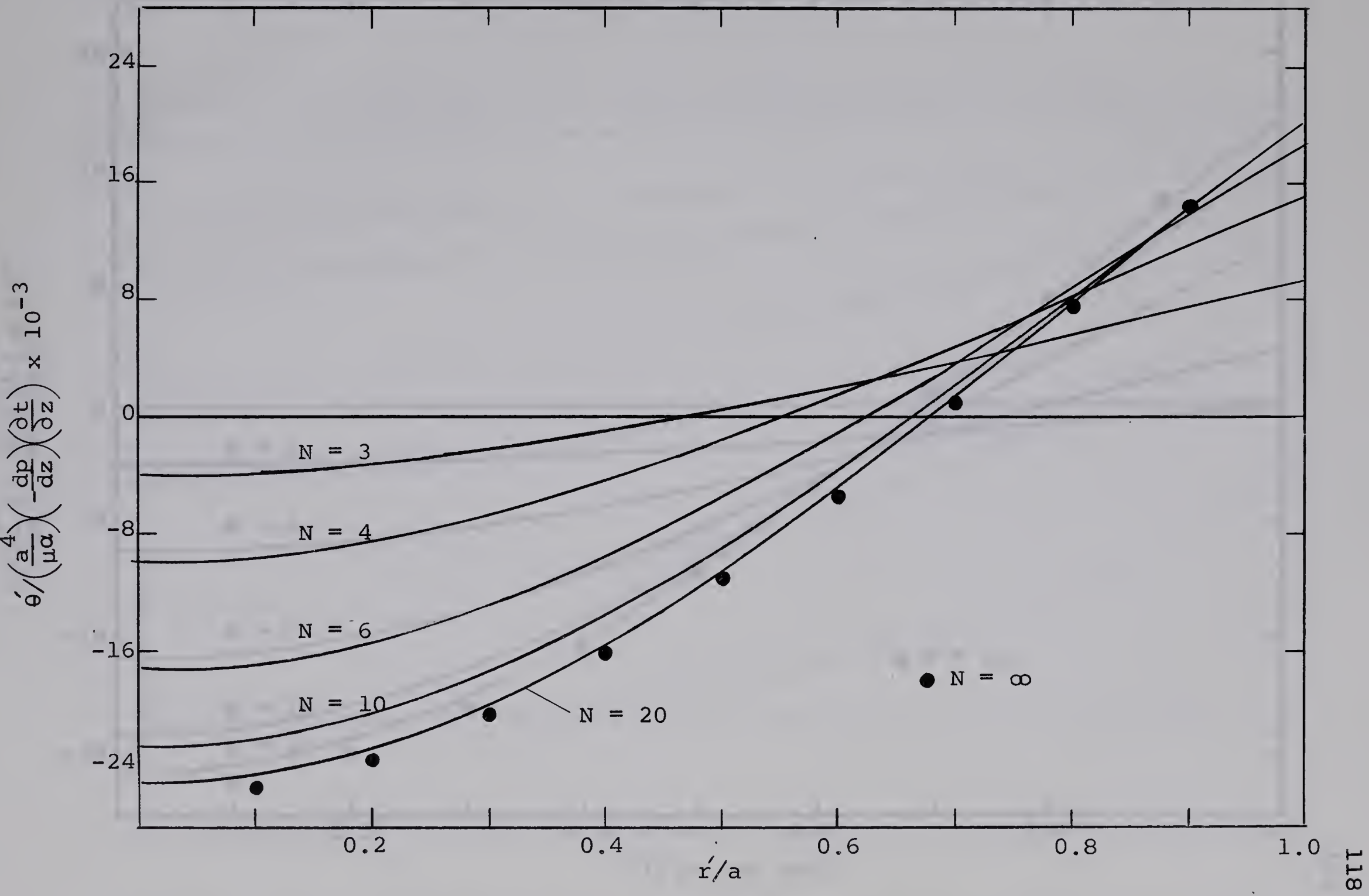

Fig. 47 Temperature profiles along $\Phi = \pi/N$ in regular polygonal ducts with uniform peripheral heat flux.

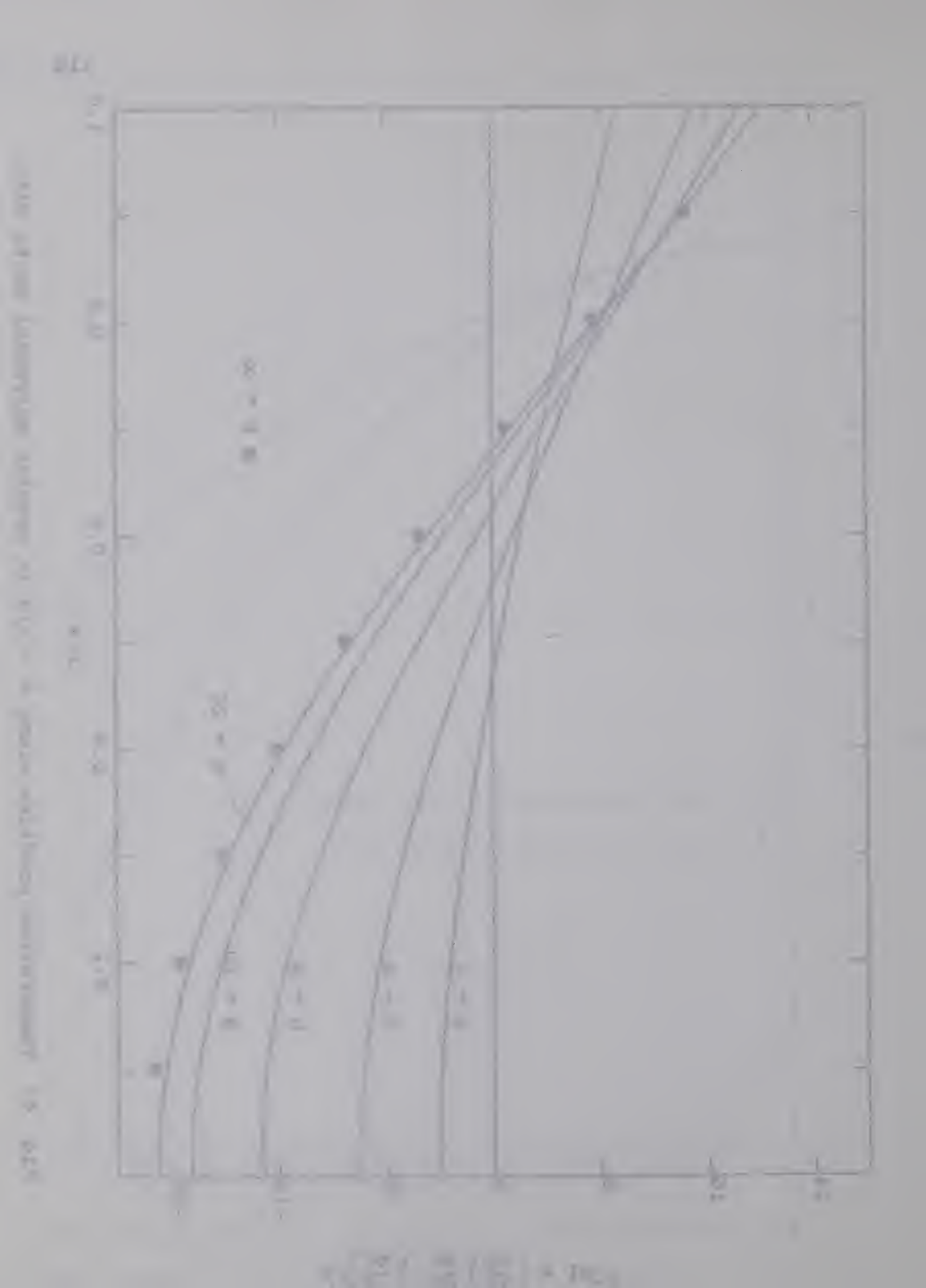

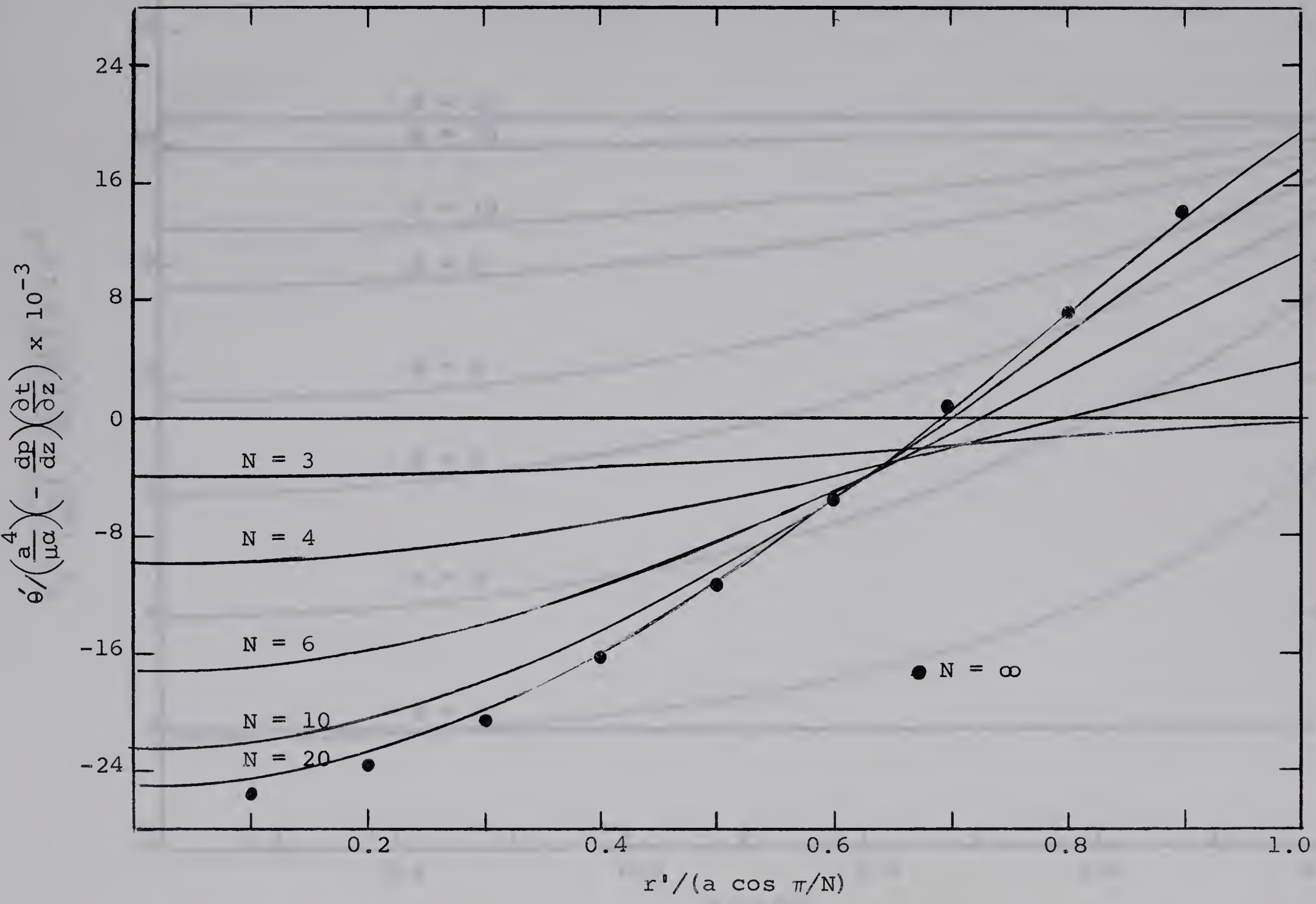

Fig. 48 Temperature profiles along $\Phi = 0$ in regular polygonal ducts with uniform peripheral heat flux.

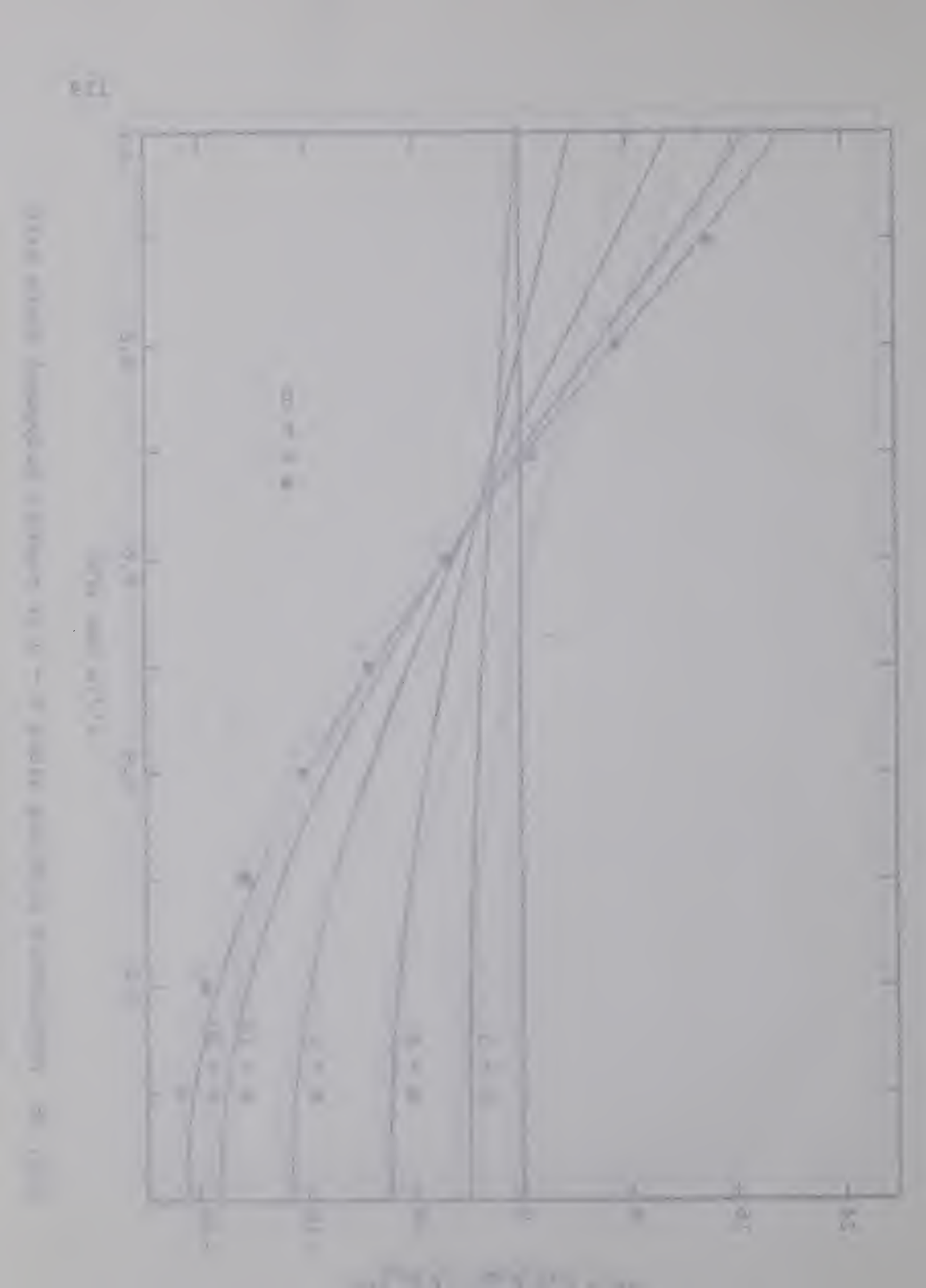

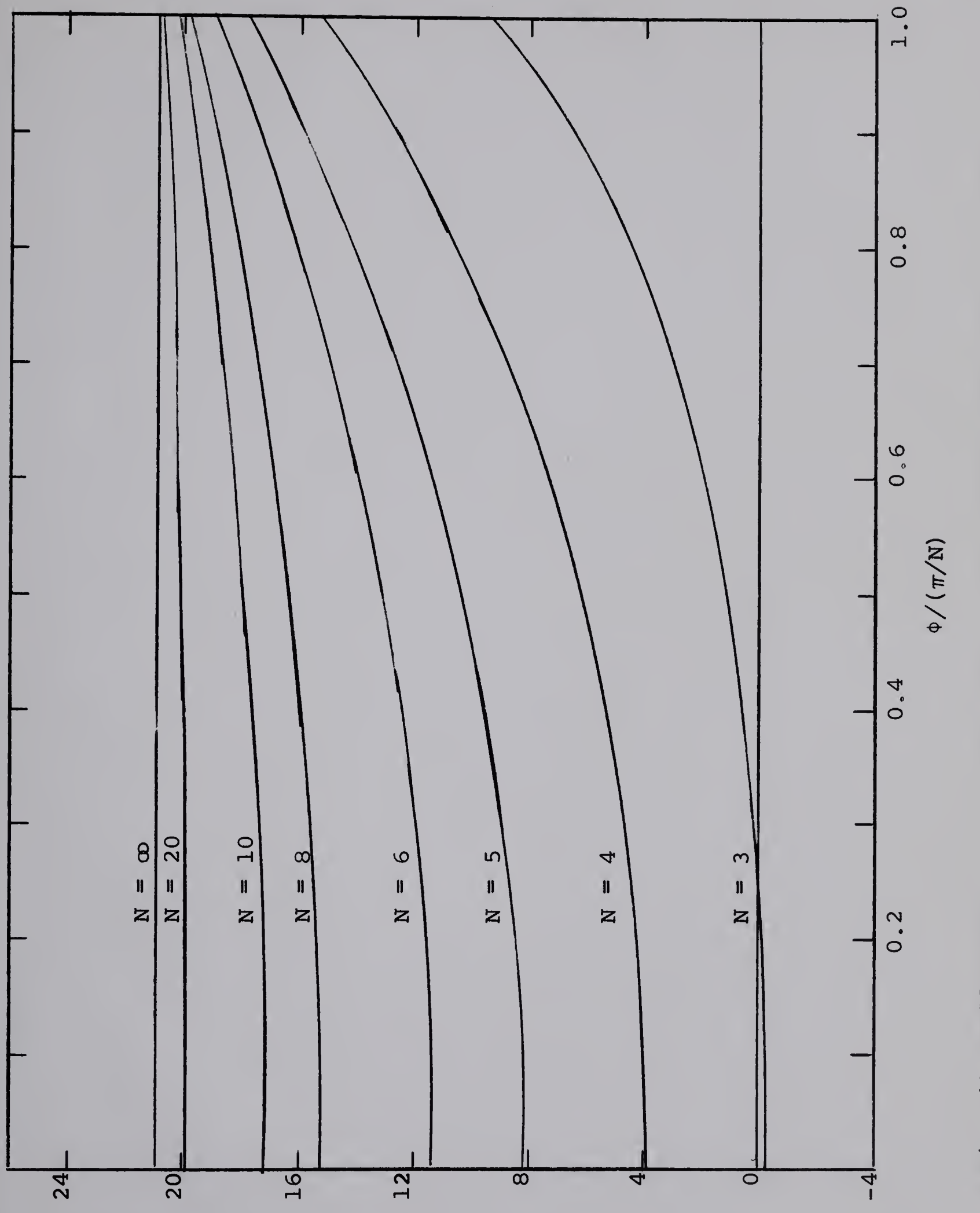

Fig. 49 Wall temperature distribution in regular polygonal ducts with uniform peripheral heat flux.

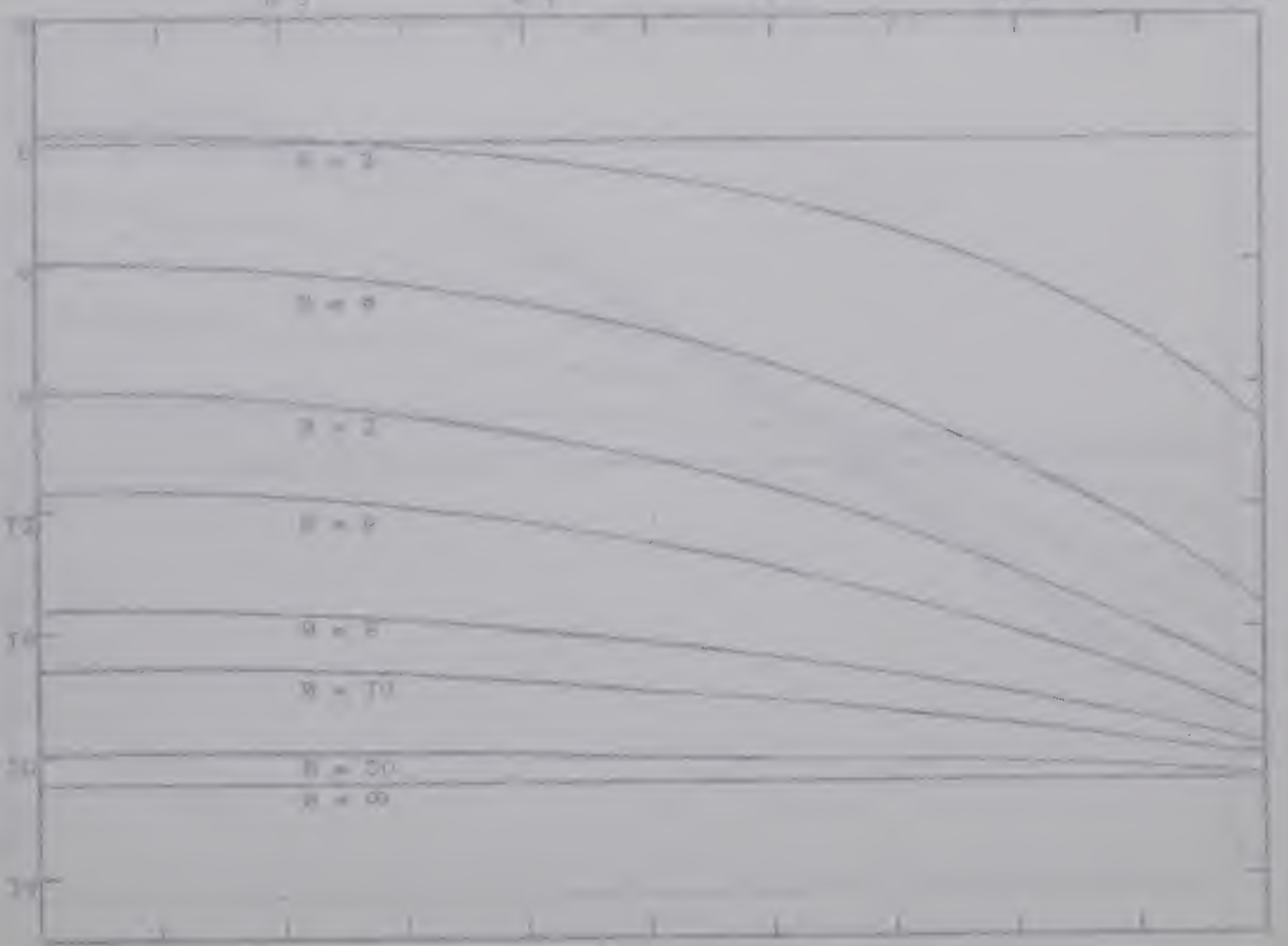
0·2
0·4
0·6
0·8
1·0
1·2
1·4
1·6
1·8
2·0
2·2
k = 2
k = 4
k = 2
k = 1
k = 0·5
k = 0·2
k = 0·1
k = 0